

The Pennsylvania State University
The Graduate School
College of Engineering

EVALUATING MODEL BEHAVIOR FOR HYDROLOGIC FORECASTING
IN GAUGED AND UNGAUGED WATERSHEDS

A Dissertation in
Civil Engineering
by
Kathryn L. van Werkhoven

© 2008 Kathryn L. van Werkhoven

Submitted in Partial Fulfillment
of the Requirements
for the Degree of

Doctor of Philosophy

August 2008

The dissertation of Kathryn L. van Werkhoven was reviewed and approved* by the following:

Thorsten Wagener
Assistant Professor of Civil Engineering
Dissertation Advisor
Chair of Committee

Patrick M. Reed
Associate Professor of Civil Engineering

Chris J. Duffy
Professor of Civil Engineering

Michael E. Mann
Associate Professor of Meteorology

Peggy Johnson
Department Head, Civil and Environmental Engineering

* Signatures are on file in the Graduate School

ABSTRACT

Understanding hydrologic model behavior for different model structures (lumped vs. distributed) and under different data scenarios (gauged vs. ungauged) is critical to effectively take advantage of advancements in models and data sources and to appropriately apply models for specific circumstances. This dissertation presents multiple studies that evaluate hydrologic model behavior for specific cases in hydrologic forecasting, with an ultimate objective of identifying appropriate models and approaches for less-developed, data-sparse regions. The cases evaluated include (1) a lumped, conceptual model in gauged watersheds across a hydroclimatic gradient, (2) a distributed, conceptual model in a gauged watershed, and (3) a lumped, parsimonious model in ungauged watersheds. For the first case, a comprehensive, global sensitivity analysis is performed to investigate how model behavior varies across watersheds with different hydroclimatic characteristics. The results of the sensitivity analysis are then used to determine if the parametric dimensionality of the model can be reduced for multi-objective optimization, without significantly impacting model performance. For the second case, a series of synthetic rainfall events are used to investigate spatially-varying model behavior across the domain of a distributed model. Lastly, for the third case, an approach for ungauged hydrologic prediction is tested for a region of southern Africa and changes in the modeled streamflow response due to projections of climate change are assessed. Overall findings demonstrate that hydrologic model behavior is a dynamic variable that varies across watersheds, time periods, and the model domain (in the distributed case). Results also highlight the limitations of existing methods and need for new dynamic methods for model identification that take patterns of model behavior into account for both lumped and distributed modeling. And finally, results for the ungauged case extend the modeling approach to less-developed countries and project that annual runoff for the study area will increase in the future, thereby highlighting the importance of such studies for water resources and flood management.

TABLE OF CONTENTS

List of Figures	vii
List of Tables	xiv
Preface	xv
Acknowledgements	xvi
Chapter 1 Introduction	1
1.1 Background	2
1.2 Current Drivers in Hydrologic Forecasting Research	4
1.3 Hydrologic Model Behavior	7
1.4 Dissertation Scope	8
1.4.1 Phase I	9
1.4.2 Phase II	11
1.4.3 Phase III	12
1.5 Organization	13
1.6 Chapter 1 References	13
Chapter 2 Phase I (a): Characterization of Watershed Model Behavior across a Hydroclimatic Gradient	17
2.1 Introduction	18
2.2 MOPEX Basins and Data	21
2.3 Methods	24
2.3.1 The Sacramento Soil Moisture Accounting Model (SAC-SMA)	24
2.3.2 Sobol' Sensitivity Analysis	26
2.3.3 Metrics for Model Evaluation	29
2.3.4 Spearman Rank Correlation	31
2.4 Approach	32
2.5 Results and Discussion	33
2.5.1 Long-term Sensitivities	33
2.5.1.1 High Flows – RMSE	34
2.5.1.2 Low Flows – TRMSE	37
2.5.1.3 Water Balance – ROCE	38
2.5.1.4 Medium Flow Regime – SFDCE	41
2.5.2 Interannual Sensitivities	43
2.5.3 Synthesis of Results	49
2.6 Summary and Conclusions	51
2.7 Chapter 2 References	55
Chapter 3 Phase I (b): Sensitivity-Guided Multi-Objective Calibration of a Lumped Watershed Model across a Hydroclimatic Gradient	59
3.1 Introduction	60
3.2 Study Watersheds	63
3.3 Methods	65
3.3.1 The Sacramento Soil Moisture Accounting Model (SAC-SMA)	65

3.3.2 Objective Functions	66
3.3.3 Epsilon Nondominated Sorted Genetic Algorithm II	68
3.3.4 Sobol' Sensitivity Analysis	70
3.4 Approach	71
3.5 Results	72
3.5.1 Reduced Parameter Sets	72
3.5.2 Optimization	74
3.5.2.1 Watershed AMI	75
3.5.2.2 Watershed EAS	81
3.5.2.3 Watershed SPR	83
3.5.2.4 Watershed GUA	87
3.6 Discussion	91
3.7 Conclusions	94
3.8 Chapter 3 References	95
Chapter 4 Phase II: Rainfall Characteristics Define the Value of Streamflow Observations for Distributed Watershed Model Identification	99
4.1 Introduction	100
4.2 Model Description	101
4.3 Sobol' Sensitivity Analysis	102
4.4 Experimental Design	105
4.5 Results	107
4.6 Conclusions	111
4.7 Chapter 4 References	115
Chapter 5 Phase III: Evaluating Climate Change Impacts in Ungauged Watersheds in Southern Africa	118
5.1 Introduction	119
5.2 Study Area and Data	122
5.2.1 The Olifants Basin	122
5.2.2 Data	125
5.3 Methods	128
5.3.1 Regionalization of Hydrologic Constraints	128
5.3.2 Development of Climate Change Time Series	129
5.3.3 Model Description	131
5.4 Approach	132
5.5 Results	134
5.5.1 Regionalization Analysis	134
5.5.2 Historical Streamflow Predictions and Verification	135
5.5.3 Future Trends in Climate Change Variables	138
5.5.4 Future Streamflow Predictions	142
5.6 Discussion and Conclusions	148
5.7 Chapter 5 References	151
Chapter 6 Synthesis	154
6.1 Summary of Scientific Contributions	155

6.2 Recommendations for Future Work.....	158
Appendix A Supplementary Figures and Tables for Chapter 4.....	161
Appendix B Supplementary Figures and Tables for Chapter 5	168

LIST OF FIGURES

Figure 2.1 Location and elevation of 12 MOPEX watersheds.	22
Figure 2.2 MOPEX watershed characteristics: (a) mean monthly runoff volume in mm (b) mean monthly precipitation (c) mean monthly potential evaporation (d) hydrologic ratios (e) flow duration curves.....	23
Figure 2.3 Conceptualization of the SAC-SMA.	25
Figure 2.4 Hydrograph components captured by the four selected evaluation metrics.....	30
Figure 2.5 Long-term Sobol sensitivity indices for 12 watersheds and 14 parameters based on a 38-year period: Total (individual + interactions) sensitivities, first-order (individual contributions) and interaction contributions for (a) RMSE, (b) TRMSE, (c) ROCE, and (d) SFDCE.	34
Figure 2.6 Scatter plots demonstrating Spearman rank correlation (R) between selected parameters' long-term Sobol sensitivity indices (SI) and long-term hydroclimatic variables across watersheds for (a) RMSE, (b) TRMSE, (c) ROCE, and (d) SFDCE. Watersheds are indicated by the marker symbols and the selected parameter is labeled on the y-axis.	36
Figure 2.7 Interannual Sobol sensitivity indices for the six driest watersheds over the period 1980-1998. The overall sensitivity (last column in each grid) is the corresponding result from the long-term analysis shown in Figure 2.5. Total annual precipitation (left axis) and the runoff coefficient (right axis) for each year is shown above each sensitivity grid.....	44
Figure 2.8 Interannual Sobol sensitivity indices for the six wettest watersheds over the period 1980-1998. The overall sensitivity (last column in each grid) is the corresponding result from the long-term analysis shown in Figure 2.5. Total annual precipitation (left axis) and the runoff coefficient (right axis) for each year is shown above each sensitivity grid.....	45
Figure 2.9 Scatter plots demonstrating Spearman rank correlation (R) between parameters' annual Sobol sensitivity indices (SI) and annual hydroclimatic variables. Each plot displays the result for a particular watershed and parameter combination. The watershed is indicated by the marker and the parameter is labeled on the y-axis.	46
Figure 2.10 Summary of SAC-SMA parameter sensitivity results and guidance for parameter estimation (based on the maximum index from the four evaluation metrics' results). Highly sensitive (black) parameters are those where the majority	

of years have an $SI > 0.1$, sensitive (gray) are those where the majority are in the range $0.01 < SI < 0.1$; and not sensitive (white) are those where the majority of years have an $SI < 0.01$50

Figure 3.1 Study watersheds’ locations, elevation ranges, and hydrographs for an average year (normal and log scale).64

Figure 3.2 Conceptualization of the SAC-SMA.66

Figure 3.3 Development of parameter sets to optimize for each sensitivity index threshold (t) in each study watershed. Part (a) indicates the parameters’ Sobol sensitivity indices for the four evaluation metrics and shows which parameters (outlined in black) have indices above the given threshold value. Part (b) illustrates how reduced-parameter sets were built by including parameters that are sensitive for RMSE *or* TRMSE (2-metric reduced set) and parameters that are sensitive for *any* of the metrics (4-metric reduced set).....73

Figure 3.4 Watershed AMI optimization results for the (a) 2-metric reduced parameter sets and the (b) 4-metric reduced parameter sets. Results of the full parameter optimization are shown in the top row of both (a) and (b). The sensitivity index threshold and the corresponding number of optimized parameters is indicated in the gray box for each case.76

Figure 3.5 Watershed AMI observed and simulated (i.e. pareto range) cumulative runoff volume curves and flow duration curves (with the high flows (0-10%) portion shown in the inset plot on a larger y-axis scale for readability). The cases presented include (a) the full parameter set optimization, (b) the ‘best’ 2-metric reduction result (c) the ‘best’ 4-metric reduction result and (d) the corresponding 2-metric for the threshold level of the ‘best’ 4-metric result (for comparison). The ‘best’ optimizations were selected subjectively as the case with the fewest parameters where model performance is not severely impacted for the metrics considered.78

Figure 3.6 Watershed EAS optimization results for the (a) 2-metric reduced parameter sets and the (b) 4-metric reduced parameter sets. Results of the full parameter optimization are shown in the top row of both (a) and (b). The sensitivity index threshold and the corresponding number of optimized parameters is indicated in the gray box for each case.80

Figure 3.7 Watershed EAS observed and simulated (i.e. pareto range) cumulative runoff volume curves and flow duration curves (with the high flows (0-10%) portion shown in the inset plot on a larger y-axis scale for readability). The cases presented include (a) the full parameter set optimization, (b) the ‘best’ 2-metric reduction result (c) the ‘best’ 4-metric reduction result and (d) the corresponding 2-metric for the threshold level of the ‘best’ 4-metric result (for comparison). The ‘best’ optimizations were selected subjectively as the case with the fewest

parameters where model performance is not severely impacted for the metrics considered.82

Figure 3.8 Watershed SPR optimization results for the (a) 2-metric reduced parameter sets and the (b) 4-metric reduced parameter sets. Results of the full parameter optimization are shown in the top row of both (a) and (b). The sensitivity index threshold and the corresponding number of optimized parameters is indicated in the gray box for each case.84

Figure 3.9 Watershed SPR observed and simulated (i.e. pareto range) cumulative runoff volume curves and flow duration curves (with the high flows (0-10%) portion shown in the inset plot on a larger y-axis scale for readability). The cases presented include (a) the full parameter set optimization, (b) the ‘best’ 2-metric reduction result (c) the ‘best’ 4-metric reduction result and (d) the corresponding 2-metric for the threshold level of the ‘best’ 4-metric result (for comparison). The ‘best’ optimizations were selected subjectively as the case with the fewest parameters where model performance is not severely impacted for the metrics considered.86

Figure 3.10 Watershed GUA optimization results for the (a) 2-metric reduced parameter sets and the (b) 4-metric reduced parameter sets. Results of the full parameter optimization are shown in the top row of both (a) and (b). The sensitivity index threshold and the corresponding number of optimized parameters is indicated in the gray box for each case.88

Figure 3.11 Watershed GUA observed and simulated (i.e. pareto range) cumulative runoff volume curves and flow duration curves (with the high flows (0-10%) portion shown in the inset plot on a larger y-axis scale for readability). The cases presented include (a) the full parameter set optimization, (b) the ‘best’ 2-metric reduction result (c) the ‘best’ 4-metric reduction result and (d) the corresponding 2-metric for the threshold level of the ‘best’ 4-metric result (for comparison). The ‘best’ optimizations were selected subjectively as the case with the fewest parameters where model performance is not severely impacted for the metrics considered.90

Figure 4.1 Spatially distributed parameter sensitivity for cases of (a) uniform total precipitation (P_{tot}) and uniform initial states (S_i) and (b) uniform precipitation and nonuniform initial states. Sensitivity indices are the total of all model parameters for a given cell. Indices are presented for the SAC-SMA and routing model analyzed simultaneously (SAC + ROUT – left two maps) and for the SAC-SMA analyzed separately (SAC only – right map).108

Figure 4.2 Spatially distributed parameter sensitivity for 4 different distributed storm events - (a) an upper basin stationary storm (b) a lower basin stationary storm (c) a storm moving downstream and (d) a storm moving upstream. Sensitivity indices are the total of all model parameters’ indices for a given cell.

In each case, indices are presented for the SAC-SMA and routing model analyzed simultaneously (SAC + ROUT – left two maps) and for the SAC-SMA analyzed separately (SAC only – right map).	109
Figure 4.3 Individual parameter grids resulting from the sensitivity analysis for Experiment 1 – uniform precipitation (P) and uniform initial states (Si).	112
Figure 4.4 Individual parameter grids resulting from the sensitivity analysis for Experiment 2 – uniform precipitation (P) and randomly varying initial states (Si).	113
Figure 4.5 Individual parameter grids resulting from the sensitivity analysis for Experiment 3 – localized precipitation (P) in the upper part of the basin and uniform initial states (Si).	114
Figure 4.6 Relative impacts of model parameters for each scenario of total precipitation (P _{tot}), initial states (Si), and model analysis (i.e., combined SAC+ROUT or SAC only). Values are percentages of total (sum of all parameters) mean areal sensitivity indices. Shades of gray also reflect the magnitude of the values.	115
Figure 5.1 Relative locations of the Limpopo Basin, the Olifants Basin, Kruger National Park, and Massingir Dam in southern Africa.	123
Figure 5.2 Elevation and mean areal precipitation of the Olifants Basin.	124
Figure 5.3 Location of (a) study watersheds within the Olifants Basin (gauged watersheds were used to generate regression relationships and source watersheds were the focus of the climate change assessment) and (b) the downscaled precipitation grid and temperature stations with respect to the source watersheds.	125
Figure 5.4 General skematic of (a) the regionalization of hydrologic constraints and (b) a constrained ensemble prediction.	129
Figure 5.5 Structure of the monthly probability distributed storage model used in this study.	132
Figure 5.6 Scatter plots of watershed characteristics (predictors) that were selected by regression analysis and streamflow indices (response variables) for (a) ROC and (b) CV. Note, that plots are included to provide a general idea of the single-variable relationships, although the final (strongest) relationships and statistical intervals (confidence and prediction intervals) were multivariate and not easily depicted in 2-dimensions.	135
Figure 5.7 Validation of ensemble predictions for 3 gauged watersheds that area also source watersheds. Reliability (R) of the confidence and prediction intervals is noted in the legend.	137

Figure 5.8 Constrained streamflow predictions for the historical period and total source area (sum of runoff from all source watersheds), generated using observations of precipitation as forcing.....	138
Figure 5.9 Regional climate change trends in mean annual precipitation (P), temperature (T), and potential evaporation (PE) for the control (1961-2000), future A (2045-2065) and future B (2081-2100) periods. Note that T and PE data were not available for model cnrm.	139
Figure 5.10 Regional climate change trends in mean monthly precipitation (P), temperature (T), and potential evaporation (PE).	141
Figure 5.11 Climate change trends in mean annual precipitation (P), temperature (T), and potential evaporation (PE) by watershed and GCM.	142
Figure 5.12 Regional climate change trends in P/PE and in the range of the prediction interval (PI) and confidence interval (CI) of the ROC for each model. Historical observed P/PE (black dot) and resulting ranges on the ROC (black and white patches) are also shown.....	143
Figure 5.13 Model mean regional ensemble simulations of hydrologic response to climate change, showing the control period (top), future A period (middle), and future B period (bottom).	144
Figure 5.14 Regional climate change trends in the range of the prediction interval (PI) and confidence interval (CI) on total volume of mean annual runoff (R) in units of million m ³ for each model – calculated from the ensemble predictions. Percent change in the mean R (mean of the range) from the control period to each of the future periods is indicated in red text. Historical ranges based on observed forcing are also shown (black and white patches).	145
Figure 5.15 Regional climate change trends in the range of the prediction interval (PI) and confidence interval (CI) on total volume of mean monthly runoff (R) in units of million m ³ for each model – calculated from ensemble predictions. The ΔR (blue line) is the monthly change (in the range mean) from the control period to the future periods divided by the total annual runoff to indicate how each month contributes to the overall change in annual runoff. The PI and CI based on observed historical forcing is shown (red lines) for comparison in the control period.	146
Figure 5.16 Watershed climate change trends in the percent change in total mean annual runoff from the control period to future A (2045-2065) and future B (2081-2100).....	147

Figure 5.17 Mean annual runoff based on the mean climate model projections across the 28 source watersheds for (a) the control period (1961-2000) (b) future A (2045-2065) and (c) future B (2081-2100). Runoff values are in units of mm to enable comparison across watersheds.	147
Figure 5.18 Projected change in annual runoff across the 28 source watersheds for (a) future A (2045-2065) and (b) future B (2081-2100).	148
Figure A.1 Metric TRMSE: Spatially distributed parameter sensitivity for cases of (a) uniform total precipitation (P_{tot}) and uniform initial states (S_i) and (b) uniform precipitation and nonuniform initial states. Sensitivity indices are the total of all model parameters for a given cell. Indices are presented for the SAC-SMA and routing model analyzed simultaneously (SAC + ROUT – left two maps) and for the SAC-SMA analyzed separately (SAC only – right map).	162
Figure A.2 Metric ROCE: Spatially distributed parameter sensitivity for cases of (a) uniform total precipitation (P_{tot}) and uniform initial states (S_i) and (b) uniform precipitation and nonuniform initial states. Sensitivity indices are the total of all model parameters for a given cell. Indices are presented for the SAC-SMA and routing model analyzed simultaneously (SAC + ROUT – left two maps) and for the SAC-SMA analyzed separately (SAC only – right map).	163
Figure A.3 Metric SFDCE: Spatially distributed parameter sensitivity for cases of (a) uniform total precipitation (P_{tot}) and uniform initial states (S_i) and (b) uniform precipitation and nonuniform initial states. Sensitivity indices are the total of all model parameters for a given cell. Indices are presented for the SAC-SMA and routing model analyzed simultaneously (SAC + ROUT – left two maps) and for the SAC-SMA analyzed separately (SAC only – right map).	164
Figure A.4 Metric TRMSE: Spatially distributed parameter sensitivity for 4 different distributed storm events - (a) an upper basin stationary storm (b) a lower basin stationary storm (c) a storm moving downstream and (d) a storm moving upstream. Sensitivity indices are the total of all model parameters' indices for a given cell. In each case, indices are presented for the SAC-SMA and routing model analyzed simultaneously (SAC + ROUT – left two maps) and for the SAC-SMA analyzed separately (SAC only – right map).	165
Figure A.5 Metric ROCE: Spatially distributed parameter sensitivity for 4 different distributed storm events - (a) an upper basin stationary storm (b) a lower basin stationary storm (c) a storm moving downstream and (d) a storm moving upstream. Sensitivity indices are the total of all model parameters' indices for a given cell. In each case, indices are presented for the SAC-SMA and routing model analyzed simultaneously (SAC + ROUT – left two maps) and for the SAC-SMA analyzed separately (SAC only – right map).	166

Figure A.6 Metric SFDCE: Spatially distributed parameter sensitivity for 4 different distributed storm events - (a) an upper basin stationary storm (b) a lower basin stationary storm (c) a storm moving downstream and (d) a storm moving upstream. Sensitivity indices are the total of all model parameters' indices for a given cell. In each case, indices are presented for the SAC-SMA and routing model analyzed simultaneously (SAC + ROUT – left two maps) and for the SAC-SMA analyzed separately (SAC only – right map).	167
Figure B.1 Maps of climatic and physical watershed characteristics for the 23 gauged watersheds, including the wetness index (PPE), elevation (ELEV), slope, and topographic index (TI). PPE is unitless (ratio), ELEV in meters, slope in degrees, and TI is unitless.	170
Figure B.2 Maps of additional physical watershed characteristics for the 23 gauged watersheds, including the normalized difference vegetation index (NDVI), landuse (LU), soil drainage rate (DRATE) and soil water content (m/m) at the permanent wilting point (WP).	171
Figure B.3 Spatial distribution of mean annual precipitation for control period (1961-2000) based on observations and downscaled climate model projections.....	172
Figure B.4 Spatial distribution of percent change in downscaled precipitation from the control period (1961-2000) to Future A (2046-2065) and Future B (2081-2100) for each model.....	173
Figure B.5 Change in mean annual precipitation based on the original (non-downscaled) global climate model projections from the three models used in this study for future A (2045-2065) and future B (2081-2100) periods. Precipitation change is measured with respect to the historical period 1961-1990.	174
Figure B.6 Model echam5 regional ensemble simulations of hydrologic response to climate change, showing the control period (top), future A period (middle), and future B period (bottom).	175
Figure B.7 Model giss regional ensemble simulations of hydrologic response to climate change, showing the control period (top), future A period (middle), and future B period (bottom).	176
Figure B.8 Model cnrm/echam5 regional ensemble simulations of hydrologic response to climate change, showing the control period (top), future A period (middle), and future B period (bottom).	177
Figure B.9 Model cnrm/giss regional ensemble simulations of hydrologic response to climate change, showing the control period (top), future A period (middle), and future B period (bottom).	178

LIST OF TABLES

Table 2.1 MOPEX Watershed Characteristics	23
Table 2.2 Description of SAC-SMA parameters and allowable ranges analyzed in this study	24
Table 2.3 Definition of the Θ symbols in Eqs. (2.4)–(2.7) of Sobol's method	29
Table 3.1 Four study watersheds' characteristics.....	64
Table 3.2 Description of SAC-SMA parameters allowable ranges and a priori values.	65
Table 3.3 Four watersheds' best-case reduced-parameter optimization specifications.....	92
Table 4.1 Description of SAC-SMA and routing parameter descriptions, a priori grid ranges, and sensitivity analysis ranges.	103
Table 4.2 Values and ranges for the two scenarios of SAC-SMA initial states.....	106
Table 5.1 Models on which the downscaled data used in this study were based and availability for precipitation (P), temperature (T), the control period (1961-2001), the future A period (2045-2065), and the future B period (2081-2100).....	127
Table 5.2 Description and ranges of model parameters.	132
Table 5.3 Streamflow indices tested for the regionalization of hydrologic constraints.	134
Table 5.4 Multivariate regression results for the selected response indices	135
Table B.1 Streamflow station information for gauges used in this study	169

PREFACE

The research presented in this dissertation represents a manifestation of questions that I began to formulate prior to pursuing a PhD, while working in South Africa and other developing countries. During that time, I was regularly confronted with challenges of lacking data, both in quality and quantity, as well as a lacking confidence in the sustainability and the underlying hydrologic theory of the technology I was implementing. At the time, though, my sources for guidance and depth of understanding were limited. My decision to return to graduate school was largely prompted by a desire to increase my understanding of hydrologic processes, variability, models, and model evaluation techniques. With that knowledge, I felt I could better recognize (or develop) appropriate approaches to hydrologic modeling in different regions of the world that effectively take into account data restrictions and hydroclimatic variability.

Through work on the studies presented in this dissertation, I steadily progressed toward this goal. In the process, I also came to realize how large the gap is between research and practice in hydrologic modeling. In research, there have been significant advances in our understanding of processes at various scales, sources and implications of uncertainty, use of remotely sensed data, methods for parameter estimation, etc. However these advances take a very long time to filter down into operational use, if they get there at all. And conversely, the issues faced in an operational environment do not always filter up into modeling approaches designed in a research setting. It is my intention throughout my career to work not only towards advancing the science and application of hydrologic modeling in less-developed as well as developed regions, but also towards closing the gap and opening greater lines of communication between research and practice. This dissertation is a big first step in that direction.

ACKNOWLEDGEMENTS

First and foremost I would like to thank my advisor, Dr. Thorsten Wagener, for his dedication, unfaltering support, and invaluable guidance throughout this PhD endeavor. I attribute a big part of my success over the last three years to his encouragement, influence and contagious enthusiasm for our science. Next, I want to thank Dr. Patrick Reed, who helped to guide me through much of the work in this dissertation and through many a computational quagmire. I am also grateful to Dr. Chris Duffy and Dr. Michael Mann for their time and constructive comments on various aspects of my research. In addition to faculty mentors, I greatly benefited from the help and previous work of a fellow student, now Dr. Yong Tang, whose coding genius laid the groundwork for my dissertation. All of the graduate students in the Water Resources Group helped me along the way at one point or another, so I send out thanks to them as well. I also gratefully acknowledge the financial support I received from the Clare Booth Luce Foundation, GE, and the Penn State College of Engineering. Thanks to these organizations, I was fortunate enough to have research freedom and travel support throughout my PhD. And one final mention with respect to technical support – I thank Brink du Plessis, Elias Nell, and Estelle van Niekerk for their invaluable help collecting the data that I used in Chapter 5 of this dissertation. Then there's my family, my parents and my sister, Lori. I would not be where I am today without their influence, constant support and patient listening over the years in all my wandering and all my endeavors, including this one. I always knew they were in my corner. Final and foremost, I thank my husband Herman. He's the reason I'm here, he's the reason I got through it, without any bruises... and just one little bump.

CHAPTER 1

Introduction

1.1 BACKGROUND

Hydrologic forecasts are a vital part of planning and mitigation strategies for the protection of human life and the ecological health of our planet. On multi-year time-scales, water resources management depends on forecasts to indicate possible changes in long-term water availability and to ensure sustainable use of our water supply. On monthly or annual time scales, forecasts provide crucial information for drought assessment and guidance of mitigation efforts. And on daily time-scales, emergency management organizations rely on hydrologic forecasts for effective flood warning and for the preparation of response personnel and resources.

In order to generate hydrologic forecasts, mathematical models of the natural processes controlling movement and storage of moisture in a watershed are needed. The approaches and tools used for watershed modeling vary widely and have evolved over the last several decades [*Singh and Woolhiser, 2002*]. Before the arrival of computers, models began as simple representations of individual components of the hydrologic cycle. Two key examples are the unit hydrograph and the rational formula, both developed by Dooge [1957; 1959], which simulate flow routing and excess rainfall, respectively. These methods, though still often used, evolved into more complete representations of the hydrologic cycle as digital computers became more commonly available. The Stanford Watershed Model (SWM), developed in the 1960s [*Crawford and Linsley, 1966*], marked the first of such models representing the complete cycle and was also the first to allow for continuous (versus single-event) simulation of the hydrologic system (a requirement for hydrologic forecasting). The SWM formed the basis for the Sacramento Soil Moisture Accounting Model (SAC-SMA) [*Burnash et al.,*

1973], which is still widely used and is currently the primary operational forecasting model in the United States. Up to this point in the evolution of models, hydrologic processes were represented conceptually, rather than explicitly by governing laws of physics. In the 1980s, the first physically-based watershed model emerged with the development of the Système Hydrologique Européen (SHE) [Abbott *et al.*, 1986]. At the time of initial development, however, physically-based models were severely limited by computing power and therefore not widely applied. This constraint has dramatically decreased over time, allowing for continued development of these models and an increase in their use and applicability. Since the 1980s, development and improvement of watershed models have increased exponentially. The resulting range of available models varies widely in complexity, data requirements, and modeling philosophy [Singh and Frevert, 2006].

Today we stand at cross-roads in the evolution of watershed models. Lack of computational constraints (relative to the past) combined with a multitude of existing models make the selection of an appropriate model for hydrologic forecasting (or other application) a formidable task. Compounding the issue, we live in a time when climate change threatens to further stress our water resources and increase the frequency of extreme events [Milly *et al.*, 2002; Milly *et al.*, 2005; Kundzewicz *et al.*, 2008]. The need for forecasts therefore in all parts of the world and under many different circumstances is growing. If the science underlying hydrologic forecasting is to advance in a direction that will confront such issues, the research community must proceed not only towards developing new models and approaches, but also towards increasing our understanding of the strengths, weaknesses, and most appropriate applications of existing models for the

variety of hydroclimatic, data availability, and economic situations that exist across this planet.

1.2 CURRENT DRIVERS IN HYDROLOGIC FORECASTING RESEARCH

The research questions that are currently at the forefront of scientific discussion related to hydrologic forecasting reflect an effort within the community to more effectively and broadly apply hydrologic models to better address today's societal needs. Wagener et al. [in review], identified the following three primary (but inter-related) drivers that encompass the impetus behind much recent and ongoing research:

- 1) The need to understand, estimate, and effectively communicate uncertainty in hydrologic predictions [e.g., *McIntyre et al.*, 2003; *Wagener and Gupta*, 2005].
- 2) The need to build hydrologic ‘models of everywhere’ – i.e., to develop the capacity to generate forecasts at any location, including interior points in a watershed (i.e., above a streamflow gauge), as well as in ungauged or poorly-gauged basins [e.g., *Sivapalan et al.*, 2003; *Beven*, 2007].
- 3) The need to predict the impacts of environmental change (such as climate and land-use change) on hydrology and water resources [e.g., *Allen and Ingram*, 2002; *Porporato et al.*, 2004; *Milly et al.*, 2005; *Poff et al.*, 2006].

The analysis of uncertainty in model predictions (Driver 1) is necessary both to recognize the current limitations of our science and to provide decision makers with better, more complete information. It also represents one way of evaluating how appropriate a model is for a particular application or situation. Computational

advancements have significantly facilitated recent progress in uncertainty analysis by making it possible to sample from high dimensional spaces and relax some very limiting assumptions that were previously necessary [McIntyre *et al.*, 2002]. Specific issues remaining include the lack of an approach in which all sources of uncertainty can be considered simultaneously (data, model structure, model states, parameter values, etc.), our limited understanding of and ways to consider model structural uncertainty, the lack of uncertainty studies for complex models and inadequate methods to clearly communicate uncertainty to decision makers.

The need for hydrologic ‘models of everywhere’ (Driver 2) stems in part from the growing recognition of the value in hydrologic predictions in all locations and on smaller spatial scales. Two major topics fall under this driver – predictions at interior points in gauged watersheds (i.e., locations upstream of the outlet point where data is available) and predictions for ungauged or poorly-gauged watersheds (i.e., where the quantity and/or quality of data is inadequate or entirely lacking). These two topics differ somewhat in their relevant approaches and issues. Both, however, are limited by the problem of identifying appropriate model parameters. Forecasts at interior locations in gauged watersheds are generated by discretizing the area into smaller model elements (e.g., sub-basins, grid elements, etc.). The result is a distributed (versus lumped) model configuration. In general to achieve reliable predictions in gauged watersheds, most models (lumped or distributed) require at least some degree of calibration to observed data. This need arises because not all model parameters can be estimated directly from measurable watershed characteristics [Wagner *et al.*, 2003]. A key question then for distributed modeling is how to best use the data at the watershed outlet to parameterize

multiple interior model elements (assuming no spatial observations such as soil-moisture are available, which is often the case). For ungauged situations, where sufficient data are not available for calibration, an alternative approach is necessary to parameterize the model [Sivapalan *et al.*, 2003]. Many studies have attempted to parameterize models of ungauged basins using relationships between the real (natural) hydrologic system structure and model parameters. However, as mentioned, most model parameters have weak relationships to measurable system characteristics and therefore model predictions for ungauged basins are often very uncertain [Wagner and Wheeler, 2006]. Thus a primary issue for modeling ungauged and poorly-gauged watersheds is the development of better approaches for extracting information about model parameters and model structure from static watershed characteristics (such as soil type, vegetation, slope, etc.).

Driver 3 (modeling environmental change) is important for understanding how changes to the system forcing (e.g., climate) or system structure (e.g., landuse) may potentially impact the overall hydrologic system response (e.g., runoff). Growing concern about water availability and improving information from climate models have recently generated an increase in the number of investigations focusing on climate change impacts for water resources. Studies vary widely in approach and study location, but collectively demonstrate a probable increase in water-stress for some parts of the world and the need for continued research on this topic [e.g., Lettenmaier *et al.*, 1999; Kiem and Franks, 2001; Nijssen *et al.*, 2001; Hay *et al.*, 2002; Arnell, 2004; Christensen *et al.*, 2004; Manabe *et al.*, 2004; Vanrheenen *et al.*, 2004; Milly *et al.*, 2005; Andersson *et al.*, 2006]. In contrast to climate change studies, landuse change impact studies have been a focus in hydrology for several decades. The topics addressed reflect the range of processes (both

natural and anthropogenic) that can affect a watershed's hydrologic response – including deforestation and reforestation [e.g., *Likens et al.*, 1977; *Swank and Crossley*, 1988; *Calder*, 1990]; forest and rangeland fires [e.g., *Parkin et al.*, 1996; *Cerda*, 1998]; urbanization [e.g., *DeWalle et al.*, 2000]; and beetle infestation and agricultural drainage [e.g., *Robinson*, 1986; *Dunn and Mackay*, 1996]. Modeling environmental change is inherently related to building ‘models of everywhere’ by the common problem of identifying appropriate parameter values. Since model parameter values reflect (in some way) the specific characteristics of a watershed or a location, structural changes (i.e., landuse) within a watershed can potentially be reflected through a change in the model parameters. If no observations of the changed system response are available, then the parameters need to be adjusted based on changes in the physical characteristics (e.g., landuse) of the system. Thus a relationship is needed (as for the ungauged case) between physical characteristics and model parameters. The success of modeling environmental change therefore also hinges on how well appropriate model parameters and model structure can be identified from static watershed characteristics.

1.3 HYDROLOGIC MODEL BEHAVIOR

A fundamental issue underlying all of the topics mentioned above is the need to understand hydrologic model behavior and changes in model behavior under varying conditions (i.e., varying watershed conditions and/or modeling approaches). A typical uncertainty analysis (Driver 1) assesses how much each source (model component or input) will affect the uncertainty in the model output [e.g., *Butts et al.*, 2004; *Clark and Vrugt*, 2006; *Ajami et al.*, 2007]. Therefore to account for all sources of uncertainty, it is

necessary to fully understand the model's structure and how it behaves under certain conditions. When moving from a lumped to a distributed configuration (i.e., for developing 'models of everywhere' – Driver 2), model behavior may vary spatially as well as across model components. Understanding the impact of spatial discretization on model behavior is essential to determine how best to use streamflow observations at the watershed outlet (i.e., to guide calibration approaches) and to determine the most appropriate spatial configuration (i.e., the degree of spatial discretization). For hydrologic modeling of ungauged watersheds (Driver 2), as well as for modeling environmental change (Driver 3), observed data are not available to evaluate and parameterize the model by usual methods. Therefore, rather than comparing the model output to observed watershed responses, the watershed model can be used to understand the real-world system behavior in ungauged locations and/or under conditions of environmental/climate change.

1.4 DISSERTATION SCOPE

The studies presented in this dissertation address multiple questions related to watershed model behavior for three different cases of hydrologic forecasting. Each case constitutes one phase of research and encompasses elements from the main drivers in hydrologic modeling research listed previously. The topics were selected also to relate to existing situations in operational hydrologic forecasting and to provide insight for the ultimate objective of increasing forecasting capabilities in less developed (and thus data sparse) regions. Phases I and II look at model behavior from an internal perspective – i.e., using observations of the natural system to understand what's going on inside of the model

structure. Phase III looks at model behavior from an external perspective – i.e., using the model response (‘external behavior’) to understand the structure of and changes in the natural system. The three phases and main questions targeted are:

Phase I: For a lumped, conceptual model in multiple gauged watersheds – How important are various model components and how appropriate is the model for representing watersheds across multiple hydroclimatic regimes? What is the impact of reducing the model's complexity (by treating some model parameters as constants) on the model's predictive performance and how does the impact change across watersheds?

Phase II: For a distributed, conceptual model in a single gauged watershed – What controls the model behavior and how does it vary spatially? What are implications of spatially-varying model behavior for the value of streamflow observations at the outlet?

Phase III: For a lumped conceptual model in ungauged and poorly-gauged watersheds – What is an appropriate approach for modeling ungauged/poorly gauged watersheds? How does the model respond to conditions of climate change and what does this tell us about future impacts on water resources in the region?

1.4.1 Phase I

Phase I represents the current situation of operational hydrologic forecasting in the United States, where a single, lumped conceptual model (SAC-SMA) is used for watersheds of many different hydroclimatic regimes. The research objective of the first step, Phase I (a), is to determine how the model represents watersheds across a range of

hydroclimatic regimes and if the model structure is appropriate (e.g., adequately or overly flexible). To investigate this question, a global sensitivity analysis is performed on the SAC-SMA to assess how the importance and behavior of model components vary across 12 watersheds of different regimes. The results indicate how strong an impact each parameter has on model predictions. Parameters found to be sensitive have a significant impact on model predictions and represent important components of the model structure. Those found to be insensitive have little impact on model predictions and represent potentially unwarranted (excessive) model complexity. The findings have implications for calibration of the SAC-SMA specifically, as well as for model identification and evaluation in general, since they allow for testing whether the actual model behavior is appropriate.

The second objective, Phase I (b), builds upon the first step and addresses whether or not the model complexity can be reduced in order to simplify model calibration, which is particularly important when the model is applied in distributed configuration or when a very large number of watersheds must be calibrated (as is the case for operational forecasting). If a particular model component is found to be unimportant (for a given watershed), then the associated parameters can theoretically be removed from the calibration process and treated as constants. Although this type of complexity reduction is commonly done in hydrologic modeling [*Cox et al.*, 2006; *Huang and Liang*, 2006], the impact on model performance and how feasible it is across different regimes has not been fully assessed. In Phase I (b), multi-objective optimizations are performed for full and partial parameter sets to determine the impact of setting the less sensitive or insensitive

model parameters to fixed a priori values. Results demonstrate the feasibility of using this approach to simplify the calibration process for hydrologic models.

1.4.2 Phase II

Phase II addresses questions related to distributed hydrologic modeling, which is the future direction of operational forecasting in the United States (and elsewhere). Throughout the hydrology community, focus is shifting from lumped to distributed model configurations due to the potential benefits that are associated with distributed modeling (i.e., forecasts at interior locations and use of spatially-distributed precipitation data) [Smith *et al.*, 2004]. The main objective of Phase II of this dissertation research is to understand the impact of a spatially-distributed configuration on overall hydrologic model behavior. Distributed models include an additional dimension of model behavior to consider (as compared to the lumped models) due to the spatial discretization of the model domain. Therefore, to fully understand the behavior of distributed models, it is necessary to investigate the relative significance of model elements for streamflow predictions at the outlet. It is also important to determine what factors are largely controlling spatial behavior (e.g., precipitation distribution, initial model states, cell location, etc.).

In Phase II, a global sensitivity analysis is performed using the Hydrology Lab Distributed Hydrologic Modeling System (HL-DHMS) of the National Weather Service (NWS). Previous work [Tang *et al.*, 2007] established methods and presented initial but inconclusive results of a global sensitivity analysis for a fully-distributed model. The results highlighted the complexity of the analysis and the fact that numerous factors can

affect model behavior in distributed models (e.g., spatially distributed forcing and initial states, and differential routing distances from cells to outlet). In a real-world system, where these factors vary simultaneously and data unavoidable contains noise, it becomes very difficult to interpret results. This study therefore uses (synthetic) virtual experiments to enable an in-depth and error free analysis. Results indicate regions across the model domain that control model behavior and the factors (e.g., precipitation distribution) that are most significant for spatial variation of model behavior.

1.4.3 Phase III

Phase III represents the situation of ungauged and poorly-gauged basins that are encountered in many (particularly less-developed) parts of the world. The primary objectives of this phase are to test an approach to model ungauged watersheds in a region where predictions are currently unavailable and apply the approach to investigate the impacts of climate change on water resources. The study focuses in the Olifants Basin (which is within Limpopo Basin) in southern Africa, where existing water stress, potentially large impacts of climate change, and transboundary cooperation issues make hydrologic forecasts a very real necessity [Levite *et al.*, 2003; FAO, 2004; Khandlhela and May, 2006]. However, most areas lack adequate data for calibration, as well as adequate resources for system sustainability, therefore data-intensive approaches to hydrologic modeling are inappropriate.

The study of Phase III uses an alternative data-modest approach in which the expected hydrologic response is constrained (rather than calibrated) using regionalized relationships between watershed characteristics (physical and climatic) and indices of

streamflow response. A parsimonious model structure is then used to obtain ensemble predictions for ungauged watersheds. The approach is tested and verified in gauged watersheds and then expanded to ungauged watersheds in a localized area of high significance for water resources in the Olifants Basin. Simulations of future runoff are produced for the ungauged watersheds based on downscaled climate change projections and the overall impacts of climate change on water resources in the region are assessed.

1.5 ORGANIZATION

The remaining chapters of this dissertation are organized by research phase (with Phase I broken into two chapters for clarity) as follows:

Chapter 2 – Phase I (a)

Chapter 3 – Phase I (b)

Chapter 4 – Phase II

Chapter 5 – Phase III

Chapter 6 presents an overall summary of the scientific contributions of this dissertation and recommendations for future work. Appendices A and B include supplementary figures and tables for Chapters 4 and 5, respectively.

1.6 CHAPTER 1 REFERENCES

- Abbott, M. B., J. C. Bathurst, J. A. Cunge, P. E. O'Connell and J. Rasmussen (1986). An Introduction to the European Hydrological System - Systeme Hydrologique Europeen, "SHE", 1. History and Philosophy of a Physically-Based, Distributed Modeling System. *J. Hydrol.*, 87(1-2), 45-59.
- Ajami, N. K., Q. Y. Duan and S. Sorooshian (2007). An integrated hydrologic Bayesian multimodel combination framework: Confronting input, parameter, and model structural uncertainty in hydrologic prediction. *Water Resour. Res.*, 43(1).

- Allen, M. R. and W. J. Ingram (2002). Constraints on future changes in climate and the hydrologic cycle. *Nature*, 419(6903), 224-232.
- Andersson, L., J. Wilk, M. C. Todd, D. A. Hughes, A. Earle, D. Kniveton, R. Layberry and H. H. G. Savenije (2006). Impact of climate change and development scenarios on flow patterns in the Okavango River. *J. Hydrol.*, 331(1-2), 43-57.
- Arnell, N. W. (2004). Climate change and global water resources: SRES emissions and socio-economic scenarios. *Global Environmental Change-Human and Policy Dimensions*, 14(1), 31-52.
- Beven, K. (2007). Towards integrated environmental models of everywhere: uncertainty, data and modelling as a learning process. *Hydrol. Earth Syst. Sci.*, 11(3), 460-467.
- Burnash, R. J. C., R. L. Ferral and R. A. McGuire (1973). A Generalized Streamflow Simulation System - Conceptual Modeling for Digital Computers, U.S. Department of Commerce, National Weather Service and State of California, Dept. of Water Resources.
- Butts, M. B., J. T. Payne, M. Kristensen and H. Madsen (2004). An evaluation of the impact of model structure on hydrological modelling uncertainty for streamflow simulation. *J. Hydrol.*, 298(1-4), 242-266.
- Calder, I. R. (1990). *Evapotranspiration in the uplands*, John Wiley, Chichester.
- Cerda, A. (1998). Changes in overland flow and infiltration after a rangeland fire in a Mediterranean scrubland. *Hydrol. Process.*, 12(7), 1031-1042.
- Christensen, N. S., A. W. Wood, N. Voisin, D. P. Lettenmaier and R. N. Palmer (2004). The effects of climate change on the hydrology and water resources of the Colorado River basin. *Climatic Change*, 62(1-3), 337-363.
- Clark, M. P. and J. A. Vrugt (2006). Unraveling uncertainties in hydrologic model calibration: Addressing the problem of compensatory parameters. *Geophysical Research Letters*, 33, L06406, doi:10.1029/2005GL025604. .
- Cox, G. M., J. M. Gibbons, A. T. A. Wood, J. Craigon, S. J. Ramsden and N. M. J. Crout (2006). Towards the systematic simplification of mechanistic models. *Ecological Modelling*, 198(1-2), 240-246.
- Crawford, N. H. and R. K. Linsley (1966). Simulation in Hydrology: Stanford Watershed Model IV, Technical Report, Vol. 39. 39, Department of Civil Engineering, Stanford University, Palo Alto, CA.
- DeWalle, D. R., B. R. Swistock, T. E. Johnson and K. J. McGuire (2000). Potential effects of climate change and urbanization on mean annual streamflow in the United States. *Water Resour. Res.*, 36(9), 2655-2664.
- Dooge, J. C. I. (1957). The rational method for estimating flood peaks. *Engineering*, 184, 311-313.
- Dooge, J. C. I. (1959). A general theory of the unit hydrograph. *J. Geophys. Res.*, 64, 241-256.
- Dunn, S. M. and R. Mackay (1996). Modelling the hydrological impacts of open ditch drainage. *J. Hydrol.*, 179(1-4), 37-66.
- FAO (2004). Drought impact mitigation and prevention in the Limpopo River Basin. A situation analysis., Food and Agriculture Organization of the United Nations - Subregional Office for Southern and East Africa, Harare.

- Hay, L. E., M. P. Clark, R. L. Wilby, W. J. Gutowski, G. H. Leavesley, Z. Pan, R. W. Arritt and E. S. Takle (2002). Use of regional climate model output for hydrologic simulations. *J. Hydrometeorol.*, 3(5), 571-590.
- Huang, M. Y. and X. Liang (2006). On the assessment of the impact of reducing parameters and identification of parameter uncertainties for a hydrologic model with applications to ungauged basins. *J. Hydrol.*, 320(1-2), 37-61.
- Khandlhela, M. and J. May (2006). Poverty, vulnerability and the impact of flooding in the Limpopo Province, South Africa. *Natural Hazards*, 39(2), 275-287.
- Kiem, A. S. and S. W. Franks (2001). On the identification of ENSO-induced rainfall and runoff variability: a comparison of methods and indices. *Hydrological Sciences Journal-Journal Des Sciences Hydrologiques*, 46(5), 715-727.
- Kundzewicz, Z. W., L. J. Mata, N. W. Arnell, P. Doll, B. Jimenez, K. Miller, T. Oki, Z. Sen and I. Shiklomanov (2008). The implications of projected climate change for freshwater resources and their management. *Hydrological Sciences Journal-Journal Des Sciences Hydrologiques*, 53(1), 3-10.
- Lettenmaier, D. P., A. W. Wood, R. N. Palmer, E. F. Wood and E. Z. Stakhiv (1999). Water resources implications of global warming: A US regional perspective. *Climatic Change*, 43(3), 537-579.
- Levite, H., H. Sally and J. Cour (2003). Testing water demand management scenarios in a water-stressed basin in South Africa: application of the WEAP model. *Physics and Chemistry of the Earth*, 28(20-27), 779-786.
- Likens, G. E., F. H. Bormann, R. S. Pierce, J. S. Eaton and N. M. Johnson (1977). *Biogeochemistry of a forested ecosystem*, Springer-Verlag, New York.
- Manabe, S., P. C. D. Milly and R. Wetherald (2004). Simulated long-term changes in river discharge and soil moisture due to global warming. *Hydrological Sciences Journal-Journal Des Sciences Hydrologiques*, 49(4), 625-642.
- McIntyre, N., H. S. Wheater and M. J. Lees (2002). Estimation and propagation of parametric uncertainty in environmental models. *Journal of Hydroinformatics*, 4, 177-198.
- McIntyre, N., T. Wagener, H. S. Wheater and Z. Siyu (2003). Uncertainty and risk in water quality modelling and management. *Journal of Hydroinformatics*, 5(4), 259-274.
- Milly, P. C. D., K. A. Dunne and A. V. Vecchia (2005). Global pattern of trends in streamflow and water availability in a changing climate. *Nature*, 438(7066), 347-350.
- Milly, P. C. D., R. T. Wetherald, K. A. Dunne and T. L. Delworth (2002). Increasing risk of great floods in a changing climate. *Nature*, 415(6871), 514-517.
- Nijssen, B., G. M. O'Donnell, A. F. Hamlet and D. P. Lettenmaier (2001). Hydrologic sensitivity of global rivers to climate change. *Climatic Change*, 50(1-2), 143-175.
- Parkin, G., G. O'Donnell, J. Ewen, J. C. Bathurst, P. E. O'Connell and J. Lavabre (1996). Validation of catchment models for predicting land-use and climate change impacts .2. Case study for a Mediterranean catchment. *J. Hydrol.*, 175(1-4), 595-613.
- Poff, N. L., B. P. Bledsoe and C. O. Cuhaciyan (2006). Hydrologic variation with land use across the contiguous United States: Geomorphic and ecological consequences for stream ecosystems. *Geomorphology*, 79(3-4), 264-285.

- Porporato, A., E. Daly and I. Rodriguez-Iturbe (2004). Soil water balance and ecosystem response to climate change. *American Naturalist*, 164(5), 625-632.
- Robinson, M. (1986). Changes in Catchment Runoff Following Drainage and Afforestation. *J. Hydrol.*, 86(1-2), 71-84.
- Singh, V. P. and D. A. Woolhiser (2002). Mathematical modeling of watershed hydrology. *Journal of Hydrologic Engineering*, 7(4), 270-292.
- Singh, V. P. and D. K. Frevert (Editors) (2006). *Watershed Models*. CRC Press, Boca Raton, FL.
- Sivapalan, M., K. Takeuchi, S. W. Franks, V. K. Gupta, H. Karambiri, V. Lakshmi, X. Liang, J. J. McDonnell, E. M. Mendiondo, P. E. O'Connell, T. Oki, J. W. Pomeroy, D. Schertzer, S. Uhlenbrook and E. Zehe (2003). IAHS decade on Predictions in Ungauged Basins (PUB), 2003-2012: Shaping an exciting future for the hydrological sciences. *Hydrological Sciences Journal-Journal Des Sciences Hydrologiques*, 48(6), 857-880.
- Smith, M. B., K. P. Georgakakos and X. Liang (2004). The distributed model intercomparison project (DMIP). *J. Hydrol.*, 298(1-4), 1-3.
- Swank, W. T. and D. A. Crossley (Editors) (1988). *Forest hydrology and ecology at Coweeta. Ecological Studies* 66, 66. Springer-Verlag, New York.
- Tang, Y., P. M. Reed, K. van Werkhoven and T. Wagener (2007). Advancing the identification and evaluation of distributed rainfall-runoff models using Sobol's global sensitivity analysis. *Water Resour. Res.*, 43, W06415, doi:10.1029/2006WR005813.
- Vanrheenen, N. T., A. W. Wood, R. N. Palmer and D. P. Lettenmaier (2004). Potential implications of PCM climate change scenarios for Sacramento-San Joaquin River Basin hydrology and water resources. *Climatic Change*, 62(1-3), 257-281.
- Wagener, T. and H. V. Gupta (2005). Model identification for hydrological forecasting under uncertainty. *Stochastic Environmental Research and Risk Assessment*, 19(6), 378-387.
- Wagener, T. and H. S. Wheater (2006). Parameter estimation and regionalization for continuous rainfall-runoff models including uncertainty. *J. Hydrol.*, 320(1-2), 132-154.
- Wagener, T., N. McIntyre, M. J. Lees, H. S. Wheater and H. V. Gupta (2003). Towards reduced uncertainty in conceptual rainfall-runoff modelling: Dynamic identifiability analysis. *Hydrol. Process.*, 17(2), 455-476.
- Wagener, T., P. Reed, K. van Werkhoven, Y. Tang and Z. Zhang (in review). Advances in the identification and evaluation of complex environmental systems models. *Journal of Hydroinformatics*.

CHAPTER 2

Phase I (a): Characterization of Watershed Model Behavior across a Hydroclimatic Gradient

Based on:

van Werkhoven, K., T. Wagener, P. Reed, and Y. Tang. (2008) Characterization of model behavior across a hydroclimatic gradient. *Water Resources Research*, 44, W01429, doi:10.1029/2007WR006271.

2.1 INTRODUCTION

Watershed-scale hydrologic models are essential for flood and drought prediction, water resources planning and allocation, erosion and sedimentation studies, nonpoint source pollution and remediation, climate and land use change assessments, hydropower operations, etc. [Singh and Frevert, 2006]. The extensive array of models that have been developed to date include both simple [e.g., Jakeman *et al.*, 1990] and highly complex structures [e.g., Abbott *et al.*, 1986; Reggiani *et al.*, 2000]. For some applications, such as operational forecasting, a single model structure may be used to represent a wide range of watersheds with varying physical and hydroclimatic characteristics. Such cases may require a model with sufficient flexibility (and therefore complexity) to represent the different watersheds. However, as a consequence of increasing model flexibility (and/or complexity) there is an associated increase in the number of model parameters that must be estimated. The potential for equifinality and over-parameterization thus also increases for complex models, resulting in parameter values that are not always easily identifiable in the calibration process [Beven, 1989]. Studies have shown [e.g., Jakeman and Hornberger, 1993; Wagener *et al.*, 2003; Wagener and Wheater, 2006] that as model complexity increases, the number of unidentifiable parameters also increases, preventing (for those unidentifiable parameters) the possibility of locating one parameter value that is any better than another in the calibration process.

Sensitivity analysis has become a popular tool in watershed modeling to explore high-dimensional parameter spaces, assess parameter identifiability, and understand sources of uncertainty. [Hornberger and Spear, 1981; Freer *et al.*, 1996; Saltelli *et al.*, 1999; Wagener *et al.*, 2001, 2003; Wagener, 2003; Hall *et al.*, 2005; Muleta and Nicklow,

2005; *Sieber and Uhlenbrook, 2005; Bastidas et al., 2006; Pappenberger et al., 2006, 2008; van Griensven et al., 2006; Demaria et al., 2007; Tang et al., 2007b; Tang et al., 2007c*]. In this context, sensitivity analysis is commonly used to determine which parameters have a significant impact on the model response and should be the focus of estimation efforts, and conversely, which have an insignificant impact (e.g., due to over-parameterization) and could be fixed to some a priori or regional estimates. In several previous studies, model output sensitivity to parameter values (herein referred to as "parameter sensitivity") has been shown to vary significantly across watersheds, time periods and time scales, and evaluation metrics [*Wagner et al., 2001; Sieber and Uhlenbrook, 2005; Demaria et al., 2007; Tang et al., 2007c; Tang et al., 2007b*]. However, no studies have characterized this variation for a single model across a well-defined hydroclimatic gradient using multiple metrics and time periods/scales. Therefore, an understanding of model behavior – and its dependency on hydroclimatic regime – remains limited.

For the case in which a model is used to simulate watersheds with widely varying characteristics, an assessment of why and how parameter sensitivities vary across watersheds for a suite of flow condition metrics can help to determine if the model structure is fully exploited and/or if it is over-parameterized in all cases. Some studies have suggested that relatively few (e.g., 3 to 5) parameters are identifiable from observations of streamflow for hydrologic models [*Jakeman and Hornberger, 1993*]. However, the existence of significant sensitivity variation across watersheds, time periods/scales, and evaluation metrics would suggest that the number of identifiable parameters found in their study is more a function of the experimental design and cannot

be generalized. A comprehensive analysis of varying model behavior would test this hypothesis as well as provide valuable understanding and guidance for calibration. Such information is particularly useful for watershed models that are used extensively in operational environments. These models often require calibration across a wide range of watersheds and are used in multiple applications. As an example, the Sacramento Soil Moisture Accounting Model (SAC-SMA) is the primary model used by the National Weather Service (NWS) River Forecast Centers (RFC) throughout the US. Several studies have presented automatic or semi-automatic methods that could facilitate calibrating this model for the hundreds of watersheds across the US, as is required for a country-wide forecasting system [Brazil, 1988; Sorooshian *et al.*, 1993; Duan *et al.*, 1994; Boyle *et al.*, 2000, 2001; Vrugt *et al.*, 2003a; Hogue *et al.*, 2006; Tang *et al.*, 2006; Vrugt *et al.*, 2006]. Other studies have focused on the development and assessment of a priori parameter estimates for the SAC-SMA [Koren, 2000; Duan *et al.*, 2001; Koren *et al.*, 2003; Anderson *et al.*, 2006; Gan and Burges, 2006]. However, to date, few sensitivity analyses of the SAC-SMA exist in the literature despite its common use in operations and hydrologic research. Furthermore, our previous work [Tang *et al.*, 2007b; Tang *et al.*, 2007c] has suggested that some common assumptions about parametric sensitivities of the SAC-SMA model structure are not valid. These findings have implications for methodologies based on a priori assumptions about parameter sensitivity, such as "step-wise" or "stepped" calibration approaches [e.g., Hogue *et al.*, 2000, 2006; Fenicia *et al.*, 2007] and warrant further investigation. Finally, as efforts continue to reformulate this model into a distributed configuration [Koren *et al.*, 2004], a complete understanding of its parameter sensitivities becomes increasingly vital.

The main objective of this study is to use Sobol's variance-based global sensitivity analysis to build a comprehensive picture of parametric sensitivity for the SAC-SMA and understand its variation across hydroclimatic regimes, flow types, time periods, and time scales. Further objectives are to determine how the variation informs us about model behavior and to what extent the variation is related to the hydroclimatic characteristics of the watersheds and/or simulated time periods. The analysis is intended to demonstrate [1] if moderate model complexity is warranted (or proven excessive) when modeling a range of watersheds, [2] comprehensive trends in SAC-SMA model behavior for calibration guidance, and [3] the validity of typical parameter sensitivity and identifiability assumptions.

2.2 MOPEX BASINS AND DATA

The hydro-meteorological datasets used in this study were developed as part of the Model Parameter Estimation Experiment (MOPEX) and include data for twelve watersheds in the US that span different hydroclimatic regimes and geographic locations [*Duan et al.*, 2006]. Previous studies [*Duan et al.*, 2006; *Gan and Burges*, 2006] summarized the performance of the SAC-SMA in these watersheds.

From the MOPEX dataset, daily precipitation and daily streamflow for 39 years (1960-1998) of data were used, along with mean monthly estimates of potential evaporation and vegetation adjustments. The relative locations of the 12 watersheds are shown in Figure 2.1 and their characteristics are listed in Table 2.1. In this table and in subsequent figures, the watersheds are ordered from dry to wet based on the wetness index, which is defined as the ratio of mean annual precipitation (P) to mean annual

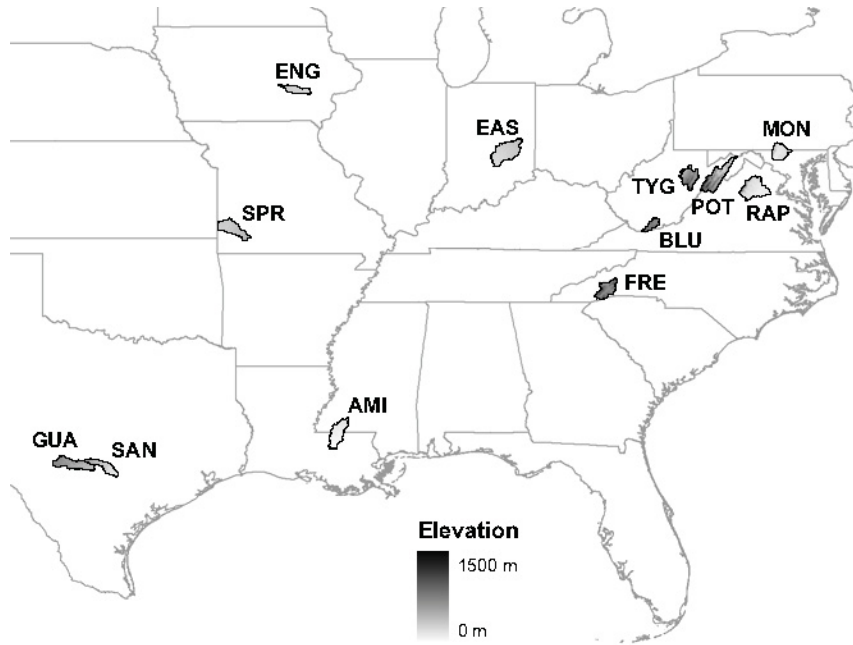


Figure 2.1 Location and elevation of 12 MOPEX watersheds

potential evaporation (PE). Throughout this paper, the watersheds will be identified using the three-letter IDs listed in Table 2.1.

As illustrated in Figure 2.1, the watersheds' drainage areas range from the smallest (BLU) case encompassing 1021 km² to the largest (EAS) watershed draining 4421 km². They are located in the general Southeastern region of the US and include a variety of topographic and land cover characteristics. The wide ranges of mean annual P (765-1564 mm/a), mean annual runoff coefficient (ROC) (0.15–0.63), and mean annual PE (711-1528 mm/a) exemplify the diverse hydroclimatic regimes represented in the dataset. A further summary of watershed characteristics is presented in Figures 2.2a-e. Additional physical characteristics of these watersheds are presented by *Duan et al.* [2006] and *Gan and Burges* [2006].

Table 2.1 MOPEX Watershed Characteristics

ID	River	Outlet Location	Area (km ²)	Mean Annual Precip. (mm)	Mean Annual ROC (Q/P)	Mean Annual PE (mm)
GUA	Guadalupe	Spring Branch, TX	3406	765	0.15	1528
SAN	San Marcos	Luling, TX	2170	827	0.22	1449
ENG	English	Kalona, IA	1484	893	0.30	994
SPR	Spring	Waco, MO	3015	1076	0.28	1094
RAP	Rappahannock	Fredericksburg, VA	4134	1030	0.37	920
MON	Monocacy	Frederick, MD	2116	1041	0.40	896
EAS	East Fork White	Columbus, IN	4421	1015	0.37	855
POT	S. Branch Potomac	Springfield, WV	3810	1042	0.33	761
BLU	Bluestone	Pipestem, WV	1021	1018	0.41	741
AMI	Amite	Denham Springs, LA	3315	1564	0.39	1073
TYG	Tygart Valley	Phillipi, WV	2372	1166	0.63	711
FRE	French Broad	Ashville, NC	2448	1383	0.58	819

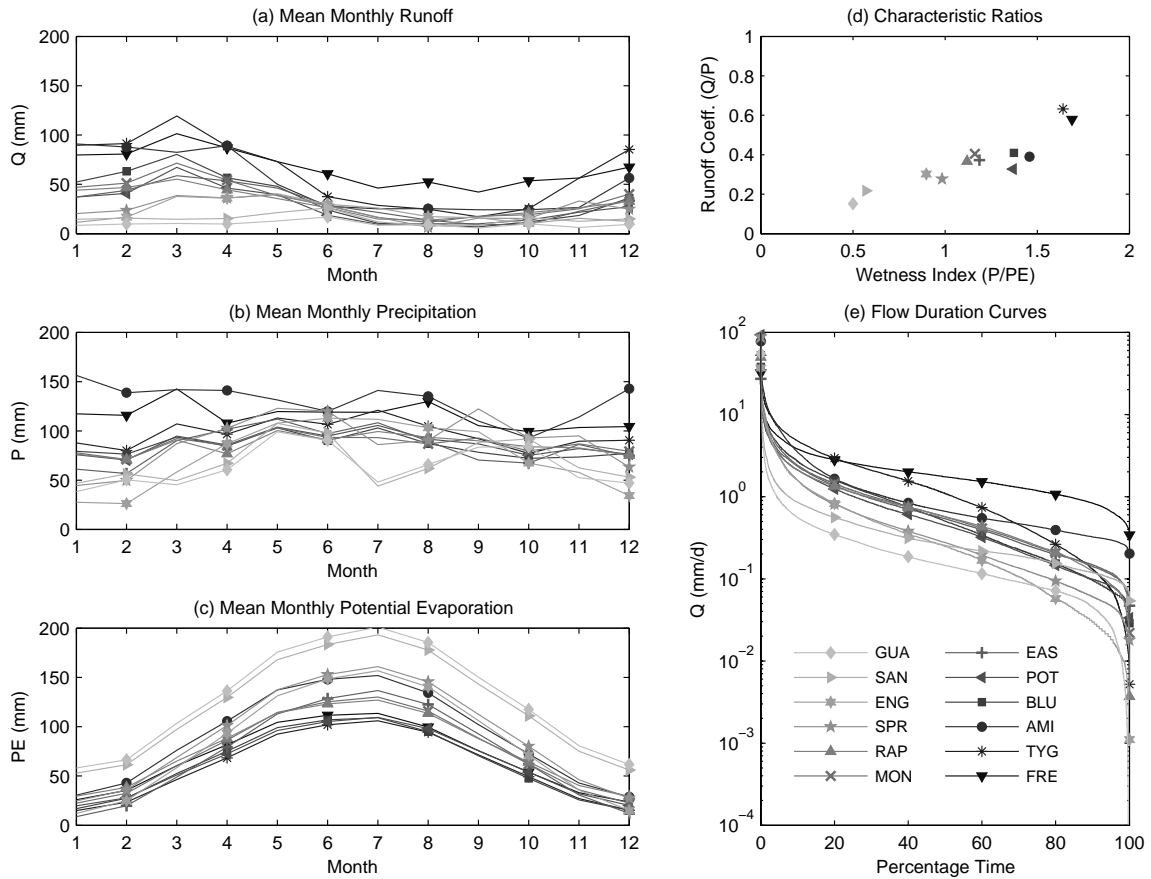


Figure 2.2 MOPEX watershed characteristics: (a) mean monthly runoff volume in mm (b) mean monthly precipitation (c) mean monthly potential evaporation (d) hydrologic ratios (e) flow duration curves.

2.3 METHODS

2.3.1 Sacramento Soil Moisture Accounting Model (SAC-SMA)

The SAC-SMA is a conceptual rainfall-runoff model that represents the soil column by an upper and lower zone of multiple storages [Burnash, 1995]. It has been used extensively in both research and operational applications where it is the primary rainfall-runoff model used for river forecasting by the National Weather Service (NWS) River Forecast Centers (RFCs) across the United States. Figure 2.3 shows the structure of the SAC-SMA and the main function of its 16 model parameters (shown in bold). Beyond these main functions, several parameters have secondary functions as part of the percolation component, which connects upper and lower zones. The representation of the percolation process is somewhat different in the SAC-SMA than in some other commonly-used watershed models (e.g., PRMS, VIC, TOPMODEL) as discussed by Clark *et al.* [in press]. In the SAC-SMA, percolation is a function of both the upper zone moisture availability and the lower zone moisture deficit (versus only moisture availability as in many other models). Therefore parameters that control the moisture content of both the upper and lower zones also impact the amount of percolation.

Table 2.2 Description of SAC-SMA parameters and allowable ranges analyzed in this study

Parameter	Units	Description	Range
UZW	mm	Upper zone tension water maximum storage	25 – 125
UZFWM	mm	Upper zone free water maximum storage	10 – 75
UZK	day ⁻¹	Upper zone free water withdrawal rate	0.2 – 0.5
PCTIM	% / 100	Percent permanent impervious area	0.0 – 0.05
ADIMP	% / 100	Percent area contributing as impervious when saturated	0.0 – 0.2
RIVA	% / 100	Percent area affected by riparian vegetation	0.0 – 0.2
ZPERC	none	Maximum percolation rate under dry conditions	20 – 300
REXP	none	Percolation equation exponent	1.4 – 3.5
PFREE	% / 100	% of percolation going directly to lower zone free water	0 – 0.5
LZW	mm	Lower zone tension water maximum storage	75 – 300
LZFPM	mm	Lower zone free water primary maximum storage	40 – 600
LZFSM	mm	Lower zone free water supplementary maximum storage	15 – 300
LZPK	day ⁻¹	Lower zone primary withdrawal rate	0.001 – 0.015
LZSK	day ⁻¹	Lower zone supplementary withdrawal rate	0.03 – 0.2

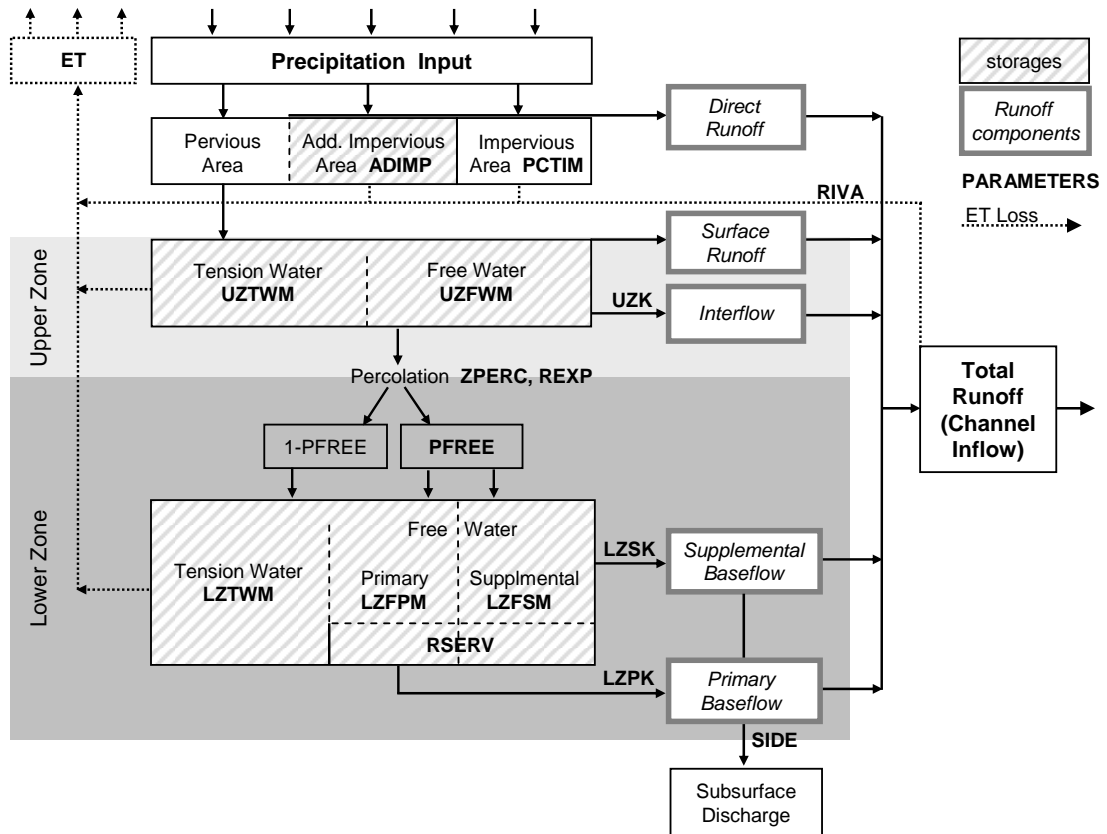


Figure 2.3 Conceptualization of the SAC-SMA.

In the parameter estimation process, two of the 16 SAC-SMA model parameters are typically set to standard values (SIDE and RSERV) for all watersheds. The remaining 14 parameters must be estimated by some means (calibration or otherwise) for each watershed. These 14 parameters were the focus of this study and are described in Table 2.2 along with the allowable ranges used in the sensitivity analyses [Anderson, 2002]. Our objective was to investigate the parameter sensitivities within the ranges defined as reasonable by the NWS for standard SAC-SMA model calibration over the variety of watershed types found in the US.

2.3.2 Sobol' sensitivity analysis

Sobol's sensitivity analysis method [Sobol', 1993], is a variance-based approach in which the model output variance is decomposed into relative contributions from individual parameters and parameter interactions. This method was selected based on previous work that demonstrated it to be more robust than other sensitivity analysis methods for the evaluation of hydrologic models [Tang *et al.*, 2007b]. In addition, Sobol's method explicitly includes the effects of parameter interactions and quantifies sensitivity with easily-compared indices, a necessity for our analysis. The method's primary drawback is its relatively large computational requirements.

In Sobol's method, sensitivity to each parameter or parameter interaction is assessed based on its percent contribution to the total output variance. The variance in model output is typically measured as the variance in a model evaluation metric such as the root-mean square error (RMSE). Throughout this section, references to the variance in model output should be interpreted as the variance in an evaluation metric. The four metrics used in this study will be described in Section 2.3.3. Sobol's variance decomposition can be represented as:

$$D(f) = \sum_i D_i + \sum_{i < j} D_{ij} + \sum_{i < j < k} D_{ijk} + D_{12\dots p} \quad (2.1)$$

where f is the distribution of model output, $D(f)$ is the total output variance; D_i is the output variance due to the i th component of the input parameter vector Θ ; D_{ij} is the output variance due to the interaction of parameter θ_i and θ_j ; D_{ijk} represents third-order interactions; $D_{12\dots p}$ represents all interactions greater than third-order; and p defines the total number of parameters. In this study, we were primarily interested in each parameter's total contribution to output variance, as well as how much of that

contribution was due to individual effects versus interactions with other parameters (i.e., the difference between the total and individual effects). The first-order and total Sobol sensitivity indices were calculated to measure these contributions and are defined as:

$$\text{first-order index: } S_i = \frac{D_i}{D} \quad (2.2)$$

$$\text{total index: } S_{Ti} = 1 - \frac{D_{\sim i}}{D} \quad (2.3)$$

where the first order index, S_i , measures the model sensitivity to the individual effect of parameter θ_i , and the total index, S_{Ti} , measures the sensitivity due to the combined effect of parameter θ_i plus its interactions with all other parameters in the analysis. In Eq. (2.3), the term $D_{\sim i}$ refers to the variance resulting from all of the parameters *except* θ_i . In other words, if parameter θ_i were removed from the analysis, the resulting reduction in output variance is equivalent to the total impact of parameter θ_i . Since the indices are ratios of a portion to the total output variance, their values range from 0 to 1 and can be directly compared. If a particular parameter has a small first order index, but a large total sensitivity index, then that parameter impacts the model primarily through parameter interactions.

The variance terms (i.e., D terms) in Eq. (2.1-2.3) can be approximated by numerical integration in a Monte Carlo framework. Distributions of model parameters are sampled and evaluated to generate distributions of model output. The total output variance, D , is simply the statistical variance of the output distribution, as follows:

$$\hat{f}_o = \frac{1}{n} \sum_{s=1}^n f(\Theta_s) \quad (2.4)$$

$$\hat{D} = \frac{1}{n} \sum_{s=1}^n f^2(\Theta_s) - \hat{f}_o^2 \quad (2.5)$$

where f is the model output, f_o is the mean model output, n is the sample size, Θ_s is the sampled parameter vector. Calculation of the variance contributions is somewhat more complicated. An important aspect of Sobol's method is the use of two different samples, generated by the same scheme and with the same number of elements. The model is evaluated using the first sample to calculate the overall output mean and variance (i.e., the combined effects of all parameters). The second sample is then used to resample each parameter, rather than setting each to a fixed value, for the calculation of total and individual variance contributions. For the latter calculations, parameter vectors are constructed systematically, with values selected from the two samples in specific combinations defined by which parameter's contribution is being calculated. The resulting distributions of the parameter vectors are evaluated to obtain the corresponding distributions of model output that are used in the approximations for D_i and $D_{\sim i}$. The expressions for D_i and $D_{\sim i}$ as defined by *Sobol'* [1993, 2001], *Hall et al.* [2005], and *Saltelli* [2002] are:

$$\hat{D}_i = \frac{1}{n} \sum_{s=1}^n f(\Theta_s^{(a)}) f(\Theta_{(-i)s}^{(b)}, \Theta_{is}^{(a)}) - \hat{f}_o^2 \quad (2.6)$$

$$\hat{D}_{\sim i} = \frac{1}{n} \sum_{s=1}^n f(\Theta_s^{(a)}) f(\Theta_{(-i)s}^{(a)}, \Theta_{is}^{(b)}) - \hat{f}_o^2 \quad (2.7)$$

where (a) and (b) are two different samples (both of size n). The Θ symbols, defined in Table 2.3, indicate from which samples the parameters values are taken. In this study Sobol's quasi-random sequence was used to sample points more uniformly in the parameter space than uncorrelated random sampling. Details of this sampling scheme can be found in the work of *Sobol'* [1967, 1993], *Brantley and Fox* [1988]; and *William et al.*, [1999].

Table 2.3 Definition of the Θ symbols in Eqs. (2.4)–(2.7) of Sobol's method

Symbol	Definition
Θ_s	Sampled parameter vector
$\Theta_{is}^{(a)}$	Parameter θ_i taken from sample (a)
$\Theta_{is}^{(b)}$	Parameter θ_i taken from sample (b)
$\Theta_{(-i)s}^{(a)}$	All parameters except θ_i taken from sample (a)
$\Theta_{(-i)s}^{(b)}$	All parameters except θ_i taken from sample (b)

2.3.3 Metrics for Model Evaluation

Applications of watershed models are inherently multi-objective [Gupta *et al.*, 1998; Madsen, 2000; Buras, 2001; Vrugt *et al.*, 2003b; Bekele and Nicklow, 2005; Tang *et al.*, 2007a]. In this study, we used four different model evaluation metrics to assess parameter sensitivity, two of which are common statistical metrics and two that are aggregate measures of overall hydrologic response. Each metric replaces the function f in the equations for Sobol's method defined above. Figure 2.4 illustrates that the metrics capture four important components of the hydrograph, including high flows, low flows, variability in mid-range flows (streamflow regime), and the long-term water balance. The high flow metric is the commonly-used Root Mean Squared Error (RMSE), defined as:

$$RMSE = \sqrt{\frac{1}{m} \sum_{t=1}^m (Q_{s,t} - Q_{o,t})^2} \quad (2.8)$$

where m is the number of timesteps, $Q_{s,t}$ is the simulated flow for timestep t , and $Q_{o,t}$ is the observed flow in timestep t . For the low flow metric, the simulated and observed flow time series are first transformed by a Box-Cox transformation (Eq. 2.9) with a λ value of 0.3, which has a similar effect as a log transformation. The RMSE of the transformed flows is then calculated to obtain a metric that emphasizes low flow, referred to here as the Transformed Root Mean Squared Error (TRMSE) (Eq. 2.10).

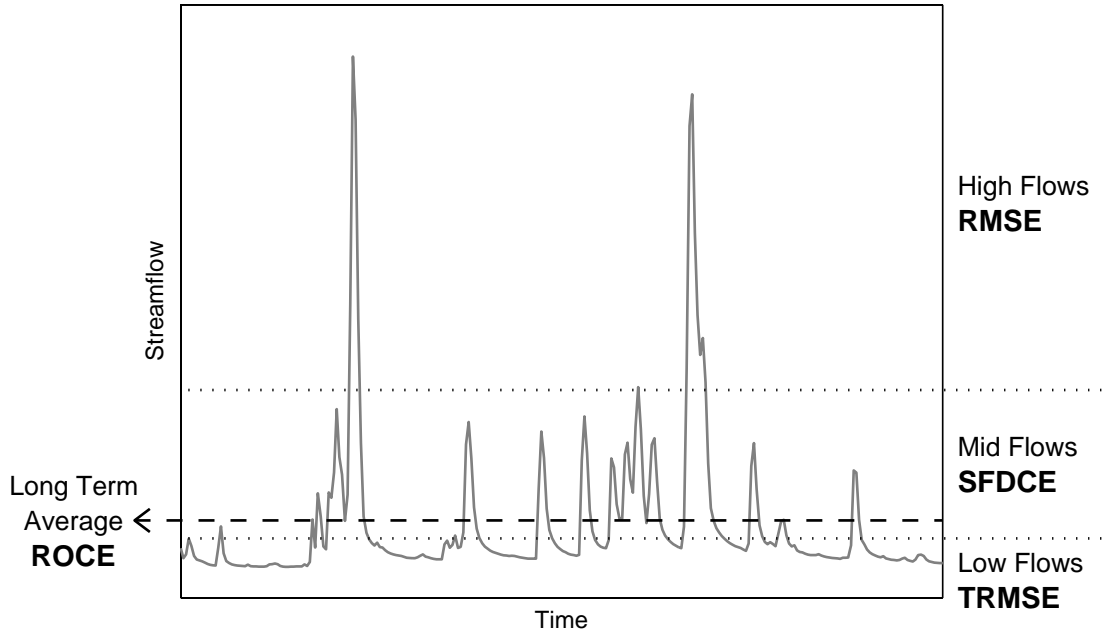


Figure 2.4 Hydrograph components captured by the four selected evaluation metrics.

$$Z = \frac{(1+Q)^\lambda - 1}{\lambda} \quad (2.9)$$

$$TRMSE = \sqrt{\frac{1}{m} \sum_{t=1}^m (Z_{s,t} - Z_{o,t})^2} \quad (2.10)$$

where m is again the number of timesteps, $Z_{s,t}$ is the transformed simulated flow for timestep t , and $Z_{o,t}$ is the transformed observed flow in timestep t . The next metric, referred to as Slope of the Flow Duration Curve Error (SFDCE), measures how well the model captures the distribution of mid-level flows. The slope of a watershed's flow duration curve indicates the variability, or flashiness, of its flow magnitudes. The SFDCE metric is thus simply the absolute error in the slope of the flow duration curve between the 30 and 70 percentile flows as follows:

$$SFDCE = abs\left(\frac{Q_{s,70} - Q_{s,30}}{40} - \frac{Q_{o,70} - Q_{o,30}}{40}\right) \quad (2.11)$$

where $Q_{s,30}$ and $Q_{s,70}$ are the 30 and 70 percentile flows of simulated flow duration curve and $Q_{o,30}$ and $Q_{o,70}$ are the 30 and 70 percentile flows of observed flow duration curve. Since this metric first combines the flows into one value (in this case slope) before calculating the error, it is an aggregate measure of overall model response and less biased by individual events. Similarly, the final metric, the Runoff Coefficient Error (ROCE) captures the overall accuracy of the water balance by first combining the flows into one characteristic hydrologic descriptor, the mean annual runoff coefficient. The absolute error in the runoff coefficient is then calculated and thus the ROCE is defined as

$$ROCE = abs\left(\frac{\bar{Q}_s}{\bar{P}} - \frac{\bar{Q}_o}{\bar{P}}\right) \quad (2.12)$$

where \bar{Q}_s and \bar{Q}_o and are the simulated and observed mean annual runoff volume, and \bar{P} is the mean annual precipitation.

2.3.4 Spearman Rank Correlation

The Spearman rank correlation coefficient was used in this study to assess the relationships between parameter sensitivities and hydroclimatic characteristics. It provided a means to quantify the strength of a monotonic relationship between two variables, with no assumptions of frequency distribution or linearity [Lehmann and D'Abbrera, 1998]. Since some of the relationships were highly nonlinear in this study (as will be shown in Section 2.2.5), the Spearman rank coefficient was preferable to a traditional linear correlation coefficient. To calculate it, values of each of the variables (in this case watershed characteristics and sensitivity indices) are ranked and the correlation is calculated based on the difference in rankings as follows:

$$R = 1 - \frac{6 \sum d^2}{v(v^2 - 1)} \quad (2.13)$$

where d is the difference in rank between the variables for a given value and v is the number of values.

2.4 APPROACH

The methods described above were used to perform a comprehensive sensitivity analysis of the SAC-SMA for 12 watersheds using 4 model evaluation metrics for both a long-term 39 year period as well as yearly periods. A Monte Carlo sampling scheme [*Saltelli, 2002; Tang et al., 2007b*] was used with 8096 samples and a warm-up period of 1 year (i.e., the first year was not included in the sensitivity calculations to allow the model states to warm-up and remove any impact of uncertain initial conditions). The method was repeated for the 4 evaluation metrics described in Section 2.3.3, resulting in 48 separate sets of sensitivity results (a "set" refers to a group of 14 individual and 14 total indices that result for the 14 model parameters in each run). The total-order Sobol indices were compared across watersheds and across the objectives to identify any visible patterns of variation in sensitivity. To quantify the variation, relationships between parameter sensitivity and several hydroclimatic characteristics were developed as scatter plots and correlation was calculated by the Spearman rank correlation method. Results of the long-term sensitivity and correlation analysis are presented in Section 2.5.1.

Beyond the long-term analysis, an interannual analysis was performed to investigate the year-to-year variation in sensitivity within each watershed. Sobol's method was applied using the same sampling scheme described above. For each sample, model simulations were again generated for a 39-year period, however, evaluation metrics and

Sobol's indices were calculated separately for each individual calendar year. Therefore, the results of each year are based on the same parameter samples and can be directly compared. As in the long-term analysis, the first year was used as a warm-up period and not included (leaving 38 separate years for analysis). Annual sensitivity indices were generated using this method for the 12 watersheds, 38 individual years, and 4 evaluation metrics. The results were plotted to identify patterns of temporal variation within watersheds, as well as to identify trends across watersheds that were masked in the long-term analysis. Relationships between interannual hydroclimatic characteristics and the interannual sensitivity indices were plotted and quantified by Spearman rank correlation. Results of the interannual sensitivity and correlation analysis are presented in Section 2.5.2. As a final step, the results from both the long-term and interannual sensitivity analyses are synthesized to provide some general overall guidance for SAC-SMA model identification in Section 2.5.3.

2.5 RESULTS AND DISCUSSION

2.5.1 Long-Term Sensitivities

In the following sections, the results are organized by the different aspects of the flow that have been assessed through the four evaluation metrics. In each section, dominant patterns of sensitivity are highlighted first, followed by discernible trends across the watersheds. Grids of long-term Sobol sensitivity indices across the 12 watersheds and 14 model parameters are presented in Figure 2.5a-d. Note that in each grid, watersheds (x-axis) are ordered from dry to wet (left to right) based on the wetness index as in previous figures and tables. The model parameters (y-axis) are generally structured with upper

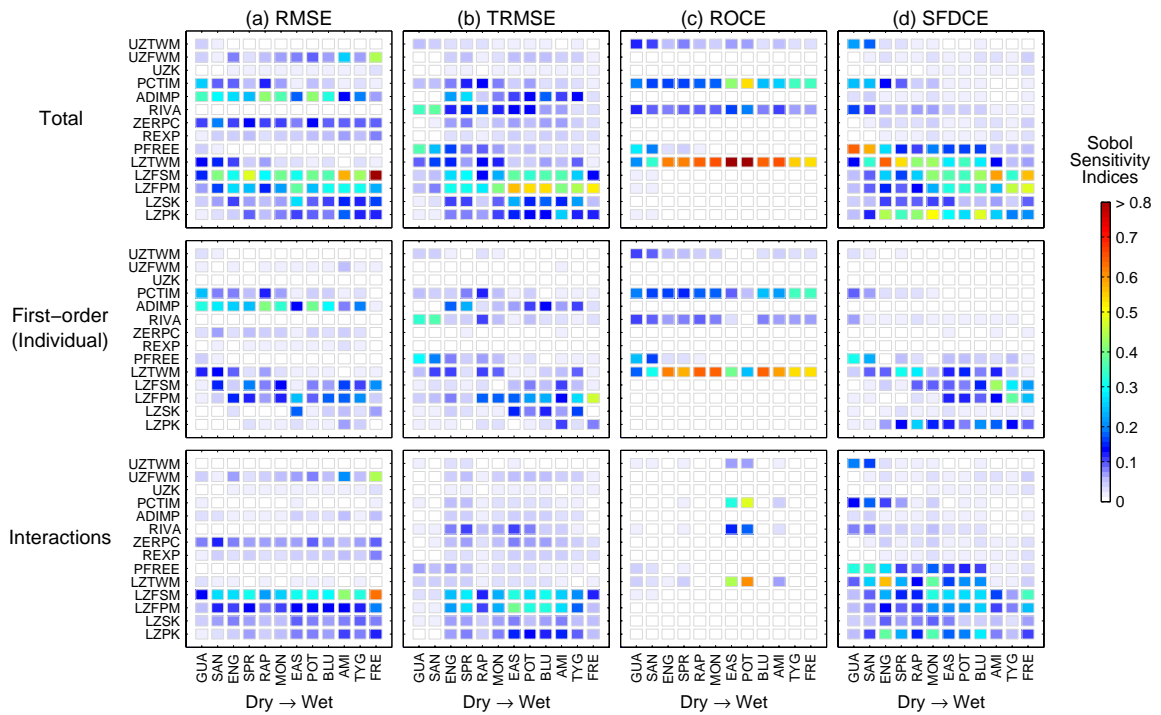


Figure 2.5 Long-term Sobol sensitivity indices for 12 watersheds and 14 parameters based on a 38-year period: Total (individual + interactions) sensitivities, first-order (individual contributions) and interaction contributions for (a) RMSE, (b) TRMSE, (c) ROCE, and (d) SFDCE.

zone parameters at the top, percolation parameters in the middle, and lower zone parameters at the bottom. Total indices (individual + interactions), first-order indices (individual) and indices representing all parameter interactions (total index – first order index) are displayed separately to demonstrate the varying impact of parameter interactions.

2.5.1.1 High Flows - RMSE

Some dominant patterns are observable in the total indices for the high flow metric (RMSE) (top grid of Figure 2.5a), where the amount of variable contributing area (ADIMP), the percolation multiplier (ZPERC), and the sizes of the lower zone free storages (LZFFM, LZFSM) are consistently sensitive across the watersheds. The

sensitivity of variable contributing area (ADIMP) reflects that parameter's impact on high peaks (mainly at the high end of its allowable range). The strong sensitivity to lower zone parameters for this metric, however, is initially surprising and counter to typical a priori assumptions that mainly upper zone parameters dominate high flow simulations. However, in the SAC-SMA, the lower zone free water storages and recession rates are directly involved in the calculation of percolation. Since percolation controls the partitioning of water between the upper and lower zones, it also impacts how much of a given event is generated by faster, higher-peaking runoff components from the upper zone (i.e., interflow, surface runoff or direct runoff) versus slower, lower-peaking components from the lower zone (baseflow). In this capacity, parameters that control percolation (including ZPERC and lower zone storages and recessions) impact high-flow simulations as reflected by the sensitivity indices. The importance of interactions among these parameters is illustrated in Figure 2.5a (middle and lower grids). In some cases (e.g., lower zone recessions – LZPK and LZSK), a parameter's total sensitivity comes almost entirely from the effects of interactions. Overall the contributions by parameter interactions are a significant part of the total sensitivity picture for RMSE.

Comparing parameter sensitivities across the watersheds for RMSE (i.e., across rows of Figure 2.5a), several trends are visible that provide insight into model behavior across hydroclimatic regimes. For example, the strong trend of increasing sensitivity from dry to wet watersheds for the upper zone free storage (UZFWM) and the opposite (though not as strong) trend for percent impervious area (PCTIM) demonstrates a shift in mechanisms for generating peaks. These trends suggest that in wet watersheds, simulated peaks are more often generated by saturation of the upper zone free water storage, while

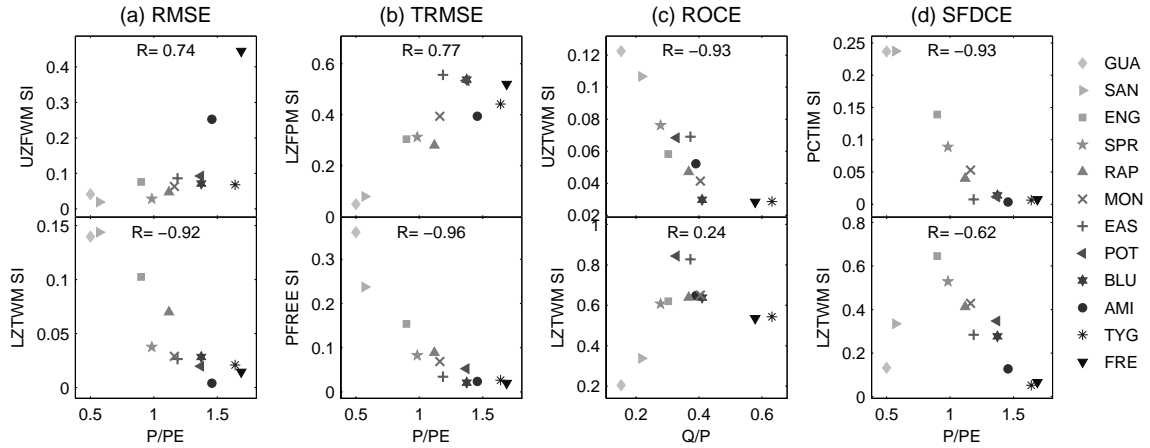


Figure 2.6 Scatter plots demonstrating Spearman rank correlation, R , between selected parameters' long-term Sobol sensitivity indices (SI) and long-term hydroclimatic variables across watersheds for (a) RMSE, (b) TRMSE, (c) ROCE, and (d) SFDCE. Watersheds are indicated by the marker symbols and the selected parameter is labeled on the y-axis.

in dry watersheds peaks are largely controlled by direct runoff from impervious areas. This observation is intuitive as dry watersheds rarely receive enough rainfall to saturate both the tension storages and upper zone free water (which is required to generate surface runoff). Thus, in many events impervious area will be the dominant or even the only mechanism of producing runoff in the model. Conversely wet watersheds regularly saturate and produce surface runoff (which 'overshadows' impervious runoff in the RMSE measure). Figure 2.6a (top) illustrates the trend of increasing upper zone free storage sensitivity with watershed wetness index. The Spearman rank correlation coefficient for this relationship is 0.74. Another informative trend is the higher sensitivities of the tension storages in dry watersheds. Figure 2.6a (bottom) shows the strong negative rank correlation ($R = -0.92$) between lower zone tension storage (LZTWM) sensitivity and watershed wetness coefficient. This indicates the greater importance or "activation" of thresholds in dry watersheds for simulating peaks. In these watersheds, longer and more frequent dry periods (and less overall volume of precipitation) lead to tension storages drying out more often. Therefore the sizes of the tension storages become important in

determining if and when thresholds are crossed and when runoff is generated. On the other hand, in wet watersheds the tension storages may regularly be full (for nearly any size) and thus not have a significant impact on peak simulations.

2.5.1.2 Low Flows - TRMSE

Moving to Figure 2.5b and the low flow (TRMSE) evaluation metric, the pattern of sensitivity is similar to that of the high flow (RMSE) metric (e.g., prominent lower zone sensitivity) though some differences exist. For example, the switch in the parameter with highest sensitivities from the secondary to primary baseflow storage (i.e., from LZFSM to LZFBM) reflects the greater importance of slower-receding (primary) baseflow for low flow versus high flow periods. In addition, the reduced sensitivity of the percolation curve multiplier (ZPERC) suggests that the percolation in dry conditions (which is when ZPERC controls percolation) is less important than it was for high flows. This result is expected since much of percolation in dry conditions goes to lower zone tension storage and does not recharge baseflow. The lower zone sensitivities in TRMSE are likely due to both the main parameter functions (i.e., control of the potential volume of baseflow and slope of recession) as well as its role in the percolation during saturated soil conditions. Another difference between the high flow (RMSE) and low flow (TRMSE) results is the reduction in upper zone free storage (UZFBM) sensitivity. This difference makes sense since this parameter primarily impacts interflow and surface runoff generation (high flow components) rather than baseflow. The emergence of some sensitivity in parameters that control evapotranspiration (ET) losses (RIVA, LZTWM, PFREE) represents additional overall shifts in model control, as ET losses have a larger impact on low flows than on

high flows. Finally, in Figure 2.5b, the contribution of interactions to total parameter sensitivity is again apparent (as for RMSE), further supporting the importance of accounting for parametric interactions.

Comparing sensitivities across watersheds for TRMSE (i.e., across rows of Figure 2.5b), we find that the overall variability is somewhat larger than it was for RMSE. There are fewer parameters in this case that are sensitive across all watersheds. Most noticeably, the two driest watersheds (SAN, GUA) have distinctly different patterns of sensitivity than the other (particularly the wettest) watersheds. The lower sensitivity for the lower zone free primary storage (LZFPM) in the dry watersheds (Figure 2.6b – top) reflects the limited importance of baseflow for low flow simulations in these watersheds (where baseflow may be intermittent). In contrast, the greater impact of ET on low flows in dry watersheds stands out strongly in the higher lower zone tension storage (LZTWM) sensitivities, riparian vegetation area (RIVA) sensitivities, and lower zone partitioning (PFREE) sensitivities. The latter trend is shown and quantified in Figure 2.6b (bottom) with Spearman rank correlations of -0.96. These parameters' impacts on ET-loss are discussed further in the next section.

2.5.1.3 Water Balance - ROCE

The overall parameter sensitivity pattern for the long-term water balance metric (ROCE) is distinctly different than that of the other metrics (Figure 2.5c). Rather than being dominated by the lower zone parameters, the pattern for ROCE is controlled across all watersheds by parameters that affect the volume of ET losses (UZTWM, PCTIM, RIVA, LZTWM). This result reflects the fact that these parameters largely control the volume

(rather than the shape) of the hydrograph, which impacts the long-term water balance. In the SAC-SMA, ET losses occur primarily from the upper and lower zone tension storages and from riparian areas. The amount of loss from each store depends on the demand (potential ET for that time of year) and on the supply (water content of the storage). The parameters that are sensitive to the long-term water balance are those that affect not only the size of these storages (i.e., the potential volume of losses), but also the amount of water that goes into these storages. For example, the percent impervious area controls the volume of runoff that enters the channel directly and is therefore unavailable to ET (i.e., it is the volume that does not enter the upper zone tension storage). Similarly, in the lower zone, percolated water is partitioned between tension and free storages by parameter PFREE. The volume that goes directly into free storage (rather than tension storage) is effectively unavailable for ET loss. These two parameters thus may be sensitive in addition to the parameters controlling the size of the ET-source zones (UZTWM, LZTWM, RIVA).

Evaluating the effects of interactions in Figure 2.5c (lower), it is clear that interactions are not significant for ROCE, in contrast to RMSE and TRMSE. The individual sensitivity pattern (middle) is nearly identical to the total sensitivity pattern (top) and the contributions from interactions (lower) are largely zero, with a few exceptions. This observation reflects that these parameters are sensitive due to their main, independent functions in the model (rather than due to any interacting process like percolation). The reasons for interaction sensitivities for a few watersheds (e.g., POT and EAS) could not be determined though these interactions may be a result of hydroclimatic

characteristics not included in this analysis (e.g., precipitation distribution) or of errors in the data.

Comparing results across watersheds for ROCE, large sensitivity differences are apparent between the two driest watersheds (SAN, GUA) and the rest of the watersheds. Here the upper zone tension storage (UZW) and the lower zone partitioning (PFR) become sensitive. These trends likely relate to the frequency or infrequency of saturation of the upper and lower zone tension storages. If the lower zone is usually dry, the percolation partitioning (PFR) is more important due to its control over the volume of percolation going into the tension storage (and eventually lost to ET as discussed above) during unsaturated lower zone conditions. If the lower zone is saturated, no percolation goes into tension storage, and the partitioning parameter has no effect. Similarly if the upper zone tension water storage is frequently full, the volume of ET loss is less variable than if this storage is often dry. ET losses always occur at the potential rate under saturated conditions, thus if a watershed's upper zone is often saturated, water balance sensitivity to upper zone tension storage will be low (and vice versa). The strong negative rank correlation associated with this trend is presented in Figure 2.6c (top). The second trend illustrated for ROCE involves the lower zone tension storage sensitivity (Figure 2.6c – lower). This trend is different than others in that it shows a non-monotonic relationship with watershed characteristics since the highest sensitivities occur for the mid-wetness watersheds. Lower sensitivities occur for both the wettest and driest watersheds, producing the inverse V shape seen in the scatter plot of this parameter in Figure 2.6c. The reduction in sensitivity for wet watersheds is again likely due to more frequent saturation of the lower zone tension storage and thus less impact of its size on

the volume of losses to ET. Similar to UZTWM, in some years the storage may fill for all parameter values and the volume of ET loss is unaffected by that parameter for those periods. Conversely in very dry watersheds there are potentially long periods in which the upper zone tension storage never fills and thus no water percolates to the lower zone (and LZTWM has no effect).

2.5.1.4 Medium Flow Regime - SFDCE

The final metric, SFDCE, evaluates the error in the slope of the flow duration curve between the 30 and 70 percentile flow magnitudes. It thus captures the distribution (i.e., the variability of flow magnitudes) within the range of mid-level flows. The hydrograph components that fall into the 30-70% range vary by watershed, but will generally include small peaks and high baseflows (e.g., just after large storms). The distribution of these flow magnitudes (i.e., relative frequencies or "flashiness") determines the steepness (or mildness) of the FDC slope. Figure 2.5d shows that, for this metric, lower zone parameters again dominate the sensitivity pattern as they did for RMSE and TRMSE. In contrast to those metrics' results however, the lower zone tension storage parameter (LZTWM) and lower zone partitioning parameter (PFREE) are also sensitive for most of the watersheds. These sensitivities, along with lower zone storages and recessions, reflect the importance of both percolation and lower zone partitioning (between tension and free storages) for reproducing the flow regimes of the watersheds. The percolation function, as mentioned, determines how much water infiltrates to slow-responding baseflow (less-variable flow magnitudes) versus how much moves through the upper zone to become faster-responding (more-variable) interflow or surface runoff. Lower zone partitioning

then impacts the amount of percolation that recharges baseflow after events (versus enters tension storage and is lost to ET). Watersheds with higher percolation and sustained baseflow generally show less variability in flow magnitude (less "flashy" regime) than those with less percolation and therefore more surface runoff and interflow. Figure 2.5d (bottom) shows that the effects of interactions for the SFDCE metric are again significant as they were for RMSE and TRMSE (where percolation was also important). If only individual effects were considered (middle plot) the parameter sensitivity results would be incomplete due to the large contribution by parameter interactions (bottom plot). The importance of interactions for RMSE, TRMSE and SFDCE, though not for ROCE, supports a hypothesis that parameter interactions in the SAC-SMA are largely a result of the percolation function.

Comparing sensitivities across the watersheds for this metric, it is seen that for the drier watersheds the ET-controlling parameters of the upper zone (UZTWM, PCTIM and RIVA) again become sensitive for SFDCE as they did for ROCE. In this case, however, the reason for their sensitivity is their impact on the variability in flow magnitudes (rather than their impact on long-term runoff volume as for ROCE). This impact is greater for dry watersheds than wet watersheds for two reasons. First, in dry watersheds the parameters will be more frequently "activated" over the 30-70 percentile range of flows (whereas in wet watersheds the upper zone will be more often full over this range of flows and UZTWM and RIVA will have less impact). Second, since relatively high flows occur less frequently in dry watersheds than in wet watersheds, the 30-70 percentile range will shift downward to include lower flows (relative to that watershed's range of flows). Therefore, the small peaks generated by impervious area and the recessions that are

affected by riparian and upper zone ET will more likely fall into the 30-70 range. Figure 2.6d (top) demonstrates the decreasing dry to wet trend ($R=-0.93$) between watershed wetness and percent impervious area sensitivity (PCTIM). Figure 2.6d (bottom) also shows a bimodal trend for lower zone tension storage (LZTWM), similar to the trend for the ROCE evaluation metric (and likely for similar reasons of saturation frequency/infrequency as discussed in Section 2.5.1.3.).

2.5.2 Interannual Sensitivities

The interannual sensitivity analysis provides additional information about the variability of parameter sensitivities and model behavior across the watersheds. Temporal patterns (Figures 2.7-2.8) were plotted to observe how sensitivities change from year to year and how much interannual variability (or consistency) is present within each watershed. For all metrics and watersheds in Figures 2.7-2.8, variability in sensitivity patterns is evident. Based on the results in Section 2.5.1, it is reasonable to infer that differences in flow and forcing characteristics from year-to-year could also result in different sensitivity patterns (as seen in Figures 2.7-2.8) from year-to-year. The interannual correlation analysis supports this premise as trends were found for all watersheds between the hydroclimatic characteristics and the parametric sensitivity results for each year. Some trends found in the interannual analysis were similar to trends in the long-term analysis (i.e., patterns across wet and dry years within a watershed are similar to long-term patterns across wet and dry watersheds). Other interannual trends, however, did not exist in the long-term analysis since they seem to represent more specific combinations of long and short-term climatic characteristics at a certain location.

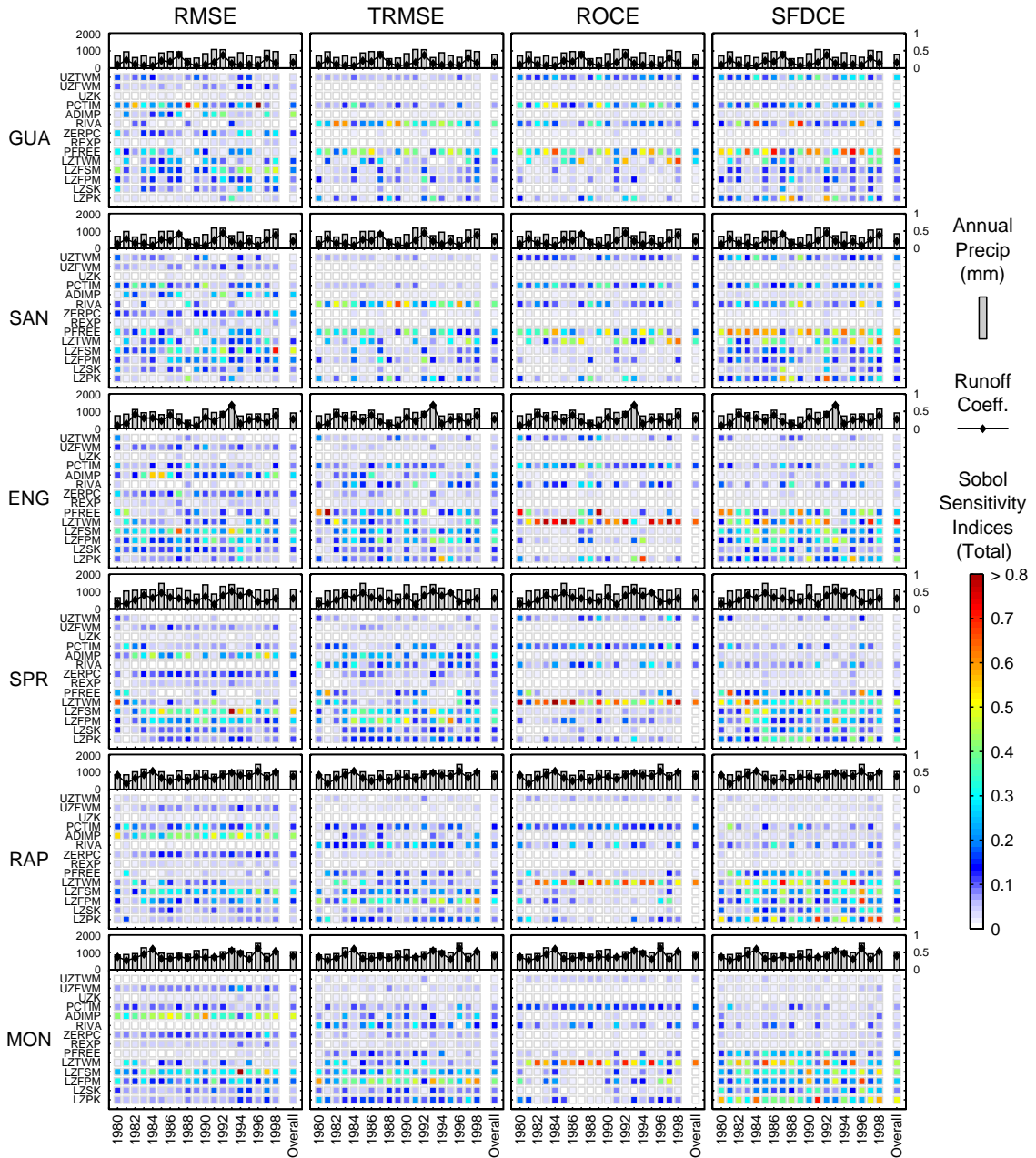


Figure 2.7 Interannual Sobol sensitivity indices for the six driest watersheds over the period 1980-1998. The overall sensitivity (last column in each grid) is the corresponding result from the long-term analysis shown in Figure 2.5. Total annual precipitation (left axis) and the runoff coefficient (right axis) for each year is shown above each sensitivity grid.

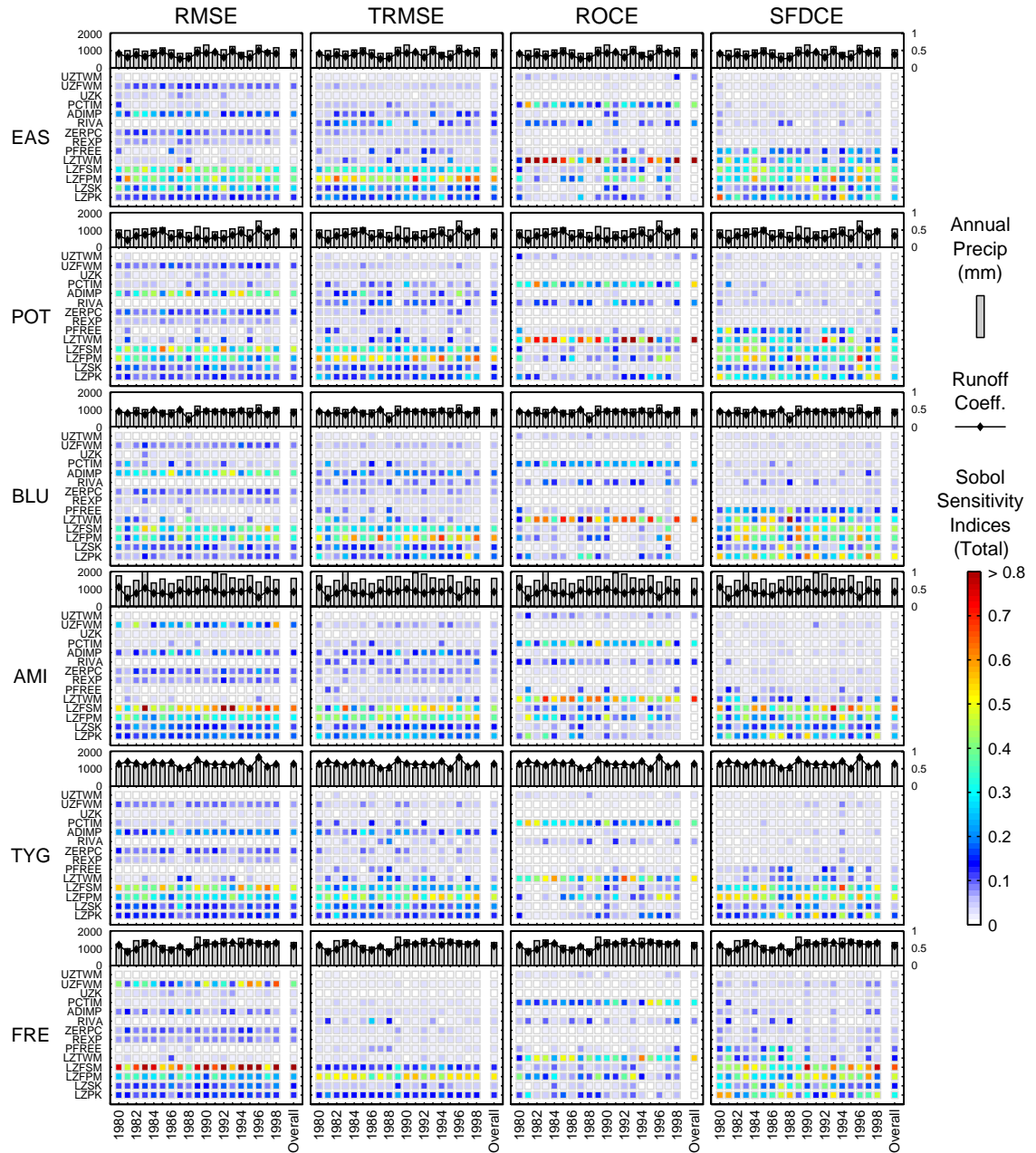


Figure 2.8 Interannual Sobol sensitivity indices for the six wettest watersheds over the period 1980-1998. The overall sensitivity (last column in each grid) is the corresponding result from the long-term analysis shown in Figure 2.5. Total annual precipitation (left axis) and the runoff coefficient (right axis) for each year is shown above each sensitivity grid.

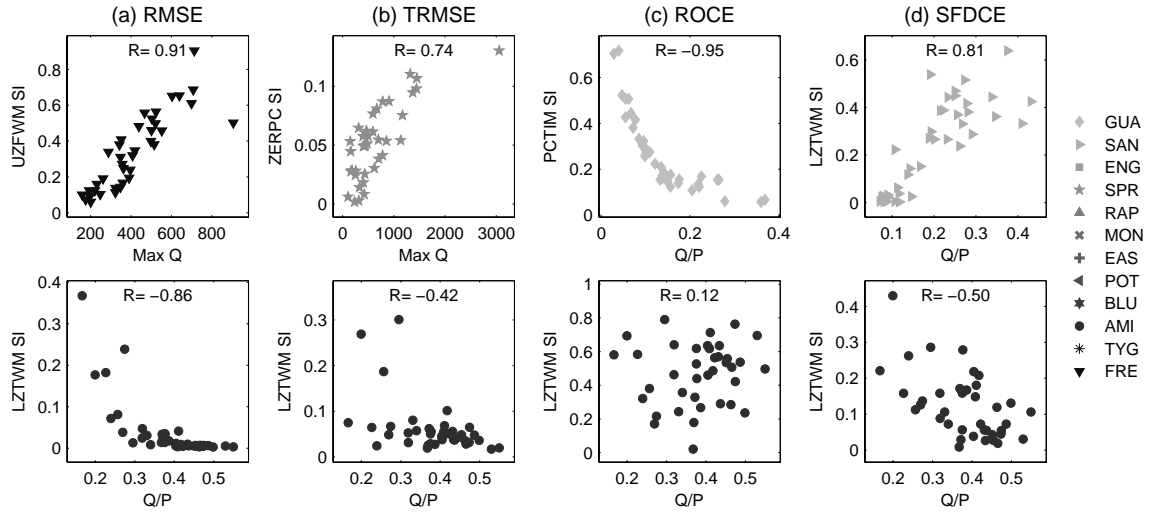


Figure 2.9 Scatter plots demonstrating Spearman rank correlation (R) between parameters' annual Sobol sensitivity indices (SI) and annual hydroclimatic variables. Each plot displays the result for a particular watershed and parameter combination. The watershed is indicated by the marker and the parameter is labeled on the y-axis.

In one bounding case, the wet conditions in the FRE watershed show an increasing trend in high flow sensitivity for the upper zone free water storage (UZFWM) with annual maximum flow in watershed FRE (top plot of Figure 2.9a). In the long-term analysis, this watershed (FRE) had the highest sensitivity to the upper zone free storage (UZFWM) parameter. The high sensitivity is attributed to more frequent saturation of the upper zones. In the interannual analysis, years with high annual maximum flow indicate when large event(s) occurred and thus when the upper zone storages of the SAC-SMA are most likely to be saturated. In such cases (as discussed in Section 2.5.1), runoff is produced in the model mainly by surface runoff (i.e., saturation excess). Thus the size of the upper zone free storage has a large impact on simulations particularly in those years, as demonstrated in Figure 2.9a. Another similar trend between the long-term and interannual analysis is the bimodal behavior of lower zone tension store sensitivity. In dry watersheds the interannual trend is positive (top Figure 2.9d) and in wet watersheds the

trend is negative (bottom Figure 2.9d). Similar reasons apply as were discussed in Section 2.5.1 (relative frequencies of lower zone saturation).

An example of a trend not apparent in the long-term analysis is the water balance (ROCE) sensitivity trend seen in watershed GUA for the percent impervious area (top of Figure 2.9c). The long-term sensitivity for this case (watershed GUA and parameter PCTIM in Figure 2.5c) was actually lower than most other watersheds. In the interannual analysis, however, percent impervious area becomes more sensitive in the dry years of watershed GUA than it does in nearly all years of other watersheds. This suggests a unique model behavior develops in the driest years of the driest watersheds that is not present for other conditions. In such cases total runoff is likely so low and storages so regularly dry, that impervious runoff from the few infrequent events is the only runoff-generating mechanism and thus has a large impact on the water balance for that year. Another difference with long-term results is exemplified by the lower zone partitioning parameter (PFREE) in watersheds SAN and GUA. This parameter is sensitive for high flows in several of the individual years. However, the sensitivity does not appear in the long-term results (last column). As discussed in Section 2.5.1, PFREE controls lower zone partitioning between tension and free water zones and generally affects low- to mid-flows and the water balance (in dry watersheds). In the dry years for these watersheds, peaks may be relatively low and PFREE will also impact the high flow metric. However, the total variance contribution to long-term results in those years is likely small (relative to years with high peaks) and the influence is therefore not discernible in the long-term result. This observation points out the potential of certain events to dominate long-term results and the ability to extract more information from the data when analyses are

performed at shorter time scales. In addition, similarities and differences between the interannual and long-term analyses highlight the influence of time scale on model behavior – a parameter’s influences will be most discernible on time scales for which the processes it controls are dominant.

A final point in the interannual results is the tendencies of some watersheds to ‘look’ like other (wet or dry) watersheds in certain years. For example, watershed RAP (see Figure 2.7) has a low flow (TRMSE) sensitivity pattern in 1998 that is generally similar (e.g., with a limited sensitivity to PFREE) to the dominant pattern in the wet watersheds. However, its pattern in 1982 resembles the overall pattern of the dry watersheds. This fluctuating sensitivity pattern could be related to the fact that this watershed has a long-term P/PE value near 1 (thus it may fluctuate between energy-limited and water-limited years). As another example, the sensitivity patterns in years when major floods occur cause patterns of drier watershed to resemble patterns of wet watershed. For example, the Mississippi Flood of 1993 is evident in watershed ENG and the Winter Flood of 1996 in the Mid-Atlantic shows up in watersheds MON and POT. This also demonstrates that two watersheds with different locations and hydroclimatic characteristics can potentially have the same sensitivity pattern in a given year (such as ENG and AMI in 1993) under extreme changes in forcing. Overall, Figures 2.7 and 2.8 emphasize the risk of assuming a model’s sensitivity based on results from a different watershed or analysis time period.

2.5.3 Synthesis of Results

Sensitivity analysis is often performed in an effort to determine which parameters are most identifiable (i.e., most sensitive) and should be the focus of calibration efforts. The results in the previous sections have demonstrated that parameter sensitivities vary depending on the hydroclimatic characteristics of the watershed and time period of analysis, as well as on the metrics used for the analysis. Based on these findings, it becomes clear that to determine parameter sensitivity for a particular watershed and period of record, it is best to perform a complete sensitivity analysis for that specific case. However, computational and time costs may often make this infeasible. Therefore, to provide some general guidance for SAC-SMA model identification, the results of the interannual and the long-term analyses are combined to create a summary of expected parameter sensitivity by watershed type and time period (Figure 2.10). Watersheds are grouped into three categories (dry, mid, and wet watersheds) based on indicated ranges of the wetness index. For each watershed group their behavior for dry, mid and wet years is classified as highly sensitive, sensitive, or not sensitive based on sensitivity indices (using the maximum index from the four evaluation metric results) of the corresponding watersheds and time periods. Highly sensitive sub-categories have a majority sensitivity index greater than 0.1 (e.g., the majority of the indices in the driest years of the dry watersheds are greater than 0.1). Sensitive sub-categories have a majority index between 0.01 and 0.1 and not-sensitive sub-categories have a majority index less than 0.01. Given a particular watershed and period of record (i.e., how wet/dry is the period), Figure 2.9 provides some general indication as to which parameters are likely to be the most

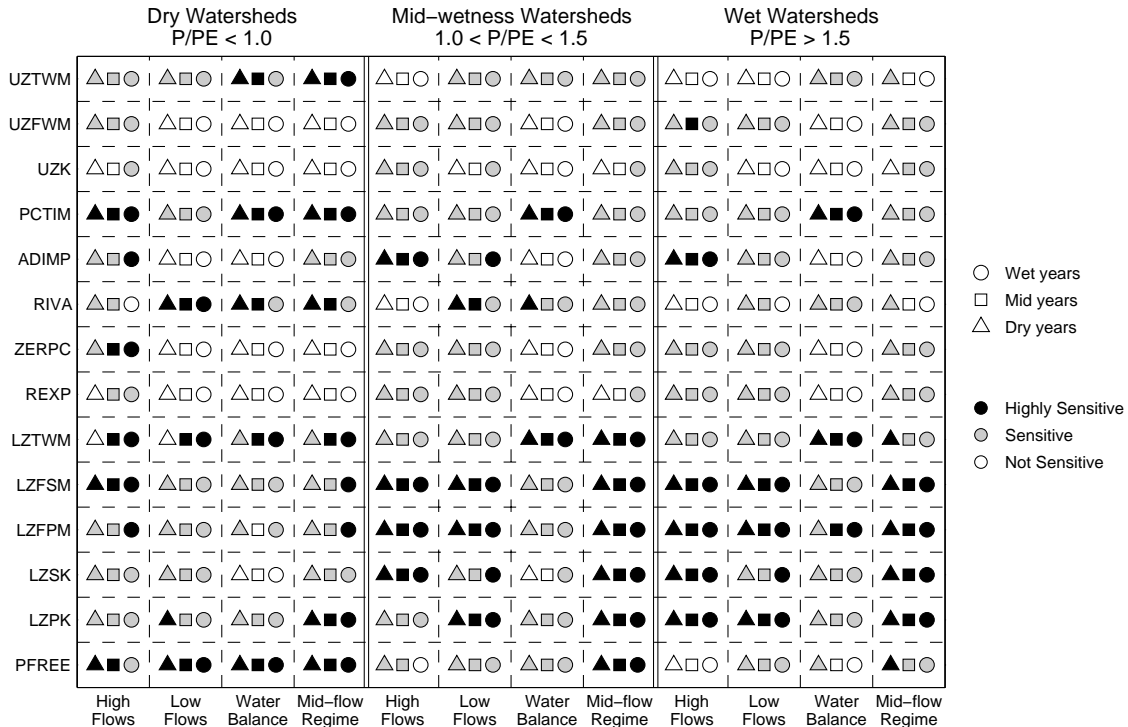


Figure 2.10 Summary of SAC-SMA parameter sensitivity results and guidance for parameter estimation (based on the maximum index from the four evaluation metrics' results). Highly sensitive (black) parameters are those where the majority of years have an SI > 0.1, sensitive (gray) are those where the majority are in the range 0.01 < SI < 0.1; and not sensitive (white) are those where the majority of years have an SI < 0.01.

identifiable, which are less (but still somewhat) identifiable, and which (if any) are largely unidentifiable.

The most evident indication in Figure 2.10 is the need to focus on the lower zone parameters (LZFSM, LZFPM, LZSK, LZPK) in model identification efforts, particularly for mid-wetness and wet watersheds. Section 2.5.1 discussed the involvement of these parameters in percolation and therefore their impact on low, mid, and high flow types. Significant information is also present for these watersheds to identify percent impervious area and lower zone tension storage using the water balance and mid-flow regime metrics. While high flows contain consistent information for identification of additional impervious area (ADIMP). Information for most of the remaining parameters

is present in mid-wetness and wet watersheds, but is weaker and less consistent (i.e., not present in all years). In dry watersheds, model identification focus should shift to parameters impacting ET losses (UZTWM, PCTIM, RIVA, LZTWM, and PFREE) as discussed throughout Section 2.5.1. The remaining parameters (including percolation-related parameters) are less consistently sensitive in dry watersheds and would require targeting specific time periods for identification.

As a final point, it should be noted that similar variation in parameter sensitivity was found at shorter time scales (e.g., intra-annual) than those presented in this paper. We performed the sensitivity analysis on some test cases at a monthly time scale. Sensitivity patterns were still largely driven by hydroclimatic variation as in the longer time scales. These results were not included in this paper as long-term and interannual variation were deemed most relevant for current calibration approaches (i.e., static parameter values are determined based on aggregates measures of model predictions for years to decades).

2.6 SUMMARY AND CONCLUSIONS

This study demonstrates that intermediate-complexity watershed models, like the SAC-SMA, include necessary flexibility for representing a wide range of watersheds located in different hydroclimatic regions. An in-depth analysis is presented of the SAC-SMA's parametric sensitivity variation across watersheds composing a hydroclimatic gradient for multiple time periods/scales and a suite of flow types. The sensitivity patterns demonstrate how different model components become dominant due to changes in forcing (hydroclimatic) conditions. This flexibility, combined with the lack of any consistently insensitive parameter (see Figure 2.10), substantiate that SAC-SMA's level

of complexity is warranted (i.e., the model is not consistently over-parameterized) for simulating watersheds across a range of hydroclimatic conditions. Results also provide detailed guidance for SAC-SMA calibration and refute some commonly employed a priori assumptions about the model's parametric sensitivity. The analysis has broader implications with respect to hydrologic model behavior and identification in general, as discussed below.

Across watersheds, we found that model behavior could be explained largely based on saturation of the upper and/or lower zones. In the upper zone, the free water storage is important in watersheds or time periods in which that zone is frequently saturated and therefore producing surface runoff. In contrast, the impact of the upper zone tension storage is greater under conditions of infrequent saturation and therefore variable ET loss. In each case, the respective conditions for sensitivity reflect conditions when the storage is actively impacting model predictions and reasonably represents the expected dominant processes. The structure of the upper zone in the SAC-SMA is similar to many hydrologic models in its partitioning between tension (ET-drained) and free water (gravity-drained) storages. Thus this moisture- and ET-driven model behavior of the upper zone would be relevant across many models.

The lower zone structure of the SAC-SMA, however, is somewhat unique (among models of similar complexity) in its coupling with the upper zone through the demand-based percolation function. As a result of the percolation structure, lower zone model behavior was found to extend beyond its more typical and assumed influences (low flows) to impact mid and high flows across most watersheds. This behavior was most

evident in watersheds with appreciable levels of lower zone saturation (mid-wetness and wet watersheds) due to the variable percolation demand in such watersheds.

The patterns in model behavior for upper zone, lower zone, and percolation components of the SAC-SMA were interpreted across dry to wet watersheds based on the above-discussed, moisture-related mechanisms. Wet watersheds and dry watersheds resulted in distinctly different patterns of parametric control. The differences were reasonable and intuitive based on differential model forcing, evapotranspiration, and storage across watersheds. Similarly within watersheds, reasonable patterns of sensitivity were produced by wet years and dry years of the analysis record. It follows that similar model behavior variations would be expected to result from non-uniform forcing and storage across a spatially distributed model domain. Wet cells would be expected to have patterns of parametric control similar to wet year/watersheds of this analysis. And likewise dry cells would be expected to follow patterns of dry years/watersheds. Thus implications of this study are likely to apply (and be compounded) for a distributed configuration of the SAC-SMA.

The differences in model behavior demonstrate that a moderate level of complexity (as in the SAC-SMA) is warranted to appropriately represent the hydrology of watersheds across a hydroclimatic gradient. Although some model components were found to be inactive for a single given watershed and/or flow type, a comprehensive evaluation across a range of watersheds and conditions revealed that nearly every model component is important in certain cases. Therefore generalizing model behavior and reducing the number of parameters that require calibration for this model would be difficult if all watersheds and all aspects of the hydrograph should be well represented.

These results also demonstrate counter-evidence for the premise that no more than 3-5 parameters can regularly be identified from hydrologic data. We show that when results are combined across four metrics, substantial information exists for 6-10 parameters (highly sensitive parameters), and 'some' information exists for most of the remaining parameters. Additionally, the fact that the dominant parameters are often similar across multiple metrics (particularly the commonly-used statistical metrics) limits the feasibility of dividing parameters into non-intersecting groups for calibration, which is the basic premise of "step-wise" or "stepped" calibration procedures.

The need to actively couple sensitivity analysis with calibration procedures is clearly indicated by the variation in sensitivity patterns found in this study. Assumptions of parametric controls based on extrapolation of sensitivity analysis results from different watersheds or time periods are likely to be invalid or inapplicable. Furthermore, some common assumptions with respect to the SAC-SMA (e.g., that lower zone parameters do not impact high flows) are incorrect, demonstrating the difficulty of discerning parametric controls a priori without rigorous computational analysis. To most effectively identify important model parameters for calibration of a given watershed and analysis period, sensitivity analysis should be performed for that specific case. Chapter 3 presents an extension of this study that investigates how parameters of varying sensitivity impact the overall model performance. Results of that study address the feasibility for different watershed types of removing (fixing to constants) parameters from the calibration process.

2.7 CHAPTER 2 REFERENCES

- Abbott, M. B., J. C. Bathurst, J. A. Cunge, P. E. O'Connell and J. Rasmussen (1986). An Introduction to the European Hydrological System - Systeme Hydrologique European, "SHE", 1. History and Philosophy of a Physically-Based, Distributed Modeling System. *J. Hydrol.*, 87(1-2), 45-59.
- Anderson, E. A. (2002). Calibration of conceptual hydrologic models for use in river forecasting. *NOAA Tech. Rep. NWS 45*, Hydrol. Lab., Silver Spring, MD.
- Anderson, R. M., V. I. Koren and S. M. Reed (2006). Using SSURGO data to improve Sacramento Model a priori parameter estimates. *J. Hydrol.*, 320(1-2), 103-116.
- Bastidas, L. A., T. S. Hogue, S. Sorooshian, H. V. Gupta and W. J. Shuttleworth (2006). Parameter sensitivity analysis for different complexity land surface models using multicriteria methods. *J. Geophys. Res.*, 111, D20101, doi:10.1029/2005JD006377.
- Bekele, E. G. and J. W. Nicklow (2005). Multiobjective management of ecosystem services by integrative watershed modeling and evolutionary algorithms. *Water Resour. Res.*, 41, W10406, doi:10.1029/2005WR004090.
- Beven, K. J. (1989). Changing ideas in hydrology - the case of physically-based models. *J. Hydrol.*, 105(1-2), 157-172.
- Boyle, D. P., H. V. Gupta and S. Sorooshian (2000). Toward improved calibration of hydrologic models: Combining the strengths of manual and automatic methods. *Water Resour. Res.*, 36(12), 3663-3674.
- Boyle, D. P., H. V. Gupta, S. Sorooshian, V. Koren, Z. Y. Zhang and M. Smith (2001). Toward improved streamflow forecasts: Value of semidistributed modeling. *Water Resour. Res.*, 37(11), 2749-2759.
- Brantley, P. and B. L. Fox (1988). Algorithm 659: Implementing Sobol's quasi-random sequence generator. *ACM Transactions on Mathematical Software*, 14, 88-100.
- Brazil, L. E. (1988). Multilevel calibration strategy for complex hydrologic simulation models. Ph. D. thesis, 217 pp, Colorado State University, Fort Collins, CO.
- Buras, N. (2001). Water resources - unresolved issues. *J. Water Resour. Plng. and Mgmt*, 127(6), 353-353.
- Burnash, R. J. C. (1995). The NWS River Forecast System - catchment model, in *Computer Models of Watershed Hydrology*, V.P. Singh (Editor), pp. 311-366, Water Resour. Publ., Highlands Ranch, CO.
- Clark, M. P., J. A. Vrugt, R. A. Woods, R. Ibbitt, A. Slater, L. E. Hay, G. H. Leavesley, T. Wagener and Q. Y. Duan (in press). Understanding the uncertainties in hydrologic models: relationships between parameter uncertainty and model structure. *Water Resour. Res.*
- Demaria, E. M., B. Njissen and T. Wagener (2007). Monte Carlo sensitivity analysis of land surface parameters using the Variable Infiltration Capacity model. *J. Geophys. Res.*, 112, D11113, doi:10.1029/2006JD007534.
- Duan, Q., S. Sorooshian and V. K. Gupta (1994). Optimal Use of the SCE-UA Global Optimization Method for Calibrating Watershed Models. *J. Hydrol.*, 158(3-4), 265-284.
- Duan, Q., J. Schaake and V. Koren (2001). A Priori estimation of land surface model parameters, in *Land Surface Hydrology, Meteorology, and Climate, Observations*

- and Modeling*, V. Lakshmi, J. Albertson and J. Schaake (Editors), pp. 77-94, AGU, Washington, D.C.
- Duan, Q., J. Schaake, V. Andreassian, S. Franks, G. Goteti, H. V. Gupta, Y. M. Gusev, F. Habets, A. Hall, L. Hay, T. Hogue, M. Huang, G. Leavesley, X. Liang, O. N. Nasonova, J. Noilhan, L. Oudin, S. Sorooshian, T. Wagener and E. F. Wood (2006). Model Parameter Estimation Experiment (MOPEX): An overview of science strategy and major results from the second and third workshops. *J. Hydrol.*, 320(1-2), 3-17.
- Fenicia, F., H. H. G. Savenije, P. Matgen and L. Pfister (2007). A comparison of alternative multiobjective calibration strategies for hydrological modeling. *Water Resour. Res.*, 43, W03434, doi:10.1029/2006WR005098.
- Freer, J., K. J. Beven and B. Ambroise (1996). Bayesian estimation of uncertainty in runoff prediction and the value of data: An application of the GLUE approach. *Water Resour. Res.*, 32(7), 2161-2173.
- Gan, T. Y. and S. J. Burges (2006). Assessment of soil-based and calibrated parameters of the Sacramento model and parameter transferability. *J. Hydrol.*, 320(1-2), 117-131.
- Gupta, H. V., S. Sorooshian and P. O. Yapo (1998). Toward improved calibration of hydrologic models: Multiple and noncommensurable measures of information. *Water Resour. Res.*, 34(4), 751-763.
- Hall, J. W., S. Tarantola, P. D. Bates and M. S. Horritt (2005). Distributed sensitivity analysis of flood inundation model calibration. *J. Hydr. Engrg.*, 131(2), 117-126.
- Hogue, T. S., H. V. Gupta and S. Sorooshian (2006). A 'user-friendly' approach to parameter estimation in hydrologic models. *J. Hydrol.*, 320(1-2), 202-217.
- Hogue, T. S., S. Sorooshian, H. V. Gupta, A. Holtz and D. Braatz (2000). A multistep automatic calibration scheme for river forecasting models. *J. Hydrometeorol.*, 1, 524-542.
- Hornberger, G. M. and R. C. Spear (1981). An Approach to the Preliminary-Analysis of Environmental Systems. *J. Environ. Manage.*, 12(1), 7-18.
- Jakeman, A. J. and G. M. Hornberger (1993). How Much Complexity Is Warranted in a Rainfall-Runoff Model. *Water Resour. Res.*, 29(8), 2637-2649.
- Jakeman, A. J., I. G. Littlewood and P. G. Whitehead (1990). Computation of the Instantaneous Unit-Hydrograph and Identifiable Component Flows with Application to 2 Small Upland Catchments. *J. Hydrol.*, 117(1-4), 275-300.
- Koren, V. (2000). Use of soil property data in the derivation of conceptual rainfall-runoff model parameters, in *Proceedings of the 15th Conference on Hydrology*, pp. 103-106, AMS, Long Beach, CA.
- Koren, V., M. Smith and Q. Duan (2003). Use of a priori parameter estimates in the derivation of spatially consistent parameter sets on rainfall-runoff models, in *Calibration of Watershed Models*, Q. Duan, H. Gupta, S. Sorooshian, H. Rosseau and R. Turcotte (Editors), pp. 239-254, AGU, Washington, D.C.
- Koren, V., S. Reed, M. Smith, Z. Zhang and D. J. Seo (2004). Hydrology Laboratory Research Modeling System (HL-RMS) of the US National Weather Service. *J. Hydrol.*, 291(3-4), 297-318.
- Lehmann, E. L. and H. J. M. D'Abbrera (1998). *Nonparametrics: Statistical Methods Based on Ranks*, Prentice-Hall, Englewood Cliffs, NJ.

- Madsen, H. (2000). Automatic calibration of a conceptual rainfall-runoff model using multiple objectives. *J. Hydrol.*, 235(3-4), 276-288.
- Muleta, M. K. and J. W. Nicklow (2005). Sensitivity and uncertainty analysis coupled with automatic calibration for a distributed watershed model. *J. Hydrol.*, 306(1-4), 127-145.
- Pappenberger, F., I. Iorgulescu and K. J. Beven (2006). Sensitivity analysis based on regional splits and regression trees (SARS-RT). *Environ. Modell. Softw.*, 21(7), 976-990.
- Pappenberger, F., K. J. Beven, M. Ratto and P. Matgen (2008). Multi-method global sensitivity analysis of flood inundation models. *Adv. Water Resour.*, 31(1), doi:10.1016/j.advwatres.2007.04.009.
- Reggiani, P., M. Sivapalan and S. M. Hassanizadeh (2000). Conservation equations governing hillslope responses: Exploring the physical basis of water balance. *Water Resour. Res.*, 36(7), 1845-1863.
- Saltelli, A. (2002). Making best use of model evaluations to compute sensitivity indices. *Comput. Phys. Commun.*, 145(2), 280-297.
- Saltelli, A., S. Tarantola and K. Chan (1999). A quantitative model-independent method for global sensitivity analysis of model output. *Technometrics*, 41, 39-56.
- Sieber, A. and S. Uhlenbrook (2005). Sensitivity analyses of a distributed catchment model to verify the model structure. *J. Hydrol.*, 310(1-4), 216-235.
- Singh, V. P. and D. K. Frevert (Editors) (2006). *Watershed Models*. CRC Press, Boca Raton, FL.
- Sobol', I. M. (1967). On the distribution of points in a cube and the approximate evaluation of integrals. *USSR Computational Math. Math. Phys.*, 7, 86-112.
- Sobol', I. M. (1993). Sensitivity estimates for nonlinear mathematical models. *Math. Model. Comput. Exp.*(1), 407-417.
- Sobol', I. M. (2001). Global sensitivity indices for nonlinear mathematical models and their Monte Carlo estimates. *Math. Comput. Simulat.*, 55, 271-280.
- Sorooshian, S., Q. Y. Duan and V. K. Gupta (1993). Calibration of Rainfall-Runoff Models - Application of Global Optimization to the Sacramento Soil-Moisture Accounting Model. *Water Resour. Res.*, 29(4), 1185-1194.
- Tang, Y., P. M. Reed and T. Wagener (2006). How effective and efficient are multiobjective evolutionary algorithms at hydrologic model calibration? *Hydrol. Earth Syst. Sci.*, 10(2), 289-307.
- Tang, Y., P. M. Reed and J. B. Kollat (2007a). Parallelization strategies for rapid and robust evolutionary multiobjective optimization in water resources applications. *Adv. Water Resour.*, 30(3), 335-353.
- Tang, Y., P. M. Reed, T. Wagener and K. van Werkhoven (2007b). Comparing sensitivity analysis methods to advance lumped watershed model identification and evaluation. *Hydrol. Earth Syst. Sci.*, 11, 793-817.
- Tang, Y., P. M. Reed, K. van Werkhoven and T. Wagener (2007c). Advancing the identification and evaluation of distributed rainfall-runoff models using Sobol's global sensitivity analysis. *Water Resour. Res.*, 43, W06415, doi:10.1029/2006WR005813.

- van Griensven, A., T. Meixner, S. Grunwald, T. Bishop, A. Diluzio and R. Srinivasan (2006). A global sensitivity analysis tool for the parameters of multi-variable catchment models. *J. Hydrol.*, 324(1-4), 10-23.
- Vrugt, J. A., H. V. Gupta, W. Bouten and S. Sorooshian (2003a). A Shuffled Complex Evolution Metropolis algorithm for optimization and uncertainty assessment of hydrologic model parameters. *Water Resour. Res.*, 39(8), 1201, doi:10.1029/2002WR001642.
- Vrugt, J. A., H. V. Gupta, L. A. Bastidas, W. Bouten and S. Sorooshian (2003b). Effective and efficient algorithm for multiobjective optimization of hydrologic models. *Water Resour. Res.*, 39(8), 1214, doi:10.1029/2002WR001746.
- Vrugt, J. A., H. V. Gupta, S. C. Dekker, S. Sorooshian, T. Wagener and W. Bouten (2006). Application of stochastic parameter optimization to the Sacramento Soil Moisture Accounting Model. *J. Hydrol.*, 325(1-4), 288-307.
- Wagener, T. (2003). Evaluation of catchment models. *Hydrol. Process.*, 17(16), 3375-3378.
- Wagener, T. and H. S. Wheater (2006). Parameter estimation and regionalization for continuous rainfall-runoff models including uncertainty. *J. Hydrol.*, 320(1-2), 132-154.
- Wagener, T., N. McIntyre, M. J. Lees, H. S. Wheater and H. V. Gupta (2003). Towards reduced uncertainty in conceptual rainfall-runoff modelling: Dynamic identifiability analysis. *Hydrol. Process.*, 17(2), 455-476.
- Wagener, T., D. P. Boyle, M. J. Lees, H. S. Wheater, H. V. Gupta and S. Sorooshian (2001). A framework for development and application of hydrological models. *Hydrol. Earth Syst. Sci.*, 5(1), 13-26.
- William, H., S. A. Teukolsky, T. V. William and P. F. Brian (1999). *Numerical recipes in C (2nd edition)*, Cambridge University Press, New York.

CHAPTER 3

Phase I (b): Sensitivity-Guided Multi-Objective Calibration of a Lumped Watershed Model across a Hydroclimatic Gradient

Based on:

van Werkhoven, K., T. Wagener, P. Reed, and Y. Tang. (in revision) Sensitivity-guided multi-objective calibration of a lumped watershed model across a hydroclimatic gradient. *Water Resources Research*.

3.1 INTRODUCTION

Watershed-scale hydrologic models are essential tools to understand and predict water movement and storage in a watershed. Before reliable predictions are possible, most, if not all, watershed models require some degree of calibration to observed streamflow data. A priori estimates of parameters, derived from available soils and land use data, may provide good starting values for the calibration process [e.g. *Koren, 2000; Duan et al., 2001; Koren et al., 2003*]. However, the spatial scale of field measurements (e.g. the data used to estimate a priori parameters) is typically much different than the spatial scale of model elements. Furthermore, most model structures are an approximation (or conceptualization) of the real hydrologic system so model parameters do not represent measurable features of the true system. Therefore, a priori parameter estimates typically must still be adjusted by calibration to achieve reliable predictions [*Beven, 1989; Wagener and Wheater, 2006*].

In the last two decades, advances in global optimization have proven useful for hydrologic model identification [*Duan et al., 1992; Sorooshian et al., 1993; Yapo et al., 1998; Vrugt et al., 2003; Wagener et al., 2003; Kollat and Reed, 2006; Tang et al., 2007a*]. Global algorithms have succeeded in overcoming some challenges of hydrologic model optimization (e.g., avoiding local optima, ridges and plateaus of the response surface) and have significantly increased the efficiency of the calibration process [*Duan et al., 1992; Tang et al., 2006*]. However, in recent years studies have begun to recognize that the complexity (i.e., number of parameters) of hydrologic models is often too large, given the amount of information contained in hydrologic data [*Beven and Binley, 1992; Wagener et al., 2001, 2003*]. As a result, most models include unidentifiable parameters –

i.e. parameters for which sufficient information does not exist in the streamflow observations (or other response variable of interest) and therefore cannot be well-identified in the calibration process. If these unidentifiable parameters are allowed to vary freely during calibration, the resulting values will have little meaning (since one value is presumably no better than another). The problem formulation for hydrologic model calibration is a key step that should include a means of dealing with unidentifiable parameters. Another issue for model calibration is the limit to the dimension of the parameter space that can feasibly be searched by current optimization algorithms. For models with a very large number of free-varying parameters (e.g. physically-based and/or distributed models), the full calibration problem may not be viable, even with the most effective algorithms.

One approach that has been applied to handle parameter unidentifiability and large (high-dimension) calibration problems is to reduce the number of free-varying parameters by fixing selected parameters to constant values [*Bastidas et al.*, 1999; *Cox et al.*, 2006; *Hogue et al.*, 2006; *Huang and Liang*, 2006; *Wagner and Wheeler*, 2006; *Wagner and Kollat*, 2007]. These previous studies have used judgment (e.g. understanding of the model structure) or computational tools like sensitivity analysis to determine which model parameters are least identifiable and can be set to constant values. However, these studies applied the approach for only one watershed or they fixed the same parameters to constant values for all watersheds in the study. *Van Werkhoven et al.* [2008] demonstrated that if a sensitivity analysis is applied for watersheds spanning a hydroclimatic gradient, the model parameters that are most sensitive may vary significantly. Thus the set of sensitive (and insensitive) parameters cannot be assumed to

be consistent across watersheds. Furthermore, previous studies have typically used only common statistical metrics of simulation error to assess parameter sensitivity. Statistical metrics quantify the distance between the observed and simulated flow time series based on assumptions about the statistical characteristics of the model residuals, but do not indicate how well the hydrologic function (e.g. water balance and flow regime) of the system is maintained by the model. The results of *van Werkhoven et al.* [2008] show that the parameters that are sensitive for one metric may be quite different than the parameters that are sensitive for another metric. Thus it is important to explicitly include hydrologically-based metrics in the sensitivity analysis and calibration process. Overall, the variation in parametric sensitivity across both watersheds and metrics implies that the selection of parameters to optimize (and fix to constants) should be done on a case-to-case basis for different watersheds (rather than by a single, static approach), using a multi-objective framework that includes hydrologic metrics in addition to typical statistical metrics.

This study investigates a sensitivity-guided approach to watershed model calibration that is applied in a multi-objective framework using the SAC-SMA model for watersheds with varying hydroclimatic regimes. Specific objectives of the study are to determine for the different watersheds (1) to what extent and at what sensitivity level model performance is impacted by setting insensitive parameters to constant, a priori values, (2) the consequence with respect to the hydrologic function of the model if the parameter reduction and optimization are based on only statistical error measures, and (3) what, if any, generalizable guidelines emerge for applying this approach across a hydroclimatic gradient.

3.2 STUDY WATERSHEDS

The watersheds used in this study are part of the Model Parameter Estimation Experiment (MOPEX), an initiative which has developed datasets for hundreds of watersheds across the US [Duan *et al.*, 2006]. Four watersheds were selected to represent distinctly different hydroclimatic regimes. The relative locations and elevation ranges of the 4 watersheds are shown in Figure 3.1, along with normal- and log-scale hydrographs for an average year. As illustrated in Figure 3.1, the watersheds are of comparable size (3015 to 4421 km²), but have different dynamic response characteristics as reflected by the watersheds' hydrographs. The most humid (and lowest-elevation) watershed, AMI, has frequent, more attenuated peaks and higher sustained baseflow, which is typical for a humid regime. The hydrograph of EAS has somewhat less frequent peaks, though it shows similar attenuation and sustained baseflow as AMI. Watershed SPR has slightly less attenuated, less frequent peaks and lower baseflow than EAS. Finally, the most arid and highest-elevation watershed, GUA, has infrequent, sharp peaks and low to intermittent baseflow as is typical for arid and semi-arid watersheds.

The characteristics listed in Table 3.1 further reflect the watersheds' diverse hydroclimatic regimes. As shown in Table 3.1, AMI is the wettest watershed in terms of both mean annual precipitation (P) and wetness index (P/PE), whereas GUA is the driest in terms of these measures. Watersheds EAS and SPR, have similar P but are different (higher in SPR) mean annual potential evaporation (PE). Thus SPR has a wetness index less than one (and is 'water-limited') while EAS has a wetness index greater than one (and is 'energy-limited') [Budyko, 1974]. Throughout discussions and figures in this paper, the watersheds are ranked from dry to wet based on the wetness index. Additional

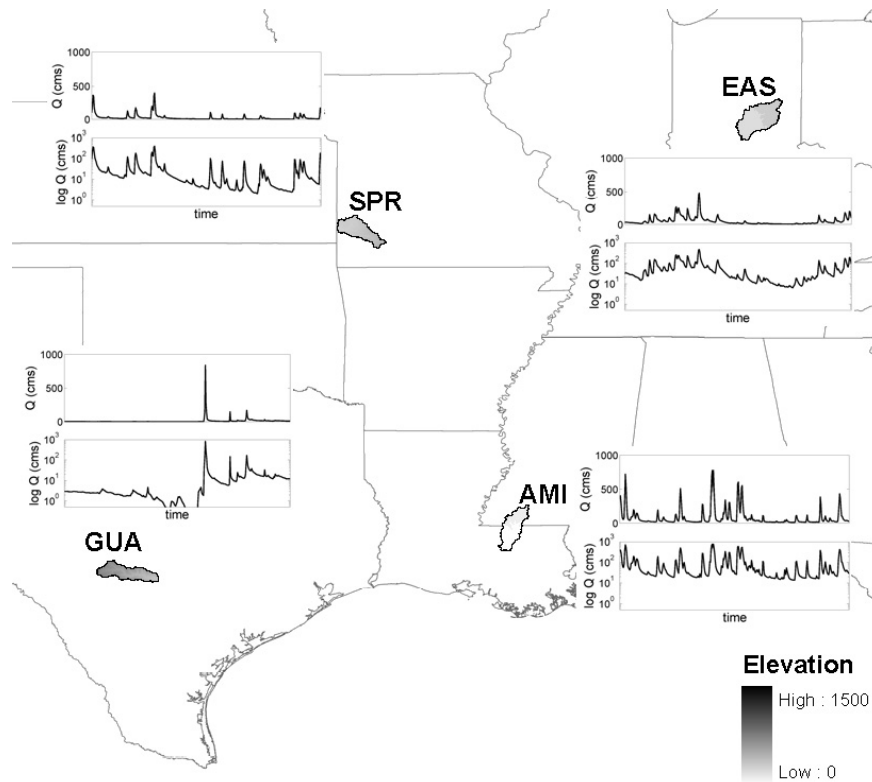


Figure 3.1 Study watersheds' locations, elevation ranges, and hydrographs for an average year (normal and log scale).

Table 3.1 Four study watersheds' characteristics.

ID	River (State)	Area (km ²)	Mean Annual P (mm)	Mean Daily Q (cms)	Mean Annual ROC (Q/P)	Mean Annual PE (mm)	Mean Annual P/PE
AMI	Amite (LA)	3315	1564	55	0.39	1073	1.46
EAS	E. Fork White (IN)	4421	1015	25	0.37	855	1.19
SPR	Spring (MO)	3015	1076	22	0.28	1094	0.98
GUA	Guadalupe (TX)	3406	765	11	0.15	1528	0.50

characteristics of these watersheds are presented by *Duan et al.* [2006]; *van Werkhoven et al.* [2008]; and *Gan and Burges* [2006]. The data used from the MOPEX dataset includes daily precipitation and daily streamflow for 39 years (1960-1998) of data, long-term mean monthly estimates of PE, and vegetation adjustments to the PE estimates.

Table 3.2 Description of SAC-SMA parameters allowable ranges and a priori values.

Parameter	Allowable Range	A Priori Values			
		AMI	EAS	SPR	GUA
UZTWM	25 – 125	62.5	53.5	54.8	31.75
UZFWM	10 – 75	35.4	30.95	32.4	18.9
UZK	0.2 – 0.5	0.36	0.36	0.37	0.27
PCTIM	0.0 – 0.05	0.011	0.011	0.011	0.011
ADIMP	0.0 – 0.2	0.063	0.063	0.063	0.063
RIVA	0.0 – 0.2	0.0	0.0	0.0	0.0
ZPERC	20 – 300	108.6	89.7	80.6	113.5
REXP	1.4 – 3.5	2.21	2.28	2.68	2.514
PFREE	0 – 0.5	0.205	0.224	0.36	0.317
LZTWM	75 – 300	256.2	229.2	204.3	131.5
LZFSM	15 – 300	31.28	37.3	33.17	23.83
LZFPM	40 – 600	128.4	129.8	64.65	70.2
LZPK	0.03-0.2	0.09	0.094	0.102	0.07
LZPK	0.001-0.015	0.009	0.007	0.006	0.004

3.3 METHODS

3.3.1 Sacramento Soil Moisture Accounting Model (SAC-SMA)

The SAC-SMA [Burnash, 1995] is a moderate-complexity lumped conceptual rainfall-runoff model that represents the soil column by upper and lower zones of multiple storages (Figure 3.2). It is the primary rainfall-runoff model used for river forecasting by the National Weather Service (NWS) River Forecast Centers (RFCs) across the United States and it has also been used extensively in research [e.g. Gupta *et al.*, 1998; Koren *et al.*, 1999; Boyle *et al.*, 2000; Boyle *et al.*, 2001; Gan and Burges, 2006; Hogue *et al.*, 2006; Tang *et al.*, 2006]. The model includes 16 parameters whose primary functions are depicted in Figure 3.2. Of these 16 parameters, two are typically set to standard values (SIDE and RSERV) in the parameter estimation process. The remaining 14 parameters must be estimated by some means (calibration or otherwise) for each watershed. These 14 parameters were the focus of this study and are listed in Table 3.2 (see Table 2.2 of Chapter 2 for parameter descriptions and units). Table 3.2 also lists the parameters' allowable ranges that were used in the multi-objective optimization [Anderson, 2002] and

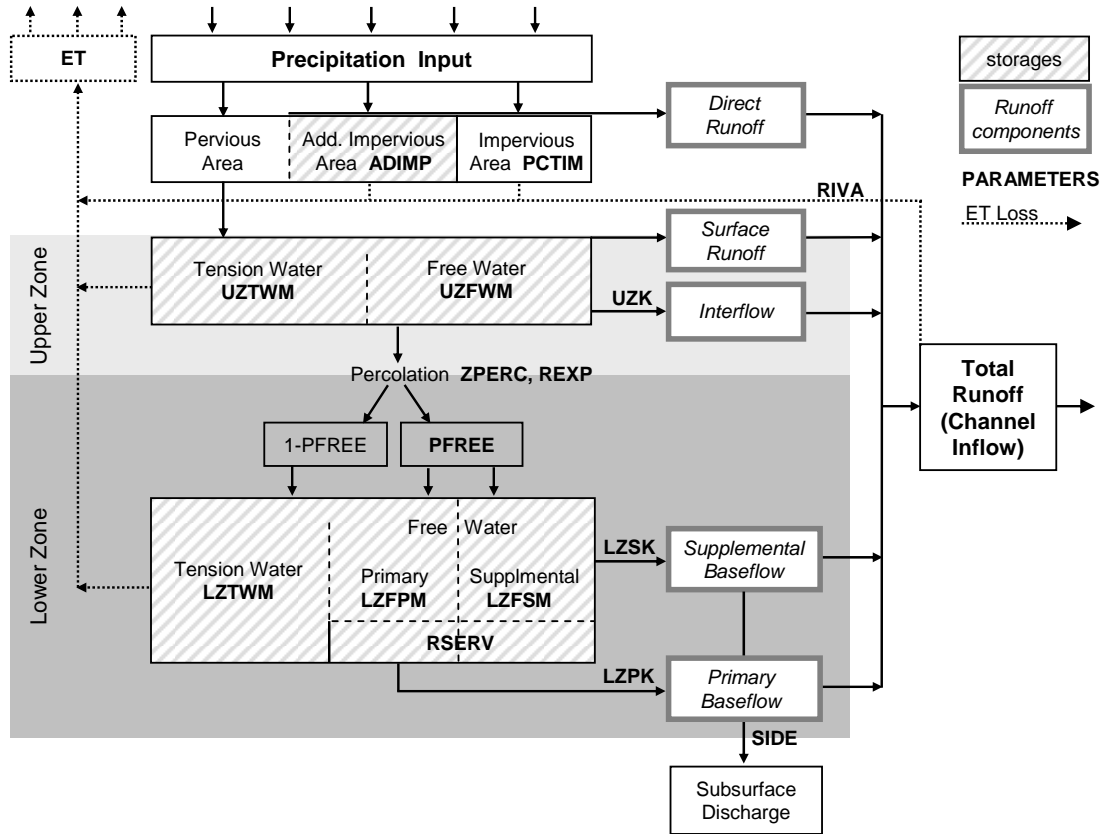


Figure 3.2 Conceptualization of the SAC-SMA.

the a priori values calculated from soils data and other watershed characteristics by *Koren* [2000]. These a priori values were assigned to a given parameter and held constant (not adjusted in optimization) if that parameter was deemed insensitive for a particular case.

3.3.2 Objective Functions

Many hydrologic modeling studies use statistically-based metrics as the primary objectives for model calibration. As discussed in Section 3.3.1, such metrics do not necessarily ensure that the hydrologic function of a watershed is well-represented. One goal of this study is to assess the implication of leaving hydrologic metrics out of the calibration process. Thus four metrics are used here – two common statistical metrics that

emphasize high and low flows and two hydrologic metrics that emphasize the water balance and the mid-range flow regime. Together, these metrics capture four different but important components of the hydrograph while allowing for a comparison between statistical and hydrologic metrics. The statistical high flow metric is the commonly-used root mean squared error (RMSE), defined as:

$$RMSE = \sqrt{\frac{1}{m} \sum_{t=1}^m (Q_{s,t} - Q_{o,t})^2} \quad (3.1)$$

where m is the number of timesteps, $Q_{s,t}$ is the simulated flow for timestep t , and $Q_{o,t}$ is the observed flow in timestep t . For the second statistical metric, the simulated and observed flow time series are first transformed by a Box-Cox transformation (Eq. 3.2) with a λ value of 0.3, which has a similar effect as a log transformation. The RMSE of the transformed flows is then calculated to obtain a metric that emphasizes low flow, referred to here as the transformed root mean squared error (TRMSE) (Eq. 3.2).

$$Z = \frac{(1+Q)^\lambda - 1}{\lambda} \quad (3.2)$$

$$TRMSE = \sqrt{\frac{1}{m} \sum_{t=1}^m (Z_{s,t} - Z_{o,t})^2} \quad (3.3)$$

where m is again the number of timesteps, $Z_{s,t}$ is the transformed simulated flow for timestep t , and $Z_{o,t}$ is the transformed observed flow in timestep t . The third metric, the runoff coefficient error (ROCE), captures the overall accuracy of the water balance by first combining the flows into one characteristic hydrologic descriptor, the mean annual runoff coefficient. The absolute error in the runoff coefficient is then calculated and thus the ROCE is defined as

$$ROCE = abs\left(\frac{\bar{Q}_s}{\bar{P}} - \frac{\bar{Q}_o}{\bar{P}}\right) \quad (3.4)$$

where \bar{Q}_s and \bar{Q}_o and are the simulated and observed mean annual runoff volume, and \bar{P} is the mean annual precipitation. The final metric is the slope of the flow duration curve error (SFDCE) and measures how well the model captures the distribution of mid-level flows. The slope of a watershed's flow duration curve indicates the variability, or flashiness, of its flow magnitudes. The SFDCE metric is thus simply the absolute error in the slope of the flow duration curve between the 30 and 70 percentile flows as follows:

$$SFDCE = abs\left(\frac{Q_{s,70} - Q_{s,30}}{40} - \frac{Q_{o,70} - Q_{o,30}}{40}\right) \quad (3.5)$$

where $Q_{s,30}$ and $Q_{s,70}$ are the 30 and 70 percentile flows of simulated flow duration curve and $Q_{o,30}$ and $Q_{o,70}$ are the 30 and 70 percentile flows of observed flow duration curve.

3.3.3 Epsilon Nondominated Sorted Genetic Algorithm II (ϵ -NSGAI)

The ϵ -NSGAI is a multi-objective evolutionary algorithm (MOEA) that has been applied and tested for a variety of system optimization problems [Kollat and Reed, 2005, 2006; Tang et al., 2006; Tang et al., 2007a]. Within the area of water resources, the algorithm has been used most extensively for the calibration of hydrologic models [e.g. Tang et al., 2006] and the design of long-term groundwater monitoring networks [e.g. Kollat and Reed, 2006]. Comparison studies have shown that the performance of the ϵ -NSGAI is equivalent or superior to other state-of-the-art MOEAs for solving water resources problems. In particular, the algorithm's strengths include its ease of implementation, reliability, and diverse representations of tradeoffs [Kollat and Reed, 2005; Tang et al., 2006].

Evolutionary algorithms in general are methods that incorporate principles of biological evolution to generate solutions with the greatest "fitness" as defined by one or more objective functions for the given system. Like the original NSGAI [Deb et al., 2002], the ϵ -NSGAI employs real-valued search operators that include simulated binary crossover (SBX) [Deb and Agrawal, 1994] and polynomial mutation as well as elitist selection strategies [Deb, 2001]. In addition, the algorithm maintains use of nondomination sorting and crowding distance to increase solution diversity as in the original version. The ϵ -NSGAI expands upon NSGAI by including the concept of ϵ -nondominance [Laumanns et al., 2004] and dynamic population sizing [Harik and Lobo, 1999]. Inclusion of ϵ -nondominance allows for user-control over the precision of the approximation to the Pareto set and thus also over the algorithm's computational cost (as shown by Kollat and Reed [2006]). Values of ϵ establish the error tolerance for each objective function – small values will more completely capture the full resolution Pareto set, while larger values will result in a more coarse approximation. Dynamic population sizing [Harik and Lobo, 1999] is a method that enables the algorithm's population size to increase or decrease commensurate with problem difficulty. The scheme uses a series of “connected runs” in which initial small populations pre-condition the search and subsequent populations are sized based on search progress. Using dynamic population sizing facilitates the implementation of ϵ -NSGAI by eliminating the need to specify the population size. For more detailed descriptions of ϵ -NSGAI, see Kollat and Reed [2005; 2006] and Tang et al. [2007].

3.3.4 Sobol' Sensitivity Analysis

The SAC-SMA parameter sensitivity analysis results that are used in this study were developed as part of previous work by *van Werkhoven et al. [2008]*. That study used Sobol's method [*Sobol'*, 1993] to determine SAC-SMA total and individual parameter sensitivities for 12 watersheds based on the four metrics described in Section 3.3.2. A subset of those results (i.e. total sensitivities for the four study watersheds) is used in this study to select sensitive versus insensitive parameters for optimization.

Sobol's sensitivity analysis method is a variance-based approach in which the model output variance is decomposed into relative contributions from individual parameters and parameter interactions. A given parameter's sensitivity in this method is quantified by the ratio of its contribution to the output variance to the full (i.e. due to all parameters) output variance, resulting in an index value ranging from 0 to 1. This index, called the Sobol' sensitivity index, can be calculated for both individual and total parameter sensitivities. The total index measures the sensitivity due to the combined effect of the parameter alone (i.e. individual sensitivity) plus its interactions with all other parameters in the analysis. This study uses total sensitivity indices since these values reflect the full impact of each parameter on the model output and are most relevant for calibration. In Sobol's method, the total output variance and the variance contributions are approximated in a Monte Carlo framework using two different samples. The model is evaluated using the first sample to calculate the full output mean and variance (i.e., the combined effects of all parameters). The second sample is then used to resample each parameter, rather than setting each to a fixed value, for the calculation of total and individual variance contributions. For more details on Sobol's method see *Sobol'* [1993,

2001], *Hall et al.* [2005], *Saltelli* [2002], *Tang et al.* [2007b], and *van Werkhoven et al.*[2008].

3.4 APPROACH

For each of the 4 study watersheds, the methods described in Section 3.3.1-3.3.3 were used to perform multi-objective optimization with varying problem formulations in order to assess the importance of including multiple hydrologic metrics and the impact of reducing the number of optimized parameters for different watersheds. First, as a baseline, the full SAC-SMA parameter space (14 parameters) was optimized for each watershed using ϵ -NSGAI and the four objective functions defined in Section 3.3.2. Then, multiple reduced-parameter sets were developed by defining four thresholds (0.05, 0.1, 0.2 and 0.3) on Sobol's sensitivity index (see Figure 3.3). These thresholds identify parameters that contribute 5, 10, 20 and 30 percent of the total output variance, respectively. SAC-SMA parameter sensitivities were obtained by Sobol's sensitivity analysis in a previous study [*van Werkhoven et al.*, 2008], which includes an in-depth discussion of the resulting parameter sensitivities. For a given threshold and objective function, all parameters having a sensitivity index greater than the threshold were defined as sensitive for that metric. Two different reduced-parameter sets were then constructed for each threshold – one based on the union of sensitive parameters for the 2 statistical metrics (RMSE and TRMSE) and one based on the union of sensitive parameters for all 4 metrics. The two reduced-parameter sets are thus referred to throughout the discussion section as the '2-metric reduction' and the '4-metric reduction'. The parameter reduction approach and associated results are discussed in more detail in Section 3.5.1. Once the

parameter sets were developed, each was optimized using ε -NSGAII and the four objective functions. Thus for each watershed a total of 9 multi-objective optimization results were obtained – the full-parameter set plus 8 reduced parameters sets (i.e. 2 sets per threshold). The tradeoff or Pareto solution sets that resulted from the multi-objective optimizations were compared across thresholds to determine the overall impact of reducing the parameter space. Results were also compared between the 2-metric and 4-metric reductions to assess the implication of ignoring hydrologic metrics in both the parameter-reduction and optimization steps of the calibration approach.

To ensure the reliability of results, the ε -NSGAII was executed for each case with 50 different random seeds and 500,000 function evaluations (thus 25,000,000 total function evaluations for each parameter set). The solution sets from all 50 seeds were combined and ε -nondomination sorting was applied to obtain the final reference set in each case. These final results are plotted in Figures 3.4, 3.6, 3.8, and 3.10 and are discussed in Sections 3.5.2-3.5.5.

3.5 RESULTS

3.5.1 Reduced Parameter Sets

The method used to develop reduced-parameter sets for SAC-SMA is depicted in Figure 3.3. Each row of the figure corresponds to one of the four threshold values (0.05, 0.1, 0.2 and 0.3) that were imposed on the Sobol sensitivity index to define ‘sensitive’ versus ‘insensitive’ parameters. The color grids (Figure 3.3a) reflect the value of the sensitivity index for each SAC-SMA parameter (y-axis) in each watershed (x-axis). For each metric, parameters with a sensitivity index greater than the given threshold are identified and are

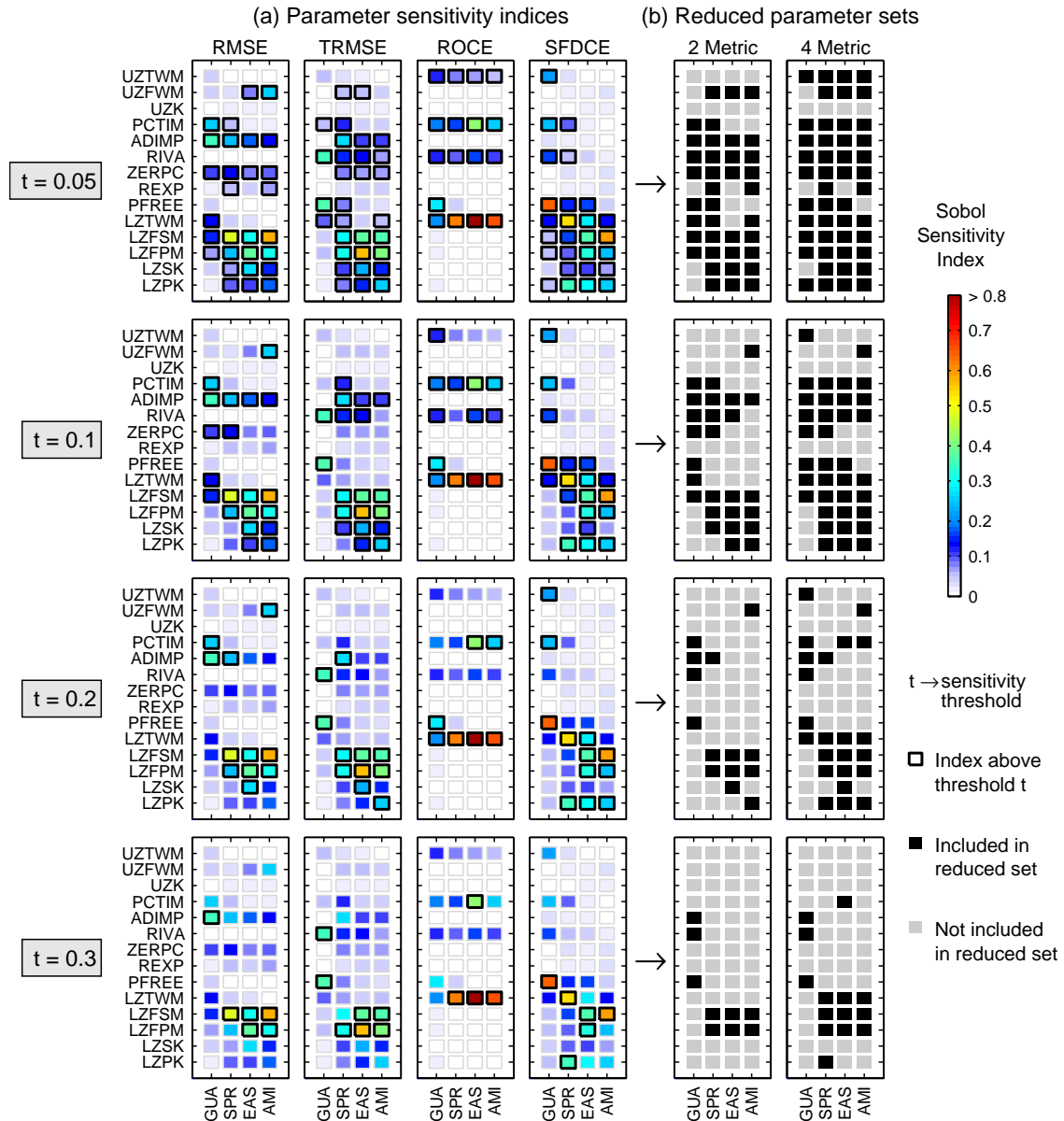


Figure 3.3 Development of parameter sets to optimize for each sensitivity index threshold (t) in each study watershed. Part (a) indicates the parameters' Sobol sensitivity indices for the four evaluation metrics and shows which parameters (outlined in black) have indices above the given threshold value. Part (b) illustrates how reduced-parameter sets were built by including parameters that are sensitive for RMSE *or* TRMSE (2-metric reduced set) and parameters that are sensitive for *any* of the metrics (4-metric reduced set).

outlined in black. From these parameters, two different reduced-parameter sets are then constructed for each threshold. The 2-metric reduced set is the union of parameters that are sensitive for RMSE and TRMSE, while the 4-metric reduced set is the union of

parameters that are sensitive for all four study metrics. The resulting parameter sets are shown in Figure 3.3b (right side of the figure) by black solid squares. The differences between the 2-metric and 4-metric sets reflect that parametric sensitivity varies significantly across the metrics (as discussed in detail in *van Werkhoven et al. [2008]*). The 4-metric sets (for a given watershed and threshold) include the same parameters as the 2-metric sets (those sensitive for RMSE or TRMSE), *in addition* to the parameters that are sensitive for ROCE and SFDCE. Thus in each case the 4-metric set will include an equal or greater number of parameters as compared to the 2-metric set.

For both cases, as the threshold increases, there are progressively fewer parameters included in the reduced sets. In the 2-metric case, applying thresholds 0.05, 0.1, 0.2 and 0.3 result in ranges of 8-12, 6-7, 3-4, and 2-3 parameters included, respectively. While the thresholds in the 4-metric case result in ranges of 10-13, 8-10, 5-6, and 3-4 parameters, respectively. The impact on the model performance of reducing the number of calibrated parameters by such extents (and based on different metrics) is presented and discussed for each watershed in Section 3.5.2.

3.5.2 Optimization

Results of the multi-objective optimizations are shown in Figures 3.4, 3.6, 3.8, and 3.10. For each watershed (i.e., each figure), the Pareto solutions from the full-parameter optimizations (top row – identical on both sides of the figure) and reduced-parameter optimizations (rows 2-5) are included for the 2-metric and 4-metric parameter reductions. Note that in all cases the optimizations resulted in a 4-objective Pareto solution set. For better interpretation and readability we have plotted the 4-objective solution set twice in 2

dimensions with color. In both, RMSE & TRMSE are plotted on x and y axis, respectively, with either ROCE (left) or SFDCE (right) shown in color (i.e. the left and right sides are the same solution set but plotted with a different metric in color). As a means of scaling and to enable comparisons, the x-axis range in each plot is equal to the watershed's mean annual flow and the y-axis is one quarter of the transformed mean annual flow. Thus the distance between points in each plot has comparable significance. The a priori (un-optimized) solution is also plotted as a point in each case for comparison. This point (and its color) represents the objective values obtained when the model is run with all 14 parameters set to a priori values (calculated using pedo-transfer functions by *Koren* [2000]). Overall these plots capture a continuum from the case of full parametric search to the case of an a priori specified parameter set attained without search.

3.5.2.1 Watershed AMI

The results of the full and reduced-parameter optimizations for AMI, the most humid of the four watersheds, are shown in Figure 3.4. In the full-parameter result (top row), some overall performance improvement is evident in the relative distance between the minimum objective values (i.e. particularly RMSE, TRMSE and SFDCE) and the a priori result. Since the a priori ROCE value is already near zero, little improvement occurs for that metric. The parameter reductions at the first level ($t=0.05$) result in only a slight change in the solution set (as compared to the full-set optimization). This reflects that little impact on performance occurs as the least sensitive parameters are removed from the analysis. In addition, at this level the 2- and 4-metric reduction results are very similar, further demonstrating the low impact of the removed parameters. Moving down

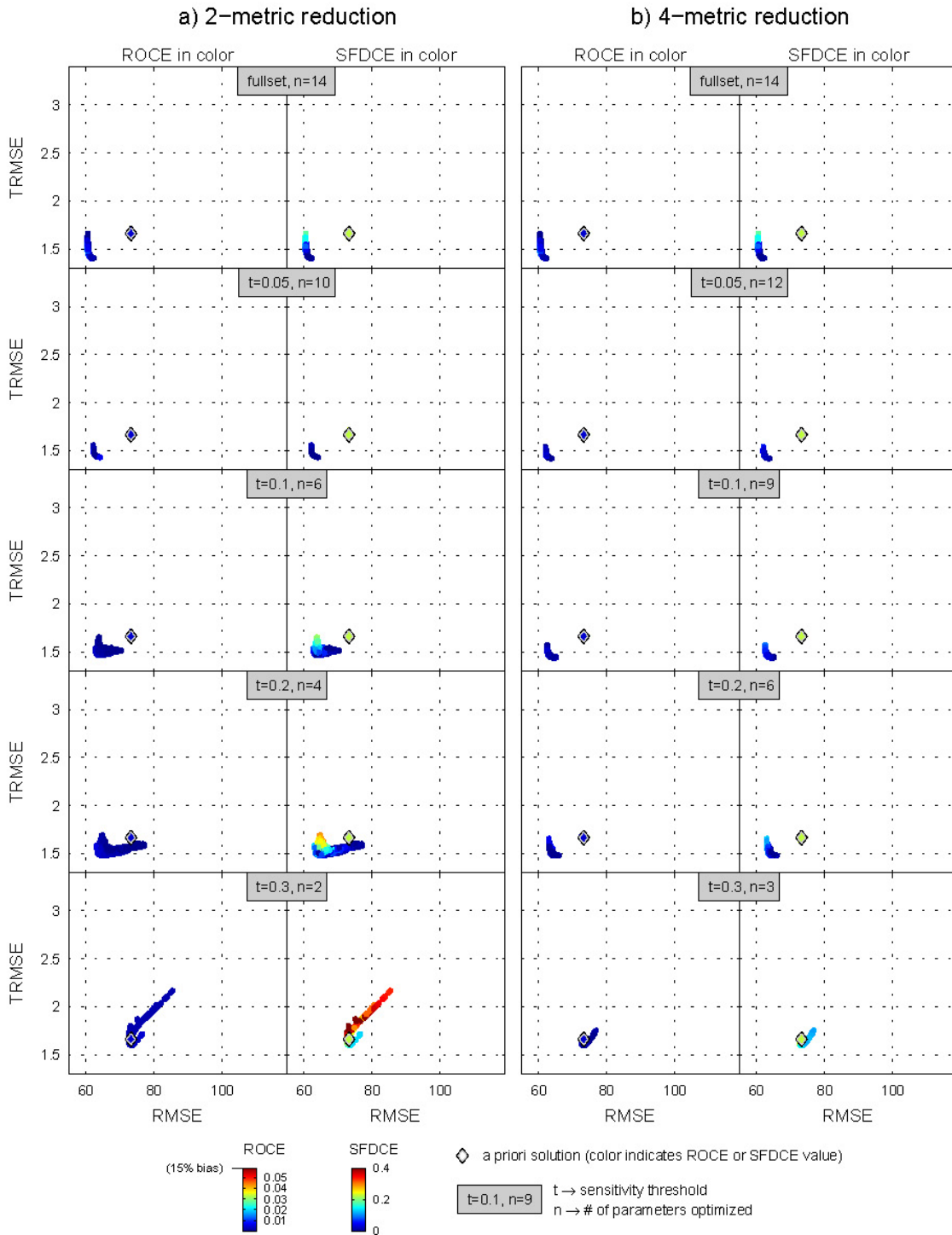


Figure 3.4 Watershed AMI optimization results for the (a) 2-metric reduced parameter sets and the (b) 4-metric reduced parameter sets. Results of the full parameter optimization are shown in the top row of both (a) and (b). The sensitivity index threshold and the corresponding number of optimized parameters are indicated in the gray box for each case.

to threshold levels of 0.1 and 0.2, some slight change on the shape of the solution set becomes apparent in for 2-metric reduction (Figure 3.4a), while the 4-metric result remains similar to the previous level. The optimum values for all metrics in both cases however do not significantly change. The shape change is likely a result of leaving out increasingly important parameters for ROCE and SFDCE – since the change disappears in the 4-metric reduction. When parameters LZTWM and PCTIM are added to the analysis for the 4-metric reduction, the solution set again is similar to the previous levels. It can be deduced however that parameter LZTWM is the primary influence on the shape difference between 3.4a and 3.4b at thresholds of 0.1 and above. Parameter PCTIM is also removed in the 2-metric reduction level 0.05 but the shape change did not occur at this level. At the final threshold level ($t=0.3$), the most significant degradation in performance occurs. Here the optimum RMSE and TRMSE values are near the a priori solution and the majority of the solution set is actually worse than the a priori value. At this level, parameters LZPK and UZFWM are removed for both the 2-metric and 4-metric reductions. As discussed by *van Werkhoven et al.* [2008], UZFWM is an important parameter for capturing high flows in wet watersheds, thus its removal particularly impacts the optimal RMSE value that is attainable for this watershed. As in the previous two levels, when LZTWM is added to the analysis from the 2-metric to the 4-metric case, the extent of the solution set reduces though the optimum values are not significantly affected.

The variation and quality of model simulations resulting from the solution sets for select cases are illustrated in Figure 3.5 by flow duration curves and cumulative runoff curves. We recognize the limitation of the flow duration curve to fully reflect the quality

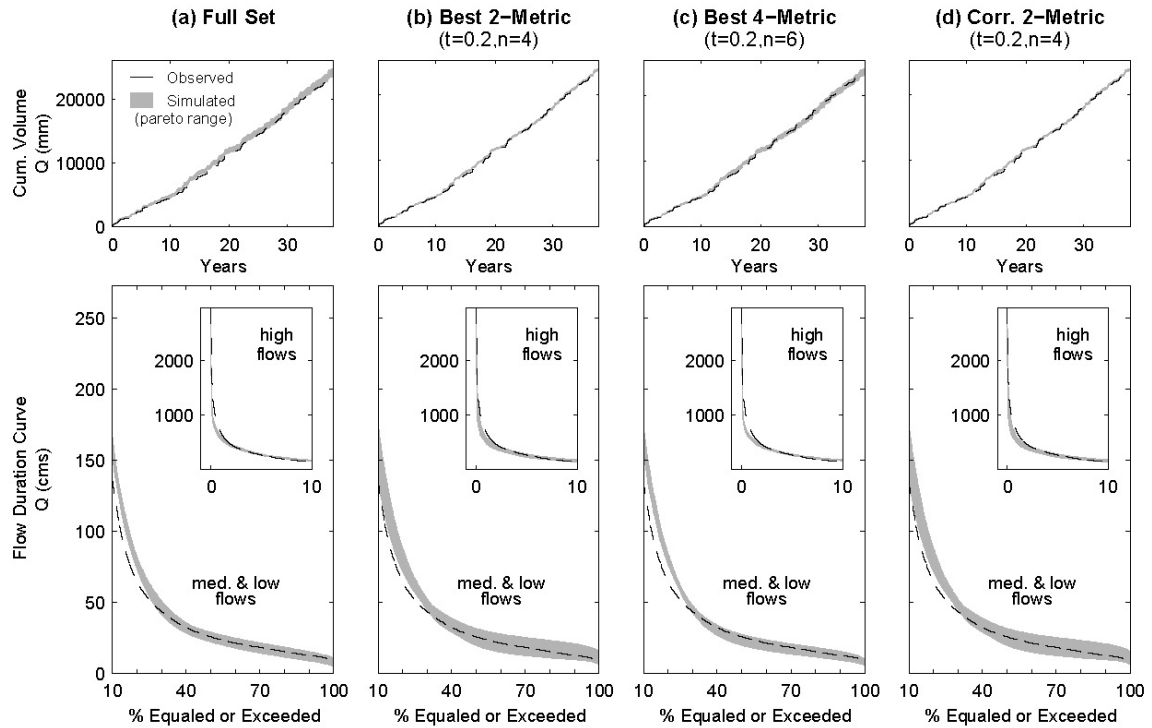


Figure 3.5 Watershed AMI observed and simulated (i.e. pareto range) cumulative runoff volume curves and flow duration curves (with the high flows (0-10%) portion shown in the inset plot on a larger y-axis scale for readability). The cases presented include (a) the full parameter set optimization, (b) the ‘best’ 2-metric reduction result (c) the ‘best’ 4-metric reduction result and (d) the corresponding 2-metric for the threshold level of the ‘best’ 4-metric result (for comparison). The ‘best’ optimizations were selected subjectively as the case with the fewest parameters where model performance is not severely impacted for the metrics considered.

of simulations since it includes no information on accurate flow timing (as time series would), only that the right distribution of flow levels occurred throughout the record. However space clearly prevents the inclusion of 38-year time series, and including only select years would make it impossible to link the metric values (which are calculated on the full 38 years) to the model outputs. Therefore these plots provide a more general indication of similarity and dissimilarity in results and (particularly) of the width or narrowness of the solution set range in each case. Figure 3.5 (and in Figures 3.7, 3.9 and 3.11) includes 4 cases – the full-parameter result, the 'best' 2-metric result (determined subjectively as the case with the fewest parameters where model performance is not severely impacted), the 'best' 4-metric result, and finally the 2-metric result

corresponding to the 'best' 4-metric result (i.e., at the same threshold level). Comparing these cases allows for a systematic assessment of the significance of including hydrologic metrics (i.e., ROCE and SFDCE) in the analysis. For watershed AMI, if the reduction and optimization were performed using only statistical metrics (Figure 3.4a), a sensitivity threshold of 0.2 might be selected to reduce the number of optimized parameters while maintaining the model performance. This case is identified as the 'best' 2-metric result and reduces the number of optimized parameters from 14 to 4 (UZFWM, LZFPM, LZFSM, LZPK). The range of model output for this case is plotted in Figure 3.5b. As compared to Figure 3.5a (full-parameter result), the width of the solution set's simulation range (gray area) on the flow duration curve is wider, which reflects the wider range of objective values in this case (particularly SFDCE and RMSE). If the analysis were performed using all four metrics (Figure 3.4b), the 'best' result occurs at the same threshold (0.2). In this case (Figure 3.5c), the number of optimized parameters would be reduced to 6 (UZFWM, PCTIM, LZTWM, LZFSM, LZFPM, LZPK). Figure 3.5d for this watershed is identical to Figure 3.5b since the 'best' 2-metric and 4-metric results occurred at the same level. In contrast to other watersheds (as will be shown in the following sections), including hydrologic metrics for AMI is less critical. This observation is likely attributable to the near-zero water balance error (ROCE) of the a priori solution. Since the a priori values yield a good water balance, optimizing the parameters highly sensitive for metric ROCE does not greatly improve performance. Overall however, the results for watershed AMI show that the model complexity (in terms of number of optimized parameters) can be significantly reduced based on a Sobol sensitivity index of 0.2, resulting in four optimized parameters.

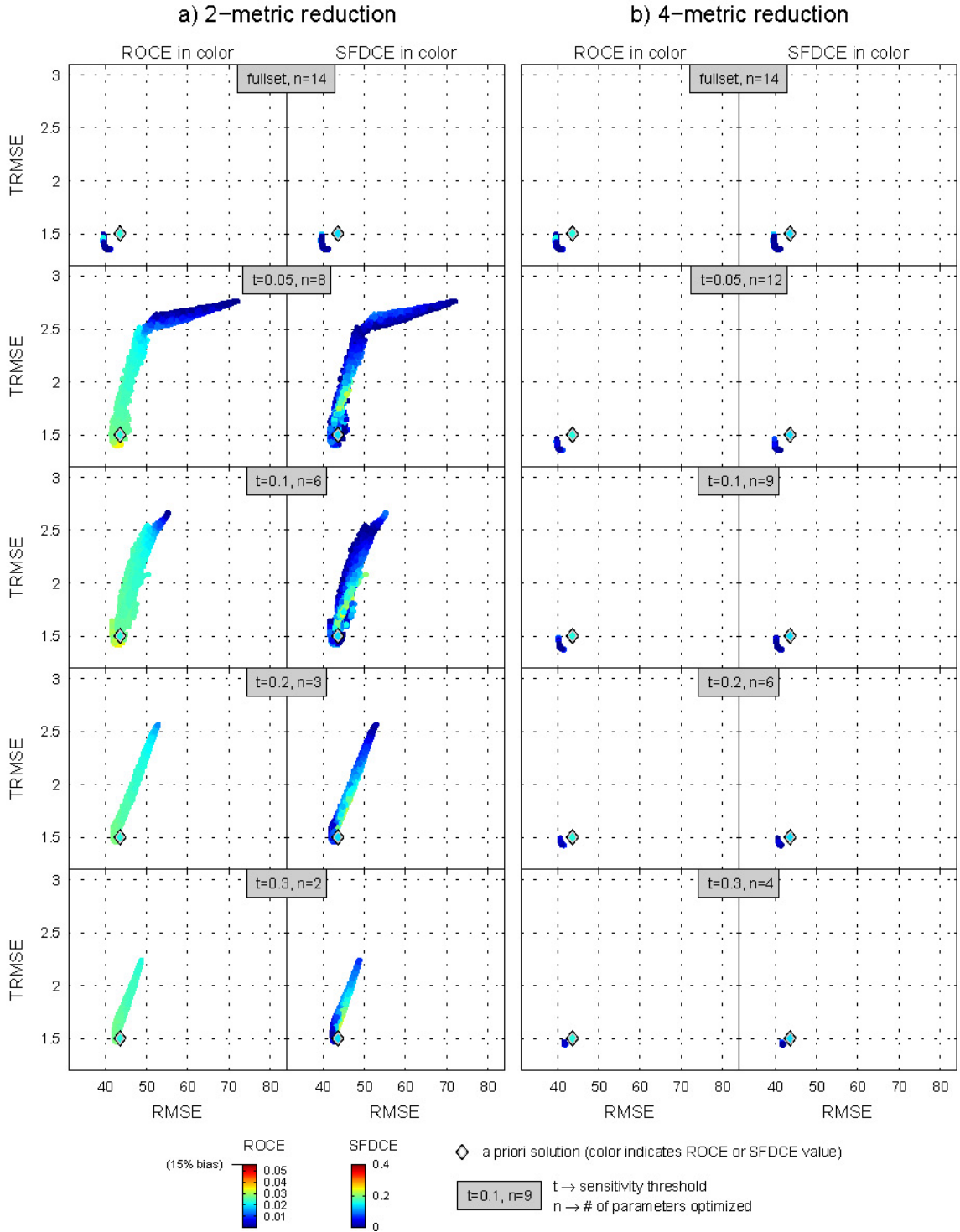


Figure 3.6 Watershed EAS optimization results for the (a) 2-metric reduced parameter sets and the (b) 4-metric reduced parameter sets. Results of the full parameter optimization are shown in the top row of both (a) and (b). The sensitivity index threshold and the corresponding number of optimized parameters are indicated in the gray box for each case.

3.5.2.2 Watershed EAS

The optimization results for watershed EAS (Figure 3.6) show some distinctly different patterns than watershed AMI. First, as seen in the full-parameter result (top row) the a priori solution is closer to the Pareto front for the statistical metrics (RMSE and TRMSE), therefore less overall improvement (in these metrics) is attainable by the optimization. In addition, the a priori water balance error (ROCE) is higher (0.03) than it was for AMI. The impact of parameter-reduction for this watershed is immediately apparent in the results of the 2-metric case at a threshold of 0.05. Here a large spread in values of RMSE and TRMSE develops in order to reach improved values of ROCE. Six parameters were removed from the analysis at this level. When four of those parameters are re-added to the analysis for the 4-metric reduction (moving from Figure 3.6a to 3.6b at level 0.05), the solution set returns to the shape and values of the full-parameter set result. The pattern of large spread in TRMSE values remains throughout the 2-metric reductions for all thresholds, while the 4-metric reductions' solution sets do not significantly change from the full-parameter set. The two parameters that are consistently different between Figure 3.6a and 6b are PCTIM and LZTWM. These two parameters are highly sensitive for metric ROCE. Therefore it makes sense that if the initial (a priori) water balance is poor, then removing these two parameters from the analysis would prevent the optimization from improving or 'fixing' the water balance (unless it reaches into regions of high error for the other metrics). As an additional observation, parameter UZFWM is included for the 2-metric reduction at a threshold of 0.05 (while it is not for $t=0.1$ and above). The region of very high RMSE error at this level (when UZFWM is included) could be a result of large peaks generated by very low values of UZFWM that

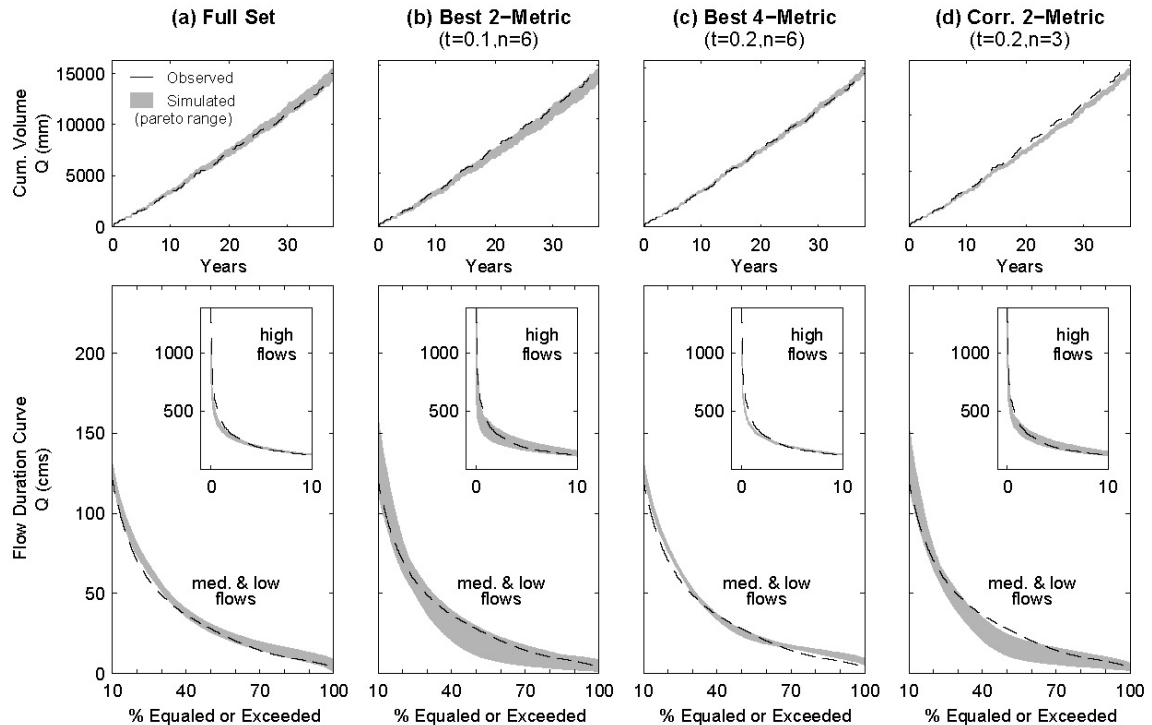


Figure 3.7 Watershed EAS observed and simulated (i.e. pareto range) cumulative runoff volume curves and flow duration curves (with the high flows (0-10%) portion shown in the inset plot on a larger y-axis scale for readability). The cases presented include (a) the full parameter set optimization, (b) the 'best' 2-metric reduction result (c) the 'best' 4-metric reduction result and (d) the corresponding 2-metric for the threshold level of the 'best' 4-metric result (for comparison). The 'best' optimizations were selected subjectively as the case with the fewest parameters where model performance is not severely impacted for the metrics considered.

are offsetting water balance error to improve the ROCE values at the expense of high RMSE error (resulting in the 'tail' at the top of the solution set in this case).

For watershed EAS, the 'best' 2-metric result occurs at a threshold of 0.1. At this level the optimum values of RMSE and TRMSE are still only slightly higher than the full-parameter result though still better than the a priori values. For each subsequent threshold these values are closer to the a priori values. A threshold of 0.1 for the 2-metric case reduces the number of parameters from 14 to 6. The model output for the full-parameter result and the 'best' 2-metric result are shown in Figures 3.7a and 3.7b, respectively. Figure 3.7b shows a wider solution set range on low, mid and high flows of the flow duration curve, as well as on the cumulative volume curve. The increased ranges

reflect the wide range of objective values that result for this case (i.e., throughout Figure 3.6a). The 'best' 4-metric reduction result is selected at a threshold of 0.2 which again includes 6 parameters (though a different 6 parameters than the 'best' 2-metric case). Figure 3.7c shows the sharper (more narrow) solution set range on the output curves that results for the 'best' 4-metric case. Comparing Figures 3.7b and 3.7c also demonstrates the importance of *which* parameters are optimized rather than *how many* are optimized. These two cases included the same number of parameters (6), however the results appear significantly better in Figure 3.7c – when all four metrics are used in the parameter-reduction. For a final comparison, the results from the 2-metric reduction corresponding to the 'best' 4-metric reduction (i.e., threshold 0.2) are included in Figure 3.7d. The wider (less sharp) range and decreased accuracy of results are evident in both the flow duration and cumulative volume curves. This demonstrates that when using a 2-metric reduction, a lower sensitivity threshold (i.e., including more parameters) would be necessary to achieve comparable results. Thus, for watershed EAS the impact of leaving the hydrologic metrics out of the analysis is significant. At all threshold levels in Figure 3.6 a large difference exists between the 2-metric reduction and 4-metric reduction. It is clearly beneficial to include hydrologic metrics in the parameter reduction process for this case. When 4 metrics are included, it appears possible to reduce the number of optimized parameter from 14 to 6, while maintaining model performance.

3.5.2.3 Watershed SPR

Figure 3.8 presents the optimization results for watershed SPR. Like EAS, the a priori solution is relatively close to the optimized solution for RMSE, TRMSE, and SFDCE. In

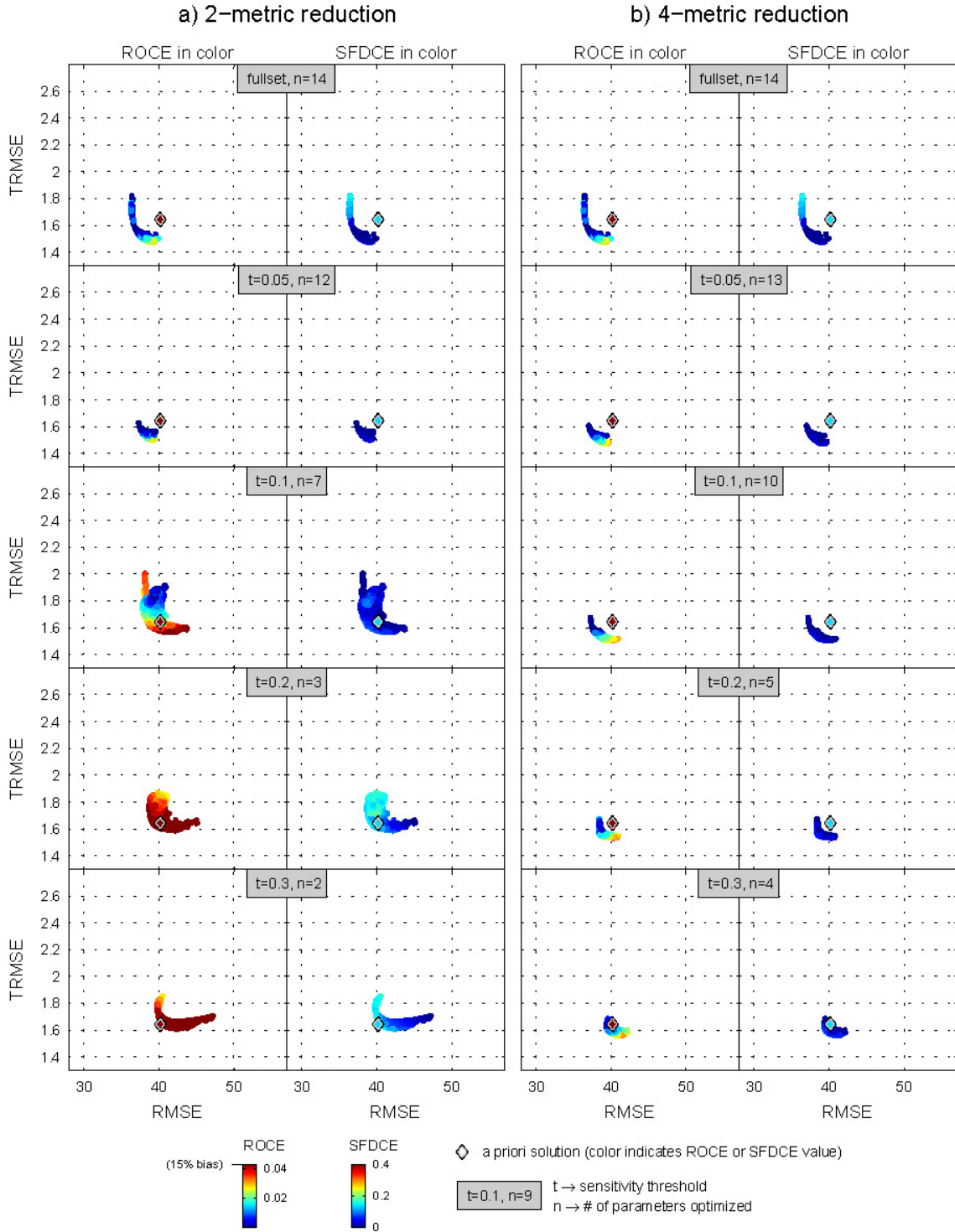


Figure 3.8 Watershed SPR optimization results for the (a) 2-metric reduced parameter sets and the (b) 4-metric reduced parameter sets. Results of the full parameter optimization are shown in the top row of both (a) and (b). The sensitivity index threshold and the corresponding number of optimized parameters are indicated in the gray box for each case.

this watershed, however, the a priori ROCE value is higher than it is for all other watersheds at 0.04 (corresponding to roughly a 15% volumetric bias). Similar to watershed AMI, the impact of the parameter reduction at the 0.05 threshold is minimal and no observable differences exist between the 2-metric and the 4-metric cases (at this level). Using this threshold, very few parameters are removed (e.g. fewer than EAS at the same level) so the small impact is not surprising. However, at a threshold of 0.1, the effect of the parameter reduction on performance becomes apparent for the 2-metric case, where 7 parameters are removed from the analysis. In this case, (as was seen in EAS) the solution set expands into a region of higher RMSE and TRMSE in order to minimize ROCE. In other words, when these 7 parameters are removed, the best simulations with respect to low flows (in particular) are in turn very poor with respect to the water balance. When 3 parameters are re-added to the analysis (LZPK, LZTWM, and PFREE) for the 4-metric reduction at the same threshold level, the results look very similar to the results at the 0.05 threshold. The same trend of large impact in the 2-metric case and less change (particularly in the shape of the solution set) for the 4-metric case continues for $t=0.2$ and $t=0.3$. However for $t=0.2$ and 0.3 , the RMSE and TRMSE values reach closer to (and become worse than) the a priori values. The two parameters that are consistently removed from the analysis between Figure 3.8a and 8b (for $t=0.1$ and above) are LZTWM and LZPK. LZTWM in particular has a very high sensitivity for this basin and it is likely that this parameter (as for AMI) is causing much of the differences seen in Figure 3.8.

The 'best' 2-metric result is selected at a threshold of 0.05, which includes 12 parameters and is therefore a small reduction with only 2 parameters removed. Above that threshold, however, results significantly degrade. The model output for the full-

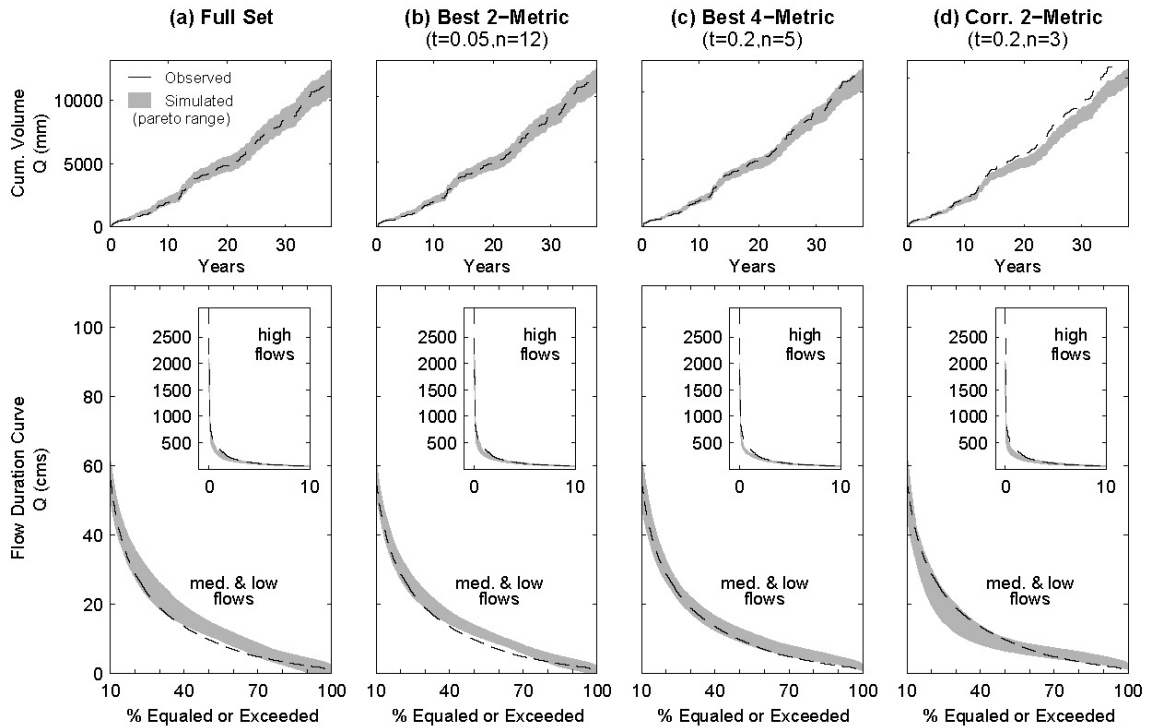


Figure 3.9 Watershed SPR observed and simulated (i.e. pareto range) cumulative runoff volume curves and flow duration curves (with the high flows (0-10%) portion shown in the inset plot on a larger y-axis scale for readability). The cases presented include (a) the full parameter set optimization, (b) the ‘best’ 2-metric reduction result (c) the ‘best’ 4-metric reduction result and (d) the corresponding 2-metric for the threshold level of the ‘best’ 4-metric result (for comparison). The ‘best’ optimizations were selected subjectively as the case with the fewest parameters where model performance is not severely impacted for the metrics considered.

parameter result and the 'best' 2-metric result are shown in Figures 3.9a and 3.9b, respectively. The two plots are very similar, reflecting the small impact of removing only 2 very insensitive parameters. The 'best' 4-metric result is selected at threshold 0.2 which includes 5 optimized parameters and is therefore a much larger reduction. Figure 3.9c shows that, on the flow duration curve, the results look again similar to Figures 3.9a and 3.9b with slight degrade on the cumulative volume. Figure 3.9d illustrates that the corresponding 2-metric result for the 'best' 4-metric result (at the same threshold level) has a significantly wider solution set range and is much further from the full-parameter result in Figure 3.7a. The wide range in most metrics of the solution set for this case are also reflected in Figure 3.8a for this case (where the majority of the set is worse than the

a priori solution). The importance of including the hydrologic metrics in this case is underpinned by the differences between Figures 3.8a and 3.8b at all threshold levels. This point is further emphasized by the better performance attained when optimizing 5 parameters for the 4-metric case at level $t=0.2$ than when optimizing 7 parameters for the 2-metric case at level $t=0.1$. With fewer parameters, better performance can be achieved if parameters are well-selected. Overall, it appears reasonable to reduce the number of optimized parameters from 14 to 5 (ADIMP, LZTWM, LZFSM, LZFPF, and LZPK) when using 4 metrics for watershed SPR.

3.5.2.4 Watershed GUA

The full-parameter optimization for GUA (the driest watershed) achieves the greatest relative improvement in high and low flow performance (i.e., in RMSE and TRMSE) from the a priori solution (as compared to the other three watersheds). Like SPR, the a priori ROCE value for GUA is also high, though the SFDCE value is lower. Like AMI and SPR, parameter reduction using a threshold of 0.05 does not have a significant impact on the performance for either the 2-metric or the 4-metric cases, though a larger number of parameters (6) are removed in this case. Increasing the threshold from 0.05 to 0.1 removes just one additional parameter (LZFPF) from the analysis, but creates a very noticeable impact on the performance. A very similar effect occurs for the 4-metric case as well, where 2 parameters are removed (LZFPF and LZPK). In both cases the resulting minimum values for each metric do not change significantly, but the change in shape reduces the potential of a good tradeoff solution (i.e., a solution where all metrics are close to their minimum). The most significant impact on performance, however, occurs at

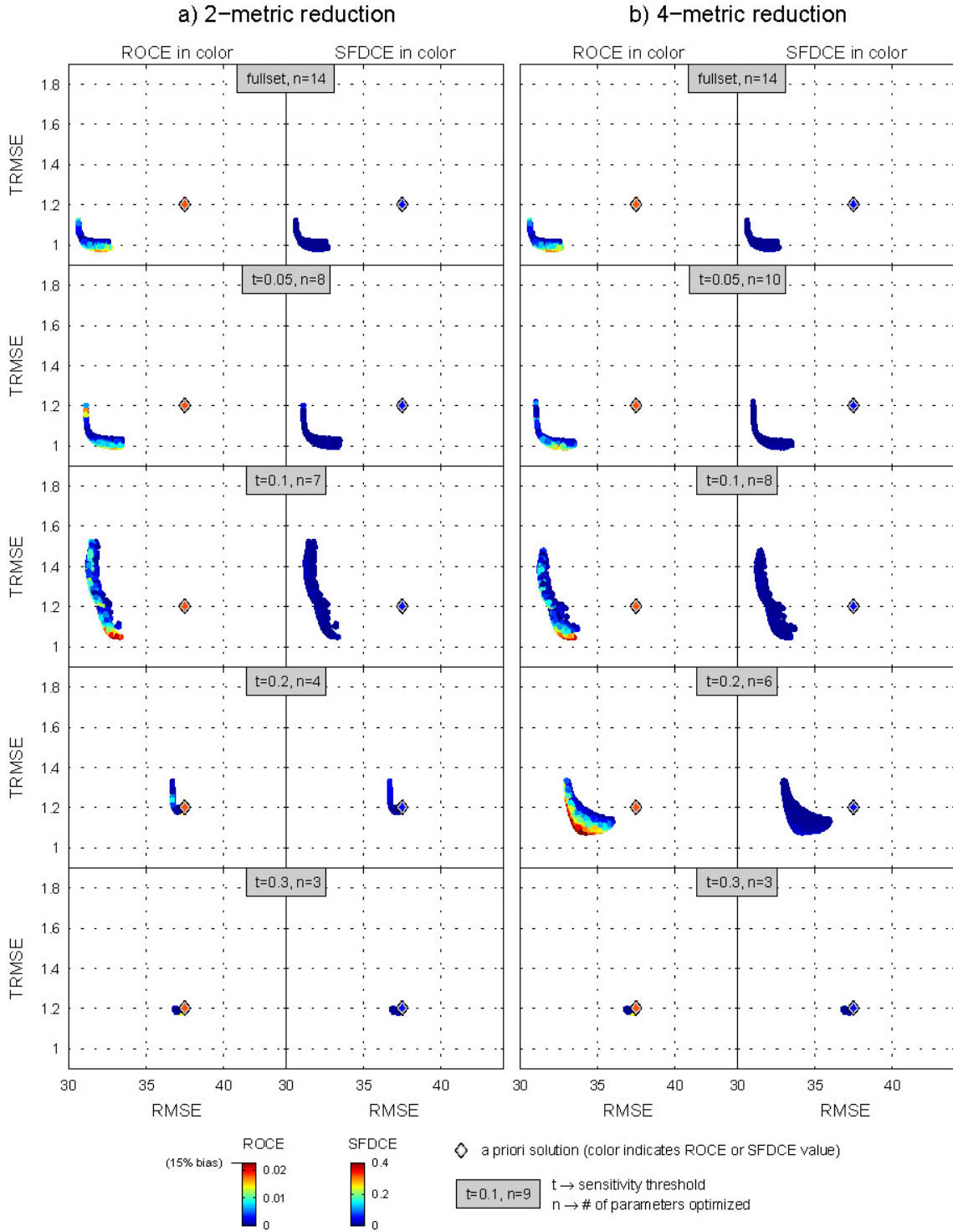


Figure 3.10 Watershed GUA optimization results for the (a) 2-metric reduced parameter sets and the (b) 4-metric reduced parameter sets. Results of the full parameter optimization are shown in the top row of both (a) and (b). The sensitivity index threshold and the corresponding number of optimized parameters are indicated in the gray box for each case.

a threshold of 0.2. At this level, RMSE and TRMSE increase to the a priori levels (and higher) for the 2-metric case. The 4-metric case shows less impact than the 2-metric case, though it is still significant as compared to lower thresholds of the 4-metric case. In addition, tradeoffs between metrics worsen again here as the best (lowest) TRMSE solutions have very high values of ROCE. It is interesting to note that the improvement in RMSE at threshold 0.2 from the 2-metric to 4-metric case, a pattern not observed in other watersheds. This is initially unexpected since the parameters that are re-added to the analysis (UZTWM and LZTWM) for the 4-metric case are not sensitive to RMSE at this threshold level. However one of these parameters (LZTWM) is in fact sensitive for RMSE at the previous level ($t=0.1$), therefore re-adding this parameter has an impact. As discussed in *van Werkhoven et al* [2008] dry watersheds have been observed to have greater overlap in parametric sensitivity between the statistical and hydrologic metrics. Thus similar trends (i.e., an observable improvement in statistical metrics from the 2-metric to 4-metric cases) are not apparent for other watersheds. As further demonstration, the final threshold level ($t=0.3$) results in the same parameter set (ADIMP, RIVA and PFREE) for both the 2-metric and 4-metric reduction in watershed GUA. Little improvement in performance is achieved by optimizing only these three parameters as the resulting solution set appears nearly as a point adjacent to the a priori solution.

The 'best' 2-metric result for this watershed is selected at a threshold of 0.05, which includes 8 parameters. Above $t=0.05$, however, the tradeoff potential and minimum values (especially over $t=0.2$) significantly degrade. The model output for the full-parameter result and the 'best' 2-metric result are shown in Figures 3.11a and 3.11b, respectively. The two plots are similar though slightly wider solution set ranges are

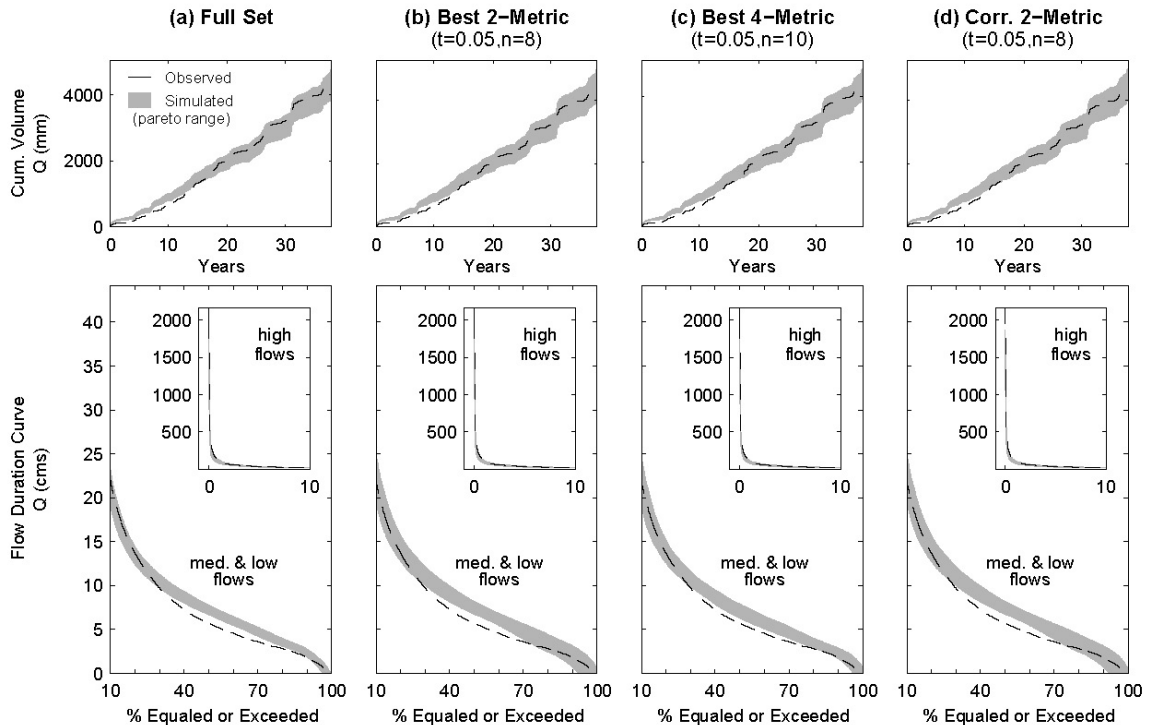


Figure 3.11 Watershed GUA observed and simulated (i.e. pareto range) cumulative runoff volume curves and flow duration curves (with the high flows (0-10%) portion shown in the inset plot on a larger y-axis scale for readability). The cases presented include (a) the full parameter set optimization, (b) the ‘best’ 2-metric reduction result (c) the ‘best’ 4-metric reduction result and (d) the corresponding 2-metric for the threshold level of the ‘best’ 4-metric result (for comparison). The ‘best’ optimizations were selected subjectively as the case with the fewest parameters where model performance is not severely impacted for the metrics considered.

apparent in Figure 3.11b. As for watershed AMI, the 'best' 4-metric result is selected at the same level as the 'best' 2-metric result and includes two additional parameters for a total of 10. Very little difference is observable between Figure 3.7b and 3.7c. (Note Figure 3.7d is identical to 7b since the 2-metric result corresponding to the 'best' 4-metric result is simply again the 'best' 2-metric result in this case). Thus, including the hydrologic metrics for this watershed appears less critical than for EAS and SPR. However, a different reason for this observation is deduced for GUA than it was for watershed AMI (i.e., the near zero a priori ROCE value). In this case, the overlap in parametric sensitivities between the statistical and hydrologic metrics caused important parameters for hydrologic metrics (e.g. LZTWM) to also be included in the 2-metric

reduction for thresholds 0.1 and 0.05. Overall, a reduction in the number of optimized parameters for this watershed appears possible to 8 parameters, the largest number for all watersheds. This likely reflects the model's limitations when representing processes in semi-arid environments, which results in the need to retain more model complexity to improve simulations.

3.6 DISCUSSION

Table 3.3 lists the specifications of the 'best' optimization results for each of the study watersheds (defined subjectively as the case for which the least number of parameters are optimized to produce results close to the full-parameter result). As shown in Table 3.3, the number of optimized parameters in these cases reduces from 14 to 4, 6, 5, and 8 parameters for AMI, EAS, SPR, and GUA, respectively. For three of the four watersheds, the recommended sensitivity threshold would be 0.2, while for one (GUA) the threshold would be 0.05. The lower threshold and greater number of parameters necessary to maintain performance for the GUA watershed (the most arid watershed) is likely related to the difficulty of modeling arid and semi-arid watersheds. More parameters are necessary to maintain acceptable performance to make up for model inadequacies. In addition, as shown in Table 3.3 the parameters that should be included for each watershed also vary. This is not surprising based on large parametric sensitivity differences that exist across the watersheds, particularly between the most arid (e.g., GUA) and most humid (e.g., AMI) watersheds. However, despite some differences, similarities persist. The lower zone free storages for example (LZFSM, LZFPM), should be included in each case due to the high sensitivity of these parameters for most watersheds.

Table 3.3 Four watersheds' best-case reduced-parameter optimization specifications.

ID	Sensitivity threshold	# of params.	Parameters included
AMI	0.2	4	UZFWM, LZFPF, LZFSM, LZPK
EAS	0.2	6	PCTIM, LZTWM, LZFPF, LZFSM, LZSK, LZPK
SPR	0.2	5	ADIMP, LZTWM, LZFPF, LZFSM, LZPK
GUA	0.05	8	PCTIM, ADIMP, RIVA, ZPERC, PREE, LZTWM, LZFPF, LZFSM

The extent and rate at which model performance declines as parameters are removed varies for each case and is dependent on several factors. First, the quality of the a priori estimates strongly influences the impact of removing parameters. Since parameters are fixed to their a priori calculated value once they are removed from the analysis, these values increasingly control the model performance as additional parameters are removed (i.e. down the columns of Figures 3.4, 3.6, 3.8, and 3.10). If the a priori solution (i.e., the metric values for the simulation using all a priori parameters) is close to the fully-optimized solution set with respect to each metric, then less decline in performance will be perceived as parameters are removed (and vice versa). In general, the a priori estimates were somewhat better for the two more humid watersheds (AMI and EAS) and the two more arid watersheds (SPR and GUA). The hydroclimatic characteristics of a watershed (e.g. arid versus humid) are a second factor in the rate of performance decline for the SAC-SMA model. As discussed above, arid systems present greater challenges for hydrologic modeling than humid systems. Therefore, model performance would be expected to decline more rapidly for arid versus humid watersheds as degrees of freedom are removed from the model. This is supported by the results of watershed GUA as compared to watershed AMI. Lastly, *which* and *how many* parameters are removed in each step impacts the extent of performance change. Thresholds values of the Sobol sensitivity index were defined to develop parameter sets (see Figure 3.3). Since

parameter sensitivities vary significantly across the watersheds, which and how many parameters are included for a given threshold also varies for each watershed, as does the impact of a particular set and number of parameters. In some cases, parameters at a lower sensitivity have a larger incremental impact than parameters at a higher sensitivity. Or similarly, a few parameters may have a larger incremental impact than several parameters. Overall, the impact on model performance of fixing parameters to a priori values is likely a complex interaction among all of these factors – the quality of the a priori estimates, the type of watershed, and parameters removed. Therefore, no generalized statement about the sensitivity level above which parameters impact performance is possible. The analysis should be performed on a case by case basis.

The same factors discussed above also impact the importance of including hydrologic metrics in sensitivity-guided calibration. The quality of the a priori estimates influences whether or not such metrics are necessary to ensure that the hydrologic function of the model is acceptable. If the a priori hydrologic metrics are poor (e.g. watershed SPR), it is particularly vital to include these metrics in the analysis to appropriately select and optimize parameters and improve the simulations. However, even if the a priori hydrologic metrics appear to be acceptable, including these metrics may still improve the optimization and result in better performance with fewer parameters (e.g. EAS, Figure 3.6b). The type of watershed also influences the importance of including hydrologic metrics. The results of watershed GUA were similar at low threshold for the 2-metric and 4-metric reductions (i.e., with or without the hydrologic metrics) implying that including these metrics did not significantly improve results. This likely occurred due to the greater overlap that exists in parametric sensitivities for the

SAC-SMA across statistical and hydrologic metrics for semi-arid watersheds. Overall the results of this study underpin the benefit for many cases of including hydrologic metrics in a sensitivity-guided multi-objective calibration approach.

3.7 CONCLUSIONS

This study demonstrates that the number of parameters that must be calibrated for hydrologic models in watersheds across a hydroclimatic gradient can be reduced without a significant impact on model performance if those parameters are selected carefully – based on parametric sensitivities specific to each watershed using both hydrologic and statistical metrics in the analysis. To arrive at this conclusion, we perform multi-objective optimization of the SAC-SMA model for four watersheds using nine different sets of optimized parameters that are selected based on global sensitivity analysis (with non-optimized parameters fixed to a priori values). Four metrics are used in the parameter selection and optimization processes, two statistically-based and two hydrologically-based. Though the experiments reveal that reducing the number of calibrated parameters is possible, a generalized approach (e.g. which sensitivity level, metrics, or parameters to use) for all watersheds is not easily identified due to the differences in parametric sensitivities across watersheds and metrics, as well as the varying quality of a priori estimates. For each watershed, the recommended sensitivity threshold and parameters to include would be different. Though overall, results suggest that in more humid watersheds (e.g. AMI) the number of optimized parameters can be reduced further than in more arid watersheds (e.g. GUA). This is likely due to the combined effect of somewhat poorer a priori estimates in the more arid watersheds and the inadequacy of the model to

represent arid and semi-arid hydrologic processes (e.g. Hortonian overland flow). The importance of including hydrologic metrics (e.g., a water balance and flow regime metric) in a sensitivity-guided calibration approach also becomes evident when comparing results across watersheds. Using only statistically-based metrics (as has been common practice) may lead to poor selection of the optimized parameters and inadequate simulation of the watershed's hydrologic function, as clearly demonstrated by the results of watersheds EAS and SPR. In formulating a sensitivity-based approach to remove less identifiable parameters from the calibration process, differences across hydroclimatic regimes should not be ignored. A dynamic approach that couples sensitivity analysis and optimization on a case-to-case basis, using both statistical and hydrologic metrics, is necessary as shown here.

3.8 CHAPTER 3 REFERENCES

- Anderson, E. A. (2002). Calibration of conceptual hydrologic models for use in river forecasting. *NOAA Tech. Rep. NWS 45*, Hydrol. Lab., Silver Spring, MD.
- Bastidas, L. A., H. V. Gupta, S. Sorooshian, W. J. Suttleworth and Z. L. Yang (1999). Sensitivity analysis of a land surface scheme using multicriteria methods. *J. Geophys. Res.*, *104*(D16), 19481-19490.
- Beven, K. and A. Binley (1992). The Future of Distributed Models - Model Calibration and Uncertainty Prediction. *Hydrol. Process.*, *6*(3), 279-298.
- Beven, K. J. (1989). Changing ideas in hydrology - the case of physically-based models. *J. Hydrol.*, *105*(1-2), 157-172.
- Boyle, D. P., H. V. Gupta and S. Sorooshian (2000). Toward improved calibration of hydrologic models: Combining the strengths of manual and automatic methods. *Water Resour. Res.*, *36*(12), 3663-3674.
- Boyle, D. P., H. V. Gupta, S. Sorooshian, V. Koren, Z. Y. Zhang and M. Smith (2001). Toward improved streamflow forecasts: Value of semidistributed modeling. *Water Resour. Res.*, *37*(11), 2749-2759.
- Budyko, M. I. (1974). *Climate and Life*, Academic, San Diego, CA.
- Burnash, R. J. C. (1995). The NWS River Forecast System - catchment model, in *Computer Models of Watershed Hydrology*, V.P. Singh (Editor), pp. 311-366, Water Resour. Publ., Highlands Ranch, CO.

- Cox, G. M., J. M. Gibbons, A. T. A. Wood, J. Craigon, S. J. Ramsden and N. M. J. Crout (2006). Towards the systematic simplification of mechanistic models. *Ecological Modelling*, 198(1-2), 240-246.
- Deb, K. (2001). *Multi-objective optimization using evolutionary algorithms*, John Wiley & Sons LTD., New York.
- Deb, K. and R. B. Agrawal (1994). Simulated binary crossover for continuous search space. Tech Rep IITK/ME/SMD-94027, Indian Institute of Technology, Kanpur.
- Deb, K., A. Pratap, S. Agarwal and T. Meyarivan (2002). A Fast and Elitist Multiobjective Genetic Algorithm: NSGA-II. *IEEE Trans. Evol. Computation*, 6, 182-197.
- Duan, Q., J. Schaake and V. Koren (2001). A Priori estimation of land surface model parameters, in *Land Surface Hydrology, Meteorology, and Climate, Observations and Modeling*, V. Lakshmi, J. Albertson and J. Schaake (Editors), pp. 77-94, AGU, Washington, D.C.
- Duan, Q., J. Schaake, V. Andreassian, S. Franks, G. Goteti, H. V. Gupta, Y. M. Gusev, F. Habets, A. Hall, L. Hay, T. Hogue, M. Huang, G. Leavesley, X. Liang, O. N. Nasonova, J. Noilhan, L. Oudin, S. Sorooshian, T. Wagener and E. F. Wood (2006). Model Parameter Estimation Experiment (MOPEX): An overview of science strategy and major results from the second and third workshops. *J. Hydrol.*, 320(1-2), 3-17.
- Duan, Q. Y., S. Sorooshian and V. Gupta (1992). Effective and Efficient Global Optimization for Conceptual Rainfall-Runoff Models. *Water Resour. Res.*, 28(4), 1015-1031.
- Gan, T. Y. and S. J. Burges (2006). Assessment of soil-based and calibrated parameters of the Sacramento model and parameter transferability. *J. Hydrol.*, 320(1-2), 117-131.
- Gupta, H. V., S. Sorooshian and P. O. Yapo (1998). Toward improved calibration of hydrologic models: Multiple and noncommensurable measures of information. *Water Resour. Res.*, 34(4), 751-763.
- Hall, J. W., S. Tarantola, P. D. Bates and M. S. Horritt (2005). Distributed sensitivity analysis of flood inundation model calibration. *J. Hydr. Engrg.*, 131(2), 117-126.
- Harik, G. R. and F. G. Lobo (1999). A parameter-less genetic algorithm, Tech Rep IlliGAL 99009, University of Illinois at Urbana-Champaign.
- Hogue, T. S., H. V. Gupta and S. Sorooshian (2006). A 'user-friendly' approach to parameter estimation in hydrologic models. *J. Hydrol.*, 320(1-2), 202-217.
- Huang, M. Y. and X. Liang (2006). On the assessment of the impact of reducing parameters and identification of parameter uncertainties for a hydrologic model with applications to ungauged basins. *J. Hydrol.*, 320(1-2), 37-61.
- Kollat, J. B. and P. M. Reed (2005). The value of online adaptive search: A performance comparison of NSGAI, epsilon-NSGAI and epsilon MOEA. *Evolutionary Multi-Criterion Optimization*, 3410, 386-398.
- Kollat, J. B. and P. M. Reed (2006). Comparing state-of-the-art evolutionary multi-objective algorithms for long-term groundwater monitoring design. *Adv. Water Resour.*, 29(6), 792-807.

- Koren, V. (2000). Use of soil property data in the derivation of conceptual rainfall-runoff model parameters, in *Proceedings of the 15th Conference on Hydrology*, pp. 103-106, AMS, Long Beach, CA.
- Koren, V., M. Smith and Q. Duan (2003). Use of a priori parameter estimates in the derivation of spatially consistent parameter sets on rainfall-runoff models, in *Calibration of Watershed Models*, Q. Duan, H. Gupta, S. Sorooshian, H. Rosseau and R. Turcotte (Editors), pp. 239-254, AGU, Washington, D.C.
- Koren, V. I., B. D. Finnerty, J. C. Schaake, M. B. Smith, D. J. Seo and Q. Y. Duan (1999). Scale dependencies of hydrologic models to spatial variability of precipitation. *J. Hydrol.*, 217(3-4), 285-302.
- Laumanns, M., L. Thiele and E. Zitzler (2004). An adaptive scheme to generate the pareto front based on the epsilon-constraint method. TIK-Report No.199, Computer Engineering and Networks Laboratory (TIK), Swiss Federal Institute of Technology (ETH), Zurich.
- Saltelli, A. (2002). Making best use of model evaluations to compute sensitivity indices. *Comput. Phys. Commun.*, 145(2), 280-297.
- Sobol', I. M. (1993). Sensitivity estimates for nonlinear mathematical models. *Math. Model. Comput. Exp.*(1), 407-417.
- Sobol', I. M. (2001). Global sensitivity indices for nonlinear mathematical models and their Monte Carlo estimates. *Math. Comput. Simulat.*, 55, 271-280.
- Sorooshian, S., Q. Y. Duan and V. K. Gupta (1993). Calibration of Rainfall-Runoff Models - Application of Global Optimization to the Sacramento Soil-Moisture Accounting Model. *Water Resour. Res.*, 29(4), 1185-1194.
- Tang, Y., P. M. Reed and T. Wagener (2006). How effective and efficient are multiobjective evolutionary algorithms at hydrologic model calibration? *Hydrol. Earth Syst. Sci.*, 10(2), 289-307.
- Tang, Y., P. M. Reed and J. B. Kollat (2007a). Parallelization strategies for rapid and robust evolutionary multiobjective optimization in water resources applications. *Adv. Water Resour.*, 30(3), 335-353.
- Tang, Y., P. M. Reed, T. Wagener and K. van Werkhoven (2007b). Comparing sensitivity analysis methods to advance lumped watershed model identification and evaluation. *Hydrol. Earth Syst. Sci.*, 11, 793-817.
- van Werkhoven, K., T. Wagener, P. Reed and Y. Tang (2008). Characterization of watershed model behavior across a hydroclimatic gradient. *Water Resour. Res.*, 44, W01429, doi:10.1029/2007WR006271.
- Vrugt, J. A., H. V. Gupta, L. A. Bastidas, W. Bouten and S. Sorooshian (2003). Effective and efficient algorithm for multiobjective optimization of hydrologic models. *Water Resour. Res.*, 39(8), 1214, doi:10.1029/2002WR001746.
- Wagener, T. and H. S. Wheater (2006). Parameter estimation and regionalization for continuous rainfall-runoff models including uncertainty. *J. Hydrol.*, 320(1-2), 132-154.
- Wagener, T. and J. Kollat (2007). Visual and numerical evaluation of hydrologic and environmental models using the Monte Carlo Analysis Toolbox (MCAT). *Environmental Modeling and Software*, 22, 1021-1033.

- Wagener, T., N. McIntyre, M. J. Lees, H. S. Wheater and H. V. Gupta (2003). Towards reduced uncertainty in conceptual rainfall-runoff modelling: Dynamic identifiability analysis. *Hydrol. Process.*, 17(2), 455-476.
- Wagener, T., D. P. Boyle, M. J. Lees, H. S. Wheater, H. V. Gupta and S. Sorooshian (2001). A framework for development and application of hydrological models. *Hydrol. Earth Syst. Sci.*, 5(1), 13-26.
- Yapo, P. O., H. V. Gupta and S. Sorooshian (1998). Multi-objective global optimization for hydrologic models. *J. Hydrol.*, 204(1-4), 83-97.

CHAPTER 4

Phase II: Rainfall Characteristics Define the Value of Streamflow Observations for Distributed Watershed Model Identification

Based on:

van Werkhoven, K., T. Wagener, P. Reed, and Y. Tang. (2008). Rainfall characteristics define the value of streamflow observations for distributed watershed model identification. *Geophysical Research Letters*, 35, doi:10.1029/2008GL034162.

4.1 INTRODUCTION

A growing shift from lumped to distributed models has been occurring within the hydrology community for a wide range of applications [Smith *et al.*, 2004]. Despite some clear advantages of distributed models, the parameter identification process can be hindered by the fact that streamflow observations are often only available for the integrated hydrologic response at the watershed outlet. Our understanding of the information contained in streamflow observations and the value of this information for distributed model identification is not yet well-established. This knowledge gap has significant implications for our ability to predict the watershed response and to inform the design of observation networks using distributed hydrologic models.

Previous studies and parameter estimation approaches for distributed conceptual models have commonly assumed that their parametric sensitivities do not vary in space and time, thus ignoring the dynamic nature of the parameter identification problem [e.g., Leavesley *et al.*, 2003; Madsen, 2003; Carpenter and Georgakakos, 2004; Muleta and Nicklow, 2005]. Tang *et al.* [2007] demonstrated that the distribution of precipitation significantly influences the location of identifiable regions within a distributed model grid, while also suggesting that other factors such as cell location and initial states may also have an influence. However the experimental structure of their study, which evaluated parameter sensitivities based on two past events of precipitation and antecedent moisture conditions, made it difficult to fully isolate and assess the impacts of individual controlling factors. Sensitivity within the routing component of the model also was not considered. Furthermore, the conclusions of this work did not account for uncertainty in the data and in the representation of the real world system, which unavoidably adds noise

to such an analysis. The use of virtual experiments is an alternative approach, which allows for the in-depth analysis of model behavior in a synthetic and thus error free environment [Bashford *et al.*, 2002; Weiler and McDonnell, 2004; Winter *et al.*, 2004].

The study presented here uses global sensitivity analysis to fully evaluate a common conceptual distributed model across the spatial domain and to identify regions (in the model grid space) that control the model response behavior. The impacts of relevant event characteristics (i.e., precipitation distribution, initial soil-moisture state distribution, and active grid cell location) on these controlling regions, and therefore on the parameters that could be identified during calibration, are isolated using specific scenarios of synthetic data. A strong relationship between event characteristics and parameter sensitivity would indicate that significant spatio-temporal variations exist in the information content of the available observations, which may bias model identification.

4.2 MODEL DESCRIPTION

Many grid-based distributed hydrologic models establish a cell-to-cell connectivity only through surface channel routing, i.e., the cells are not connected in the subsurface [e.g., Liang *et al.*, 2004] Several more complex, integrated models that include subsurface connectivity have also been developed [e.g., VanderKwaak and Loague, 2001; Panday and Huyakorn, 2004; Kollet and Maxwell, 2006; Qu and Duffy, 2007], however, the simpler surface-connected models continue to be widely used in both research and operational environments. One example of such a simpler model is used here – the National Weather Service's (NWS) Hydrology Laboratory Distributed Hydrologic

Modeling System (HL-DHMS) [Koren *et al.*, 2004]. The HL-DHMS is based on a structure of approximately 4 x 4 km grid cells, each of which consists of a conceptual water balance component, a hillslope routing component, and a channel routing component. The Sacramento Soil Moisture Accounting Model (SAC-SMA) [Burnash, 1995] is typically used as the water balance component (see Figure 2.3) and the kinematic wave method is used for hillslope and channel routing. The 14 main SAC-SMA parameters are included in the analysis (Table 4.1). For kinematic wave hillslope (overland) routing, only the roughness parameter (hill- n) is included in the analysis, as the other two parameters (slope and drainage density) were estimated from DEM data as part of the Distributed Model Intercomparison Project (DMIP) of the NWS [Reed *et al.*, 2004] and are usually not considered variable. For channel routing, we used the ‘rating curve’ method of HL-DHMS [see Koren *et al.*, 2004] in which the two parameters q_o and m of the kinematic wave equation $q=q_oA^m$ are estimated directly rather than by calculating them from physical properties of the channel. Thus a total of 17 parameters (14 SAC-SMA, 1 hillslope routing, and 2 channel routing) were included for each grid cell in the sensitivity analyses of this study (see Table 4.1). Note that the hillslope and channel routing models are treated as one combined model in the discussion and presentation of results.

4.3 SOBOL’ SENSITIVITY ANALYSIS

Sobol's sensitivity analysis method [Sobol', 1993] is a variance-based approach in which the model output variance is decomposed into relative contributions from individual parameters and parameter interactions, as follows:

Table 4.1 Description of SAC-SMA and routing parameter descriptions, a priori grid ranges, and sensitivity analysis ranges.

Parameter	Description	NWS a priori grid range	Sensitivity analysis range
uztwm	Upper zone tension water maximum storage	24 – 65	19.2 – 78
uzfwm	Upper zone free water maximum storage	11 – 54	8.8 – 64.8
uzk	Upper zone free water withdrawal rate	0.19 – 0.76	0.152 – 0.912
pctim	% permanent impervious area	0	0 – 0.05
adimp	% saturated impervious area	0	0 – 0.2
riva	% area affected by riparian vegetation	0	0 – 0.2
zperc	Maximum dry condition percolation rate	34 – 117	27.2 – 140.4
rexp	Percolation equation exponent	2.11 – 2.89	1.69 – 3.47
pfree	% percolation going to lower zone free water	0.2 – 0.46	0.16 – 0.55
lztwm	Lower zone tension water max storage	77 – 208	61.6 – 249.6
lzfpw	Lower zone free water primary max storage	11 – 49	8.8 – 58.8
lzfsm	Lower zone free water supp. max storage	24 – 161	19.2 – 193.2
lzpk	Lower zone primary withdrawal rate	0.051 – 0.22	0.0408 – 0.264
lzsk	Lower zone supplementary withdrawal rate	0.0021 – 0.0146	0.00168 – 0.0175
hill-n	Overland roughness coefficient	0.15	0.12 – 0.18
qo	Channel routing coefficient	0.195 – 0.4525	0.156 – 0.543
m	Channel routing exponent	1.263	1.0104 – 1.5156

$$D(f) = \sum_i D_i + \sum_{i<j} D_{ij} + \sum_{i<j<k} D_{ijk} + D_{12\dots p} \quad (4.1)$$

where p is the total number of parameters, f is the distribution of model output, $D(f)$ is the full model output variance, D_i is the output variance due to the i th component of the input parameter vector Θ , D_{ij} is the output variance due to the interaction of parameters θ_i and θ_j ; and the final two terms represent third-order and greater interactions. In this study, each model parameter in each grid cell is treated as an individual parameter. Thus the total number of parameters analyzed (1326) is the number of parameters per cell (17) times the total number of cells (78). A given parameter's sensitivity is quantified by the ratio of its variance contribution to the full (i.e., due to all parameters) output variance, resulting in an index value ranging from 0 to 1. The ‘total’ Sobol sensitivity index used in this study reflects the combined effect of the parameter alone (i.e., individual sensitivity) plus its interactions with all other parameters in the analysis. The total index, S_{Ti} , is defined as:

$$S_{Ti} = 1 - \frac{D_{\sim i}}{D} \quad (4.2)$$

where D is the full output variance and $D_{\sim i}$ is the variance resulting from all of the parameters *except* θ_i . In other words, if parameter θ_i were removed from the analysis, the resulting reduction in output variance is equivalent to the total impact of parameter θ_i . Using a Monte Carlo framework, the full output variance is approximated as the statistical variance of the output distribution and the variance contribution $D_{\sim i}$ is approximated as follows:

$$\hat{D}_{\sim i} = \frac{1}{n} \sum_{s=1}^n f(\Theta_s^{(a)}) f(\Theta_{(-i)s}^{(a)}, \Theta_{is}^{(b)}) - \hat{f}_o^2 \quad (4.3)$$

where (a) and (b) are two different samples (both of size n), f_o is the output statistical mean, $\Theta_s^{(a)}$ implies that all parameters are taken from sample (a) , $\Theta_{(-i)s}^{(a)}$ implies that all parameters *except* θ_i are taken from sample (a) , and $\Theta_{is}^{(b)}$ implies that parameter θ_i is taken from sample (b) . For more details on Sobol's method see *Sobol'* [1993], *Saltelli* [2002], or *van Werkhoven et al.* [2008]. For the purpose of this study, the model output variance is measured by the commonly-used root mean square error (RMSE), which we assume is appropriate to capture event-based behavior. The RMSE is defined as,

$$RMSE = \sqrt{\frac{1}{m} \sum_{t=1}^m (Q_{s,t} - Q_{o,t})^2} \quad (4.4)$$

where m is the number of time steps, $Q_{s,t}$ is the simulated flow for time step t , and $Q_{o,t}$ is the observed flow in time step t . For each sensitivity analysis, we used a sample size (n) of 3000, which is adequate based on minimum sample size recommendations for Sobol's method (500-1000) reported by *Saltelli et al.* [2008]. The number of model simulations required for Sobol's method is equal to $n(k+2)$, where n is the sample size (3000) and k is

the number of parameters (1326). Thus a total of 3,984,000 model simulations were performed for each sensitivity analysis experiment discussed in Section 4.4.

4.4 EXPERIMENTAL DESIGN

The sensitivity analysis experiments in this study were performed using synthetic data designed to isolate and characterize the controlling factors of distributed model behavior. The grid structure of the Blue River Basin in southern Oklahoma was used as the study basin for the analyses. The basin is represented using 78 grid cells in an elongated shape (see Figures 4.1-4.2) resulting in a total basin area of 1248 km². Five scenarios of precipitation were designed, including a spatially-uniform frontal storm event and four spatially-distributed convective storm events (an upper basin stationary storm, lower basin stationary storm, a storm moving downstream in the basin, and a storm moving upstream in the basin). The precipitation events were temporally distributed using design storm hyetographs defined by the US Department of Agriculture Soil Conservation Service [1986] for convective and frontal events. The spatial structure of the storm cell for the convective events is based on a circular Gaussian distribution with maximum intensity at the cell center [*Sivapalan and Wood, 1987; Morin et al., 2006*]. For each of the five scenarios, we applied a maximum 24-hour precipitation accumulation (P_{tot}) of 157 mm, based on the 10-year return period for a 24-hour event for the basin location (i.e., applied to the cell center for the convective cases and all cells for the uniform case). The spatial and temporal distributions of P_{tot} are shown in Figures 4.1a (uniform case) and Figure 4.2a-d (convective cases). In addition to multiple scenarios of precipitation, we applied two different scenarios of initial soil-moisture states (S_i) to allow for an

assessment of the impact of initial states on model behavior. The first scenario assumed that values of S_i were spatially-homogeneous and the values represent wet basin conditions. To obtain reasonable values, a large uniform precipitation event was simulated and the six SAC-SMA model states that occurred following the event were selected as initial states for the first scenario (Table 4.2). For the second scenario, random values of the initial states were assigned to each cell to reflect typical dry conditions. As described by *Grayson and Bloschl* [2001], the spatial correlation of soil-moisture states declines as a watershed becomes dry and can approach a random spatial pattern with little or no remaining influence of watershed physical characteristics. Thus, the assumption of randomly-distributed initial states was used for the variable-state scenario and to represent dry conditions.

Table 4.2 Values and ranges for the two scenarios of SAC-SMA initial states.

State	Description	Scenario 1 constant	Scenario 2 range
uztwc	Upper zone tension water contents	0.5	0.0 – 1.0
uzfwc	Upper zone free water contents	0	0.0 – 1.0
adimpc	Additional impervious area contents	1	0.0 – 1.0
lztwc	Lower zone tension water contents	1	0.0 – 1.0
lzfsc	Lower zone free water supplemental contents	0.5	0.0 – 1.0
lzfpc	Lower zone free water primary contents	1	0.0 – 1.0

A total of six sensitivity analysis experiments were designed by combining the five precipitation scenarios and two initial states scenarios as follows: (1) uniform P_{tot} and uniform S_i , (2) uniform P_{tot} and random S_i , (3) upper storm P_{tot} and uniform S_i , (4) lower storm P_{tot} and uniform S_i , (5) moving upstream P_{tot} and uniform S_i , and (6) moving downstream P_{tot} and uniform S_i . Experiments (1) and (2) allow for an assessment of the impact of cell location and initial states, respectively. While experiments (3)-(6) focus on the impact of non-uniform precipitation distribution on model behavior across the basin. For each experiment, Sobol's method is executed twice – once to analyze the SAC-SMA

model and routing model parameters simultaneously and once to analyze the SAC-SMA model parameters separately. Synthetic observations of streamflow were generated by running the HL-DHMS with a priori values provided by the NWS. In the sensitivity analyses, parameter values were allowed to vary across a range equal to the a priori grid minimum value minus 20% and the a priori grid maximum plus 20%. The experiments were performed using a 1-hour model time step over a 10-day period.

4.5 RESULTS

Results of the sensitivity analyses are shown in Figures 4.1 and 4.2. Each section of the figures (e.g., Figure 4.1a) corresponds to one of the sensitivity experiments described above. In each case, the spatial distributions of total accumulated rainfall (P_{tot}) and resulting sensitivity indices are plotted, along with the synthetic streamflow hydrographs. The three maps of sensitivity indices correspond to the two separate executions of Sobol's method for each case. The first two sensitivity index grids ("SAC + ROUT") are the results for the SAC-SMA model (left) and routing model (middle) when all parameters of the two models were analyzed simultaneously. The third grid ("SAC only") is the results for the SAC-SMA model when analyzed separately (i.e., with routing parameters fixed to constant a priori values). The cell values reflect the sum of all the parameters' indices for the given model (i.e., the sum of 14 indices for SAC-SMA and the sum of 3 parameters for the routing model). Grids of individual parameter results were generated and are included as Figures 4.3-4.5 for experiments (1)-(3). In addition, parameter contributions to the total mean areal sensitivity in each case are summarized in Figure 4.6. The reason for the two executions of Sobol's method for each case is the

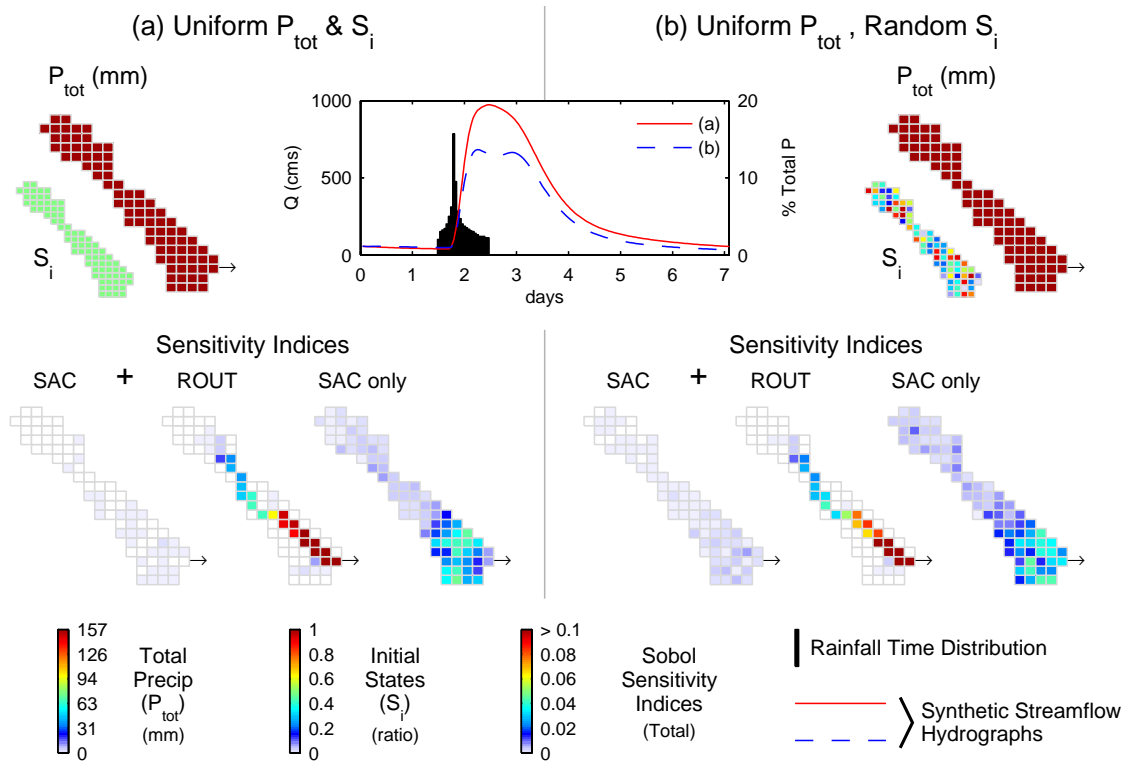


Figure 4.1 Spatially distributed parameter sensitivity for cases of (a) uniform total precipitation (P_{tot}) and uniform initial states (S_i) and (b) uniform precipitation and nonuniform initial states. Sensitivity indices are the total of all model parameters for a given cell. Indices are presented for the SAC-SMA and routing model analyzed simultaneously (SAC + ROUT – left two maps) and for the SAC-SMA analyzed separately (SAC only – right map).

dominance of the routing model when the two models are run together (e.g., see Figure 4.1a – SAC + ROUT), which caused the SAC-SMA results to be masked.

The first experiment’s results (uniform P_{tot} and uniform S_i – Figure 4.1a) clearly show the impact of cell location on model sensitivity. The importance of routing parameters significantly increases along the channel toward the basin outlet. A region of high sensitivity near the outlet also emerges in the “SAC only” analysis. Since both rainfall and initial states are spatially constant in this case, the main pattern of spatial variation in sensitivity can be attributed to cell location with respect to the outlet. Some small scale variation is likely also due to numerical approximation in the sensitivity analysis. The impact of initial states can be assessed by comparing Figures 4.1a and 4.1b.

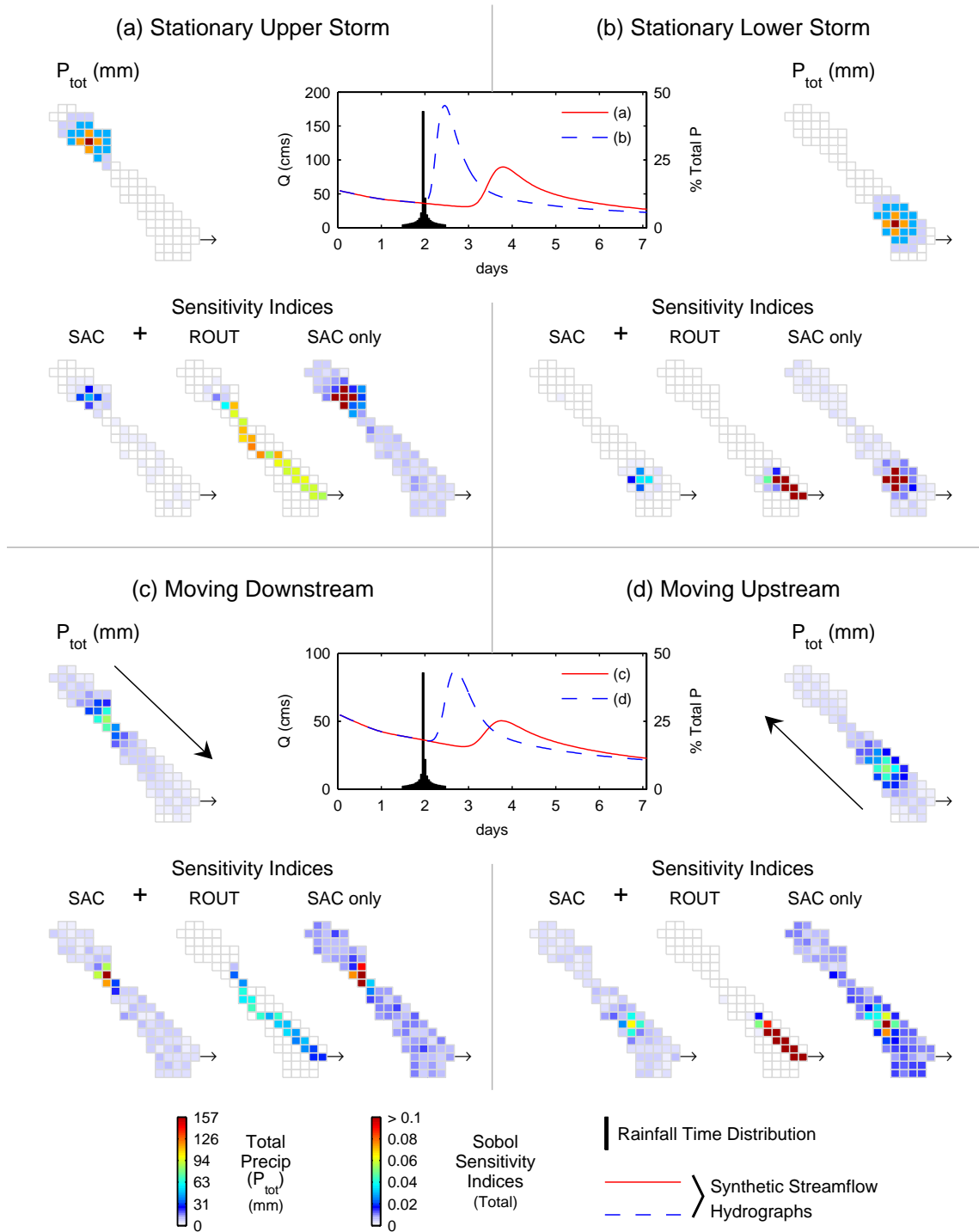


Figure 4.2 Spatially distributed parameter sensitivity for 4 different distributed storm events - (a) an upper basin stationary storm (b) a lower basin stationary storm (c) a storm moving downstream and (d) a storm moving upstream. Sensitivity indices are the total of all model parameters' indices for a given cell. In each case, indices are presented for the SAC-SMA and routing model analyzed simultaneously (SAC + ROUT – left two maps) and for the SAC-SMA analyzed separately (SAC only – right map).

The dominant patterns of sensitivity (increase towards the outlet) are maintained with some slight increase in variation in the upper part of the basin. The impact of initial states thus appears minimal in comparison to the impact of cell location.

Figure 4.2 demonstrates the strong impact of the precipitation spatial distributions on the model sensitivity distributions. For all storms (Figures 4.2a-d), the dominance of the routing parameters is less pronounced as some measurable sensitivity occurs for SAC-SMA at the location of the storm center for the combined (SAC+ROUT) analyses (as opposed to Figure 4.1). In these cases, the routing parameter sensitivity no longer increases continuously towards the basin outlet as was seen in Figure 4.1. Here the routing sensitivity appears to be impacted by the location of the precipitation event with respect to the basin outlet, resulting in a somewhat more even distribution of sensitivity from the localized precipitation to the outlet (e.g., Figure 4.2a). For the two stationary events (i.e., Figures 4.2a and 4.2b), the “SAC only” cases resulted in very clear correlations to the total precipitation distribution. The sensitivity in the remainder of the basin (where precipitation did not occur) is primarily due to the lower zone parameters, which control the baseflow that results from initial soil moisture states. Thus while some information exists in the data for the baseflow components of the model across the full grid (if the initial states are wet), information exists only where precipitation occurs for the surface runoff components. Similar results are found for the two dynamic storms (Figures 4.2c and 4.2d) although, in those cases, the precipitation (and thus sensitivity) occurs across most of the grid with a few cells of highest accumulation (and thus highest sensitivity) where the storm is located at maximum intensity. Overall the sensitivity experiments in Figure 4.2 demonstrate that when localized precipitation occurs in the

basin, the precipitation distribution becomes the dominant control on spatial information content across the model domain. Results for three additional metrics – TRMSE, ROCE and SFDCE (defined in Chapter 2) – are included in Appendix A.

4.6 CONCLUSIONS

This study demonstrates that the information contained in integrated observations of streamflow response for distributed watershed model identification is not evenly distributed in space and time across the model domain. These results are representative for distributed models that connect cells through the channel without explicit subsurface connectivity, though the strong impact of precipitation distribution is likely to extend to more complex models. We show that for the type of model used here, regions of high information content are controlled by the spatial distribution of precipitation, as well as the location of a particular cell with respect to the watershed outlet. Thus, given the spatiotemporal variability of precipitation, information content for distributed model identification also becomes a dynamic variable. New dynamic procedures are required to account for this effect and optimally utilize the observations for model calibration. Ignoring the dynamic nature of information content (e.g., adjusting parameters in regions where precipitation did not occur for a given event) may introduce significant parameter estimation error. Results also indicate that for some storm types, the value of streamflow observations for model identification is limited to a finite distance upstream of the gauge. This knowledge combined with an analysis of dominant precipitation patterns for a given region would provide valuable guidance for the optimal design of streamflow observational networks.

Uniform P_{tot} & S_i – All Parameters

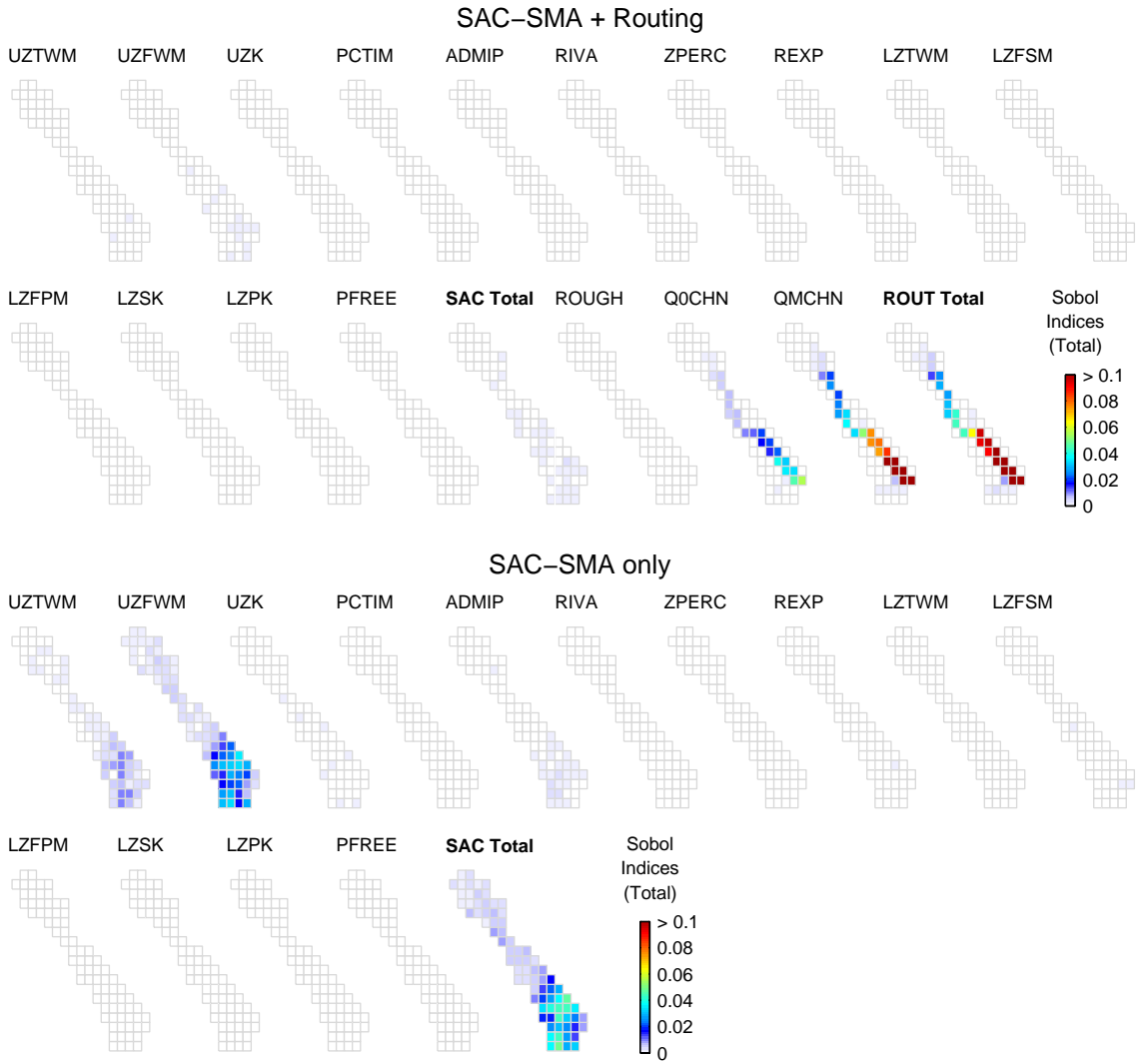


Figure 4.3 Individual parameter grids resulting from the sensitivity analysis for Experiment 1 – uniform precipitation (P) and uniform initial states (S_i)

Uniform P_{tot} , Random S_i – All Parameters

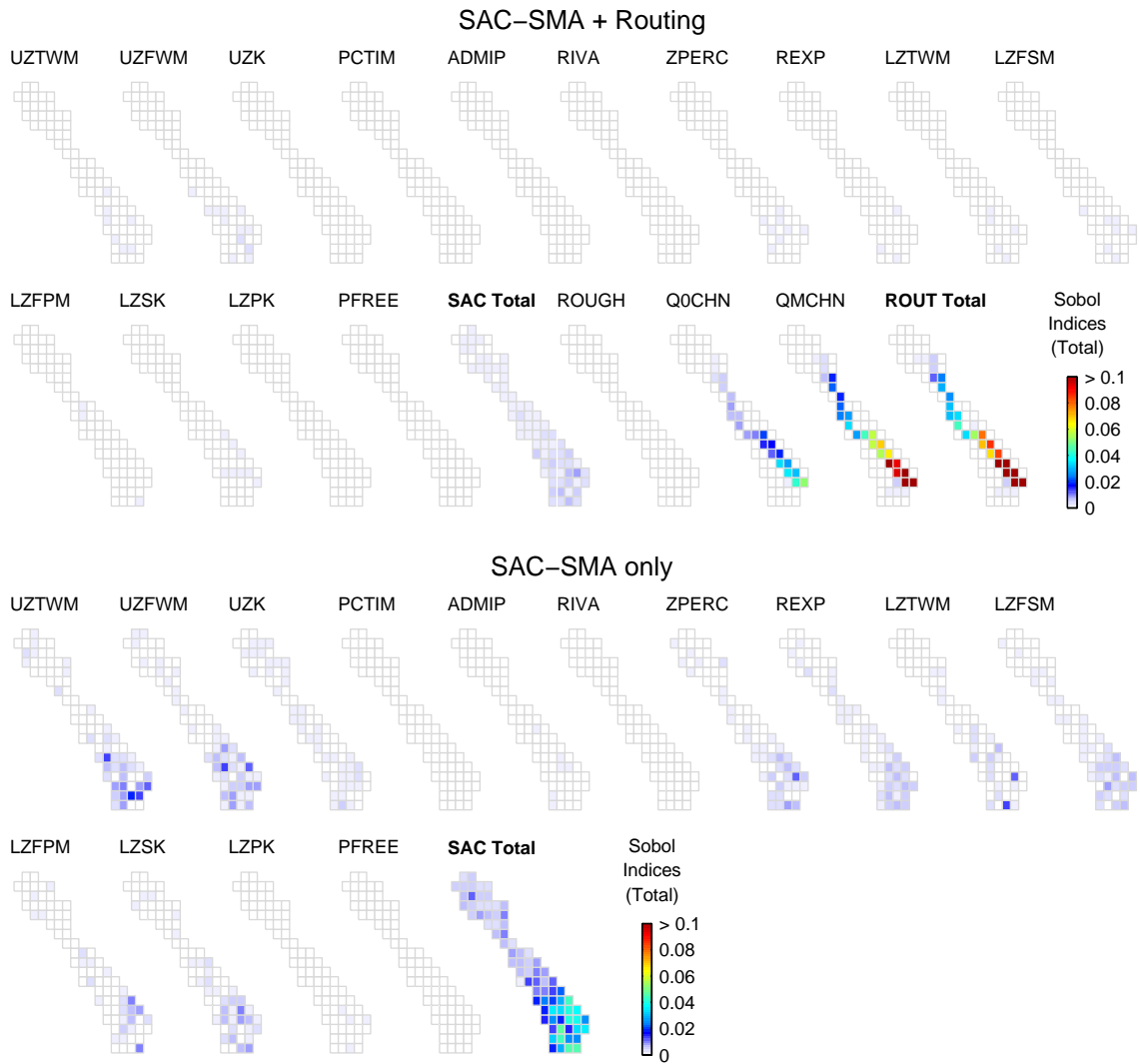


Figure 4.4 Individual parameter grids resulting from the sensitivity analysis for Experiment 2 – uniform precipitation (P) and randomly varying initial states (S_i)

Upper Storm – All Parameters

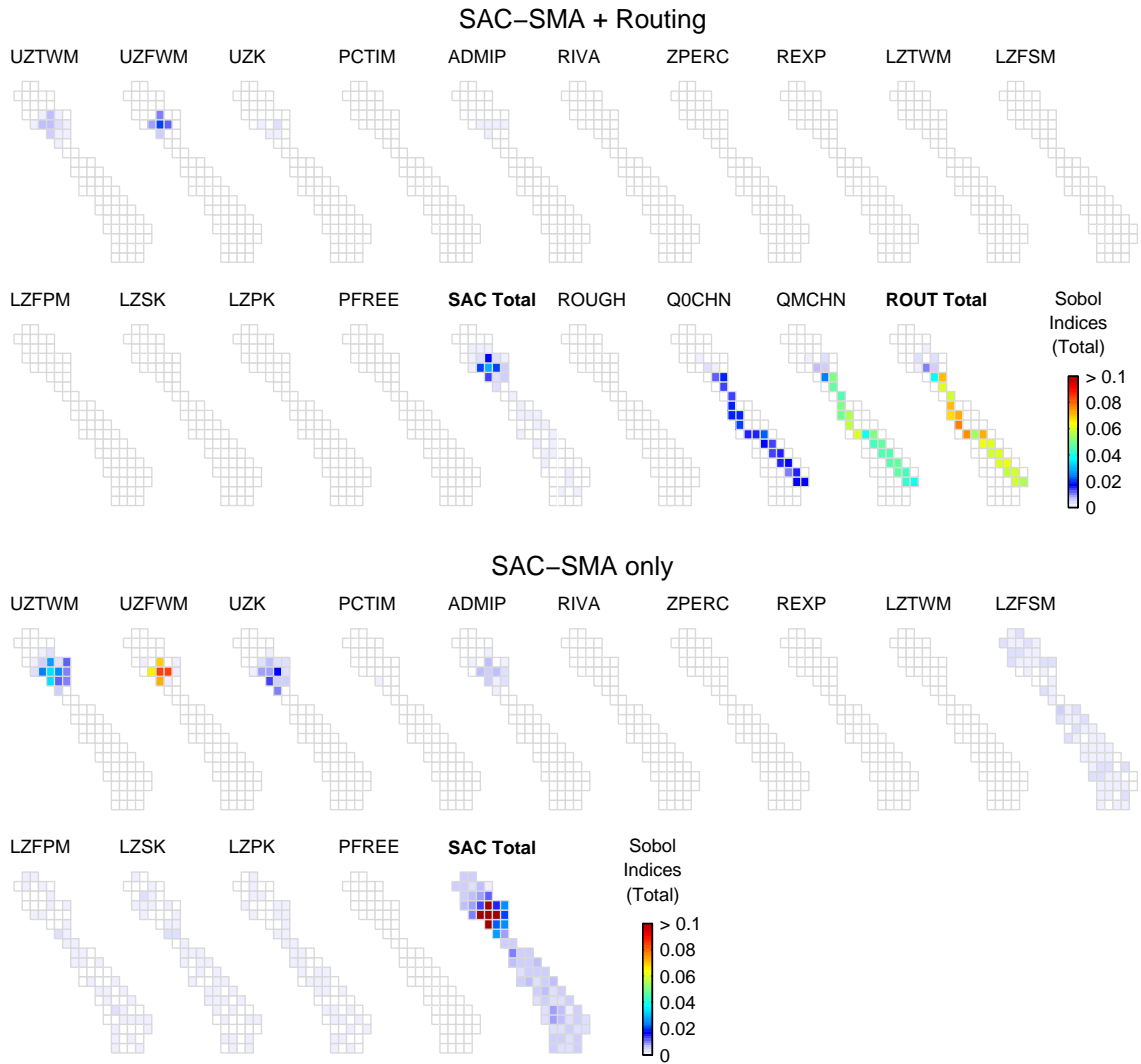


Figure 4.5 Individual parameter grids resulting from the sensitivity analysis for Experiment 3 – localized precipitation (P) in the upper part of the basin and uniform initial states (Si)

	Uniform		Uniform Random		Upper Uniform		Lower Uniform		Moving down Uniform		Moving up Uniform	
	SAC + ROUT		SAC only		SAC + ROUT		SAC only		SAC + ROUT		SAC only	
	SAC + ROUT	SAC only	SAC + ROUT	SAC only	SAC + ROUT	SAC only	SAC + ROUT	SAC only	SAC + ROUT	SAC only	SAC + ROUT	SAC only
uztwm	0.5	18.2	1.1	15.8	2.5	18.9	1.2	12.1	10.7	19.5	4.8	15.6
uzfwm	1.7	70.1	1.8	15.3	3.9	34.4	4.7	62.6	10.6	14.8	5.3	17.6
uzk	0.3	2.2	0.7	6.5	0.8	8.2	0.3	3.3	4.0	7.9	1.2	3.0
pctim	0.0	0.5	0.1	0.6	0.1	0.6	0.1	0.8	0.4	0.3	0.2	0.4
adimp	0.3	4.8	0.3	1.4	0.7	5.1	0.6	6.7	2.5	3.7	1.7	4.9
riva	0.0	0.0	0.0	0.0	0.0	0.1	0.0	0.0	0.1	0.1	0.0	0.1
zperc	0.0	0.2	1.2	10.7	0.0	0.0	0.0	0.1	0.0	0.0	0.0	0.1
rexp	0.1	0.7	0.8	11.0	0.0	0.2	0.0	0.1	0.0	0.1	0.1	0.1
lztwm	0.0	0.2	0.8	7.4	0.0	0.1	0.0	0.1	0.0	0.1	0.0	0.1
lzfsm	0.1	1.5	1.1	11.8	1.1	12.8	0.4	4.7	8.7	22.3	5.4	21.6
lzfpn	0.0	0.2	0.6	7.8	0.6	6.3	0.4	4.0	5.0	9.9	3.9	14.2
lzsk	0.1	1.1	1.3	10.3	0.7	6.9	0.3	2.1	5.2	10.1	2.7	7.6
lzpk	0.0	0.2	0.2	1.2	0.7	6.6	0.3	3.3	5.5	11.4	3.4	14.7
pfree	0.0	0.0	0.0	0.1	0.0	0.0	0.0	0.0	0.0	0.0	0.0	0.0
hill-n	0.0		0.0		0.0		0.0		0.0		0.0	
q _o	20.6		20.8		22.9		21.7		13.4		17.9	
m	76.1		69.0		65.7		70.1		33.9		53.3	

Figure 4.6 Relative impacts of model parameters for each scenario of total precipitation (P_{tot}), initial states (S_i), and model analysis (i.e., combined SAC+ROUT or SAC only). Values are percentages of total (sum of all parameters) mean areal sensitivity indices. Shades of gray also reflect the magnitude of the values.

4.7 CHAPTER 4 REFERENCES

- Bashford, K., K. Beven and P. Young (2002). Observational data and scale-dependent parameterizations: explorations using a virtual hydrological reality. *Hydrol. Process.*, 16, 293-312.
- Burnash, R. J. C. (1995). The NWS River Forecast System - catchment model, in *Computer Models of Watershed Hydrology*, V.P. Singh (Editor), pp. 311-366, Water Resour. Publ., Highlands Ranch, CO.
- Carpenter, T. M. and K. P. Georgakakos (2004). Continuous streamflow simulation with the HRCDHM distributed hydrologic model. *J. Hydrol.*, 298(1-4), 61-79.
- Grayson, R. and G. Bloschl (Editors) (2001). *Spatial Patterns in Catchment Hydrology: Observations and Modeling*. Cambridge University Press, Cambridge, UK.
- Kollet, S. J. and R. M. Maxwell (2006). Integrated surface-groundwater flow modeling: A free-surface overland flow boundary condition in a parallel groundwater flow model. *Adv. Water Resour.*, 29(7), 945-958.
- Koren, V., S. Reed, M. Smith, Z. Zhang and D. J. Seo (2004). Hydrology Laboratory Research Modeling System (HL-RMS) of the US National Weather Service. *J. Hydrol.*, 291(3-4), 297-318.
- Leavesley, G., L. Hay, R. J. Viger and S. L. Markstrom (2003). Use of a priori parameter estimation methods to constrain calibration of distributed parameter models, in *Calibration of Watershed Models*, Q. Duan, H. Gupta, S. Sorooshian, H. Rosseau and R. Turcotte (Editors), pp., American Geophysical Union.
- Liang, X., J. Z. Guo and L. R. Leung (2004). Assessment of the effects of spatial resolutions on daily water flux simulations. *J. Hydrol.*, 298(1-4), 287-310.

- Madsen, H. (2003). Parameter estimation in distributed hydrological catchment modelling using automatic calibration with multiple objectives. *Adv. Water Resour.*, 26(2), 205-216.
- Morin, E., D. C. Goodrich, R. A. Maddox, X. G. Gao, H. V. Gupta and S. Sorooshian (2006). Spatial patterns in thunderstorm rainfall events and their coupling with watershed hydrological response. *Adv. Water Resour.*, 29(6), 843-860.
- Muleta, M. K. and J. W. Nicklow (2005). Sensitivity and uncertainty analysis coupled with automatic calibration for a distributed watershed model. *J. Hydrol.*, 306(1-4), 127-145.
- Panday, S. and P. S. Huyakorn (2004). A fully coupled physically-based spatially-distributed model for evaluating surface/subsurface flow. *Adv. Water Resour.*, 27(4), 361-382.
- Qu, Y. Z. and C. J. Duffy (2007). A semidiscrete finite volume formulation for multiprocess watershed simulation. *Water Resour. Res.*, 43, W08419, doi:10.1029/2006WR005752.
- Reed, S., V. Koren, M. Smith, Z. Zhang, F. Moreda, D. J. Seo and DMIP Participants (2004). Overall distributed model intercomparison project results. *J. Hydrol.*, 298(1-4), 27-60.
- Saltelli, A. (2002). Making best use of model evaluations to compute sensitivity indices. *Comput. Phys. Commun.*, 145(2), 280-297.
- Saltelli, A., M. Ratto and T. Andres (2008). *Global sensitivity analysis: Gauging the worth of scientific models*, John Wiley & Sons, Inc., New York.
- Sivapalan, M. and E. F. Wood (1987). A Multidimensional Model of Nonstationary Space-Time Rainfall at the Catchment Scale. *Water Resour. Res.*, 23(7), 1289-1299.
- Smith, M. B., D. J. Seo, V. I. Koren, S. M. Reed, Z. Zhang, Q. Duan, F. Moreda and S. Cong (2004). The distributed model intercomparison project (DMIP): motivation and experiment design. *J. Hydrol.*, 298(1-4), 4-26.
- Sobol', I. M. (1993). Sensitivity estimates for nonlinear mathematical models. *Math. Model. Comput. Exp.*(1), 407-417.
- Tang, Y., P. M. Reed, K. van Werkhoven and T. Wagener (2007). Advancing the identification and evaluation of distributed rainfall-runoff models using Sobol's global sensitivity analysis. *Water Resour. Res.*, 43, W06415, doi:10.1029/2006WR005813.
- U.S. Department of Agriculture Soil Conservation Service (1986). *Urban Hydrology for Small Watersheds*, Tech. Release no. 55, Washington, DC.
- van Werkhoven, K., T. Wagener, P. Reed and Y. Tang (2008). Characterization of watershed model behavior across a hydroclimatic gradient. *Water Resour. Res.*, 44, W01429, doi:10.1029/2007WR006271.
- VanderKwaak, J. E. and K. Loague (2001). Hydrologic-response simulations for the R-5 catchment with a comprehensive physics-based model. *Water Resour. Res.*, 37(4), 999-1013.
- Weiler, M. and J. McDonnell (2004). Virtual experiments: a new approach for improving process conceptualization in hillslope hydrology. *J. Hydrol.*, 285(1-4), 3-18.

Winter, C. L., E. P. Springer, K. Costigan, P. Fasel, S. Mniszewski and G. Zyvoloski
(2004). Virtual watersheds: Simulating the water balance of the Rio Grande basin.
Computing in Science & Engineering, 6(3), 18-26.

CHAPTER 5

Phase III: Evaluating Climate Change Impacts for Ungauged Watersheds in Southern Africa

5.1 INTRODUCTION

Southern Africa is a water-stressed and flood-prone region. Unreliable, episodic rainfall patterns cause both recurring drought and frequent flooding [Staudenrausch and Flugel, 2001; Aldhous, 2003; Reason *et al.*, 2005]. Due to poor infrastructure and a poverty-stricken population in much of the region, the impact of flood and drought can be particularly devastating [FAO, 2004; Khandlhela and May, 2006]. Climate change may further exacerbate the problems by reducing available water resources and increasing the risk of large floods [Schulze *et al.*, 2001; Milly *et al.*, 2002; Milly *et al.*, 2005]. Given these issues, maintaining a network of hydrometeorologic gauges should be a priority in the region for monitoring and prediction of drought and floods. However, as in many parts of the world, networks are declining as socio-economic and health issues use up the few resources available [Stokstad, 1999; Houghton-Carr and Fry, 2006]. In recent years, the scientific community has recognized the need to focus research on improving hydrologic predictions in ungauged and poorly-gauged basins [Sivapalan *et al.*, 2003]. The work presented in this chapter extends a recently-developed approach for modeling ungauged basins in southern Africa to investigate the hydrologic impact of climate change, a topic of great concern in this region that is considered highly vulnerable to climate change impacts [Meadows, 2005; Milly *et al.*, 2005; Kundzewicz *et al.*, 2008].

The study focuses on the Olifants Basin, which is part of the Limpopo Basin in southeastern Africa. The Limpopo Basin is shared by four countries – Mozambique, South Africa, Botswana, and Zimbabwe (Figure 5.1). As of yet, no hydrologic model has been implemented for cooperative operational forecasting in the Limpopo region due to lack of forcing and streamflow data for model calibration in much of the area [DuPlessis,

2007]. Though, cross-border cooperation and information exchange is vital for water management and flood warning. The Olifants Basin, for example, makes up the contributing area to Mozambique's Massingir Dam, which is located just over the border from South Africa (Figure 5.1). Mozambique relies heavily on this dam for water supply and flood control in its southern provinces [FAO, 2004]. In addition to transboundary issues, the Olifants Basin is characterized by a semi-arid climate, seasonal patterns, impacts of ENSO, and fully-allocated resources, making effective water management critical [Levite *et al.*, 2003], particularly in the face of a changing climate. The vulnerability and importance of water resources management in the Olifants Basin, led the UNESCO-International Hydrological Program to designate it as a Hydrology for the Environment, Life, and Policy (HELP) basin. This designation demonstrates an international recognition of the significance of the basin from a water resources perspective [IWMI, 2004].

Several recent studies have used predictions from Global Climate Models (GCMs) to investigate potential impacts of climate change on water resources on a global scale [Milly *et al.*, 2002; Gordon *et al.*, 2005; Milly *et al.*, 2005; Nohara *et al.*, 2006; Sheffield and Wood, 2008]. However analyzing impacts at regional and local scales, requires downscaling of GCM data since localized variations in climate (e.g., orographic effects on precipitation) cannot be resolved at the low resolution (3-5°) of GCMs. Thus, studies of regional and local climate change impacts are less common and none (to the author's knowledge) have been performed for the Olifants Basin. Recent work by Hewitson and Crane [2006] presented and applied a new method of empirical downscaling for South Africa. The resulting downscaled climate variables (i.e.,

precipitation and temperature) provide forcing for hydrologic models to assess climate change impacts on water resources in the region.

Data and resource scarcity, however, make the use of many common hydrologic modeling approaches with large data and maintenance requirements infeasible. Most notably, since the majority of models require some level of calibration to observed streamflow data, an alternative approach to parameterize the model becomes necessary when observed streamflow data is unavailable. Methods presented in the past have focused primarily on either regionalizing model parameters using watershed characteristics in nearby basins or calculating model parameters from watershed properties such as soil type, landuse and topography. However neither approach has been overly successful in producing reliable predictions in ungauged basins [*Beven, 1989; Wagener and Wheeler, 2006*]. Other recent studies have indicated that, alternatively, relationships between hydrologic response signatures and watershed characteristics (physical and hydroclimatic) can be developed by regression analysis [*Eng and Milly, 2007; Yadav et al., 2007*]. Adding uncertainty bounds to the relationship forms constraints on an ungauged watershed's hydrologic response [*Yadav et al., 2007*]. Model simulations (for any model) that fall within the constraints can then be identified, forming an ensemble of acceptable simulations. By the same method, constrained hydrologic responses to future scenarios of climate change can be developed.

The work presented here tests this ungauged modeling approach for watersheds within the Olifants Basin in southern Africa and evaluates the potential for applying the approach in other parts of the Limpopo Basin where information is even more limited. The approach is applied to investigate climate change impacts in an area with

disproportionately high runoff and thus high significance for water resources management.

5.2 STUDY AREA AND DATA

5.2.1 The Olifants Basin

The Olifants Basin is located in the southern part of the Limpopo Basin and includes an area of roughly 75,000 km² above its confluence with the mainstem of the Limpopo River in Mozambique (Figure 5.1). The topography of the basin is characterized by low elevation in the east, a sharp rise in elevation up to an escarpment near the center, and high elevation in the western part of the basin. Climate patterns are significantly influenced by the topography and, as such, are highly variable across the basin. The mean annual precipitation ranges from 300 mm up to 1800 mm in localized areas along the escarpment (Figure 5.2), while the mean value for the basin as a whole is 630 mm. A distinct rainy season exists throughout the basin from October to April, with highest accumulations typically occurring in December and January. Seasonality and high rainfall variability (spatial and temporal) contribute to the basin's propensity for both droughts and floods [Levite *et al.*, 2003; FAO, 2004; de Lange *et al.*, 2005].

Water resources are heavily allocated and developed throughout the basin, and even over-allocated in some areas. Irrigation makes up over 50% of the water demand, primarily going to large-scale, commercial farms. Small scale irrigation (for smallholder farms) is also increasingly becoming a priority with a growing effort to improve food security and conditions for the poor communities (some of the poorest in the country) in the Olifants region [IWMI, 2004; FAO, 2004; de Lange *et al.*, 2005]. Mining, power



Figure 5.1 Relative locations of the Limpopo Basin, the Olifants Basin, Kruger National Park, and Massingir Dam in southern Africa.

generation, and industrial activities are also prominent and contribute significantly to water demand, while also making the basin important for South Africa's economy. Environmental flow requirements are also of concern, particularly through the protected Kruger National Park which is located in the eastern (downstream) portion of the basin (Figure 5.1). Maintaining dry season flows and reducing the impact from upstream industrial effluent are critical for the ecological integrity of the park [*de Lange et al.*, 2005].

Within the Olifants Basin, 23 gauged headwater watersheds were identified that do not have substantial impacts from major dams and diversions (based on information available). They are relatively spread across the basin (Figure 5.3) with the exception of

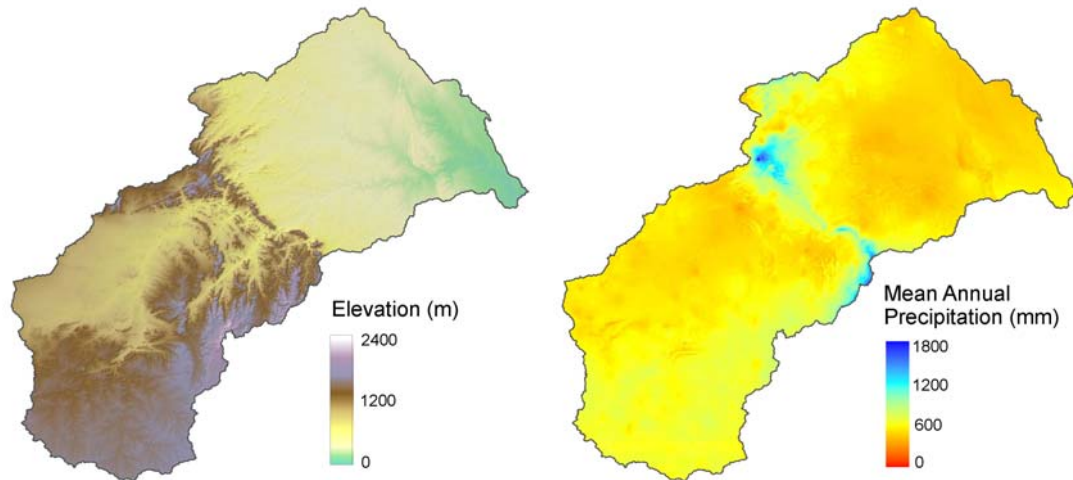


Figure 5.2 Elevation and mean areal precipitation of the Olifants Basin.

the driest and least developed areas, where few or no gauges have been installed beyond the mainstem of the river (which are affected by abstractions and dams and therefore not included). The gauged watersheds are used in the regionalization analysis that is described in Section 5.3.1. For the climate change assessment, several ungauged watersheds were identified in an area of the basin that is critical for water resources. As previously mentioned and shown in Figure 5.2, a distinct region of higher rainfall occurs along the escarpment near the center of the basin. This relatively small area produces a large portion (approximately 40%) of the total annual runoff. Nine of the gauged watersheds are located within this area. Nineteen additional ungauged headwater watersheds were delineated to cover the remainder of the area (as well as possible). The resulting 28 watersheds (9 gauged, 19 ungauged) make up 11% of the Olifants basin area while generating approximately 37% of the total annual runoff. They are referred to throughout this study as the ‘source watersheds’.

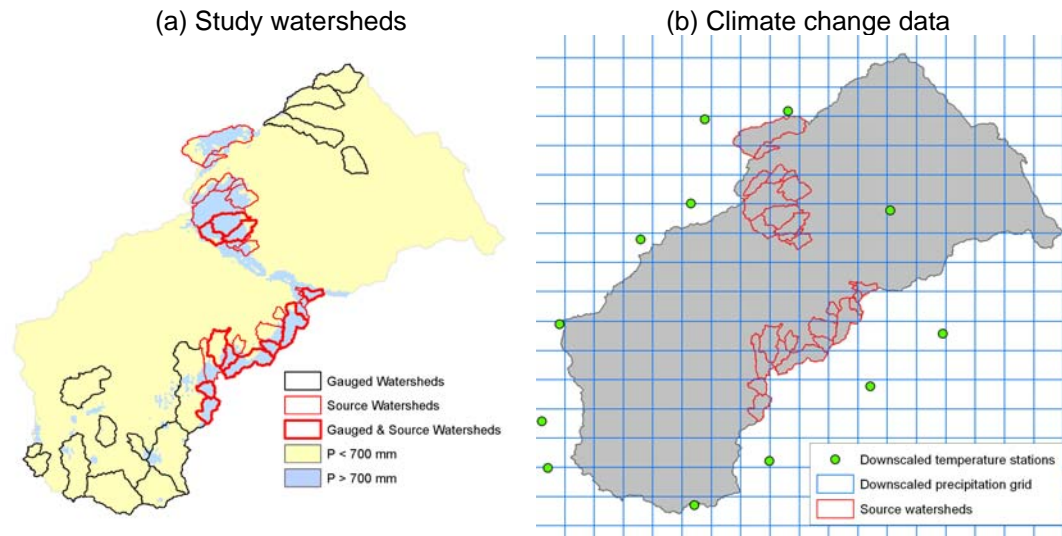


Figure 5.3 Location of (a) study watersheds within the Olifants Basin (gauged watersheds were used to generate regression relationships and source watersheds were the focus of the climate change assessment) and (b) the downscaled precipitation grid and temperature stations with respect to the source watersheds.

5.2.2 Data

Data for this study were collected from a variety of sources. Grids of physical characteristics for the Limpopo region, including elevation (90 m) and vegetation cover, were obtained from the International Water Management Institute (IWMI). IWMI maintains data for the Limpopo Basin (which covers the Olifants Basin) since it is one of the institute's 'Challenge Program River Basins'. Grids of historical mean annual and mean monthly precipitation, temperature and potential evaporation (A-pan based) for all of South Africa were obtained from datasets that accompany the South African Atlas of Climatology and Agrohydrology [Schulze, 2006]. Due to the lack of available observed time series, monthly time series of potential evaporation were generated based on these historical mean monthly values. The Department of Water Affairs and Forestry (DWA) of the South African government provided historical monthly time series (1920-1989) of precipitation, which were developed as part of a comprehensive water resources study

entitled 'Water Resources 90' (WR90). The WR90 time series include mean areal precipitation values calculated from precipitation stations for areas referred to as 'rain zones' (areas with spatially-consistent precipitation characteristics). Within the Olifants Basin, the rain zones are roughly the size (and in many cases correspond exactly) to the watersheds delineated for this study. For watersheds larger than the rain zones, weights were calculated to combine rain zones' values into an appropriate mean areal value. The DWAF also provided historical time series of streamflow observations for the 23 gauged watersheds via the Hydrology division's data distribution site. The website location and a table of station information are included in Appendix B.

Data representing scenarios of future climate in the form of downscaled, gridded (0.25° resolution) precipitation data and station-based temperature data were obtained from the University of Cape Town (UCT), Climate Systems Analysis Group (Figure 5.3). The data were downscaled from the Intergovernmental Panel on Climate Change (IPCC) Assessment Report 4 (AR4) datasets by the empirical procedure developed by *Hewitson and Crane* [2006]. This procedure is based on a concept of self-organizing maps, which are used to characterize the state of the atmosphere surrounding each grid cell and its associated precipitation probability density function. The downscaled data are based on the SRES A2 scenario, which is generally regarded as a 'worst case' scenario. Although the SRES A1B scenario is more regularly used in impact assessments, relatively small differences in runoff have been shown to occur for southern Africa between the two scenarios [*Sheffield and Wood*, 2008]. Furthermore, the difference between the scenarios is likely to be less than the overall uncertainty incurred by the downscaling and regionalization procedures used in this study.

Table 5.1 Models on which the downscaled data used in this study were based and availability for precipitation (P), temperature (T), the control period (1961-2001), the future A period (2045-2065), and the future B period (2081-2100).

Model	Group (Country)	Control (1961-2001)	Future A (2045-2065)	Future B (2081-2100)	P	T
ECHAM5/ MPI-OM	Max Planck Institute for Meteorology (Germany)	✓	✓	✓	✓	✓
GISS-ER	NASA/Goddard Institute for Space Studies (USA)	✓	✓	✓	✓	✓
CNRM	Météo-France/Centre National de Recherches Météorologiques (France)	✓	✓	✓	✓	
NCEP	The National Centers for Environmental Prediction (NCEP) Reanalysis Project (USA)	✓			✓	✓

The GCMs on which the downscaled data are based are listed Table 5.1. NCEP results, which were downscaled by the same method and are used in the analyses for additional comparison in the historical (control) period, are also included. Note that downscaled temperature was not available for model CNRM-CM3. Therefore, in order to take advantage of as much available data as possible, CNRM precipitation was combined with both ECHAM and GISS temperature data to create two additional cases of future climate. This was considered reasonable since variability between models was not large for temperature, as will be shown in Section 5.5.3. Two additional datasets were initially available from UCT but were not included in the analysis due to record length and quality issues. These include the CGCM3 model from the Canadian Centre for Climate Modeling and Analysis (for which the future B period was not available) and the IPSL-CM4 model from the Institut Pierre Simon Laplace (for which a phase shift existed in the seasonal rainfall pattern, indicating problems with the data).

5.3 METHODS

5.3.1 Regionalization of Hydrologic Constraints

A model-independent method of regionalizing constraints on watershed response [Yadav *et al.*, 2007] was used to obtain hydrologic predictions in the source watersheds. The first step of the method is to develop relationships by regression analysis between watershed physical or climatic characteristics and indices of the dynamic watershed response. Examples of response indices include the runoff coefficient (ROC) (i.e., the ratio of annual runoff to annual precipitation), frequency of large events, coefficient of variation (CV) of flow, mean summer/winter runoff, etc. Yadav *et al.*[2007] discuss a wide range of potential streamflow indices. The appropriate indices to use depend on the specific characteristics of runoff in the region of interest and the modeling objectives. Relationships between the selected response variable (the streamflow index) and one or more predictor variables (physical or climatic watershed characteristics) are developed by single and/or multivariate regression analysis. The predictor or group of predictors that is found to produce the strongest relationship with the selected index is identified. Uncertainty bounds are applied to the resulting relationship (based on the statistical confidence interval, prediction interval, or other method) to obtain constraints on the expected watershed response any new value(s) of the predictor(s) (i.e., the climatic/physical characteristics of an ungauged watershed).

The second step of the method uses the constraints to build an ensemble of 'acceptable' simulations with any hydrologic model. The simplest approach to do this is by Monte Carlo analysis to generate a large (e.g. 10,000) number of model simulations. Streamflow indices are calculated for each simulation and those with values that fall

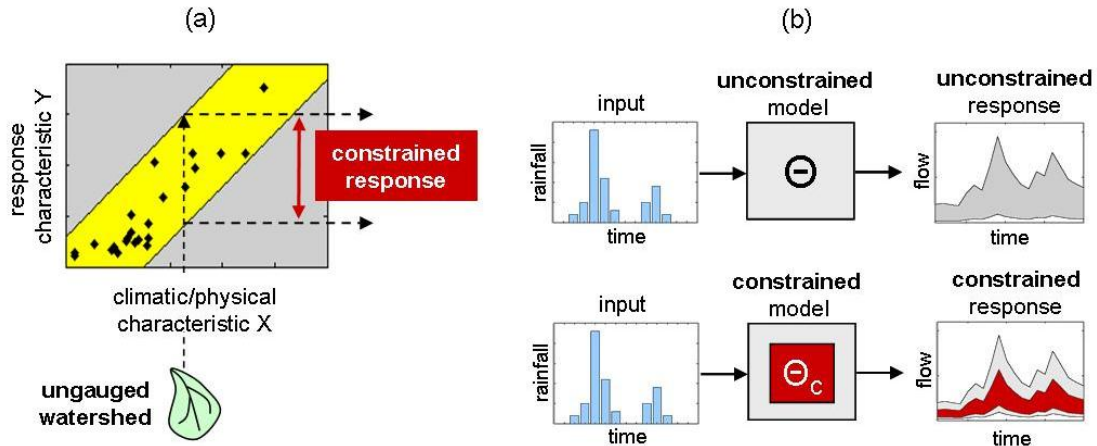


Figure 5.4 General schematic of (a) the regionalization of hydrologic constraints and (b) a constrained ensemble prediction.

within the constraints are retained. The collection of retained simulations forms the resulting ensemble prediction for the ungauged basin. A general depiction of the method is provided in Figure 5.4. For more detail on the overall method see *Yadav et al.* [2007].

5.3.2 Development of Climate Change Time Series

Downscaled time series of precipitation for each source watershed were calculated simply from the grid cell or cells that covered the area of each watershed (see Figure 5.3). Downscaled climate change projections for temperature, however, were available only at specific station locations (rather than on a continuous grid as precipitation). In order to obtain representative time series of temperature for each watershed, a two-step weighting and adjustment procedure was performed. The first step used simple Thiessen polygons to calculate weights for each watershed's surrounding stations. The Thiessen method, which is commonly applied for mean areal rainfall calculation and also applicable for temperature, assumes that any point in a watershed is best represented by the nearest station to that point. However, the stations are somewhat sparsely distributed across the Olifants Basin (Figure 5.3), particularly given the large differences in elevation in the

vicinity of the source watersheds. Therefore a second step was performed to adjust the Thiessen station weights based on relative differences between the mean monthly temperature at a station (T_i) and the mean monthly temperature over the portion of a watershed's area that station is assumed to represent (i.e. the intersection of the station's Thiessen polygon and the watershed area) [Fiedler, 2003]. Using historical, gridded temperature patterns (which account for temperature differences due to elevation), the mean areal value of temperature (MAT_i) over each intersection area was obtained. Station weight adjustment factors were then calculated as the ratio of MAT_i/T_i and applied to the original Thiessen weights to obtain new, scaled weights. By using the adjusted weights to calculate temperature time series, localized differences in temperature due to elevation differences were taken into account.

Potential evaporation time series were generated from temperature time series using the Hargreaves method [Hargreaves and Samani, 1985], which is the temperature-based method recommended by Shuttleworth [1993] since it explicitly accounts for solar radiation. The Hargreaves equation defines evaporation as

$$E = 0.0023 S_o \sqrt{\Delta_T} (T + 17.8) \quad (5.1)$$

where T is the temperature in °C, and Δ_T is the difference between mean monthly maximum and mean monthly minimum temperatures, and S_o is the water equivalent of extraterrestrial radiation (mm/day) given by

$$S_o = 15.392 d_r (\omega_s \sin \phi \sin \delta + \cos \phi \cos \delta \sin \omega_s) \quad (5.2)$$

$$\omega_s = \arccos(-\tan \phi \tan \delta) \quad (5.3)$$

$$\delta = 0.4093 \sin \left(\frac{2\pi}{365} J - 1.405 \right) \quad (5.4)$$

$$d_r = 1 + 0.033 \cos\left(\frac{2\pi}{365} J\right) \quad (5.5)$$

where ω_s is the sunset hour angle (in radians), ϕ is the latitude of the site, δ is the solar declination (in radians), d_r is the relative distance between the earth and sun, and J is the Julian day number. Hargreaves equation yields an estimate for reference crop evaporation, which can also be treated as an approximation of potential evaporation [Shuttleworth, 1993].

5.3.3 Model Description

The hydrologic model used in this study is a lumped, parsimonious model structure that has been widely applied [Moore, 2007]. The model conceptualizes the runoff generation process by a single store that accounts for variable watershed capacity via a probability distributed storage function (Figure 5.5). The Pareto distribution, which is most commonly applied and is used here, is specified by the parameter b . Excess precipitation occurs when the soil moisture store overflows, indicated in Figure 5.5 as OV1 (entire watershed overflows) and OV2 (variable area overflows). Evaporation (E) loss in the model is the product of moisture availability (contents/capacity) and the potential evaporation (PE) adjusted by a factor E_{adj} to account for differences in actual vegetation cover from the reference PE vegetation cover. To represent surface runoff at a monthly time scale (when a time lag in surface runoff is not observed), excess precipitation is routed directly to the channel. To represent baseflow, drainage from the soil moisture store occurs at a rate K_d , where it is in turn routed through a linear reservoir to the channel at the rate K_s . Total runoff (Q) from the model is the sum of surface runoff and baseflow. The five model parameters and associated ranges are listed in Table 5.2.

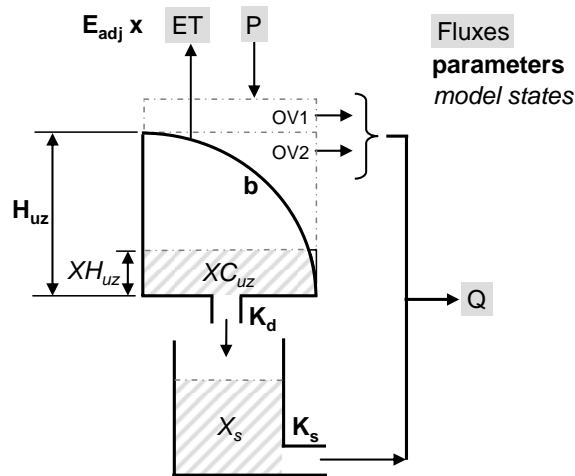


Figure 5.5 Structure of the monthly probability distributed storage model used in this study.

Table 5.2 Description and ranges of model parameters. Ranges were obtained from previous studies using this model [Moore, 2007; Yadav *et al.*, 2007] and from literature (for E_{adj}) [Chow *et al.*, 1988].

Parameter	Description	Units	Range
H_{uz}	Maximum storage capacity of the watershed	mm	1 – 400
b	Exponent defining the spatial variability of capacity	none	0 – 2
E_{adj}	Evaporation adjustment for vegetation	none	0.2 – 1.3
K_d	Drainage rate to baseflow	d^{-1}	0 – 1
K_s	Residence time of baseflow linear reservoir	d^{-1}	0 – 1

5.4 APPROACH

The methods described above are used in this study to develop predictions of the hydrologic response to climate change in the Olifants Basin. First, the regionalization analysis described in Section 5.3.1 was performed to obtain constraints for the ungauged watersheds. Streamflow indices that effectively capture the dominant response behavior characteristics were selected by reviewing hydrographs and testing the reliability of ensembles using various combinations of indices to constrain the simulations. Mean values of watershed physical and climatic characteristics were calculated for the 23 gauged watersheds. Multivariate regression analysis was then performed using a step-

wise method to identify the predictor(s) from the set of available watershed characteristics that has strongest relationship, and thus the most predictive power, for the selected response variables (i.e., the streamflow indices). Once the set of predictors and response variables was selected, a validation analysis was performed to test the modeling approach in the gauged watersheds and establish confidence for applying the approach in the ungauged watersheds. Finally, hydrologic response constraints were obtained for each ungauged watershed based on the value of its predictor (watershed characteristic) including the corresponding statistical confidence and prediction limits of the regionalized relationship. Constrained historical simulations for the ungauged basins were obtained by Monte-Carlo analysis.

To evaluate the impacts of climate change in the source watersheds, time series of future precipitation and temperature were created based on the downscaled precipitation and temperature data for each model and time period. Temperature time series were transformed into potential evaporation by Hargreaves method. Predictions of future watershed climatic characteristics (i.e., the predictors of the regionalized relationships for hydrologic response) were then calculated for each available model, time period (Table 5.1), and source watershed. Updated constraints were obtained from the regionalized relationship for each case and ensemble predictions of streamflow were generated by Monte Carlo analysis. The resulting ensemble predictions of streamflow were assimilated and compared for each period to assess the potential impacts of climate change on water resources in the high runoff-producing region of the Olifants Basin.

5.5 RESULTS

5.5.1 Regionalization Analysis

To identify appropriate hydrologic indices for the regionalization procedure, hydrographs of the 23 gauged watersheds were evaluated. It was found that the main streamflow characteristics that vary across the region are flow volume (i.e., the mean flow) and flow variability (i.e. the regime or 'peakiness' of the hydrograph). Multiple streamflow indices that describe these two characteristics were tested (Table 5.3) to determine how well each (and each combination) constrains the hydrograph and captures the observations. The two indices selected were the runoff coefficient (ROC) and the coefficient of variation of flow (CV). These two indices were used further in the regionalization analysis.

Table 5.3 Streamflow indices tested for the regionalization of hydrologic constraints.

Streamflow Index	Description	Units
Mean	Mean monthly flow	mm
Variance	Variance of monthly flow	mm
Coefficient of variation	Ratio of the standard deviation to the mean monthly flow	none
Runoff coefficient	Ratio of total runoff to total precipitation	none
Median	Median monthly flow	mm
Maximum	Maximum monthly flow	mm
Max/Mean	Ratio of maximum to mean monthly flow	none
Minimum	Minimum monthly flow	mm
Mean annual	Mean annual flow	mm
Max annual	Maximum annual flow	mm
Min annual	Minimum annual flow	mm
# Zero months	Number of months with zero flow	months
Min/Max	Ratio of minimum annual to maximum annual flow	none
High pulse count	Number of periods with flow greater than the 3 x median	periods
Low pulse count	Number of periods with flow less than 1/3 x median	periods

Several watershed physical and climatic characteristics (based on available data) were calculated and tested as predictors in the regionalization analysis, including the wetness index (P/PE), elevation (ELEV), slope (SL), topographic index (TI), land use index (LU), soil wilting point (WP), soil drainage rate (DR), and the normalized difference vegetation index (NDVI). The TI is defined as $\ln(a/\tan B)$ where a is the total

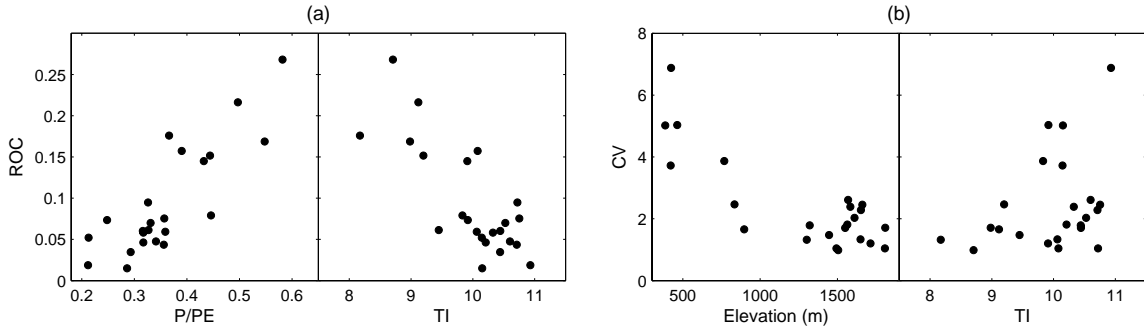


Figure 5.6 Scatter plots of watershed characteristics (predictors) that were selected by regression analysis and streamflow indices (response variables) for (a) ROC and (b) CV. Note, that plots are included to provide a general idea of the single-variable relationships, although the final (strongest) relationships and statistical intervals (confidence and prediction intervals) were multivariate and not easily depicted in 2-dimensions.

upstream area and B is slope. Maps of these characteristics for the 23 gauged watersheds are included in Appendix B. Results of multivariate regression indicate that the ROC is best predicted by P/PE and TI, while the CV is best predicted by ELEV and TI (Table 5.4). The relationship of ROC with P/PE and TI indicates that overall runoff volume is impacted by both climate and topography. The influence of P/PE on ROC is expected as greater rainfall volume should produce greater runoff. The influence of TI on ROC likely relates to the fact that higher slopes tend to reduce infiltration and increase runoff. Similarly, high sloping watersheds often result in higher, faster peaks and thus greater variability of flow. Therefore, the relationship between TI and CV is also intuitive. The strong influence of elevation on CV could be related to the higher slopes that occur in the areas of highest elevation in the Olifants Basin. Elevation could also be acting as a surrogate for other watershed characteristics that might vary with elevation in this region (e.g. geology) and for which no information was available.

Table 5.4 Multivariate regression results for the selected response indices, where R^2 is the coefficient of determination and the P-value indicates the statistical significance of the relationship between the given predictor has on the response variable. Low values (<0.05) indicate a statistically significant relationship.

Response variable	Predictor 1 – P value	Predictor 2 – P value	R^2
ROC	P/PE – 0.000	TI – 0.005	77.63
CV	Elev – 0.000	TI – 0.003	76.03

5.5.2 Historical Streamflow Predictions and Verification

Using the final regionalized relationships described above, ensemble predictions were generated for several gauged watersheds to verify the approach and provide confidence that reliable predictions can be produced in the ungauged watersheds. To do so, each validation basin was removed from the regression analysis to obtain unbiased constraints. Monte Carlo analysis was performed and the resulting ensemble simulations for three watersheds are included in Figure 5.7. These three gauged watersheds are also source watersheds, therefore the reliability of their results should provide a good indication of the reliability that can be achieved in the other (ungauged) source watersheds. Visually, the confidence and predictions limits on the hydrographs in Figure 5.7 constrain the observations reasonably well. Reliability (percent of the observed hydrograph contained within the interval) values range from 0.88 to 0.97 for the prediction interval and 0.74 to 0.88 for the confidence interval. Since the approach performs well in the gauged basins, it is assumed that predictions in the ungauged basins will have similar reliability.

The historical ensemble predictions from all of the 28 source watersheds were assimilated into a regional ensemble prediction (the total runoff from all 28 watersheds) by adding the upper and lower bounds from each watershed. The regional constrained hydrograph is shown in Figure 5.8. Several examples of individual watersheds' results are included in Appendix B. These historical source watershed predictions (regional and individual watersheds) were compared with predictions based on future projections of climate change to determine potential impacts on water resources as described in the following sections.

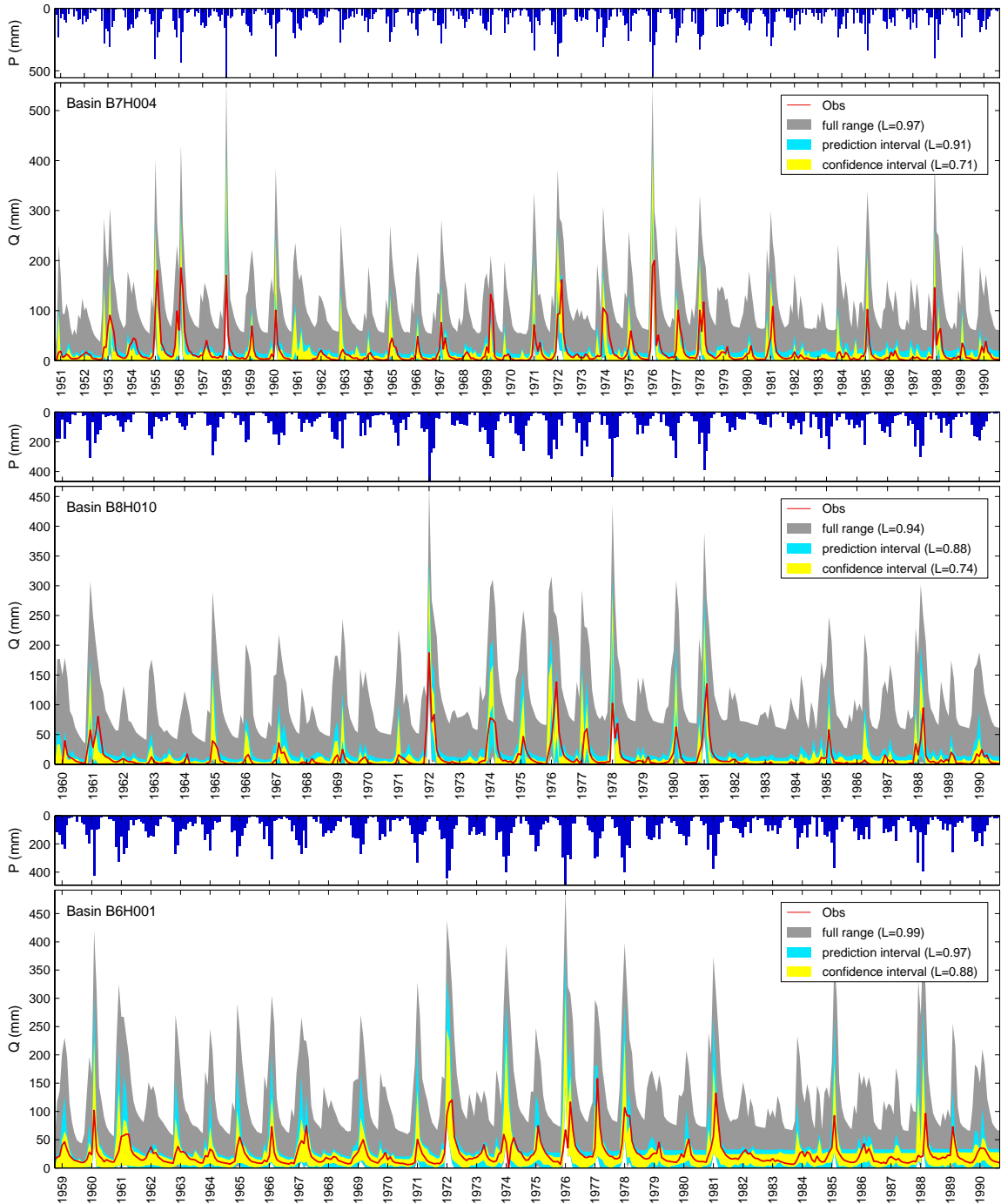


Figure 5.7 Validation of ensemble predictions for 3 gauged watersheds that area also source watersheds. Reliability (L) of the confidence and prediction intervals is noted in the legend.

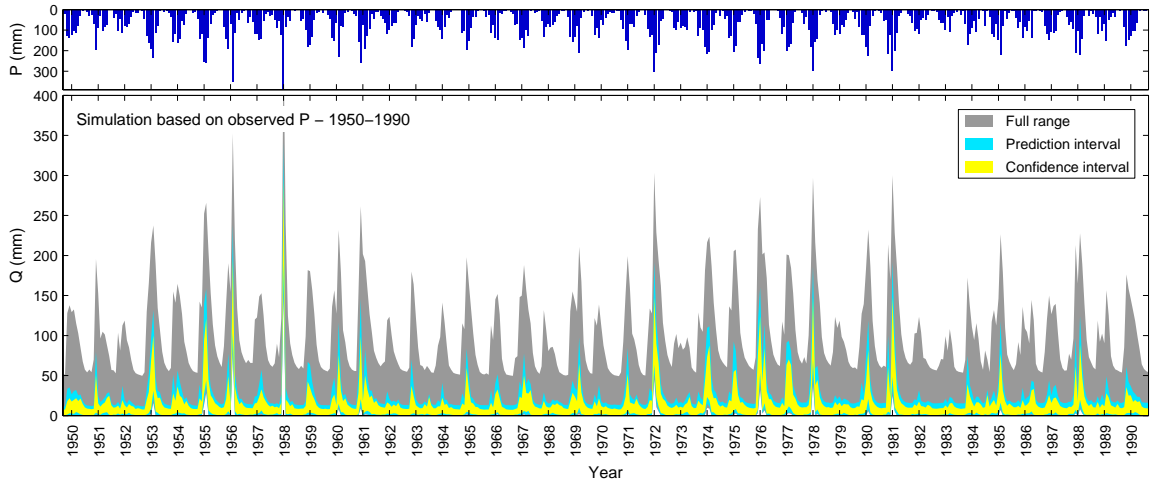


Figure 5.8 Constrained streamflow predictions for the historical period and total source area (sum of runoff from all source watersheds), generated using observations of precipitation as forcing.

5.5.3 Future Trends in Climate Variables

The overall trends in downscaled precipitation, temperature and potential evaporation for the control (1961-2000), future A (2045-2065) and future B (2081-2100) periods are shown in Figure 5.9. Regional values of each climate variable were calculated by area-weighting the mean annual values of each individual watershed. Figure 5.9 clearly shows a strong increasing pattern in all variables and all models. Mean annual temperature increases over the region by roughly 2 degrees from control to future A and 4.5-5.5 degrees from control to future B. The change in temperature causes an increase in potential evaporation of 100 mm from control to future A and 350 mm from control to future B. Good agreement between models exists for temperature and potential evaporation (since it is calculated by temperature) and also between the observed and modeled values in the control period. The changes in temperature generally agree with multi-model mean values reported for the region for scenario A2 in the IPCC AR4 [Meehl *et al.*, 2007].

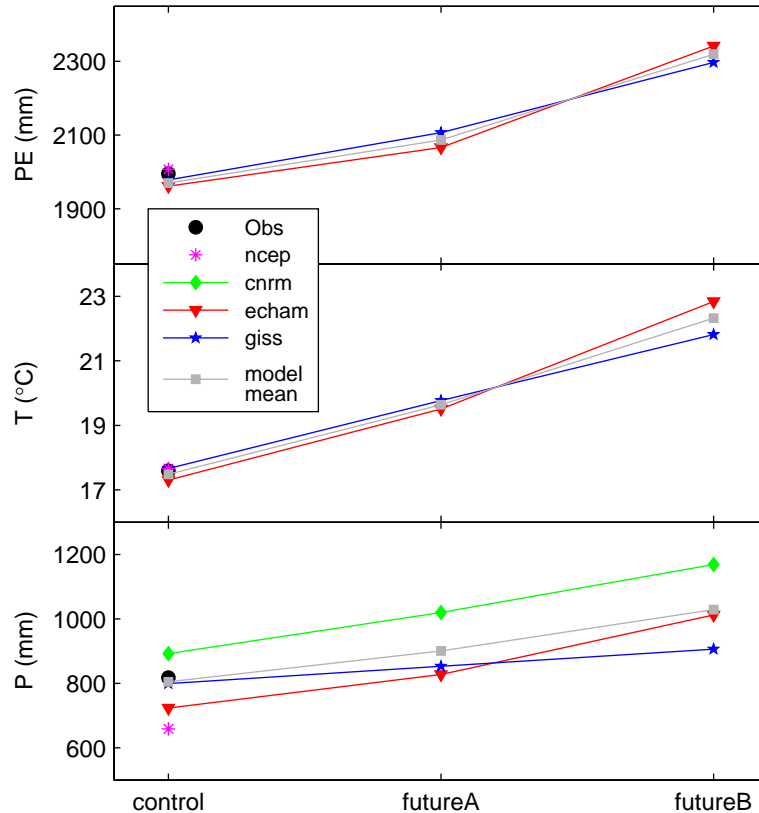


Figure 5.9 Regional climate change trends based on downscaled mean annual precipitation (P), temperature (T), and potential evaporation (PE) for the control (1961-2000), future A (2045-2065) and future B (2081-2100) periods. Note that T and PE data were not available for model CNRM.

All models also show an increasing trend in precipitation after downscaling, although variation exists in the magnitude of the values in each period and amount of the increase (Figure 5.9). Spatial distributions of the historical (control) downscaled and observed precipitation, as well as distributions of changes in future precipitation for each model over the Olifants region are included in Figures B.3-B.4 of Appendix B. The highest rainfall magnitude occurs in each period for model CNMA, while the largest change from the control occurs for model ECHAM. Model GISS shows the least change in regional precipitation and closest agreement to the observed in the control period. The model mean also shows good agreement with the observed value. Note that NCEP data shows significantly lower mean annual precipitation for the region than the observed.

This data was included only for comparison purposes since it is used in the downscaling process.

The overall increasing trend in precipitation differs from the ensemble mean result reported for the region in the IPCC AR4, which generally shows a slight decreasing trend over interior southeastern Africa [Meehl *et al.*, 2007]. However significant variability exists across the models that are included in the ensemble mean (i.e. roughly half show an increasing trend and half a decreasing trend). Variability also exists in sign of the precipitation change across the original (non-downscaled) results of the three GCMs used in this study (Figure B.5 in Appendix B). Thus these three models are assumed generally reflective of the variability across the IPCC ensemble (i.e. they are not a sub-sample of models with only wetting trends as might be suspected based on the increasing trends in downscaled data). Consistent increasing trends and agreement between models (though different models than used in this study) for the downscaled precipitation was also shown by Hewitson and Crane [2006]. The downscaling method extracts states of the atmosphere from GCM simulations and uses them in combination with self-organizing maps generated by observed data to predict precipitation values (i.e., it does not use any GCM precipitation scheme). Thus, since the downscaling process uses only atmospheric states from each GCM, a difference between the trends in mean annual precipitation found in this study and that of the GCM results is not entirely surprising and is not cause for concern. Furthermore, the downscaled precipitation accounts for the strong influence of orographic effects in the Olifants Basin, also leading to differences and greater confidence in results as compared to the GCM precipitation projections.

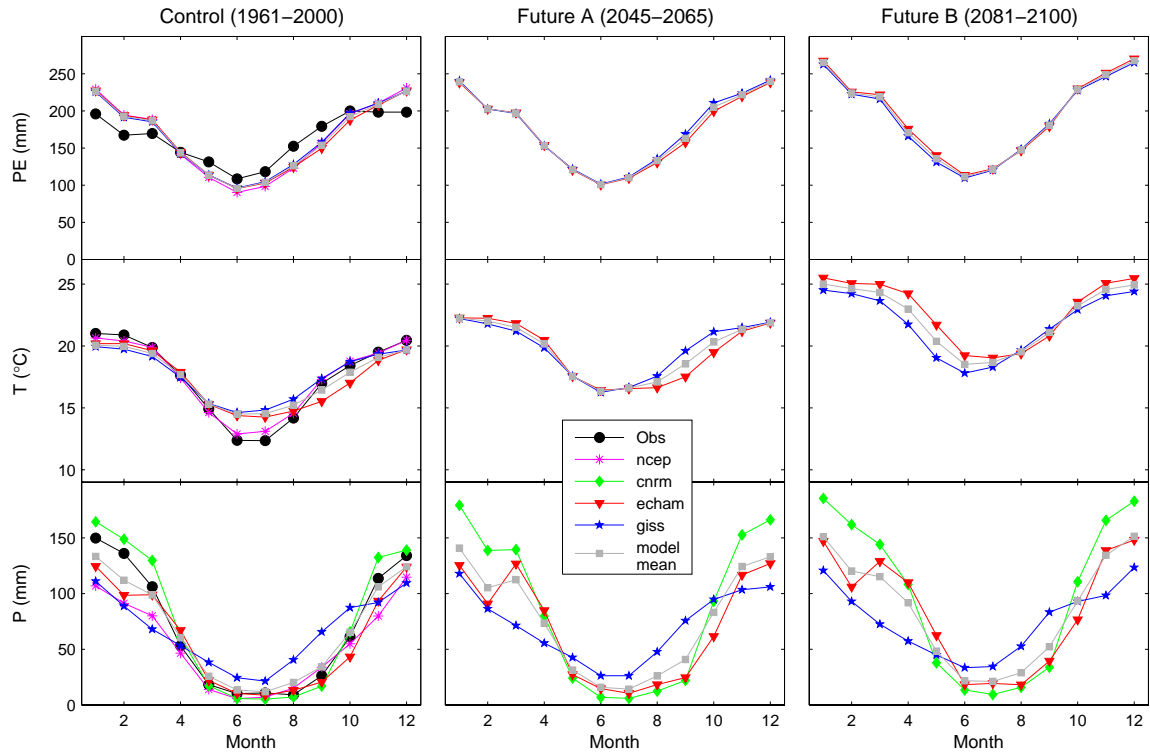


Figure 5.10 Regional climate change trends in mean monthly precipitation (P), temperature (T), and potential evaporation (PE).

Trends in regional mean monthly precipitation (Figure 5.10) show a greater increase in precipitation in the summer months, as well as the distinct pattern of seasonality. The pattern for model GISS, however, is somewhat shifted and reduced (i.e., less difference between summer and winter). Temperature and potential evaporation show a more uniform increase for all months from the control period to the future periods. In Figure 5.11, trends are presented for the 28 individual source watersheds (ordered left to right from observed wet to dry). Here, spatial variability in variables and in their agreement with observations (for precipitation) is evident. The precipitation trends for model GISS reveal some additional issues with this model (in addition to its reduced seasonality pattern) in its significant over-predictions for several watersheds (primarily the smallest watersheds therefore the bias is not apparent in the regional

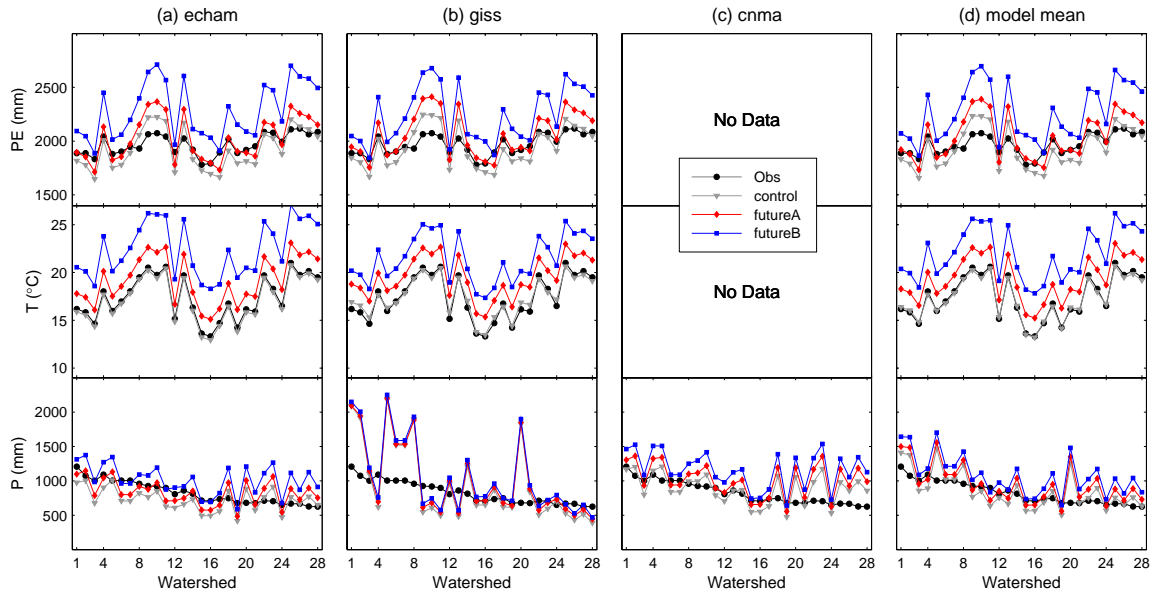


Figure 5.11 Climate change trends in mean annual precipitation (P), temperature (T), and potential evaporation (PE) by watershed and GCM.

results). Regardless, the overall increasing trend in the three variables is consistent across all watersheds and models.

5.5.4 Future Streamflow Predictions

Future values of mean annual P/PE were calculated from the downscaled precipitation and potential evaporation time series for each source watershed, model, and time period. These values were used along with static TI values to obtain future constraints on the watersheds' ROCs from the regionalized relationship defined in Section 5.5.1. The resulting ROC ranges provide the first indication of how mean annual runoff volume might change under scenarios of future climate. Figure 5.12 shows the regional trends in P/PE and ROC for each model (based on the area-weighted mean from all source watersheds). Observed values are also included for comparison ('observed' ROC ranges are constraints obtained based on observed historical precipitation). All models, except GISS, show an increase in ROC in both periods in the future. The model mean agrees

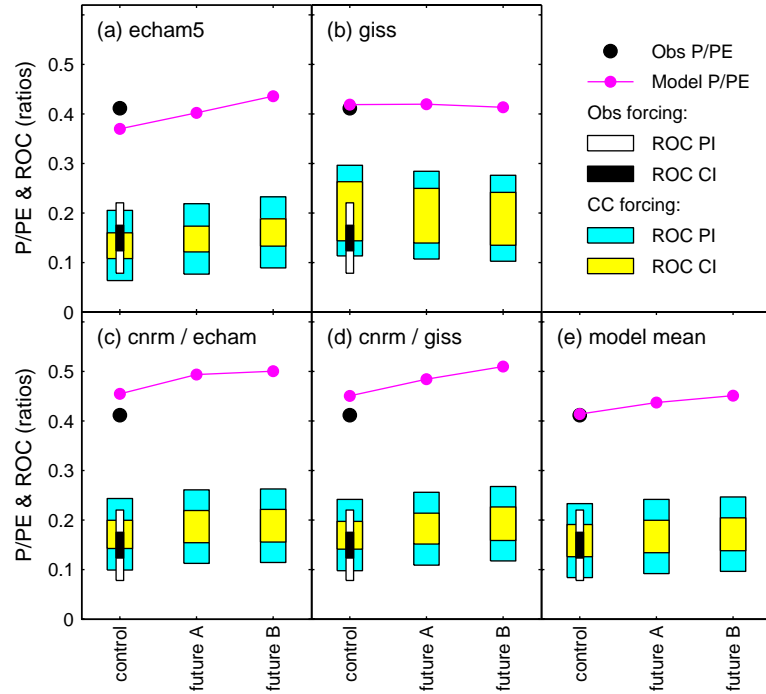


Figure 5.12 Regional climate change trends in P/PE and in the range of the prediction interval (PI) and confidence interval (CI) of the ROC for each model. Historical observed P/PE (black dot) and resulting ranges on the ROC (black and white patches) are also shown.

well in the control period with the observed P/PE and ROC range. The rising trends in the P/PE ratios (and thus ROC ranges) indicate that the increase in precipitation is greater than the increase in potential evaporation, in all but the GISS climate projections.

Using the ROC and CV constraints, ensemble predictions of streamflow were generated by Monte-Carlo analysis for each watershed, climate model and time period. The results of all watersheds were combined into a regional ensemble hydrograph (as done for the historical simulations) to assimilate the climate trends over the entire source-area. The regional hydrographs for the model mean and three periods are shown in Figure 5.13 and the rest are included in Appendix B. From the hydrographs, estimates of mean annual and mean monthly runoff volume (Q) were calculated (Figure 5.14). In all cases, mean annual runoff volume increases though the increase is small for model GISS. Percent change from the control (1961-2000) ranges from 2% to 24% in future A (2045-

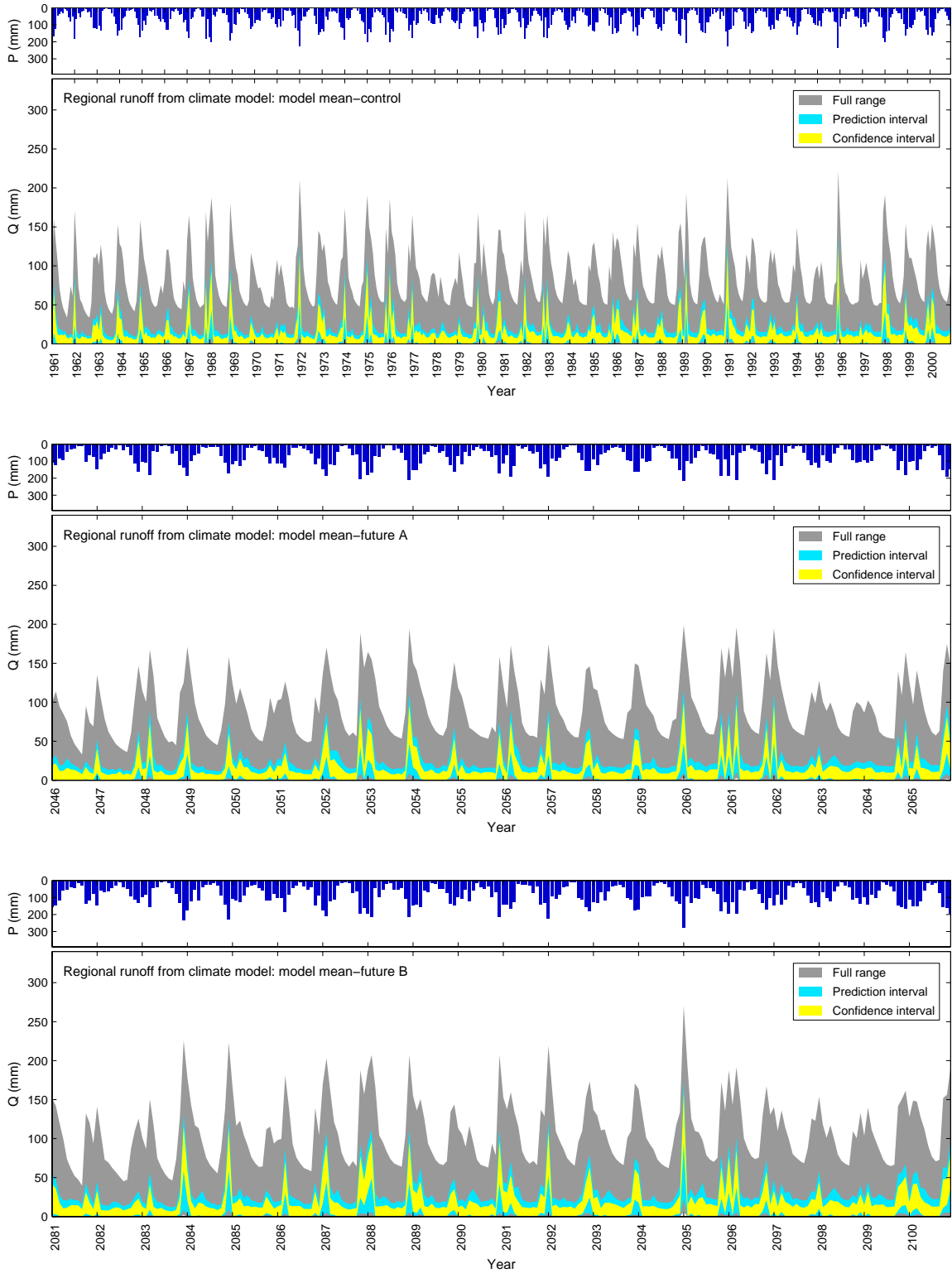


Figure 5.13 Model mean regional ensemble simulations of hydrologic response to climate change, showing the control period (top), future A period (middle), and future B period (bottom).

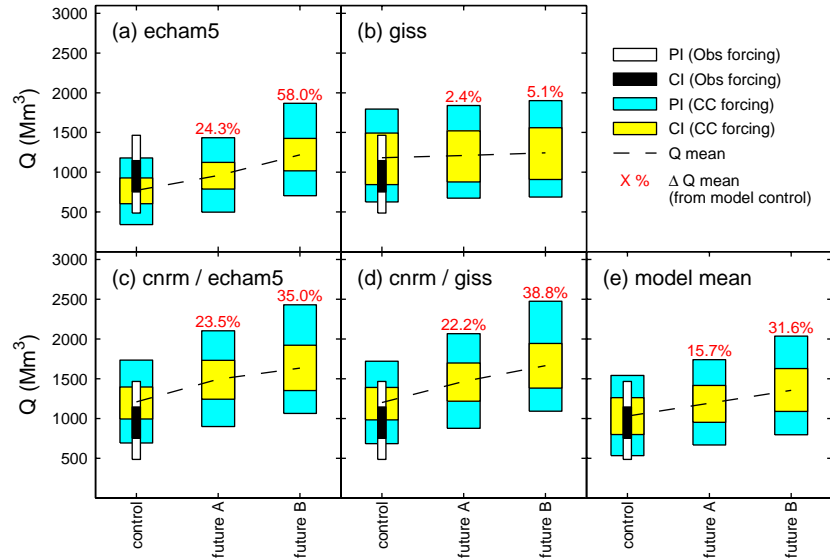


Figure 5.14 Regional climate change trends in the range of the prediction interval (PI) and confidence interval (CI) on total volume of mean annual runoff (Q) in units of million m^3 for each model – calculated from the ensemble predictions. Percent change in the mean Q (mean of the range) from the control period to each of the future periods is indicated in red text. Historical ranges based on observed forcing are also shown (black and white patches).

2065) and from 5% to 58% in future B (2081-2100). The model mean, which is closest to observations in the control period and provides the 'best estimate' of projected changes in runoff, increases by 16% in future A and by another 16% (for a total increase of 32%) in future B.

The runoff increase, however, is not evenly distributed throughout the year. Mean monthly runoff volume and the monthly change in volume from the control to future periods is shown in Figure 5.15. The majority of the increase occurs in the rainy season (Oct – Apr), with variation between models in the months that see the greatest increase. All models are consistent in projections that dry season runoff volume will remain essentially the same.

Breaking the trend down by watersheds (Figure 5.16), the percent change in mean annual runoff volume is positive in nearly all cases, though the magnitude of the change

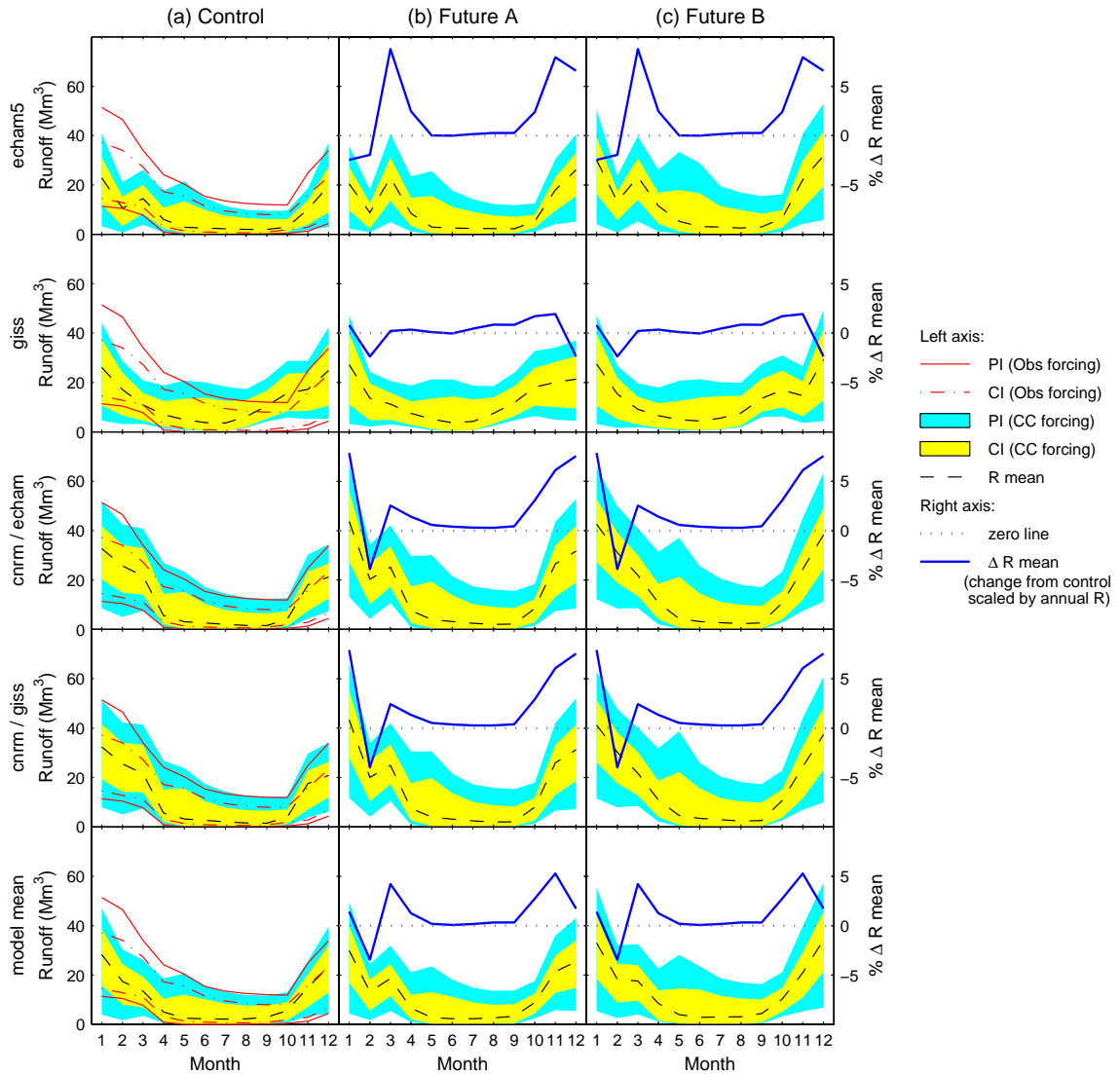


Figure 5.15 Regional climate change trends in the range of the prediction interval (PI) and confidence interval (CI) on total volume of mean monthly runoff (Q) in units of million m^3 for each model – calculated from ensemble predictions. The ΔQ (blue line) is the monthly change (in the range mean) from the control period to the future periods divided by the total annual runoff to indicate how each month contributes to the overall change in annual runoff. The PI and CI based on observed historical forcing is shown (red lines) for comparison in the control period.

is variable. The spatial patterns of runoff volume and projected changes in runoff are shown in Figures 5.17-5.18 for the model mean result. The watersheds with the highest runoff are located in the southeast part of the region, which corresponds to an area of very high rainfall (see Figure 5.2). The relative change in runoff, however, is greatest in the southwest (drier) watersheds, as well as some of the northern watersheds.

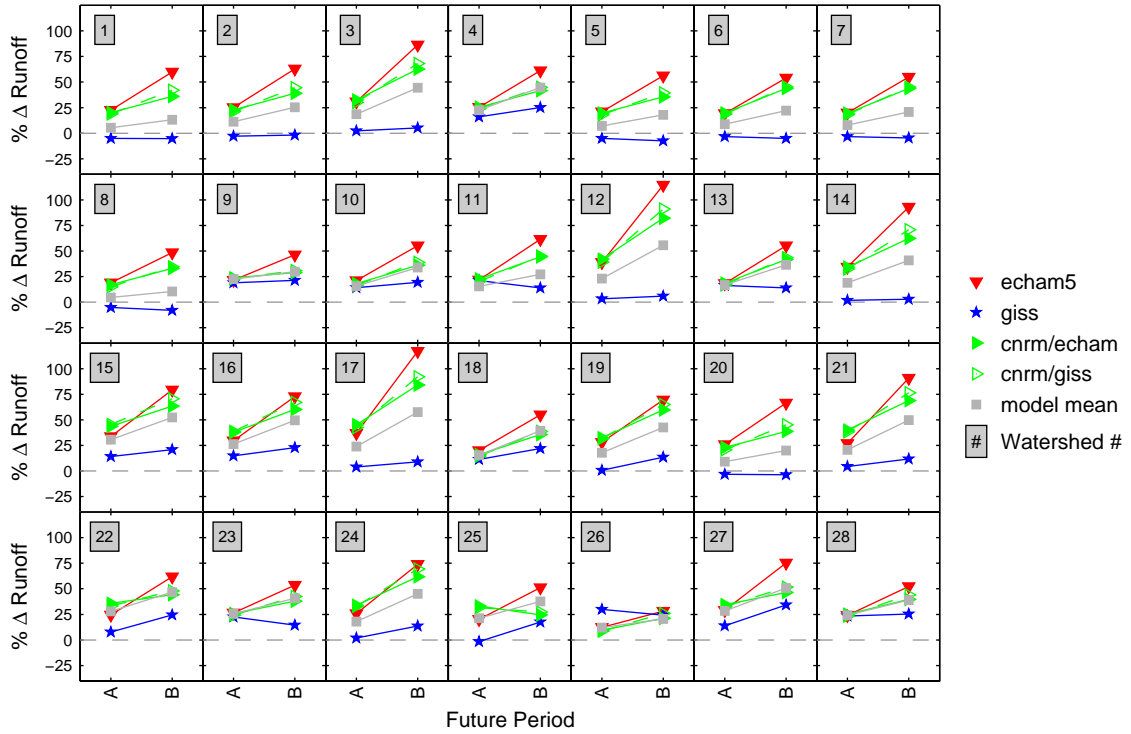


Figure 5.16 Watershed climate change trends in the percent change in total mean annual runoff from the control period to future A (2045-2065) and future B (2081-2100).

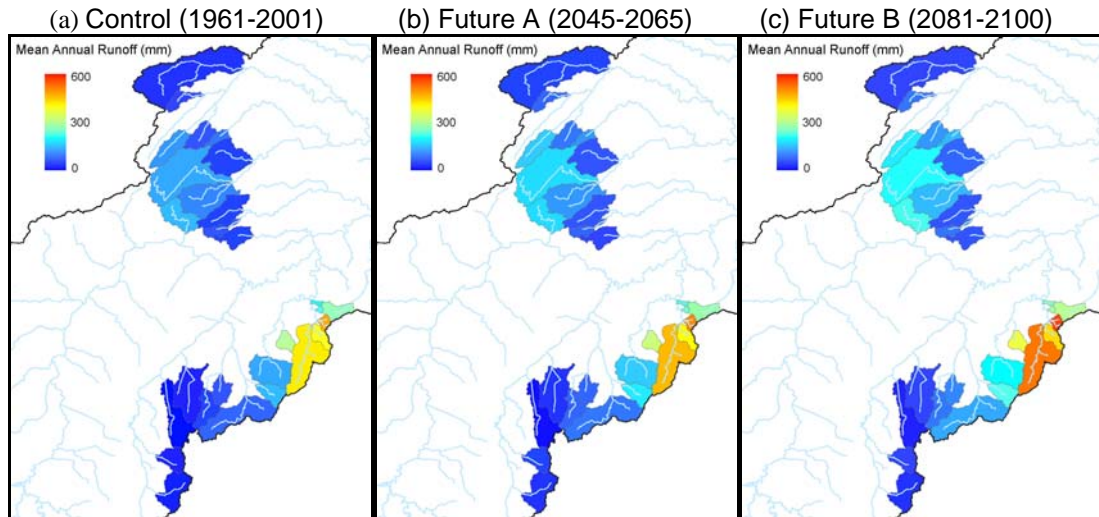


Figure 5.17 Mean annual runoff based on the mean climate model projections across the 28 source watersheds for (a) the control period (1961-2000) (b) future A (2045-2065) and (c) future B (2081-2100). Runoff values are in units of mm to enable comparison across watersheds.

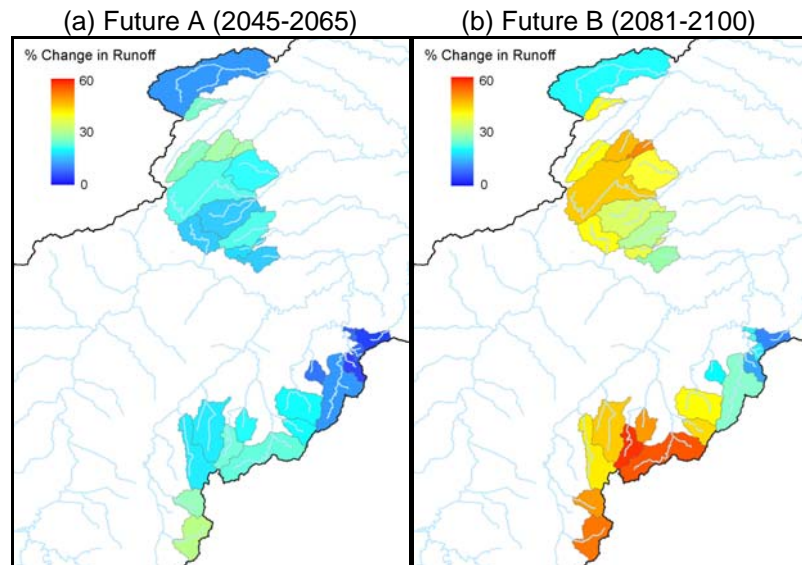


Figure 5.18 Projected change in annual runoff across the 28 source watersheds for (a) future A (2045-2065) and (b) future B (2081-2100).

5.6 DISCUSSION AND CONCLUSIONS

Two primary outcomes emerge from this study – (1) positive support for the regionalization method for ungauged hydrologic predictions and (2) an assessment of climate change impacts on water resources in a high-runoff area of the Olifants Basin. The method presented here is distinct from past methods in that it is model independent and based on relationships between watershed physical/climatic characteristics and dynamic streamflow response indices. Verification of the method in several gauged watersheds shows high reliability and thus confidence in the approach. The quality of results suggests good potential for expanding the method to other parts of the Olifants Basin and beyond to other, more data sparse tributaries of the Limpopo Basin. Furthermore, the method's low data requirements and compatibility with simple model structures make it more appropriate and feasible for use in developing countries than other data-intensive approaches.

The climate change assessment of this study shows a projected increase in regional mean annual runoff of approximately 16% by 2065 and 32% by 2100 (based on the model mean result). The projections in mean annual runoff volume have overall positive implications for water resources availability, but negative implications with respect to flood risk. Since the Olifants basin is a semi-arid region with high water demand from agriculture and industry, much concern has been raised as to whether the water supply will be able to meet the needs of all users in the future, particularly given forecasted increases in demand. Our results suggest that a decline in water availability due to increasing demand may be offset by an increasing volume of runoff in some regions. However, the seasonal pattern indicates that the additional volume will arrive almost entirely during the rainy season, when low flows and drought are less common. If the demand increase, on the other hand, is evenly distributed throughout the year, a greater deficit could still be experienced in the future during the dry season, when drought is most prevalent. In addition to implications for industrial, agricultural, and domestic users, dry season low flows are also of great ecological concern for protected areas such as Kruger National Park, which is located downstream of the study area.

The seasonal difference in the runoff trend re-emphasizes the importance of water resources management in the basin. Additional rainwater harvesting projects may become necessary to store the larger volume of rainy season runoff that is projected to occur so that it is available to meet demands during the dry season. Rainwater harvesting has been shown to have high potential in the region of southern Africa as a solution to overcome intra-seasonal dry periods and meet agricultural water needs [*Brown and Hansen, 2008*].

Small-scale rainwater harvesting projects may also become crucial to sustain the increasing number of smallholder farms that are developing within the region.

In contrast, more runoff in the rainy season implies increased flood risk and greater challenges for flood management. The Olifants region is flood prone and the majority of floods occur during the rainy season. If runoff increases as projected here, the frequency of floods is likely to increase as well. Based on the spatial distribution of the runoff change (Figures 5.17-5.18), a greater flood risk could potentially be seen in watersheds that may have been less prone to flood in the past (e.g., the drier watershed in the southwest where the relative runoff increase is higher) and therefore where flood protection might not be as strong. Our results highlight the need for effective flood management and prediction throughout the region. Implementing a cooperative, operational flood forecasting system, using methods for ungauged hydrologic prediction such as those presented here, is a critical step toward improving the regional ability to prevent and mitigate the negative impacts of floods.

This study demonstrates an effective regionalization-based method for hydrologic prediction in ungauged basins in southern Africa. The approach has been applied to assess the impacts of climate change on water resources in an area of particular importance for water resources in the region. Trends of increasing rainy season runoff emphasize the importance of water storage, to capture the short term increase and sustain demand through the dry season, as well as flood management, to mitigate the associated rise in flood risk. More broadly, this study contributes to the pressing need for advancement in our understanding of hydrologic prediction in poorly gauged basins throughout the world. In many regions, like southern Africa, a lack of local ground-based

data hinders the development of a hydrologic forecast system and declining networks indicate that the situation is not improving. The ability to cope, in such regions, with the projected intensification of water-related issues in the face of climate change hinges on the development and application of data-modest approaches to hydrologic modeling, such as the methods presented here.

5.7 CHAPTER 5 REFERENCES

- Aldhous, P. (2003). The world's forgotten crisis - Over a billion people cannot get clean water, and things are getting worse. *Nature*, 422(6929), 251-251.
- Beven, K. J. (1989). Changing ideas in hydrology - the case of physically-based models. *J. Hydrol.*, 105(1-2), 157-172.
- Brown, C. and J. Hansen (2008). *Agricultural Water Management and Climate Risk - Report to the Bill and Melinda Gates Foundation*, The International Research Institute for Climate and Society.
- Chow, V. T., D. Maidment and L. W. Mays (1988). *Applied Hydrology*, McGraw-Hill, New York.
- de Lange, M., D. J. Merrey, H. Levite and M. Svendsen (2005). Water Resources Planning and Management in the Olifants Basin of South Africa: Past, Present and Future, in *Irrigation and River Basin Management*, M. Svendsen (Editor), pp. 145-168, CAB International, Wallingford, UK.
- DuPlessis, B. (2007). Personal correspondence to K. van Werkhoven - 4/3/2007. Dept of Water Affairs and Forestry, Republic of South Africa, Pretoria.
- Eng, K. and P. C. D. Milly (2007). Relating low-flow characteristics to the base flow recession time constant at partial record stream gauges. *Water Resour. Res.*, 43(1), 1-8.
- FAO (2004). Drought impact mitigation and prevention in the Limpopo River Basin. A situation analysis., Food and Agriculture Organization of the United Nations - Subregional Office for Southern and East Africa, Harare.
- Fiedler, F. (2003). Simple, practical method for determining station weights using Thiessen polygons and isohyetal maps. *Journal of Hydrologic Engineering*, 8(4), 214-218.
- Gordon, L. J., W. Steffen, B. F. Jonsson, C. Folke, M. Falkenmark and A. Johannessen (2005). Human modification of global water vapor flows from the land surface. *PNAS*, 102(21).
- Hargreaves, G. H. and Z. A. Samani (1985). Reference Crop Evapotranspiration from Temperature. *Applied Engineering and Agriculture*, 1(2), 96-99.
- Hewitson, B. C. and R. G. Crane (2006). Consensus between GCM climate change projections with empirical downscaling: Precipitation downscaling over South Africa. *International Journal of Climatology*, 26(10), 1315-1337.

- Houghton-Carr, H. and M. Fry (2006). The decline of hydrological data collection for development of integrated water resources management tools in Southern Africa. In: S. Demuth, A. Gustard, E. Planos, F.N. Scatena and E. Servat (Editors), *Fifth FRIEND World Conference*. IAHS, Havana, Cuba.
- IWMI (2004). Olifants River Designated 'Demonstration' HELP Basin, *Africa Water Update*. International Water Management Institute, (2), pp. 1-2.
- Khandlhela, M. and J. May (2006). Poverty, vulnerability and the impact of flooding in the Limpopo Province, South Africa. *Natural Hazards*, 39(2), 275-287.
- Kundzewicz, Z. W., L. J. Mata, N. W. Arnell, P. Doll, B. Jimenez, K. Miller, T. Oki, Z. Sen and I. Shiklomanov (2008). The implications of projected climate change for freshwater resources and their management. *Hydrological Sciences Journal- Journal Des Sciences Hydrologiques*, 53(1), 3-10.
- Levite, H., H. Sally and J. Cour (2003). Testing water demand management scenarios in a water-stressed basin in South Africa: application of the WEAP model. *Physics and Chemistry of the Earth*, 28(20-27), 779-786.
- Meadows, M. E. (2005). Global Change and Southern Africa. *Geographical Research*, 44(2), 135-145.
- Meehl, G. A., T. F. Stocker, W. D. Collins, P. Friedlingstein, A. T. Gaye, J. M. Gregory, A. Kitoh, R. Knutti, J. M. Murphy, A. Noda, S. C. B. Raper, I. G. Watterson, A. J. Weaver and Z. C. Zhao (2007). Global Climate Projections, in *Climate Change 2007: The Physical Science Basis. Contribution of Working Group I to the Fourth Assessment Report of the Intergovernmental Panel on Climate Change*, S. Solomon, D. Qin, M. Manning, Z. Chen, M. Marquis, K.B. Averyt, M. Tignor and H.L. Miller (Editors), pp. 749-884, Cambridge University Press, Cambridge, United Kingdom and New York, NY, USA.
- Milly, P. C. D., K. A. Dunne and A. V. Vecchia (2005). Global pattern of trends in streamflow and water availability in a changing climate. *Nature*, 438(7066), 347-350.
- Milly, P. C. D., R. T. Wetherald, K. A. Dunne and T. L. Delworth (2002). Increasing risk of great floods in a changing climate. *Nature*, 415(6871), 514-517.
- Moore, R. J. (2007). The PDM rainfall-runoff model. *Hydrol. Earth Syst. Sci.*, 11(1), 483-499.
- Nohara, D., A. Kitoh, M. Hosaka and T. Oki (2006). Impact of climate change on river discharge projected by multimodel ensemble. *J. Hydrometeorol.*, 7(5), 1076-1089.
- Reason, C. J. C., S. Hachigonta and R. F. Phaladi (2005). Interannual variability in rainy season characteristics over the Limpopo region of southern Africa. *International Journal of Climatology*, 25(14), 1835-1853.
- Schulze, R. (Editor), (2006). *South African Atlas of Climatology and Agrohydrology*, WRC Report 1489/1/06. Water Research Commission, Pretoria, RSA.
- Schulze, R., J. Meigh and M. Horan (2001). Present and potential future vulnerability of eastern and southern Africa's hydrology and water resources. *South African Journal of Science*, 97(3-4), 150-160.
- Sheffield, J. and E. F. Wood (2008). Projected changes in drought occurrence under future global warming from multi-model, multi-scenario, IPCC AR4 simulations. *Climate Dynamics*, 31(1), 79-105.

- Shuttleworth, W. J. (1993). Evaporation, in *Handbook of Hydrology*, D. Maidment (Editor), pp., McGraw-Hill, New York.
- Sivapalan, M., K. Takeuchi, S. W. Franks, V. K. Gupta, H. Karambiri, V. Lakshmi, X. Liang, J. J. McDonnell, E. M. Mondono, P. E. O'Connell, T. Oki, J. W. Pomeroy, D. Schertzer, S. Uhlenbrook and E. Zehe (2003). IAHS decade on Predictions in Ungauged Basins (PUB), 2003-2012: Shaping an exciting future for the hydrological sciences. *Hydrological Sciences Journal-Journal Des Sciences Hydrologiques*, 48(6), 857-880.
- Staudenrausch, H. and W. A. Flugel (2001). Development of an integrated water resources management system in Southern African catchments. *Physics and Chemistry of the Earth Part B-Hydrology Oceans and Atmosphere*, 26(7-8), 561-564.
- Stokstad, E. (1999). Hydrology - Scarcity of rain, stream gages threatens forecasts. *Science*, 285(5431), 1199-1200.
- Wagener, T. and H. S. Wheater (2006). Parameter estimation and regionalization for continuous rainfall-runoff models including uncertainty. *J. Hydrol.*, 320(1-2), 132-154.
- Yadav, M., T. Wagener and H. Gupta (2007). Regionalization of constraints on expected watershed response behavior for improved predictions in ungauged basins. *Adv. Water Resour.*(30), 1756-1774.

CHAPTER 6

Synthesis

6.1 SUMMARY OF SCIENTIFIC CONTRIBUTIONS

This dissertation presents a series of studies that evaluate hydrologic model behavior and modeling approaches from the perspective of different situations that exist in hydrologic forecasting. Phase I (a) applies a comprehensive sensitivity analysis to investigate how the behavior of a widely-used, lumped, conceptual model varies across a range of watersheds with diverse physical and hydroclimatic characteristics. The primary scientific contributions of this work are (1) an understanding that distinctly different patterns of parametric control occur for watersheds of different hydroclimatic regime, (2) evidence that common assumptions about parametric controls for the specific model are invalid, and (3) demonstration that the complexity level of the model is warranted to adequately represent the response of watersheds across a hydroclimatic gradient. These findings are directly relevant for operational forecasting and calibration guidance (for users of the SAC-SMA), and more broadly for the development of effective model evaluation and identification approaches.

Phase I (b) of this dissertation builds upon the sensitivity analysis of Phase I (a) to investigate if removing insensitive parameters from model calibration is feasible without a significant impact on model performance. The two main contributions that emerged from this study are (1) evidence that this type of sensitivity-based complexity reduction is possible without substantial decline in model performance if applied on a case-to-case basis (i.e., it is sufficient to only adjust some key parameters during calibration) and (2) demonstration that calibration procedures need to be expanded beyond statistical error metrics to include metrics that capture important hydrologic characteristics of the model response to achieve realistic model behavior. The contributions of Phase I (b) are relevant

for SAC-SMA optimization, particularly as a distributed version of the model becomes more widely implemented (and the magnitude of the calibration problem for forecasting operations increases significantly), though they provide guidance for this class of model in general. The contributions of Phase I (b) also more broadly suggest that the development of approaches to dynamically couple multi-objective sensitivity analysis and optimization are needed to deal with the widening discrepancy (as more complex models are developed) between the information content of hydrologic data and number of parameters that can be identified. Overall consequences of Phase I (two steps combined) are that an evaluation of model behavior is as important as an evaluation of model performance to assess the appropriateness of a model. And, lastly, it is only necessary to calibrate a small number of parameters, but which specific parameters within the model structure varies and thus a more complex model structure might be justified.

Phase II of this dissertation evaluates the spatially-varying behavior of a distributed hydrologic model and how characteristics of rainfall, antecedent soil moisture, and grid cell location control the variation of model behavior across the model domain. The important scientific contributions of Phase II are a demonstration that (1) information content of streamflow data is a dynamic property (in space and time) that is controlled largely by characteristics of rainfall events, (2) for certain storm types the value of streamflow observations for model identification is limited to a finite distance upstream from the gauge. The first contribution is of primary importance for the development of new, dynamic calibration methods for distributed models as existing methods incorrectly assume static and spatially-uniform information content. The second contribution is relevant for the optimal design of streamflow observational networks for which an

estimation of the true information content of data is crucial. A consequence of this phase is the realization that previous approaches to model identification do not allow us to properly assess the value of observations in the context of spatially distributed modeling.

The study in Phase III evaluated an approach for modeling ungauged watersheds in southern Africa and applied the approach to assess potential hydrologic impacts of climate change in a region with disproportionately high runoff and significance for water resources. Phase III results have two primary contributions – (1) the extension of the regionalization of flow characteristics approach to a less-developed country and the verification that this modeling approach is a viable option to produce reliable streamflow predictions in ungauged watersheds in such regions (where data availability is limited) and (2) projections that annual runoff over the study area will increase in the future by a seasonal pattern, with the majority of the increase occurring during the months of the rainy season. Extension and verification of the modeling approach is relevant and important for hydrologic forecasting in the region, where a lack of data has prevented the establishment of forecasting capabilities. The projections of increasing future runoff as a result of climate change have implications for the importance of rainwater harvesting (due to the seasonal distribution of the runoff increase), as well as for flood management in the region. Specifically, the projections suggest that the strategic placement of new reservoirs or expansion of existing facilities (to store the water where it falls) could significantly reduce impacts of both droughts and floods in the Olifants Basin.

All of the methods for modeling and evaluation of model behavior presented throughout this dissertation are applicable for any hydrologic model structure. Therefore, these studies not only provide insight into patterns of behavior that are specific for the

given models (e.g. the SAC-SMA), but they also introduce highly useful tools and methodologies for evaluation of hydrologic model behavior in general. Such tools will become increasingly valuable as the development and use of complex, integrated models continues and hydrologic models become more broadly applied across the world. The challenges hydrologists face to understand, parameterize, and appropriately apply models will unquestionably become greater in the future.

6.2 RECOMMENDATIONS FOR FUTURE WORK

Recommendations of future work are identified for each phase that would build upon and expand the study's findings. The sensitivity analysis of Phase I (a) was performed at both long-term and inter-annual time scales. The variation in sensitivity found at the inter-annual time scale as compared to the long-term time scale point out that, in addition to variation across watersheds, model behavior also varies in time within a watershed. Performing the analysis on even shorter time scales (e.g. monthly, daily) in the same watersheds could provide greater insight into the time-varying nature of model behavior. The multi-objective optimization of Phase I (b) yielded solution sets that varied widely in size and complexity across the results. From an optimization/computational perspective, it would be useful to more fully evaluate the optimization dynamics associated with the different solution sets to better understand how and why the size and complexity differences occur. From a hydrologic modeling and calibration perspective, it would be of benefit to perform the analysis for additional watersheds to establish guidance for a sensitivity threshold level that could be used in an actively coupled sensitivity-based calibration approach.

In Phase II, the results of the distributed sensitivity analysis for uniform storms revealed that the spatial extent of information content did not reach the upstream portion of the watershed. Further investigation of the areal extent of information content for uniform storms is worthwhile. Interesting extensions, for example, could include adding interior gauges and testing the resulting sensitivity pattern, as well as changing the watershed size and/or event size (total volume of precipitation) of the uniform storm to find conditions for which full coverage of information occurs. In addition, the results of this study implied that a new distributed model calibration approach is needed that dynamically takes into account the spatial distribution of rainfall in order to optimally utilize available information. Therefore, the development of such an approach is recommended as a continuation of the work of Phase II.

The first recommendation to extend the work of Phase III is to expand the regionalization analysis into other parts of the Limpopo Basin. To do this, it would also be of benefit to investigate the feasibility of using other types of streamflow response information (e.g. 'soft data') in the regionalization analysis, which may be available where stream gauge data is not. Along with expanding into other regions, the ungauged modeling approach should also be expanded to predictions on a daily step. In conjunction, a rigorous analysis of satellite-based daily precipitation data is recommended to identify and correct (if possible) systematic biases in the data that occur for the region, so that the data could be used as daily forcing for hydrologic models. Lastly, performing the climate change analysis at the daily time scale is also recommended, particularly given the results of greater runoff on the monthly time scale, to assess potential changes in extreme events due to climate change. This would provide

a more complete picture of the potential consequences of climate change for flood risk in the region.

APPENDIX A

Supplementary Figures for Chapter 4

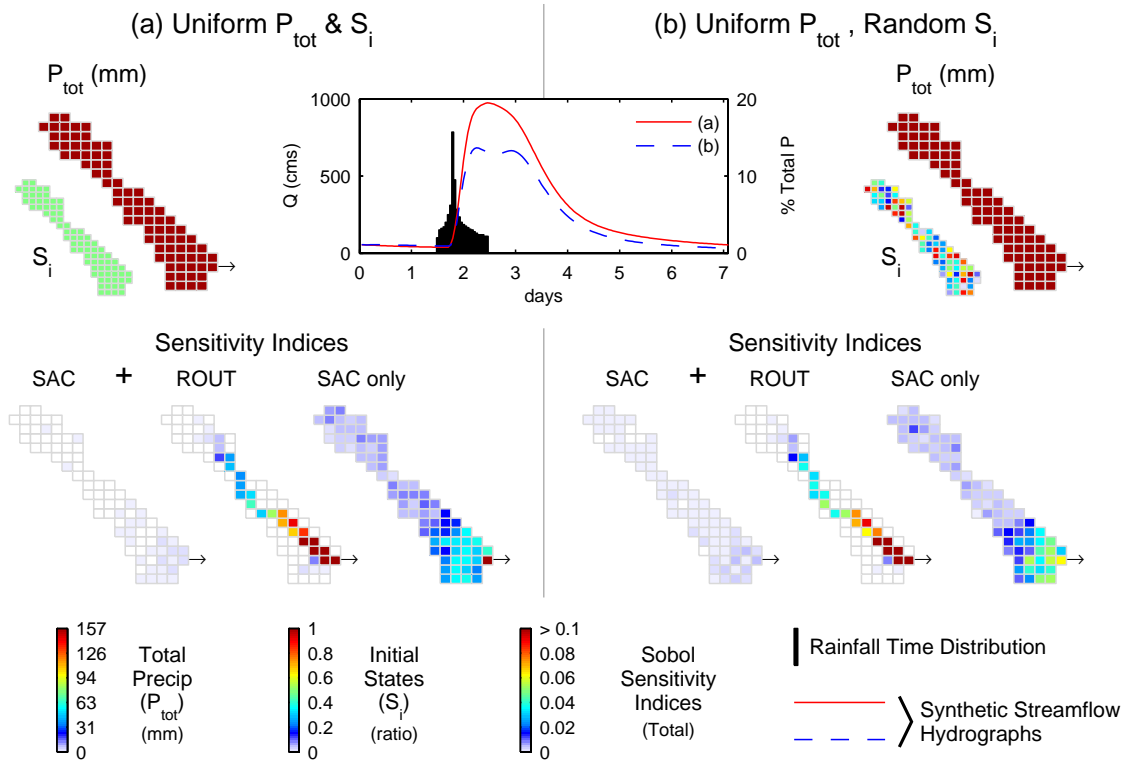


Figure A.1 Metric TRMSE: Spatially distributed parameter sensitivity for cases of (a) uniform total precipitation (P_{tot}) and uniform initial states (S_i) and (b) uniform precipitation and nonuniform initial states. Sensitivity indices are the total of all model parameters for a given cell. Indices are presented for the SAC-SMA and routing model analyzed simultaneously (SAC + ROUT – left two maps) and for the SAC-SMA analyzed separately (SAC only – right map).

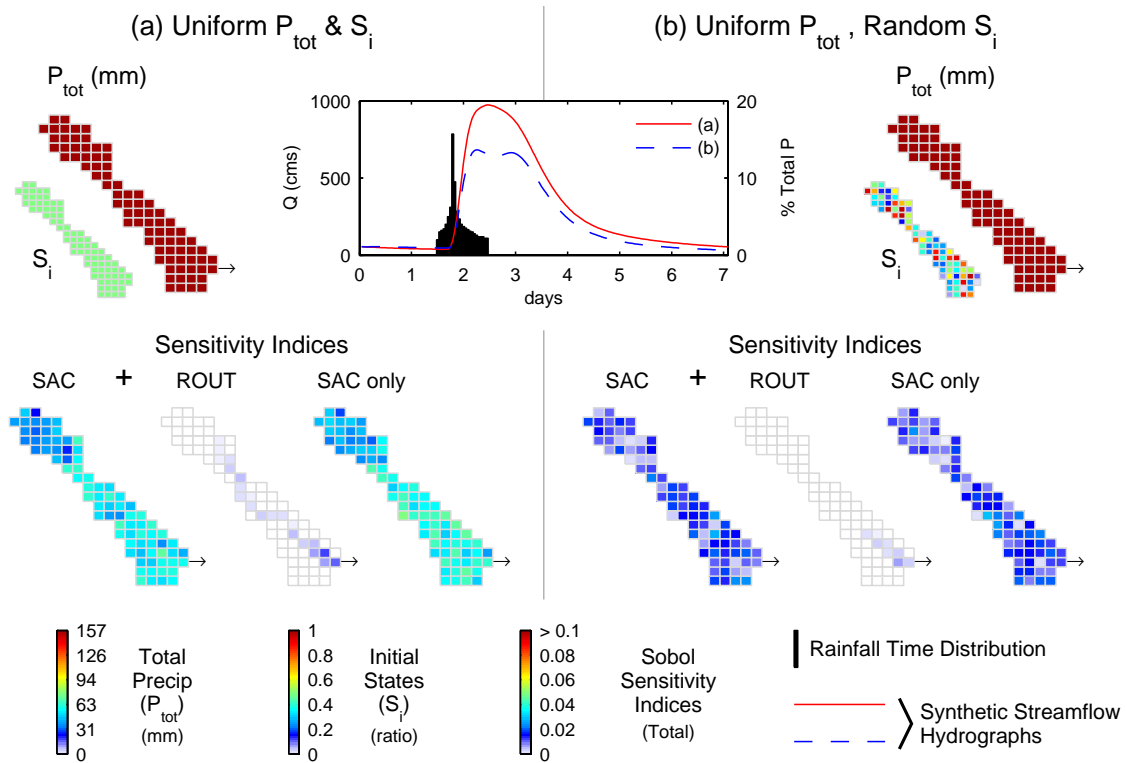


Figure A.2 Metric ROCE: Spatially distributed parameter sensitivity for cases of (a) uniform total precipitation (P_{tot}) and uniform initial states (S_i) and (b) uniform precipitation and nonuniform initial states. Sensitivity indices are the total of all model parameters for a given cell. Indices are presented for the SAC-SMA and routing model analyzed simultaneously (SAC + ROUT – left two maps) and for the SAC-SMA analyzed separately (SAC only – right map).

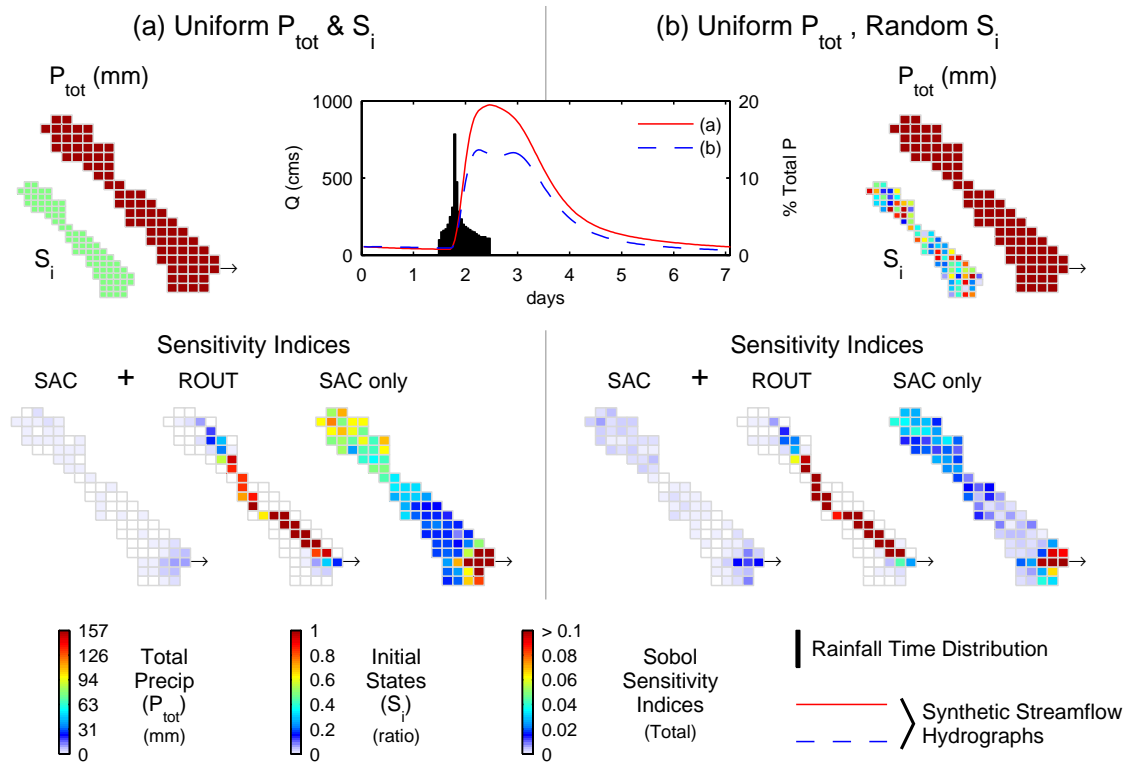


Figure A.3 Metric SFDCE: Spatially distributed parameter sensitivity for cases of (a) uniform total precipitation (P_{tot}) and uniform initial states (S_i) and (b) uniform precipitation and nonuniform initial states. Sensitivity indices are the total of all model parameters for a given cell. Indices are presented for the SAC-SMA and routing model analyzed simultaneously (SAC + ROUT – left two maps) and for the SAC-SMA analyzed separately (SAC only – right map).

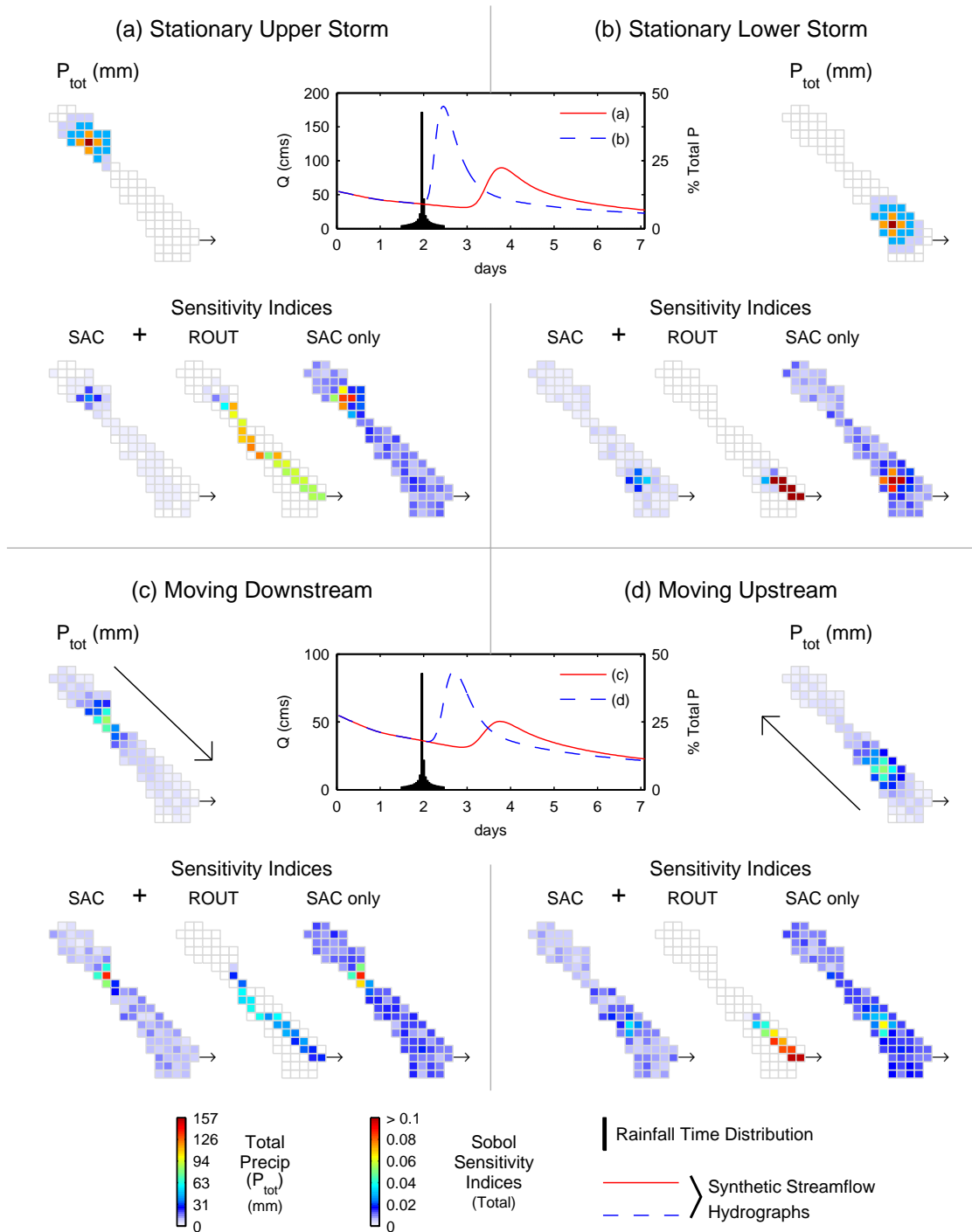


Figure A.4 Metric TRMSE: Spatially distributed parameter sensitivity for 4 different distributed storm events - (a) an upper basin stationary storm (b) a lower basin stationary storm (c) a storm moving downstream and (d) a storm moving upstream. Sensitivity indices are the total of all model parameters' indices for a given cell. In each case, indices are presented for the SAC-SMA and routing model analyzed simultaneously (SAC + ROUT – left two maps) and for the SAC-SMA analyzed separately (SAC only – right map).

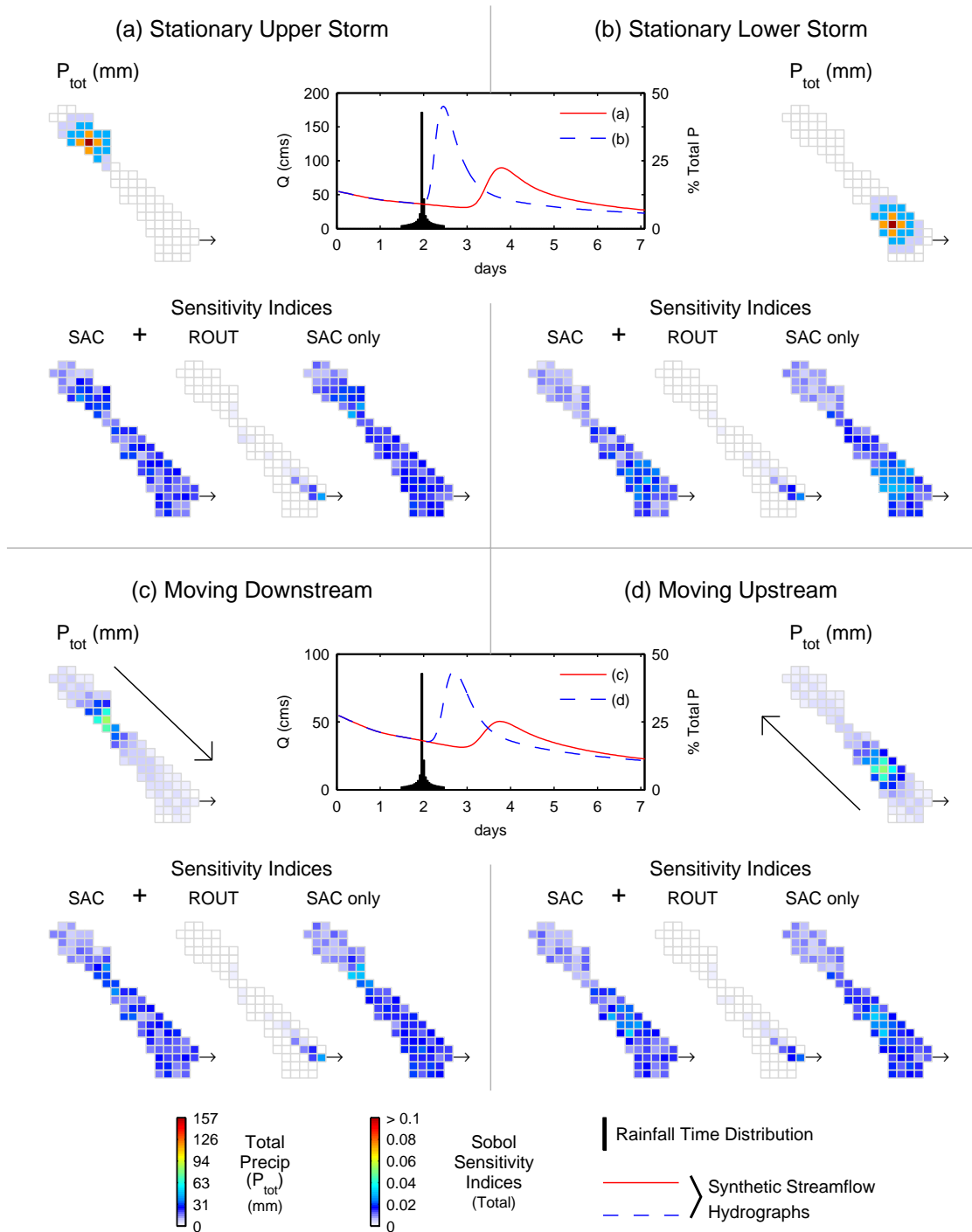


Figure A.5 Metric ROCE: Spatially distributed parameter sensitivity for 4 different distributed storm events - (a) an upper basin stationary storm (b) a lower basin stationary storm (c) a storm moving downstream and (d) a storm moving upstream. Sensitivity indices are the total of all model parameters' indices for a given cell. In each case, indices are presented for the SAC-SMA and routing model analyzed simultaneously (SAC + ROUT – left two maps) and for the SAC-SMA analyzed separately (SAC only – right map).

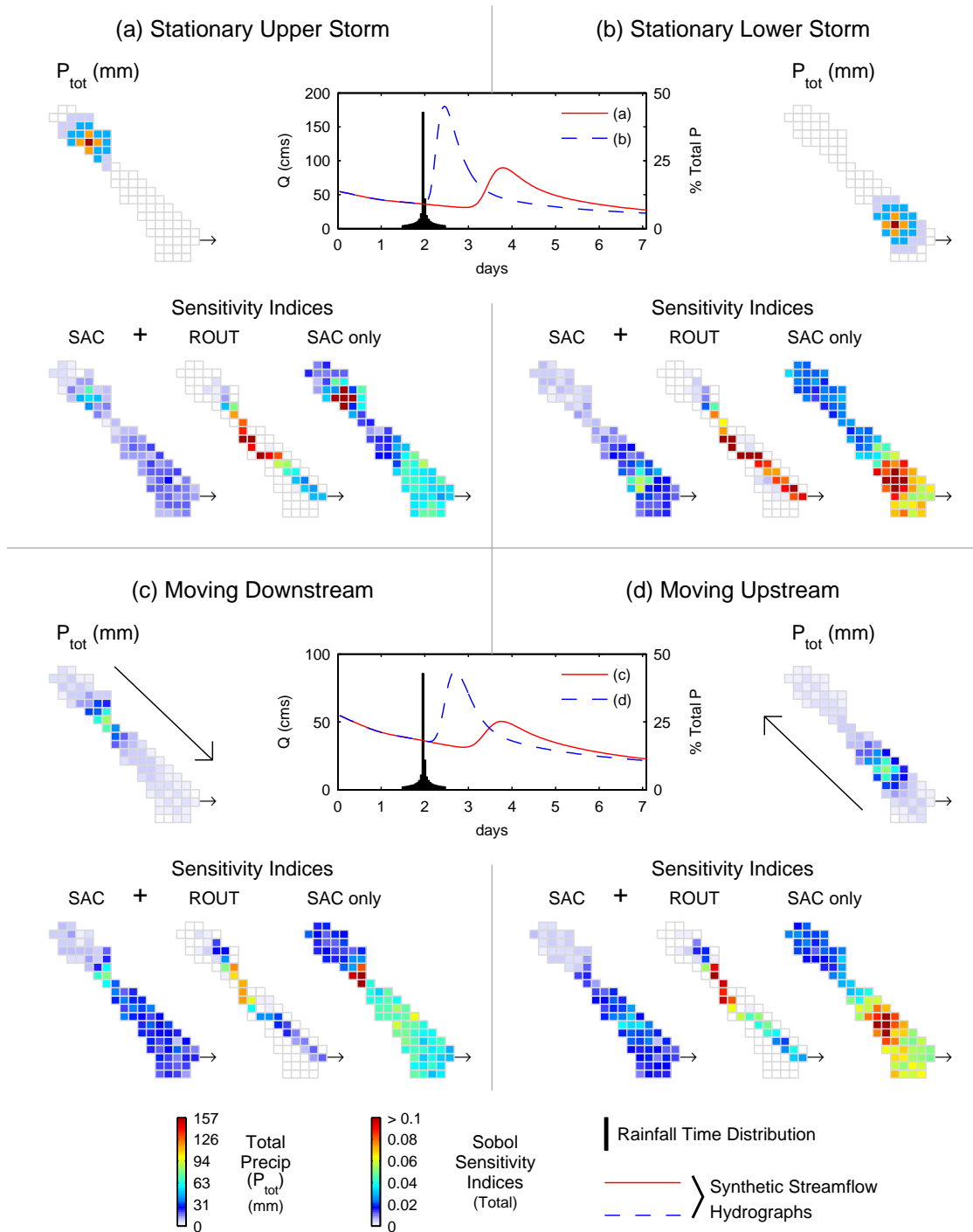


Figure A.6 Metric SFDCE: Spatially distributed parameter sensitivity for 4 different distributed storm events - (a) an upper basin stationary storm (b) a lower basin stationary storm (c) a storm moving downstream and (d) a storm moving upstream. Sensitivity indices are the total of all model parameters' indices for a given cell. In each case, indices are presented for the SAC-SMA and routing model analyzed simultaneously (SAC + ROUT – left two maps) and for the SAC-SMA analyzed separately (SAC only – right map).

APPENDIX B

Supplementary Figures for Chapter 5

Table B.1 Streamflow station information for gauges used in this study

ID	Tributary	Lat.	Long.	Upstream Area	Start Record	End Record	% Missing
B1H001	Blyde	24.68	30.80	518	1909	2007	34.0
B1H002	Spookspruit	25.82	29.34	252	1956	2007	5.6
B1H004	Klipspruit	25.67	29.17	376	1959	2007	6.6
B1H012	Little Olifants	25.81	29.59	1503	1978	2007	0.1
B1H018	Olifants	26.22	29.46	985	1989	2007	0.2
B1H021	Steenkoolspruit	26.14	29.27	1356	1990	2007	0.2
B2H004	Osspruit	25.92	28.59	123	1984	2007	0.0
B2H007	Koffiespruit	26.00	28.66	317	1985	2007	0.1
B2H014	Wilge	25.83	28.88	1086	1990	2007	0.3
B3H007	Moses	25.27	29.18	971	1980	2007	3.3
B4H003	Steelpoort	25.03	29.86	2240	1957	2007	3.0
B4H005	Waterval	25.04	30.22	188	1960	2007	0.0
B4H007	Klein-spekboom	25.01	30.50	151	1968	2007	0.9
B4H009	Dwars	24.91	30.10	448	1966	2007	6.2
B4H010	Dorps	25.08	30.44	526	1979	2007	0.4
B7H004	Klaserie	24.56	31.03	136	1950	2007	10.1
B7H010	Ngwabitsi	24.04	30.43	318	1960	2007	9.7
B7H013	Mohlapitse	24.17	30.10	263	1970	2007	15.5
B8H010	Letsitele	23.89	31.36	477	1960	2007	0.4
B8H011	Tsende	23.57	31.43	432	1960	2007	2.9
B9H001	Shisha	22.84	31.24	648	1960	2007	9.8
B9H002	Shingwidzi	23.22	31.22	810	1983	2007	1.8
B9H004	Mphongola	22.95	31.23	739	1983	2007	9.0

Data source: <http://www.dwaf.gov.za/hydrology/cgi-bin/his/cgihis.exe/station>

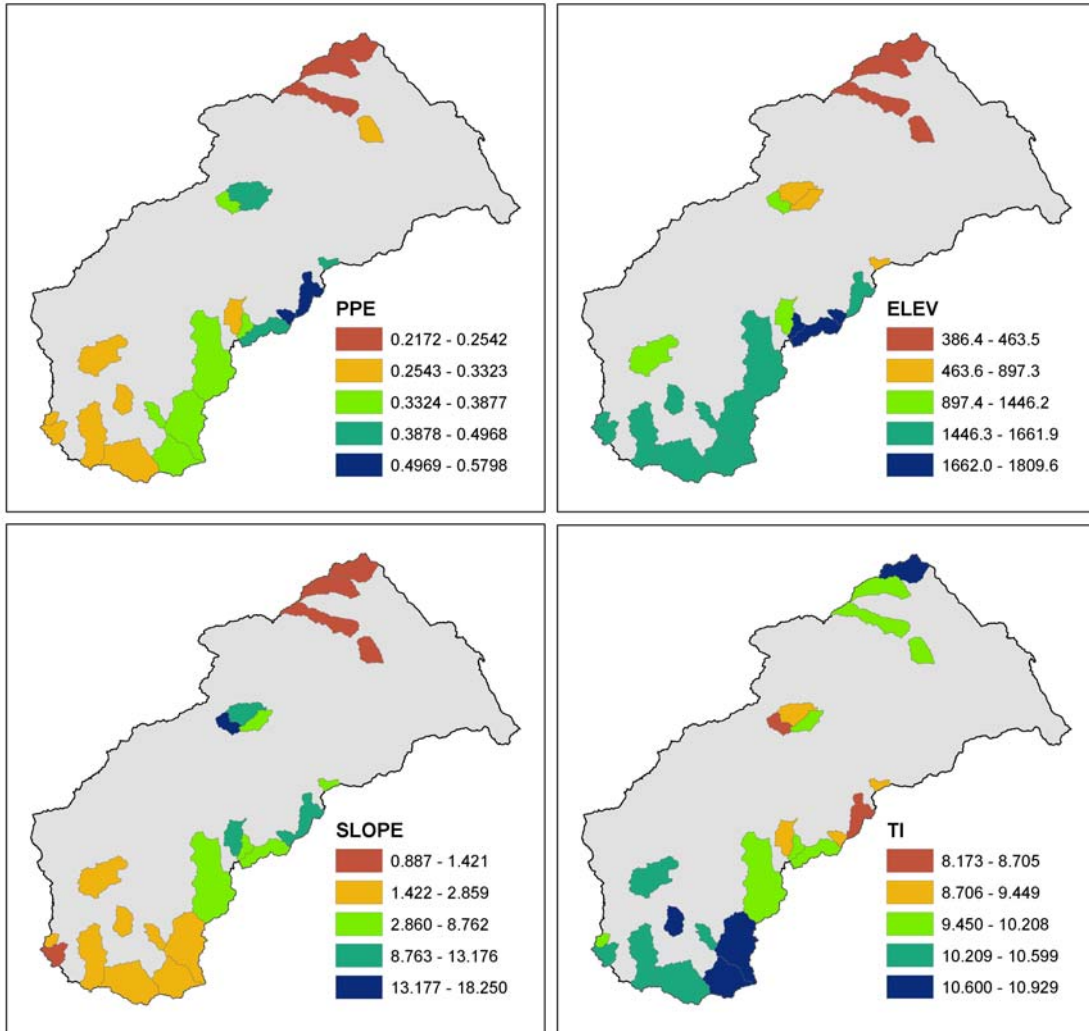


Figure B.1 Maps of climatic and physical watershed characteristics for the 23 gauged watersheds, including the wetness index (PPE), elevation (ELEV), slope, and topographic index (TI). PPE is unitless (ratio), ELEV in meters, slope in degrees, and TI is unitless.

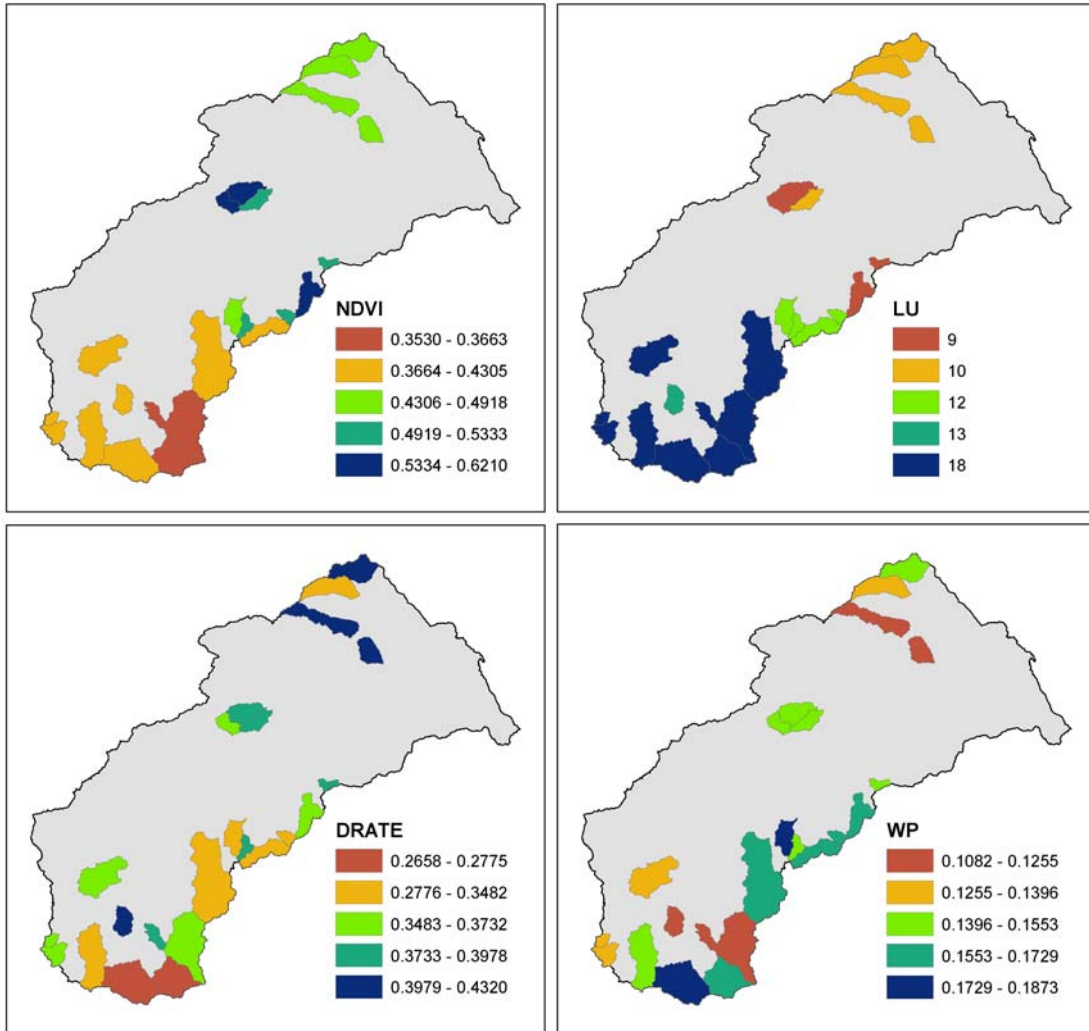


Figure B.2 Maps of additional physical watershed characteristics for the 23 gauged watersheds, including the normalized difference vegetation index (NDVI), landuse (LU), soil drainage rate (DRATE) and soil water content (m/m) at the permanent wilting point (WP). LU values are integer land cover classes defined as:

- 9 – close deciduous forest
- 10 – deciduous woodland
- 12 – open deciduous shrubland
- 13 – closed grassland
- 18 – cropland (> 50%)

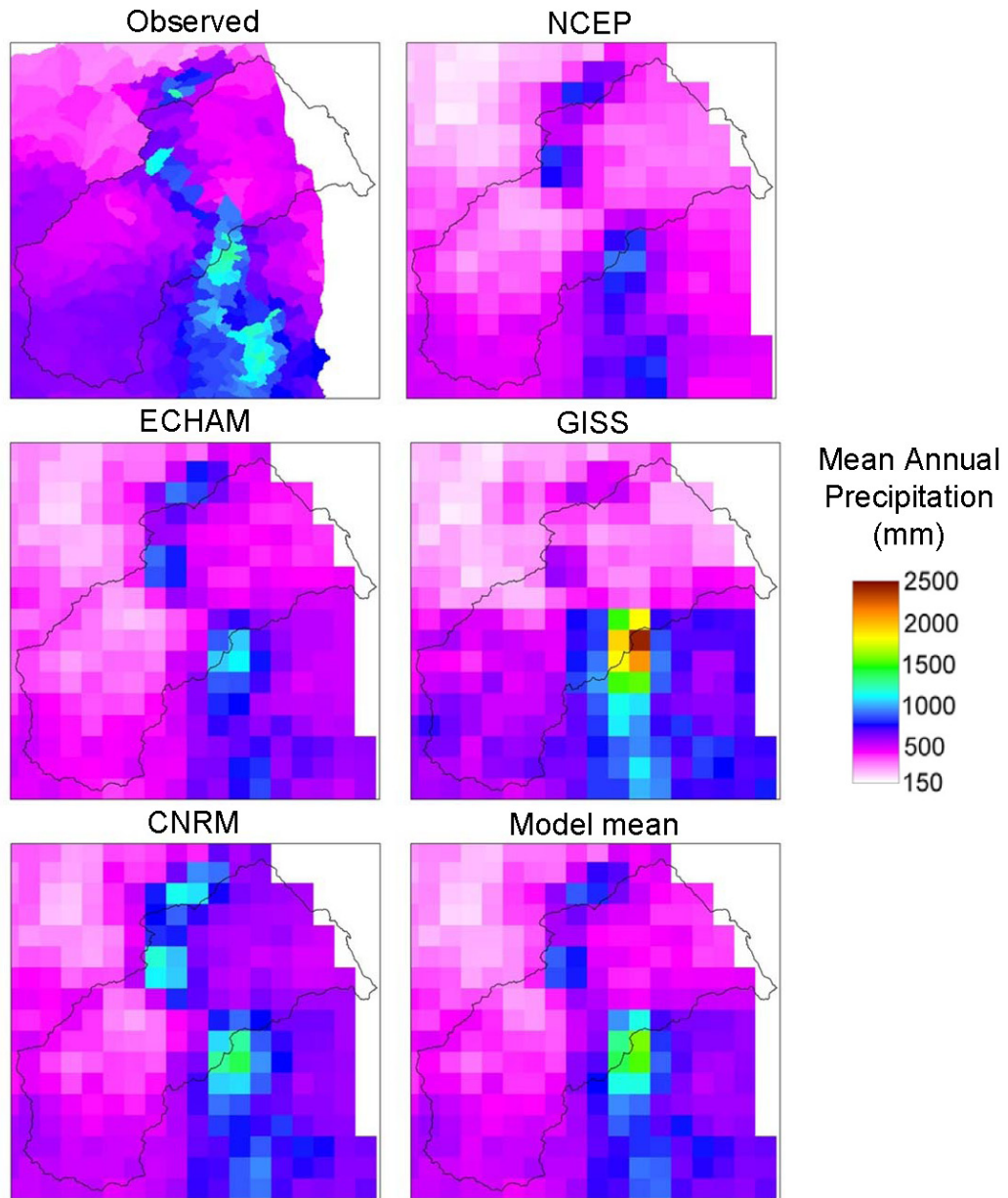


Figure B.3 Spatial distribution of mean annual precipitation for control period (1961-2000) based on observations and downscaled climate model projections.

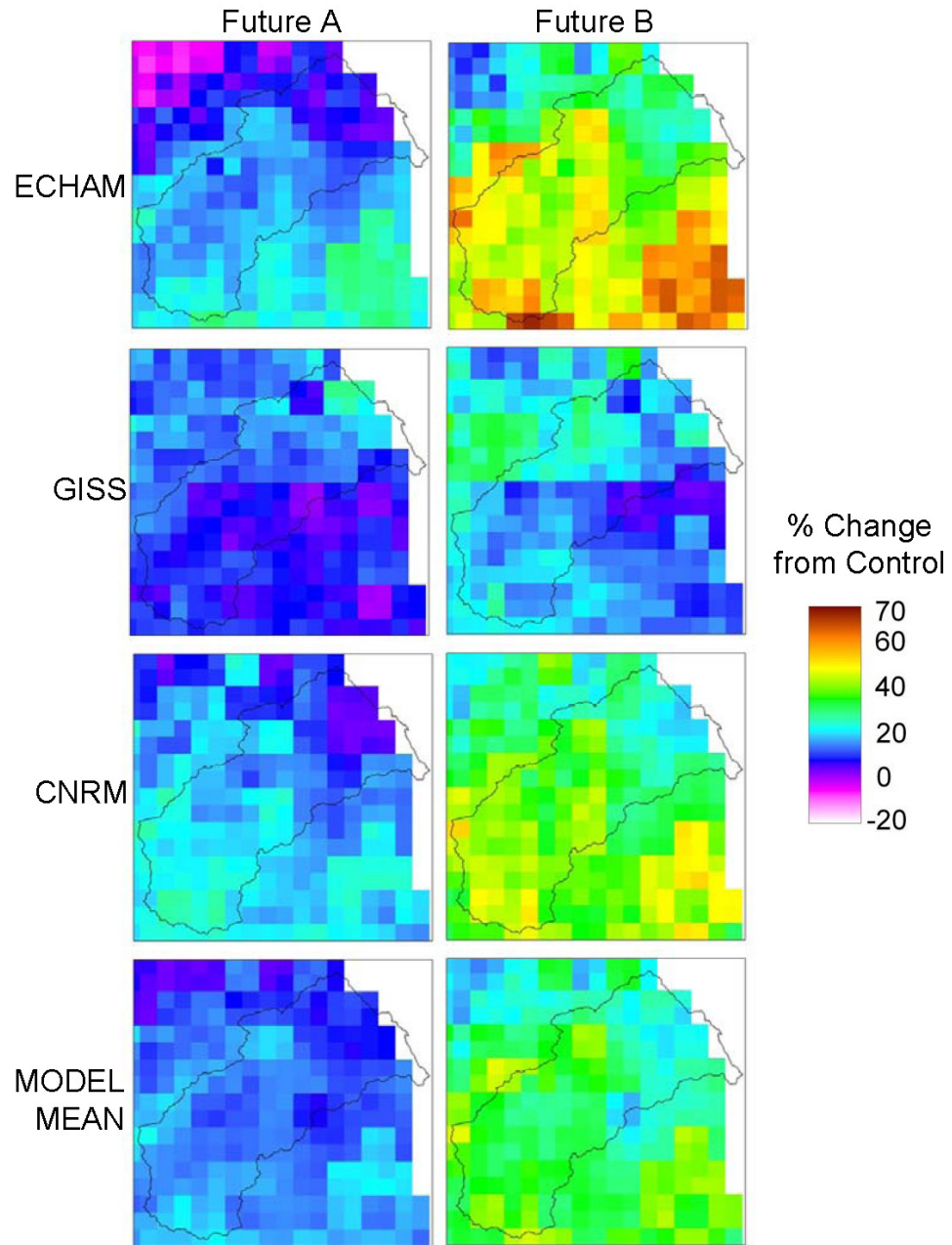


Figure B.4 Spatial distribution of percent change in downscaled precipitation from the control period (1961-2000) to Future A (2046-2065) and Future B (2081-2100) for each model.

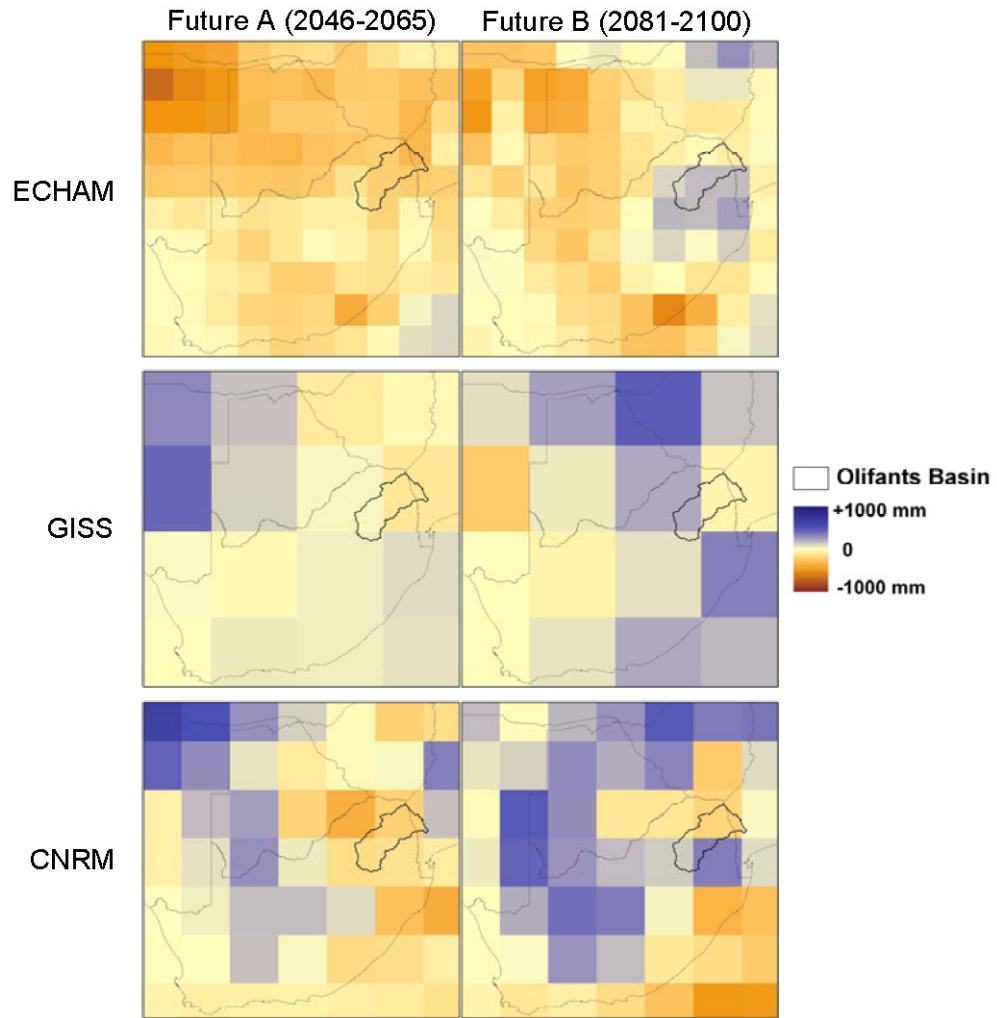


Figure B.5 Change in mean annual precipitation based on the original (non-downscaled) global climate model projections from the three models used in this study for future A (2045-2065) and future B (2081-2100) periods. Precipitation change is measured with respect to the historical period 1961-1990.

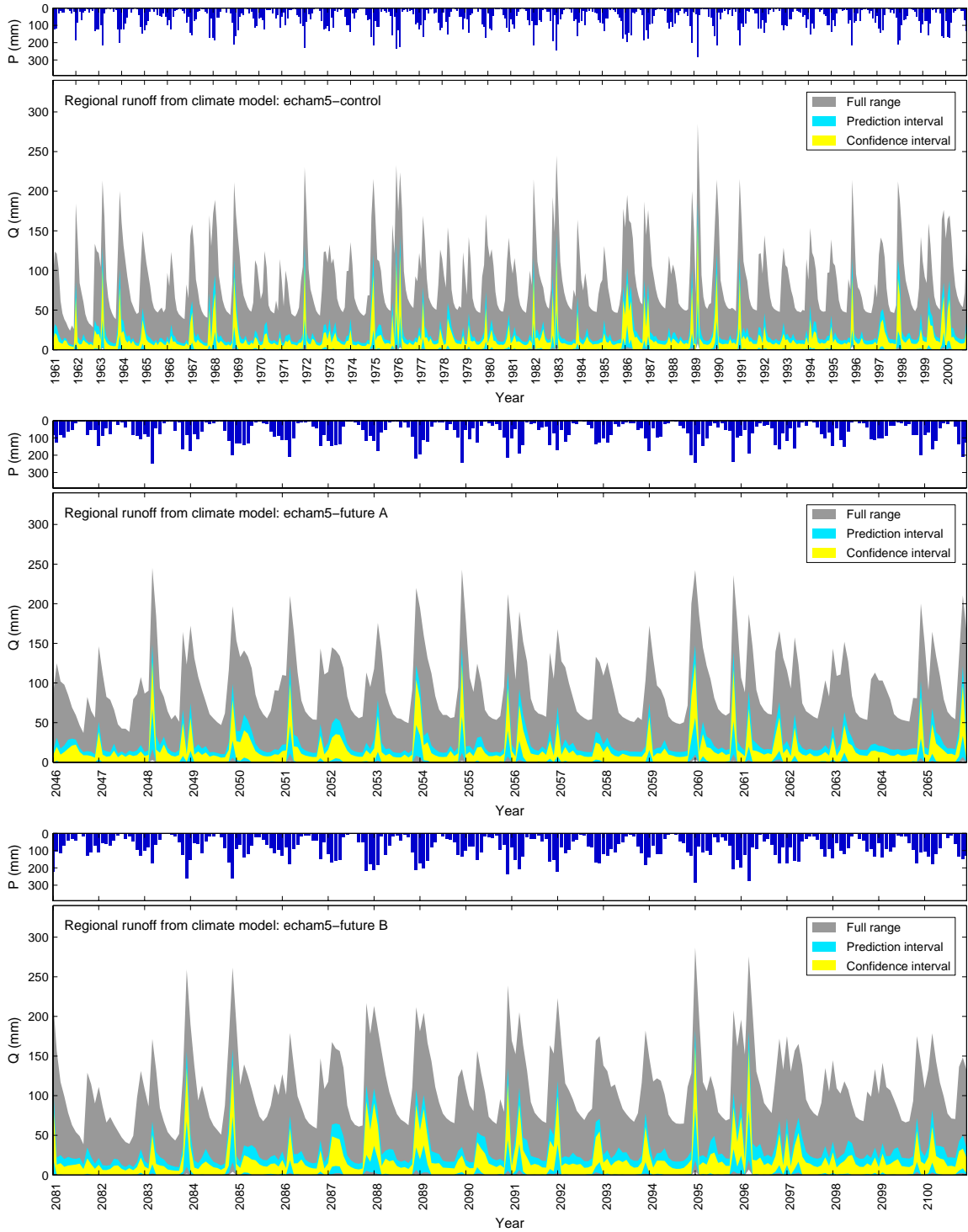


Figure B.6 Model echam5 regional ensemble simulations of hydrologic response to climate change, showing the control period (top), future A period (middle), and future B period (bottom).

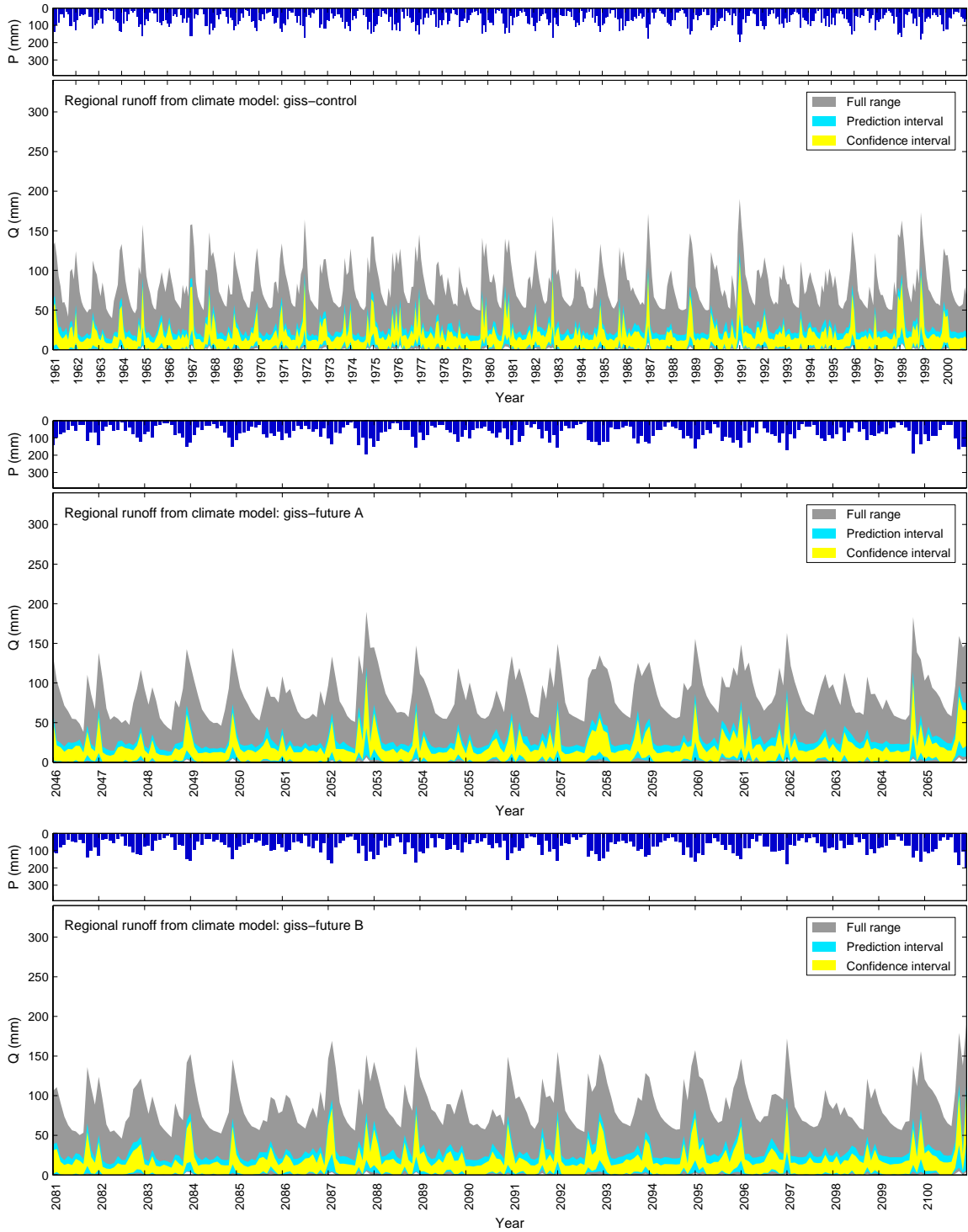


Figure B.7 Model giss regional ensemble simulations of hydrologic response to climate change, showing the control period (top), future A period (middle), and future B period (bottom).

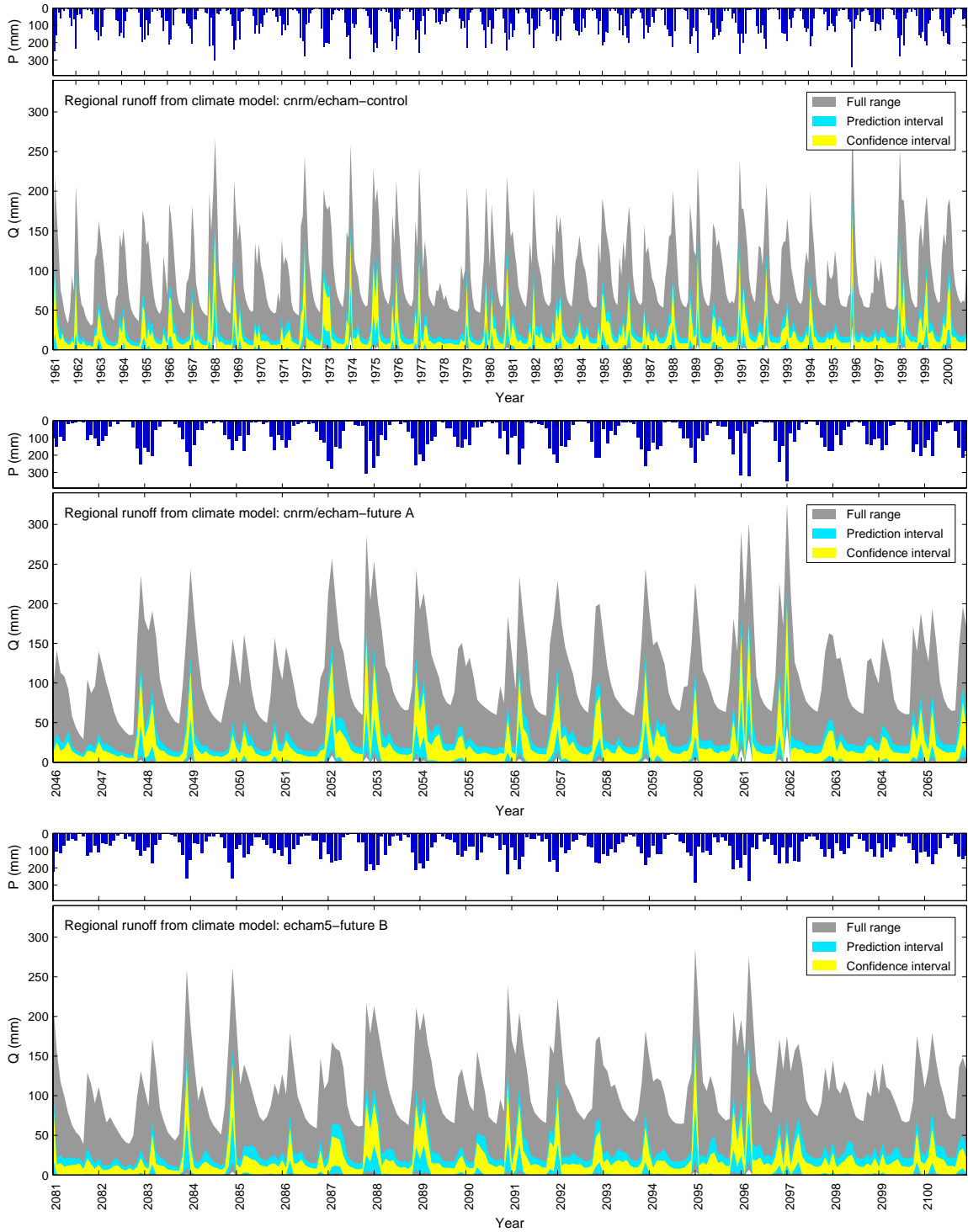


Figure B.8 Model cnrm/echam5 regional ensemble simulations of hydrologic response to climate change, showing the control period (top), future A period (middle), and future B period (bottom).

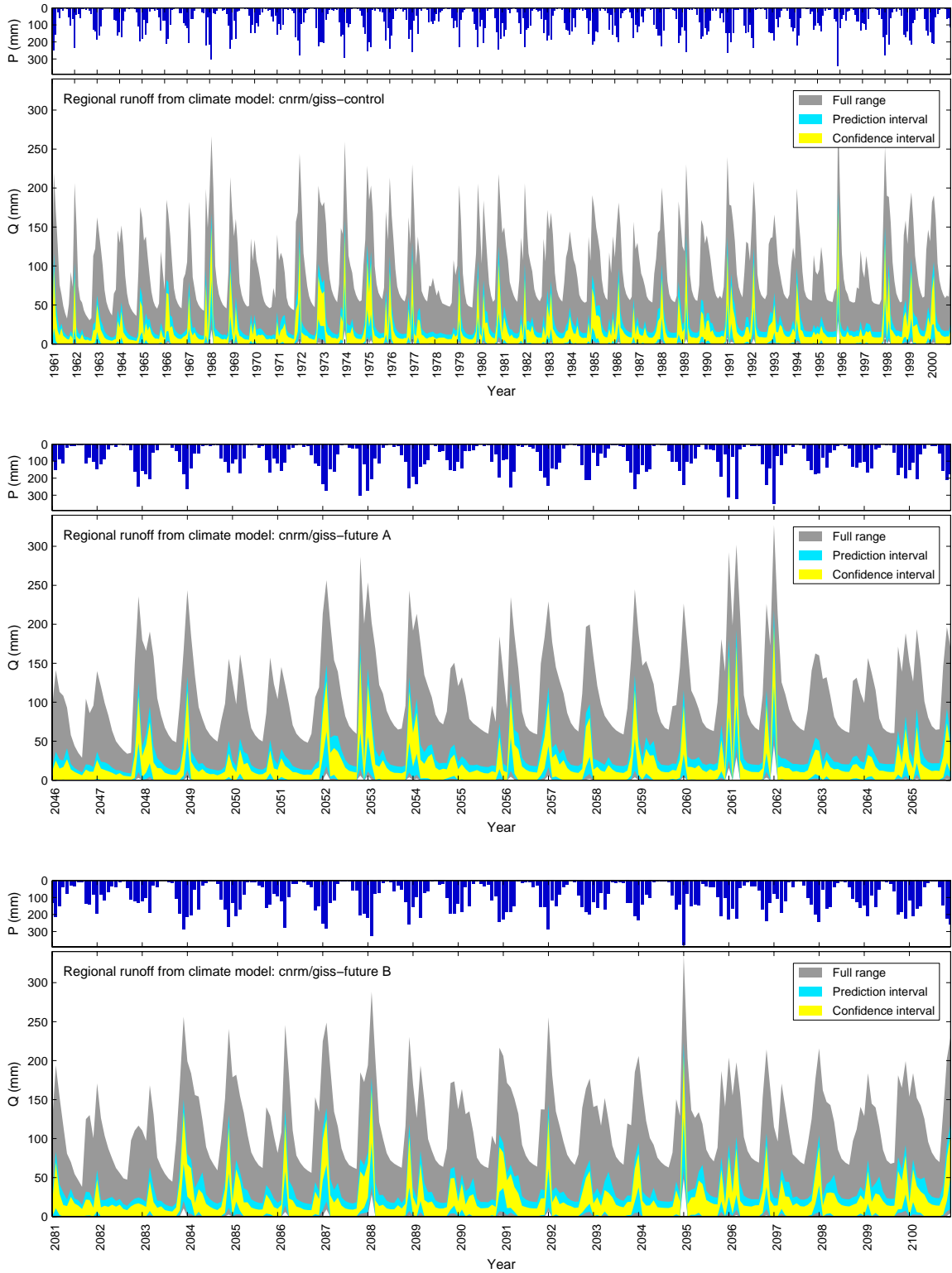


Figure B.9 Model cnrm/giss regional ensemble simulations of hydrologic response to climate change, showing the control period (top), future A period (middle), and future B period (bottom).

Vita
Kathryn L. van Werkhoven

EDUCATION

PhD Candidate, Civil and Environmental Engineering, Penn State University, State College, PA, expected Aug 2008, Dissertation: Evaluating model behavior for hydrologic forecasting in gauged and ungauged watersheds.

M.S., Hydrology and Water Resources, University of Arizona, Tucson, AZ, Aug 1999, Thesis: Analysis of the utility of remote sensing data for urban hydrologic modeling.

B.S., Engineering and Environmental Science, University of Notre Dame, Notre Dame, IN, May 1997

AWARDS AND HONORS

Outstanding Student Paper Award, AGU Fall Meeting 2007
GE Faculty for the Future Fellowship, 2007-2008
Outstanding Student Paper Award, AGU Fall Meeting 2006
Clare Luce Booth Fellowship, 2005-2007
Penn State College of Engineering Fellowship, 2005-2007
NSF Graduate Traineeship in Hydrology, University of Arizona, 1997-98

PROFESSIONAL EXPERIENCE

Engineer, Department of Water Affairs and Forestry, Government of South Africa
Pretoria, South Africa, 2004 –2005

Water Resources Engineer, Riverside Technology, inc.
Fort Collins, CO, 1999 – 2003

SELECTED PUBLICATIONS

van Werkhoven, K., T. Wagener, P. Reed, and Y. Tang (in revision). Sensitivity-guided multi-objective optimization of a lumped watershed model across a hydroclimatic gradient. *Water Resources Research*.

van Werkhoven, K., T. Wagener, P. Reed, and Y. Tang (2008). Rainfall characteristics define the value of streamflow observations for distributed watershed model identification. *Geophysical Research Letters*, 35, doi:10.1029/2008GL034162

van Werkhoven, K., T. Wagener, P. Reed, and Y. Tang. (2008). Characterization of watershed model behavior across a hydroclimatic gradient. *Water Resources Research*. doi:10.1029/2007WR006271.

Wagener, T., P. Reed, **K. van Werkhoven**, Y. Tang and Z. Zhang (in review). Advances in the identification and evaluation of complex environmental systems models. *Journal of Hydroinformatics*.

Tang, Y., P. Reed, **K. van Werkhoven**, and T. Wagener (2007). Advancing the identification and evaluation of distributed rainfall-runoff models using global sensitivity analysis. *Water Resources Research*, 43, doi:10.1029/2006WR005813.

Tang, Y., P. Reed, T. Wagener, and **K. van Werkhoven** (2007). Comparing sensitivity analysis methods to advance lumped watershed model identification and evaluation. *Hydrology and Earth System Sciences*, 11, 793-817.